Formation and Dynamics of Oil Ganglia in Porous Media

A Dissertation

Presented to

the Faculty of the Department of Chemical Engineering

University of Houston

Houston, Texas

In Partial Fulfillment

of the Requirements for the Degree

Doctor of Philosophy in Chemical Engineering

by

Madalena Maria Gomes de Queiroz Dias

July, 1984

Copyrighted by

Madalena Maria Gomes de Queiroz Dias

July, 1984

Formation and Dynamics of Oil Ganglia in Porous Media

Madalena Maria Gomes de Queiroz Dias

Approved:

Alkiviades A. Payatakes
Chairman of the Committee
A. C. Payatakes, Professor
Chemical Engineering

H. Deans, Professor
Chemical Engineering

R. W. Flumerfelt, Professor
Chemical Engineering

C. Dalton, Professor
Mechanical Engineering

J. H. Lienhard, Professor
Mechanical Engineering

H. W. Prengle Jr., Associate Dean
Cullen College of Engineering

Dan Luss, Professor and Chairman

Acknowledgments

I wish to express my gratitude to those whose contribution was fundamental in the completion of this work.

- Professor Alkiviades C. Payatakes, my Research Advisor, for his guidance, counsel and friendship throughout the course of this work.
- Professor Alírio Rodrigues, Department of Chemical Engineering, University of Porto, Porto, Portugal, whose counsel and encouragement made this dream come true.
- Dr. W. Preeg, director of Fluid Mechanics-Nuclear, Schlumberger-Doll Research, Ridgefield, Connecticut, for giving me the opportunity of working at that research center, during the summer of 1983. Some of the numerical calculations presented in Chapter 5 were performed at SDR. The unlimited access to their computing facilities was greatly appreciated.
- Dr. R. Chandler, director of Electrical Engineering, Schlumberger Well Services, Houston, Texas, for making possible the use of their computing facilities to type this dissertation.
- Drs. J. D. Chen, P. S. Hammond, J. Koplik, T. J. Lasseter. D. Wilkinson and J. F. Willemsen at SDR, for many useful discussions and suggestions.
- Mr. C. Thornton at SWS, for taking the time to introduce me to TEX, the excellent word processor and typesetting system that produced this paper.
- To INVOTAN, Portugal, for their NATO Science Fellowship.
- Mrs. Carol Maddox and Ms. Elizabeth Strauch, for taking the time to proofread this paper.
- To my family and friends, for just being there when they were needed.

This work was performed under financial support of the Department of Energy and the Schlumberger-Doll Research Center.

To my parents and my husband

E aqueles que por obras valerosas
Se vão da lei da Morte libertando

Luís Vaz de Camões, in "Os Lusíadas"

Formation and Dynamics of Oil Ganglia in Porous Media

An Abstract of a Dissertation

Presented to

the Faculty of the Department of Chemical Engineering

University of Houston

Houston, Texas

In Partial Fulfillment

of the Requirements for the Degree

Doctor of Philosophy in Chemical Engineering

by

Madalena Maria Gomes de Queiroz Dias

July, 1984

Abstract

Immiscible displacement through porous media is a process encountered in many situations, including secondary and tertiary oil recovery processes. Secondary recovery is usually carried out by waterflooding. Water is injected into the reservoir, and as this water advances through the porous formation, it leaves behind some residual oil, in the form of discrete blobs of oil, called ganglia. This residual oil, which, in certain cases, may represent up to two thirds of the initial oil in place, is the target of tertiary oil recovery. In later stages of some tertiary processes (e.g. chemical flooding), the displacement may degenerate to a relative inefficient immiscible mode. The successful completion of this recovery process depends on the mobilization and reconnection of these oil ganglia and on the formation of large blobs of oil, which constitute an oil bank.

Traditionally, two alternative approaches, based upon either a macroscopic or a microscopic scale, are used to treat analytically the problem of multiphase flow in porous media. It is the goal of this work to set forth a reliable description of the set of phenomena occurring at a characteristic length of the order of 1 to 100 grain diameters, namely microdisplacement and ganglion dynamics. To this end, a simulation method based on a network of constricted unit cells and a set of rules for fluid displacement is developed. As will be seen, this simulation method has some advantages when compared with previous attempts to model this problem, namely percolation processes, networks of tubes of the sphere-and-capillary type and the quasistatic criterion for ganglion mobilization.

This simulation method is then used to simulate the fate of a solitary oil ganglion under an applied polymer flood (ganglion dynamics) and the invasion by water of an initially oil-filled network (imbibition processes). In both cases, a qualitative description of the phenomena observed is given, and variables of importance in the study of large populations of ganglia are calculated for several values of the relevant physical and operational parameters. The average ganglion velocity, the break-up and stranding coefficients and the break-up mode probability are calculated from ganglion dynamics simulations. Simulations of imbibition processes give the ganglion size and volume distributions and the residual oil saturation.

Table of Contents

Page

Table of Contents i

List of Figures iv

List of Tables xiv

Chapter 1. Introduction 1

1.1 Importance and Motivation 1

1.2 Objectives 3

Chapter 2. Theoretical and Experimental Background 5

2.1 Porous Media 5

2.1.1 Prototype Porous Media 6

2.1.2 Model Porous Media 9

2.2 Flow Regimes 10

2.3 Displacement in Single Capillaries and in Doublets 16

2.3.1 Equilibrium and Motion of Menisci 16

2.3.2 Thickness of the Lubrication Film 20

2.3.3 Pinch-off, Snap-off and Dynamic Breakup 22

2.3.4 Trapping and Mobilization of Oil Droplets and Ganglia . . . 26

2.3.5 Motion of Oil Droplets and Ganglia in Capillary Tubes 28

2.3.6 Coalescence of Oil Droplets and Ganglia 29

2.4 Immiscible Displacement. Formation of Ganglia 30

2.4.1 Percolation Models 32
2.4.2 Networks of Converging-Diverging Tubes 37
2.5 Ganglion Dynamics 39
2.5.1 Mobilization and Quasistatic Displacement of a Solitary Ganglion 39
2.5.2 Dynamic Displacement of Ganglia. Experimental Observations 49
2.5.3 Dynamics of Ganglion Populations 51

Chapter 3. Modeling of Oil Ganglion Motion 57

3.1 Introduction 57
3.2 Network Model 59
3.3 Analogy Concepts 64
3.4 Permeability and Network Isotropy 71
3.5 Macroscopic Pressure Gradient and Boundary Conditions 73
3.6 Conductance and Pressure Drop Across an Interface 76
3.6.1 Single Phase Flow Conductance 76
3.6.2 Two Phase Flow Conductance 77
3.6.3 Pressure Drop Across an Interface 79
3.6.4 Effective Conductance and Effective Pressure Drop Across an Interface 80
3.7 Motion Rules and Interface Rupture Mechanisms 83
3.7.1 Treatment of Xerons 84
3.7.2 Treatment of Hygrons. Interface Rupture Criterion 92
3.8 Computational Aspects 109
3.8.1 Simulation Algorithm 111
3.8.2 Block Diagram 112
3.8.3 Choice of Network Size 113
3.8.4 Choice of Number of Compartments 117

Chapter 4. Oil Ganglion Dynamics 122

4.1 Introduction 122
4.2 Individual Simulations. Motion and Fission 128
4.2.1 Influence of the Capillary Number 133
4.2.2 Influence of the Viscosity Ratio 136
4.2.3 Influence of the Macroscopic Pressure Gradient 138
4.2.4 Influence of the Network Topology 142

4.3 Average Ganglion Velocity 146
4.3.1 Ganglion Velocity in a Monolayer Square Beadpack 147
4.3.2 Ganglion Velocity in a 100 × 200 Sandpack 153
4.4 Fissioning and Stranding 163
4.4.1 The Breakup and the Stranding Coefficients 163
4.4.2 Break-up Mode 183

Chapter 5. Modeling of Imbibition and Dynamic Invasion Processes 192

5.1 Introduction 192
5.2 Simulation Model 193
5.2.1 Boundary Conditions 194
5.2.2 Formation and Stranding of Ganglia 196
5.3 Free Imbibition Simulations 199
5.4 Imbibition and Dynamic Invasion Simulations 200

Chapter 6. Summary and Suggestions for Future Work 238

6.1 Summary and Conclusions 238
6.2 Suggestions for Future Work 243

Appendix A. FORTRAN 77 Listings of Computer Codes 246

A.1 Listing of Program GANDYN Used to Simulate the Motion of a Solitary Oil Ganglion 247
A.2 Listing of Program IMBSIM used for Imbibition and Dynamic Invasion Simulations 260
A.3 Listing of Subroutines Called by Program GANDYN and/or IMBSIM 278

Appendix B. Description of Dimensionless Unit Cell 292

Appendix C. Determination of the Porous Medium Model Constants for the Monolayer Square Beadpack Network 294

Appendix D. Determination of the Hydraulic Conductance Equivalent to a Long Network 297

Notation 3010

Literature References 306

List of Figures

Page

2.1 Mobilization of a ganglion. a) No Flow; ganglion at equilibrium. b) The non-wetting phase flows from left to right with pressure gradient less than the critical value required for mobilization. c) If the pressure gradient exceeds the critical value for mobilization, a rheon takes place. From Payatakes (1982) 41

2.2 Concepts involved in the quasistatic criterion for mobilization 44

2.3 Evolution of an 8-pore ganglion undergoing quasistatic displacement for $Ca = 4.8 \times 10^{-4}$ and $\kappa = 7.0$. From Hinkley (1982) 48

2.4 Evolution and breakup of the 8-pore ganglion of Figure 2.3 when subject to dynamic displacement for $Ca = 1.5 \times 10^{-3}$ and $\kappa = 7.0$. From Hinkley (1982) 50

2.5 Evolution and breakup of an oil ganglion undergoing dynamic displacement. From Rapin (1980) 52

2.6 Evolution and breakup of an 8-pore oil ganglion undergoing dynamic displacement. From Hinkley (1982) 53

3.1 Typical unit cell of the porous medium model. From Payatakes *et al* (1980) 61

3.2 Two dimensional depiction of a cubic network of unit cells. A CEVS, a UC and an EUC are identified, as well as an 8-CEVS ganglion (solid line circles) and a 2-CEVS ganglion (dashed line circles) 63

3.3 Depiction of a $N_x \times N_y = 6 \times 7$ cubic network showing the nodes numbering system and in the inset the branches numbering system 65

3.4 (a) Depiction of a 7-CEVS ganglion on a two-dimensional square network and (b) its electric network 68
3.5 Flow configuration calculation example. The direction of the macroscopic pressure gradient is at an angle ϕ' 75
3.6 Representation of a gate unit cell divided into ten compartments showing compartments k_G and k_P used to calculate the effective conductance and the effective pressure drop respectively . . 81
3.7 Stages of a 6-CEVS ganglion motion simulation. Occurrence of a xeron 85
3.8 Sequential pictures of a moving 6-pore oil ganglion. Demonstration of a xeron. From Hinkley (1982) 87
3.9 Stages of an 8-CEVS ganglion motion simulation. Occurrence of two simultaneous xerons into CEVS's sharing a same unit cell . . . 89
3.10 Stages of a 12-CEVS ganglion motion simulation. Occurrence of a xeron into a CEVS sharing a GUC with another CEVS 91
3.11 Stages of a 2-CEVS ganglion motion simulation. Occurrence of a hygron 93
3.12 Sequential pictures of a moving 2-pore oil ganglion. Demonstration of a hygron. From Hinkley (1982) 94
3.13 Stages of a 12-CEVS ganglion motion simulation. Occurrence of a hygron, after redistribution of oil 96
3.14 Stages of a 12-CEVS ganglion motion simulation. Formation of an oil thread with subsequent rupture of the interface 98
3.15 Stages of a 12-CEVS ganglion motion simulation. Formation of an oil thread without rupture of the interface 99
3.16 Stages of a 10-CEVS ganglion motion simulation. Formation of an oil thread surrounding a grain without rupture of the interface 100
3.17 Stages of a 10-CEVS ganglion motion simulation. Formation of an oil thread surrounding a grain with subsequent rupture of the interface 102
3.18 Schematic representation of an oil thread formed between two pores 103
3.19 Schematic representation of an oil thread surrounding a grain . . . 104
3.20 Sequential pictures of a moving oil ganglion. Demonstration of interface rupture with simultaneous breakup. From Rapin

(1980) 105
3.21 Sequential pictures of a moving oil ganglion. Demonstration of reconnection through an oil thread. From Rapin (1980) 106
3.22 Stages of a 10-CEVS ganglion motion simulation. Example of reconnection through an oil thread 110
3.23 Block diagram of the ganglion dynamics simulation code 114
3.24 Plot of the CPU time per simulation step, t_{CPU} , *versus* the total number of nodes, N_p 116
3.25 Plot of the normalized average radius of influence, ς, *versus* the reduced ganglion volume, v^* 118
3.26 Example of influence of the number of compartments, N_c , on the qualitative behaviour of an 8-CEVS ganglion 120
3.27 Plot of the percent error for u^* *versus* the number of compartments, N_c , for various values of v^* and $Ca = 10^{-4}$ 121
4.1 Plot of the throat size probability distribution function, $F_d(d)$. From Payatakes *et al* (1980) 124
4.2 Dependence of the advancing contact angle, θ_a^o , and the receding contact angle, θ_r^o , on the equilibrium contact angle, θ_e , for various levels of surface roughness. From Morrow (1975) 129
4.3 Dependence of the dynamic contact angle, θ, on the interfacial velocity, u_i , for $\theta_e = 10°$ 130
4.4 Dependence of the dynamic contact angle, θ, on the interfacial velocity, u_i , for $\theta_e = 30°$ 131
4.5 Dependence of the dynamic contact angle, θ, on the interfacial velocity, u_i , for an oil-brine system. From Hinkley (1982) 132
4.6 Stages of a 12-CEVS ganglion motion simulation in a network representing a 100×200 sandpack for $Ca = 2 \times 10^{-4}$, $\kappa = 1.0$, and $\phi' = 45°$ 134
4.7 Stages of a 12-CEVS ganglion motion simulation in a network representing a 100×200 sandpack for $Ca = 4 \times 10^{-4}$, $\kappa = 1.0$, and $\phi' = 45°$ 135
4.8 Stages of a 12-CEVS ganglion motion simulation in a network representing a 100×200 sandpack for $Ca = 10^{-3}$, $\kappa = 1.0$, and $\phi' = 45°$ 136
4.9 Stages of a 8-CEVS ganglion motion simulation in a network of monosized unit cells for $Ca = 10^{-3}$, $\kappa = 7.0$, and $\phi' = 90°$ 139

4.10 Stages of a 8-CEVS ganglion motion simulation in a network of monosized unit cells for $Ca = 10^{-3}$, $\kappa = 7.0$, and $\phi' = 70°$ 140

4.11 Stages of a 8-CEVS ganglion motion simulation in a network of monosized unit cells for $Ca = 10^{-3}$, $\kappa = 7.0$, and $\phi' = 45°$ 141

4.12 Stages of a 8-CEVS ganglion motion simulation in a network of monosized unit cells for $Ca = 5 \times 10^{-4}$, $\kappa = 7.0$, and $\phi' = 45°$ . . . 143

4.13 Stages of a 8-CEVS ganglion motion simulation in a network representing a 100×200 sandpack for $Ca = 5 \times 10^{-4}$, $\kappa = 7.0$, and $\phi' = 45°$ 144

4.14 Stages of a 8-CEVS ganglion motion simulation in a network representing a 100×200 sandpack for $Ca = 5 \times 10^{-4}$, $\kappa = 7.0$, and $\phi' = 45°$ 145

4.15 Comparison between experimental and theoretical values of the reduced time-averaged ganglion velocity, u^*, *versus* the reduced ganglion volume, v^*, for various Ca values and $\kappa = 0.56$ 149

4.16 Comparison between experimental and theoretical values of the reduced time-averaged ganglion velocity, u^*, *versus* the reduced ganglion volume, v^*, for various Ca values and $\kappa = 7.3$ 150

4.17 Plot of the reduced time-averaged ganglion velocity, u^*, *versus* the reduced ganglion volume, v^*, in a 100×200 sandpack for various Ca values. $\kappa = 7.0$, $\theta_e = 0°$ 154

4.18 Plot of the reduced time-averaged ganglion velocity, u^*, *versus* the reduced ganglion volume, v^*, in a 100×200 sandpack for various Ca values. $\kappa = 1.0$, $\theta_e = 0°$ 155

4.19 Plot of the reduced time-averaged ganglion velocity, u^*, *versus* the reduced ganglion volume, v^*, in a 100×200 sandpack for various Ca values. $\kappa = 0.6$, $\theta_e = 0°$ 156

4.20 Plot of the reduced time-averaged ganglion velocity, u^*, *versus* the capillary number, Ca, in a 100×200 sandpack for various values of v^*. $\kappa = 7.0$, $\theta_e = 0°$ 157

4.21 Plot of the reduced time-averaged ganglion velocity, u^*, *versus* the capillary number, Ca, in a 100×200 sandpack for various values of v^*. $\kappa = 1.0$, $\theta_e = 0°$ 158

4.22 Plot of the reduced time-averaged ganglion velocity, u^*, *versus* the capillary number, Ca, in a 100×200 sandpack for various values of v^*. $\kappa = 0.6$, $\theta_e = 0°$ 159

4.23 Plot of the reduced time-averaged ganglion velocity, u^*, *versus* the reduced ganglion volume, v^*, in a 100 × 200 sandpack for various Ca values. $\kappa = 7.0$, $\theta_e = \theta_a^o = \theta_r^o = 10°$ 161

4.24 Plot of the reduced time-averaged ganglion velocity, u^*, *versus* the reduced ganglion volume, v^*, in a 100 × 200 sandpack for various Ca values. $\kappa = 7.0$, $\theta_e = \theta_a^o = \theta_r^o = 30°$ 162

4.25 Plot of the reduced time-averaged ganglion velocity, u^*, *versus* the reduced ganglion volume, v^*, in a 100 × 200 sandpack for various Ca values. $\kappa = 7.0$, $\theta_e = 10°$, $\theta_a^o = 11.4°$, $\theta_r^o = 0°$ 164

4.26 Plot of the reduced time-averaged ganglion velocity, u^*, *versus* the reduced ganglion volume, v^*, in a 100 × 200 sandpack for various Ca values. $\kappa = 7.0$, $\theta_e = 30°$, $\theta_a^o = 34.2°$, $\theta_r^o = 9.1°$ 165

4.27 Plot of the reduced time-averaged ganglion velocity, u^*, *versus* the reduced ganglion volume, v^*, in a 100 × 200 sandpack for various Ca values. $\kappa = 7.0$, $\theta_e = 10°$, $\theta_a^o = 11.4°$, $\theta_r^o = 0°$. Rate-dependent contact angle as in curve (c), Figure 4.3 166

4.28 Plot of the reduced time-averaged ganglion velocity, u^*, *versus* the reduced ganglion volume, v^*, in a 100 × 200 sandpack for various Ca values. $\kappa = 7.0$, $\theta_e = 10°$, $\theta_a^o = 11.4°$, $\theta_r^o = 0°$. Rate-dependent contact angle as in curve (d), Figure 4.3 167

4.29 Plots of $(\omega\ell/\Delta z)$ and $(\psi\ell/\Delta z)$, *versus* the normalized length of migration, z/ℓ in a 100 × 200 sandpack, for a 4-CEVS ganglion, $\kappa = 7.0$ and a) $Ca = 10^{-3}$; b) $Ca = 5 \times 10^{-3}$. 171

4.30 Plots of $(\omega\ell/\Delta z)$ and $(\psi\ell/\Delta z)$, *versus* the normalized length of migration, z/ℓ, in a 100 × 200 sandpack, for a 5-CEVS ganglion, $\kappa = 7.0$ and a) $Ca = 10^{-3}$; b) $Ca = 5 \times 10^{-3}$. 172

4.31 Plots of $(\omega\ell/\Delta z)$ and $(\psi\ell/\Delta z)$, *versus* the normalized length of migration, z/ℓ, in a 100 × 200 sandpack, for a 5-CEVS ganglion, $\kappa = 1.0$ and a) $Ca = 10^{-3}$; b) $Ca = 5 \times 10^{-3}$. 173

4.32 Plots of $(\omega\ell/\Delta z)$ and $(\psi\ell/\Delta z)$, *versus* the normalized length of migration, z/ℓ, in a 100 × 200 sandpack, for a 5-CEVS ganglion, $\kappa = 0.6$ and a) $Ca = 10^{-3}$; b) $Ca = 5 \times 10^{-3}$. 174

4.33 Plots of $(\omega\ell/\Delta z)$ and $(\psi\ell/\Delta z)$, *versus* the normalized length of migration, z/ℓ, in a 100 × 200 sandpack, for a 7-CEVS ganglion, $\kappa = 7.0$ and a) $Ca = 10^{-3}$; b) $Ca = 5 \times 10^{-3}$. 175

4.34 Plots of $(\omega\ell/\Delta z)$ and $(\psi\ell/\Delta z)$, *versus* the normalized length of migration, z/ℓ, in a 100×200 sandpack, for a 10-CEVS ganglion,

$\kappa = 7.0$ and a) $Ca = 10^{-3}$; b) $Ca = 5 \times 10^{-3}$. 176

4.35 Plots of $(\omega\ell/\Delta z)$ and $(\psi\ell/\Delta z)$, *versus* the normalized length of migration, z/ℓ, in a 100×200 sandpack, for a 10-CEVS ganglion, $\kappa = 1.0$ and a) $Ca = 10^{-3}$; b) $Ca = 5 \times 10^{-3}$. 177

4.36 Plots of $(\omega\ell/\Delta z)$ and $(\psi\ell/\Delta z)$, *versus* the normalized length of migration, z/ℓ, in a 100×200 sandpack, for a 10-CEVS ganglion, $\kappa = 0.6$ and a) $Ca = 10^{-3}$; b) $Ca = 5 \times 10^{-3}$. 178

4.37 Plots of $(\omega\ell/\Delta z)$ and $(\psi\ell/\Delta z)$, *versus* the normalized length of migration, z/ℓ, in a 100×200 sandpack, for a 15-CEVS ganglion, $\kappa = 1.0$ and a) $Ca = 10^{-3}$; b) $Ca = 5 \times 10^{-3}$. 179

4.38 Plot of the normalized stranding coefficient, $\lambda\ell$, *versus* the normalized length of migration, z/ℓ, in a 100×200 sandpack, for 4, 5 and 7-CEVS ganglia, $\kappa = 7.0$ and $Ca = 10^{-3}$. 181

4.39 Plot of the normalized break-up coefficient, $\phi\ell$, *versus* the normalized length of migration, z/ℓ, in a 100×200 sandpack, for 4, 5 and 7-CEVS ganglia, $\kappa = 7.0$ and $Ca = 10^{-3}$. 182

4.40 Plot of the normalized stranding coefficient, $\lambda\ell$, *versus* the reduced ganglion volume, v^*, in a 100×200 sandpack, for $\kappa = 7.0$ and various Ca values. 184

4.41 Plot of the normalized break-up coefficient, $\phi\ell$, *versus* the reduced ganglion volume, v^*, in a 100×200 sandpack, for $\kappa = 7.0$ and various Ca values. 185

4.42 Plot of the normalized break-up coefficient, $\phi\ell$, *versus* the reduced ganglion volume, v^*, in a 100×200 sandpack, for $\kappa = 1.0$ and various Ca values. 186

4.43 Plot of the normalized break-up coefficient, $\phi\ell$, *versus* the reduced ganglion volume, v^*, in a 100×200 sandpack, for $\kappa = 0.6$ and various Ca values. 187

4.44 Plot of the break-up mode probability, $W(w,v)\Delta v$, *versus* the reduced ganglion volume, v^*, in a 100×200 sandpack, for $\kappa = 7.0$ and $Ca = 0.7 \times 10^{-3}$, with the mother ganglion reduced ganglion volume, w/v_{CEVS}, as a parameter. The symmetrical right half of the plot is not shown. 189

4.45 Plot of the break-up mode probability, $W(w,v)\Delta v$, *versus* the reduced ganglion volume, v^*, in a 100×200 sandpack, for $\kappa = 7.0$ and $Ca = 10^{-3}$, with the mother ganglion reduced ganglion volume, w/v_{CEVS}, as a parameter. The symmetrical right half

of the plot is not shown. 190

4.46 Plot of the break-up mode probability, $W(w,v)\Delta v$, *versus* the reduced ganglion volume, v^*, in a 100×200 sandpack, for $\kappa = 7.0$ and $Ca = 5 \times 10^{-3}$, with the mother ganglion reduced ganglion volume, w/v_{CEVS}, as a parameter. The symmetrical right half of the plot is not shown. 191

5.1 Depiction of a two-dimensional square network saturated with oil, showing the position of the oil-water interfaces at $t = 0$. 195

5.2 Stages of free imbibition simulations in a 15×30 network (100× 200 sandpack) for $\kappa = 50$. 201

5.3 Stages of free imbibition simulations in a 15×30 network (100× 200 sandpack) for $\kappa = 1$. 202

5.4 Stages of free imbibition simulations in a 15×30 network (100× 200 sandpack) for $\kappa = 0.2$. 203

5.5 Plot of the capillary number, Ca, at various cross-sections of the network *versus* the dimensionless axial distance, z/ℓ, during a simulated free imbibition for a) $\kappa = 50$; b) $\kappa = 1$; c) $\kappa = 0.2$. . . . 204

5.6 Plot of the final ganglion size frequency distribution functions for free imbibition simulations in a 15×30 network (100×200 sandpack) for $\kappa = 50$. a) frequency of ganglia, $f(s)$, *versus* the number of CEVS's occupied by the ganglion, s. b) frequency of ganglia, $f(v^*)$, *versus* the reduced ganglion volume, v^*. 207

5.7 Plot of the final ganglion size frequency distribution functions for free imbibition simulations in a 15×30 network (100×200 sandpack) for $\kappa = 1$. a) frequency of ganglia, $f(s)$, *versus* the number of CEVS's occupied by the ganglion, s. b) frequency of ganglia, $f(v^*)$, *versus* the reduced ganglion volume, v^*. 208

5.8 Plot of the final ganglion size frequency distribution functions for free imbibition simulations in a 15×30 network (100×200 sandpack) for $\kappa = 0.2$. a) frequency of ganglia, $f(s)$, *versus* the number of CEVS's occupied by the ganglion, s. b) frequency of ganglia, $f(v^*)$, *versus* the reduced ganglion volume, v^*. 209

5.9 Plot of the acceptance fraction, $a_d(d)$, *versus* the unit cell throat diameter, d, for free imbibition simulations on a 15×30 network (100×200 sandpack) for various values of κ. 210

5.10 Stages of imbibition simulation in a 15×30 network (100×200 sandpack) for $Ca = 10^{-8}$ and $\kappa = 50$ 212

5.11 Stages of imbibition simulation in a 15 × 30 network (100 × 200 sandpack) for $Ca = 10^{-5}$ and $\kappa = 50$ 213

5.12 Stages of imbibition simulation in a 15 × 30 network (100 × 200 sandpack) for $Ca = 10^{-3}$ and $\kappa = 50$ 214

5.13 Stages of imbibition simulation in a 15 × 30 network (100 × 200 sandpack) for $Ca = 10^{-8}$ and $\kappa = 1$ 215

5.14 Stages of imbibition simulation in a 15 × 30 network (100 × 200 sandpack) for $Ca = 10^{-5}$ and $\kappa = 1$ 216

5.15 Stages of imbibition simulation in a 15 × 30 network (100 × 200 sandpack) for $Ca = 10^{-3}$ and $\kappa = 1$ 217

5.16 Stages of imbibition simulation in a 15 × 30 network (100 × 200 sandpack) for $Ca = 10^{-8}$ and $\kappa = 0.2$ 218

5.17 Stages of imbibition simulation in a 15 × 30 network (100 × 200 sandpack) for $Ca = 10^{-5}$ and $\kappa = 0.2$ 219

5.18 Stages of imbibition simulation in a 15 × 30 network (100 × 200 sandpack) for $Ca = 10^{-3}$ and $\kappa = 0.2$ 220

5.19 Plot of the final ganglion size frequency distribution functions for imbibition simulations in a 15 × 30 network (100 × 200 sandpack) for $Ca = 10^{-8}$ and $\kappa = 50$. a) frequency of ganglia, $f(s)$, *versus* the number of CEVS's occupied by the ganglion, s. b) frequency of ganglia, $f(v^*)$, *versus* the reduced ganglion volume, v^* 222

5.20 Plot of the final ganglion size frequency distribution functions for imbibition simulations in a 15 × 30 network (100 × 200 sandpack) for $Ca = 10^{-5}$ and $\kappa = 50$. a) frequency of ganglia, $f(s)$, *versus* the number of CEVS's occupied by the ganglion, s. b) frequency of ganglia, $f(v^*)$, *versus* the reduced ganglion volume, v^* 223

5.21 Plot of the final ganglion size frequency distribution functions for imbibition simulations in a 15 × 30 network (100 × 200 sandpack) for $Ca = 10^{-3}$ and $\kappa = 50$. a) frequency of ganglia, $f(s)$, *versus* the number of CEVS's occupied by the ganglion, s. b) frequency of ganglia, $f(v^*)$, *versus* the reduced ganglion volume, v^* 224

5.22 Plot of the final ganglion size frequency distribution functions for imbibition simulations in a 15 × 30 network (100 × 200 sandpack) for $Ca = 10^{-8}$ and $\kappa = 1$. a) frequency of ganglia, $f(s)$, *versus* the number of CEVS's occupied by the ganglion, s. b) frequency of ganglia, $f(v^*)$, *versus* the reduced ganglion volume, v^* 225

5.23 Plot of the final ganglion size frequency distribution functions for imbibition simulations in a 15×30 network (100×200 sandpack) for $Ca = 10^{-5}$ and $\kappa = 1$. a) frequency of ganglia, $f(s)$, *versus* the number of CEVS's occupied by the ganglion, s. b) frequency of ganglia, $f(v^*)$, *versus* the reduced ganglion volume, v^* 226

5.24 Plot of the final ganglion size frequency distribution functions for imbibition simulations in a 15×30 network (100×200 sandpack) for $Ca = 10^{-3}$ and $\kappa = 1$. a) frequency of ganglia, $f(s)$, *versus* the number of CEVS's occupied by the ganglion, s. b) frequency of ganglia, $f(v^*)$, *versus* the reduced ganglion volume, v^* 227

5.25 Plot of the final ganglion size frequency distribution functions for imbibition simulations in a 15×30 network (100×200 sandpack) for $Ca = 10^{-8}$ and $\kappa = 0.2$. a) frequency of ganglia, $f(s)$, *versus* the number of CEVS's occupied by the ganglion, s. b) frequency of ganglia, $f(v^*)$, *versus* the reduced ganglion volume, v^* 228

5.26 Plot of the final ganglion size frequency distribution functions for imbibition simulations in a 15×30 network (100×200 sandpack) for $Ca = 10^{-5}$ and $\kappa = 0.2$. a) frequency of ganglia, $f(s)$, *versus* the number of CEVS's occupied by the ganglion, s. b) frequency of ganglia, $f(v^*)$, *versus* the reduced ganglion volume, v^* 229

5.27 Plot of the final ganglion size frequency distribution functions for imbibition simulations in a 15×30 network (100×200 sandpack) for $Ca = 10^{-3}$ and $\kappa = 0.2$. a) frequency of ganglia, $f(s)$, *versus* the number of CEVS's occupied by the ganglion, s. b) frequency of ganglia, $f(v^*)$, *versus* the reduced ganglion volume, v^* 230

5.28 Plot of the acceptance fraction, $a_d(d)$, *versus* the unit cell throat diameter, d, for free imbibition simulations on a 15×30 network (100×200 sandpack) for $\kappa = 50$ and various Ca values 232

5.29 Plot of the acceptance fraction, $a_d(d)$, *versus* the unit cell throat diameter, d, for free imbibition simulations on a 15×30 network (100×200 sandpack) for $\kappa = 1$ and various Ca values 233

5.30 Plot of the acceptance fraction, $a_d(d)$, *versus* the unit cell throat diameter, d, for free imbibition simulations on a 15×30 network (100×200 sandpack) for $\kappa = 0.2$ and various Ca values 234

5.31 Plot of the average water saturation, $S_w - S_{wi}$, versus time, t, for imbibition simulations on a 15×30 network (100×200 sandpack), for various values of Ca and κ 236

5.32 Plot of the residual oil saturation, S_{or} , versus the capillary number , Ca, for imbibition simulations on a 15×30 network (100×200 sandpack), for various values of κ 237

List of Tables

Page

3.1 Analogies between the Hydraulic and the Electric Networks 67

4.1 Experimental and theoretical analysis of a 100 × 200 sandpack. From Payatakes *et al* (1980) 125

4.2 Experimental and theoretical analysis of the Monolayer Square Beadpack Apparatus used by Hinkley (1982) 126

Chapter 1

Introduction

1.1 Importance and Motivation

The displacement through porous media of one fluid by another fluid, immiscible with the first, is a process encountered in many situations (e.g. gas absorbers; packed distillation columns; drainage and imbibition in solids; laboratory measurements of relative permeabilities; mercury porosimetry). Among these, oil production is perhaps the single most important process.

Oil is produced from natural deposits that occur within the interstices of porous rock formations such as sand, sandstone, limestone and dolomite. In nearly all instances, the production of oil is achieved in three different stages: primary, secondary and tertiary oil recovery.

During primary recovery the oil flows spontaneously into the production wells due to the high reservoir pressure. It is estimated that after primary recovery only 10% to 20% of the oil in the reservoir has been produced.

Secondary recovery is usually carried out by waterflooding methods. Water is injected into strategically located oil wells surrounding the producing well. It is estimated that on the average, two thirds of the oil initially in place remains trapped in the reservoir at the end of the secondary flooding. Two main causes can be identified. First, incomplete sweeping of the reservoir by the flood can leave zones of untouched oil. Second, even in the best contacted areas of the reservoir a substantial portion of oil is left behind as it is microscopically by-passed and it gets stranded. This residual oil exists in the form of discrete ganglia and occupies 25% to 50% of the porous space, whereas the rest is occupied by the aqueous phase. A *ganglion* is a nodular blob of a non-wetting phase which occupies at least one and usually several adjoining pores of the void space in a permeable medium. Typically, oil ganglia at this stage have sizes ranging from one to fifteen pore volumes. This remaining oil is the target of tertiary or enhanced oil recovery.

Chemical flooding is one of the most promising processes in enhanced oil recovery. A "chemical slug" is injected into the reservoir followed by a polymer drive slug. The role of the polymer solution is to control mobility, namely to suppress fingering. The chemical slug is usually a mixture of water, surfactant, cosurfactant and sodium chloride. At optimal conditions, chemical flooding begins as a miscible process and is very efficient. As the flood advances, compositional changes of the chemical slug deteriorate the displacement process to a less efficient immiscible mode (Healy and Reed, 1974; Healy, Reed and Stenmark, 1976; Nelson and Pope, 1977).

Phenomena of immiscible displacement also occur in systems that involve three or more fluids. The complexity of such systems, however, makes their treatment

more difficult. In this work attention is focused on two-fluid systems, and although the results can be applied to any pair of immiscible fluids, since much of the work is related to oil recovery the terms oil (oleic phase) and water (aqueous phase) will refer to the displaced and the displacing phase respectively. This work will be restricted to the case where the oleic phase is non-wetting whereas the aqueous phase is wetting. The reverse case where oil is wetting and water is non-wetting is substantially different. In the first case the capillary forces assist the invasion, whereas in the second case they resist invasion. Furthermore, in the case of a wetting displacing phase, the displaced phase is usually separated from the solid by a film of water, whereas if the displacing phase is non-wetting, the displaced phase clings to the wall and the water channels through the oil (see e.g. Craig, 1971).

1.2 Objectives

Flow through porous media offers the possibility of two alternative analytical approaches, based upon either the scale of pore dimensions or the scale of the macroscopic system. For the flow of a single (incompressible, Newtonian) fluid, Darcy's law applies and the problem is reduced to the relatively simple problem of determining the absolute permeability. If, on the other hand, more than one fluid flows, particularly if strong capillary forces are present, it is not completely clear what the valid macroscopic laws are (see. e.g., Scheidegger, 1974). In this case, the first problem is to determine which macroscopic equations are relevant, and in particular, whether the multi-phase generalization of Darcy's law is correct, and then one may ask how the relevant parameters depend on the system variables.

The objective of this work is to set forth a reliable microscopic description of the set of phenomena occurring at a scale of the order of 1 to 100 grain diameters. To this end, the text is divided as follows.

- A review of previous experimental and theoretical work on microdisplacement of two fluids in porous media is made in Chapter 2.
- In Chapter 3 a simulation method based on a network of constricted unit cells and a set of rules for fluid displacement is developed.
- The fate of a single ganglion in an infinite network is studied, both qualitatively and quantitatively in Chapter 4. Variables of importance in the study of large populations of ganglia (i.e., ganglion velocity and breakup coefficient) are calculated as functions of the relevant physical parameters (i.e., the capillary number, the viscosity ratio between the two fluids and the ganglion size).
- In Chapter 5 an extension of the simulation method is developed in order to simulate the invasion by water of a network initially filled with oil. Simulations with several different parameters such as the capillary number and viscosity ratio are presented, and the conditions for the formation of ganglia are discussed. The residual oil saturation and the size and volume distributions of ganglia are calculated. These two parameters are also important in the analysis of large populations of ganglia.
- Conclusions and recommendations for future work are proposed in Chapter 6.

Chapter 2

Theoretical and Experimental Background

2.1 Porous Media

Porous media are numerous and diverse. Here attention is focused on a pertinent class of prototype porous media, namely oil reservoir rock formations, and on *model porous media* which are simpler structures used in experimental studies of displacement processes.

In the remainder of this work, the term *pore* will be used to denote any void space within the porous medium, irrespective of size and shape. Large pores with size comparable to that of the grains are called *chambers* and the narrow pores connecting chambers are referred to as *throats.* In previous works these variables were referred respectively as "pores" and "constrictions" (Payatakes, Tien, Turian, 1973) and "pores" and "throats" (Wardlaw and Cassan, 1978).

A porous medium may be characterized by its porosity, pore geometry, heterogeneity and anisotropy. The *throat size distribution*, the *chamber size distribution*,

the *chamber-to-throat size ratio* and the *throat-to-chamber coordination number* are the most relevant characteristics of pore geometry and topology (Payatakes, Tien and Turian, 1973: Wardlaw and Cassan, 1978; Payatakes, Ng and Flumerfelt, 1980; Chandler *et al* . 1982; Koplik, 1982; Koplik and Lasseter, 1982; Wilkinson and Willemsen. 1983). Also, in the case of two-phase flow it is important to specify the wettability with respect to the pair of fluids.

Mathematical descriptions of the porous medium, called *porous medium models*, are very expedient tools to analyze flow through porous media. Some of these models will be discussed in other sections.

2.1.1 Prototype Porous Media

Oil bearing rocks are of numerous and diverse configurations, origins and composition. Extensive studies of reservoir rock structures have been done. Potter and Mast (1962) developed a method of measuring sandstone shape fabrics, using photographs of thin sections. In this same work a good review of previous works is given. A classification of carbonate rocks with emphasis on their genetic aspects is given in Choquette and Pray (1972).

Quantitative photomicrography of pore casts and mercury porosimetry or a combination of both methods have been used to characterize pore geometry and structure of carbonate rocks and sandstones (Dullien and Dhawan, 1974 and 1975; Wardlaw, 1976a, 1976b; Wardlaw and Taylor, 1976; Schmidt, McDonald and Platt, 1977; Wardlaw and Cassan, 1978; Wardlaw, 1980). More recently Lin and Cohen (1982) and Lin and Hamasaki (1983) developed a method for quantitative analysis and 3-D display of pore geometries.

Rock structures are usually characterized by their porosity, pore geometry and a set of characteristic scales.

The porosity of reservoir rocks varies in a range from 0.02 to 0.28 (Wardlaw and Cassan, 1978).

Pore geometries are as diverse as existing rock structures. In a study with dolomite rocks, Wardlaw (1976b) showed by visual inspection of pore casts that during the continued growth of dolomite crystals, initially polyhedral voids tend to be reduced in size and take the form of tetrahedral voids interconnected by sheet-like spaces.

The pore space can be divided into chambers and throats. The chamber size is characterized by the equivalent volumetric diameter, the *chamber diameter*. A wide range of randomly distributed chamber diameters is observed in reservoir rocks, typically from 5 to 100 μm (Dullien and Dhawan, 1975). A throat is characterized by its width, length and thickness. The *throat width* is comparable to the chamber diameter and the *throat length* is comparable to the *grain diameter* (*ca* 50 μm). The *throat thickness* is a randomly distributed variable ranging from 1 to 10 μm. Results reported by Wardlaw and McKellar (1981) indicate that the calculation of throat thickness distributions is not a simple matter, and it should involve combined information from mercury porosimetry on one hand and from stereological studies of pore casts on the other. It has been suggested elsewhere (Payatakes and Dias, 1984) that the throat thickness distribution can be isolated with proper analysis of porosimetry data performed with the help of algorithms simulating mercury invasion in a porous structure that already incorporates the results of the stereological analysis.

Two other geometric properties are also of prime importance. The chamber-to-throat diameter ratio which can be as small as 3 and as large as 100, usually has a value close to 10. The chamber-to-throat coordination number (number of throats connected to a given chamber) usually takes values from 4 to 7, but it can vary in a wider range from 2 to 15 (Wardlaw, 1980).

A medium is said to be *homogeneous* with respect to a certain property if that property is independent of macroscopic position within the medium. Otherwise the medium is said to be *heterogeneous*. A medium is said to be *isotropic* with respect to a certain property if that property is independent of direction within the medium. If at a point within the medium a property of the medium (e.g., permeability or thermal conductivity) varies with direction, the medium is said to be *anisotropic* at the considered point with respect to that property. The main property of flow through porous media is permeability. Hence, in general, the terms isotropy and anisotropy are used with respect to the medium's permeability. In natural materials, anisotropy is encountered in soils and in geological formations that serve as reservoirs and aquifiers. Sediments are commonly deposited in such a way that their permeability in one direction (usually along the plane of deposition) is greater than in other directions. Muskat (1937) lists 65 pairs of sand samples, more than two-thirds of which have a larger permeability in the direction parallel to the bedding plane than normal to it. The quotient of the two values ranged from 1 to 42. Johnson and Hughes (1948) and Johnson and Breston (1951) performed directional permeability measurements on various oil sandstones and concluded that flow through consolidated sands may be 25% to 30% less in one geographic direction than in another. Greenkorn, Johnson and Shallenberger (1964) studied the direc-

tional permeability of heterogeneous anisotropic porous media. Of the core plugs studied they found that about 60% showed significant point anisotropy. The permeability tensor of such media consists of two parts: a) a point-to-point variation which depends on grain size and b) a point variation which depends on bedding.

2.1.2 Model Porous Media

The most common model porous media are unconsolidated packs such as beadpacks and sandpacks, and photoetched glass plates.

Random packings of beads or sand are, for the most part, three dimensional and have a porosity of the order of 40% . As in the case of reservoir rocks, the pore space is divided in chambers and throats. The chamber diameter is *ca* 0.80 to 0.86 times the mean volumetric grain diameter, and the throats are relatively short and can be characterized by a single length, the *throat diameter* (Payatakes, Tien and Turian,1973; Payatakes and Neira, 1977). The size distribution of the throat diameter can be obtained from the initial drainage curve and its mean value is *ca* 0.37 times the mean volumetric grain diameter. This results in a chamber-to-throat diameter ratio value of *ca* 2.2, which is considerably smaller than the corresponding values for consolidated sands. These low values for the chamber-to-throat diameter ratio and the difference in throat lengths are of major importance when comparing displacement processes in unconsolidated and consolidated structures, since they strongly affect the breakup of the oleic phase (see Section 2.3.4).

Another point in which granular packings and reservoir rocks vary is their isotropy or anisotropy. Experimental studies by Fontugne (1969) and Rice *et al* (1970) using sandpacks show that the permeability in the plane of bedding is

isotropic and only slightly larger than the permeability normal to it. For this reason, granular packings are usually considered to be isotropic while reservoir rocks are known to be anisotropic (see previous section).

Monolayer packings of beads have also been used (Batycky and Singhal, 1977; Rapin, 1980; Hinkley, 1982). Being planar and easy to construct, their main attraction is that they allow the observation of the flow phenomena without having to match the refraction index of one of the fluids with that of the beads.

Photoetched glass plates are also planar porous media, having the same advantage of easy observation. The major advantage is the fact that they can be tailored as required in order to observe the behavior of the two fluids in various situations. Davis and Jones (1968) and McKellar and Wardlaw (1982) give methods for the construction of photoetched glass plates. Displacement studies in this type of media are reported by Mattax and Potter (1961), Wardlaw (1980), Lenormand and Bories (1980), Mahers, Wright and Dave (1981), Chatzis and Dullien (1981), Wardlaw and McKellar (1982), McKellar and Wardlaw (1982), Wardlaw (1982) and Lenormand, Zarcone and Sarr (1983) among others.

2.2 Flow Regimes

Multiphase flow in porous media can be treated on a macroscopic scale or on a microscopic scale.

Fractional Flow Theory is usually used for the macroscopic treatment. This theory, first proposed by Leverett (1938) and Buckley and Leverett (1942), assumes that the superficial velocity of each fluid is related to the pressure gradient a by

Darcy-like expression. Good reviews of this subject are found in Craig (1971), Wooding and Morel-Seytoux (1976) and Peaceman (1977).

In this work attention is focused on microdisplacement, that is, on flow phenomena at the pore scale. Due to the small pore dimensions and low flow rates the flow regime of interest is in the domain of creeping flow. The flow phenomena depend on the geometry and topology of the porous medium, on the physical properties of both fluids (viscosity, density, interfacial tension and contact angles), and on the externally imposed macroscopic pressure gradient. The flow is also "history" dependent, since it depends locally on the value of the oil saturation as well as on the way in which the oleic phase is distributed. Two dimensionless groups are often used to characterize the displacement mode:

- The *Capillary Number*, $Ca \equiv \mu_w v_f / \sigma_{ow}$, where μ_w and v_f are respectively the viscosity and superficial velocity of the aqueous phase and σ_{ow} is the interfacial tension between the two fluids.
- The *viscosity ratio* defined as $\kappa \equiv \mu_o / \mu_w$, where μ_o is the viscosity of the oleic phase.

Payatakes and Dias (1984) proposed a partial classification of the displacement phenomena in flow regimes based on the values of Ca and κ , the connected or disconnected form of the oleic phase, and the transient or steady nature of the flow. Below, a short description of the various flow regimes is given. In subsequent sections various regimes of importance for this work will be discussed in detail.

In this discussion it is assumed that the oleic phase is initially connected and fills the porous medium (save for a small amount of connate water). Water is brought into contact with it so that the two fluids are now separated by a set of

interfaces residing in pores near the front layer of the medium. The displacement process may occur in many ways.

- *Free Imbibition* occurs spontaneously when the aqueous phase invades the porous medium driven only by the capillary forces. These capillary forces resulting from the presence of the oil-water interfaces remain within relatively narrow bounds throughout the displacement process, whereas the viscous resistance to the flow changes as the aqueous phase invades the porous medium. The capillary number takes values on a wide range (10^{-9} to 10^{-4}). Due to the large Ca values achieved, the displacement of oil by water usually occurs in many pores simultaneously. Nevertheless, since the process is driven by capillary suction, the water pathways tend to pass through the narrowest pores accessible at every stage. In general, very large ganglia are not present in the porous medium at the end of the displacement process. The formation of large ganglia is prevented by the simultaneous invasion by water of several pores, and even if a large ganglion is formed, due to the large Ca values, it may keep moving until it breaks into smaller ganglia, which then become stranded.

- *Quasistatic Imbibition* is achieved in a similar fashion as free imbibition, only now a backpressure is applied in order to counterbalance the capillary suction and to obtain vanishingly small flow rates (Wilkinson and Willemsen, 1983). In this way the displacement is very slow, and the water seeks at each step the smallest accessible pore. Since, in most cases of interest, even large throats are small compared to the chamber size, a chamber is invaded only after all the adjoining throats have been invaded. The process is then controlled by the invasion of the *smallest accessible chamber*. (Chandler *et al* , 1982; Wilkinson

and Willemsen, 1983). One of the important characteristics of this flow regime is that, just before breakthrough (i.e., the stage at which the first connected pathway of water spanning the entire length of the sample is formed), the oleic phase is mostly connected and branches throughout the entire medium. There is no "front" separating the domains of the two fluids. After breakthrough, the water pathways begin to connect with each other leading to the eventual formation of ganglia. When a ganglion is created it becomes stranded immediately, since Ca is very small. In this way very large ganglia (with sizes comparable to that of the medium itself) may be formed.

- *Imbibition with Constant Influx and Nearly Constant Ca Value* is in many respects similar to both free imbibition and quasistatic imbibition. A back-pressure is applied across the porous medium and continuously adjusted to compensate for the changes on the viscous resistance as the aqueous phase displaces the oleic phase. In this way the influx of water is kept constant at some usually small but finite value. The applied pressure drop is negative and its magnitude increases with time if $\kappa > 1$ and is positive and its magnitude decreases with time if $\kappa < 1$. Although the influx is kept constant at the entrance, the local value of Ca at any point within the porous medium and in particular at the *transition zone* may be significantly different than that at the entrance. Since the local value of the oil saturation changes with time the flux of water at a given cross section passing through the transition zone is not equal to the influx of water at the entrance. If the Ca value imposed at the entrance is very small (say, less than 10^{-6}) the capillary forces dominate and the process approaches quasistatic imbibition conditions. Simultaneous invasion of various

pores is not likely to occur, and ganglia created under these conditions became stranded immediately.

- *Dynamic Invasion* is obtained by applying a sizable pressure difference across the porous medium so that it becomes the dominant driving force, whereas the capillary suction plays a secondary assisting role. Depending on the value of the viscosity ratio, the invasion develops in different ways. If $\kappa \ll 1$, the viscosity ratio is said to be favorable and a macroscopically smooth interface develops. If the viscosity ratio is unfavorable that is, $\kappa \geq 1$, the front becomes unstable and the formation of *viscous fingers* occurs. In this regime, the capillary forces are, negligible compared with the viscous forces; the several advancing interfaces tend to follow paths of least viscous resistance. Since, for the most part, chambers are substantially larger than throats, here the process is controlled by the the invasion of the *largest accessible throats*. Dynamic invasion may be performed at constant influx or at constant pressure drop. The overall performance in both cases is usually similar. To maintain a constant influx (nearly constant Ca) in the case of *dynamic invasion with constant influx and favorable viscosity ratio*, the applied pressure difference must increase with time, whereas in the case of *dynamic invasion with constant influx and unfavorable viscosity ratio*, the applied pressure difference must decrease with time. In the case of *dynamic invasion with constant pressure drop and favorable viscosity ratio* the value of Ca decreases continually with time and may decrease to a point where displacement takes the form of imbibition, whereas in the case of *dynamic invasion with constant pressure drop and unfavorable viscosity ratio* the Ca number increases with time making fingering more pronounced.

At the end of any of these invasion processes, some of the oleic phase originally in the porous medium remains trapped in the form of ganglia. These ganglia may be as large as the porous medium (quasistatic imbibition, Wilkinson and Willemsen, 1983) or as small as a 1-pore ganglion. Some of these ganglia may become mobilized if a new flood with a much larger capillary number (say $Ca = 10^{-4}$) is performed. It should be noticed that now, contrary to the cases of imbibition and dynamic invasion, the capillary forces resist the displacement of the oil. Depending on the capillary number, the displacement of ganglia can take different characteristics:

- *Quasistatic Displacement of Ganglia* is observed if the value of Ca is just slightly larger than the critical value for mobilization (Payatakes, 1982). It is characterized by the invasion by oil of one (and only one) of the downstream chambers and the invasion by water of one (maybe two) upstream chambers.
- *Dynamic Displacement of Ganglia* occurs when the value of Ca exceeds the critical value by a sizable amount, and it presents characteristics somewhat different than those of quasistatic displacement of ganglia (Payatakes, 1982). The ganglion may now move through different pathways simultaneously as one or more interfaces advance simultaneously in the porous medium.
- *Dynamics of Ganglion Populations* studies the collective behavior of a large population of ganglia, some of which are moving and some of which are stranded (Payatakes, Ng, Flumerfelt , 1980; Payatakes, 1982).

All the displacement processes described above are transient in nature. One particular steady state process, usually performed in the laboratory, deserves attention.

- *State Dynamic Displacement* is established if a mixture of water and oil is

fed continuously through the porous medium. After some time a dynamic equilibrium is established and the flow becomes steady on a macroscopic scale. This type of flow is used in some standard relative permeability measurements methods (Craig, 1971).

2.3 Displacement in Single Capillaries and in Doublets

The analysis of immiscible displacement in porous media and the development of simulation algorithms to be used in conjunction with suitable porous medium models require information on some aspects of the equilibrium and the motion of menisci, the thickness and the stability of the lubrication film, the mechanisms of breakup and stranding, and the motion of ganglia and bubbles in converging-diverging tubes.

Single capillaries of uniform or varying cross section and doublets of capillaries do not adequately represent the complexity of porous media (see Section 2.1.1), but they can be used to obtain some of the required experimental information.

2.3.1 Equilibrium and Motion of Menisci

Haines (1930) observed that, when a water-air interface moves through a porous medium, it does so in an episodic manner. It slowly creeps forward until an instability develops at some throat, "jumps" through the corresponding chamber, and begins another period of creeping motion. As shown by Heller (1968) these *Haines jumps* take place very rapidly and the local displacement process appears to be

controlled by the period of slow advancement between jumps. Since static configurations of the interface are not stable at all positions within converging-diverging pores, the occurrence of jumps is a characteristic of flow through porous media.

Melrose (1965) estimated the minimum pressure drop required for displacement in various pore models, and Melrose and Brandner (1974) developed a criterion for the stability of a single ganglion in a water-wet system. Oh and Slattery (1979) calculated the static positions of a fluid segment in a sinusoidal pore as a function of pressure drop, and Giordano and Slattery (1983) developed an integral inequality for the Helmholtz free energy in a dynamic, open, multiphase system, able to predict the stable, static positions of a fluid-fluid interface in a sinusoidal pore as a function of the pressure drop. A review on meniscus stability was given recently by Michael (1981).

A contact line is formed at the intersection of two immiscible fluids and a solid. The mutual interaction between the three materials in the immediate vicinity of the contact line affects the statics and dynamics of the entire flow field. West (1911) and Washburn (1921) were the first to analyze the displacement of one immiscible fluid by another through a circular capillary. The progress of a liquid flowing under its own capillary pressure in a horizontal cylindrical capillary can be theoretically described by the Washburn equation

$$L^2 = \frac{\sigma r t \cos\theta}{2\mu} , \tag{2.1}$$

where L is the length of the liquid column at time t, μ its viscosity, r is the radius of the capillary, σ is the liquid-vapor interfacial tension and θ is the contact angle. Equation (2.1) was first derived by Lucas (1918). It can be derived from Poiseuille's law (Poiseuille, 1840a, 1840b, 1842) for viscous flow by assuming that the pressure

drop (ΔP) across the liquid-vapor interface is given by the Young-Laplace equation (Young, 1805; Laplace, 1806) for a hemispherical interface

$$\Delta P = \frac{2\sigma \cos\theta}{r} \,. \tag{2.2}$$

The Washburn equation has been verified experimentally for tubes with radius from 400 to 3 μm (see for example, Fisher and Lark, 1971). Fisher and Lark (1971) extended these experiments to tubes with smaller diameters and reported good agreement with Equation (2.1) for liquid-vapor menisci for water (for $r \geq 0.3\ \mu m$) and for cyclohexane (for $r > 0.2\,\mu m$). For water in capillaries with $r < 0.3\,\mu m$ the deviations seemed to arise due to the creation of bubbles.

The Washburn equation provides satisfactory results so long as the interest is in overall effects in tubes with large length-to-diameter ratios. If the length-to-diameter ratio is small (say less than 10), then the details of the flow near the moving meniscus, which are disregarded by the Washburn analysis, become important.

As pointed out by Huh and Scriven (1971), the displacement over a solid surface of the three-phase contact line where the interface between a liquid and a second, immiscible fluid intersects the solid is a *prima facie* violation of the no-slip boundary condition of fluid mechanics. For if one fluid displaces another from the solid surface, both must move relative to the surface sometime during the process, thus resulting in a *moving contact line.* Huh and Scriven (1971) have given a historical review of ideas and observations, commencing with the rolling motion or fountain effect described by West (1911) and later by Rose (1961). Schwartz, Rader and Huey (1964) have shown experimentally this rolling effect by injecting a small amount of dye into a short length of transparent liquid in a capillary tube. It is also apparent

from this work that the no-slip boundary condition is obeyed at the solid-fluid boundary.

A careful study of the kinematics of the flow near the three-phase contact line, formed when the fluid-fluid interface meets the solid boundary at a finite angle, has been done by Dussan and Davis (1974). Their experimental work demonstrates the presence of a rolling motion and shows mathematically that the moving contact line and the no-slip boundary condition are kinematically compatible. Further work on the moving contact angle has been reported by Dussan (1976), Wooding and Morel-Seytoux (1976) and Hocking (1976, 1977).

It is evident that the dynamics of displacement near the contact line although important on a small scale (smaller than pore size), is very difficult to understand. An alternative approach, useful for simple calculations, is to regard the motion of the interface between the two fluids as being controlled by the same condition which governs the equilibrium state of a stationary interface, namely the Young-Laplace equation (Equation 2.2), only now θ is the apparent dynamic contact angle of the moving meniscus.

Dynamic contact angles have been the object of extensive studies. Wenzel (1936), Bartell and Shepperd (1953a, 1953b), Shepperd and Bartell (1953) and Padday (1960) were among the first to relate surface roughness to hysteresis of contact angles. The rate-dependency of the dynamic contact angle was shown experimentally by Rose and Heins (1962) and has been studied by several researchers both experimentally (Elliot and Riddiford, 1967; Blake, Everett and Haynes, 1967; Blake, 1968; Blake and Haynes 1969; Padday, 1969; Hoffman, 1974; Rillaerts and Joos, 1980; Welygan and Burns, 1980; Mason and Yadav, 1983; Kloubek, 1983)

and theoretically (Weiland and Davis, 1981; Kafka and Dussan, 1979). A good review on this subject is given by Dussan (1979). The key observation is that when a meniscus advances (away from the wetting phase), its *advancing contact angle*, θ_a , is larger than the intrinsic or equilibrium value, θ_e , and that when a meniscus recedes (towards the wetting phase), its *receding contact angle*, θ_r , is smaller than θ_e . The extrapolated values of θ_a and θ_r in the limit as the velocity of the contact line goes to zero are referred to as θ_a^o and θ_r^o and are usually different from θ_e (most commonly, $\theta_a^o \geq \theta_e \geq \theta_r^o$). This apparent nonuniqueness in the static contact angle is referred to as *contact angle hysteresis*.

Morrow (1975) found experimentally empirical relations between θ_a^o , θ_r^o and θ_e for several fluid systems and several degrees of surface roughness ranging from smooth to severe roughness. Despite the numerous experimental work done on the calculation of dynamic contact angles a general correlation between the dynamic contact angle and the pertinent dimensionless groups has not yet been obtained.

2.3.2 Thickness of the Lubrication Film

When a non-wetting fluid displaces a wetting fluid in a capillary tube (drainage), the displacement is not complete and a thin film of the fluid initially present is often left behind in the tube walls. This process becomes very important when the conditions of the reservoir are such that the oil is the wetting fluid and it is being displaced by the non-wetting fluid, water. Even in the more usual case where oil is the non-wetting fluid and water the wetting fluid, drainage phenomena may occur locally, especially for large Ca values. Another important case is the displacement of ganglia where the downstream interfaces of the ganglia undergo a drainage-like

process.

Fairbrother and Stubbs (1935) performed experiments by displacing a viscous fluid with air in a straight capillary tube for $Ca \leq 0.014$, and found an empirical relationship between the fraction of viscous fluid that remains in the tube, m, and Ca. Later, Taylor (1961) expanded the range of Ca values and showed experimentally that the Fairbrother and Stubbs correlation is valid for Ca as large as 0.09, but not beyond. This correlation may also be expressed in terms of the film thickness normalized by the tube radius, ξ ($\xi \approx 0.5m$, if $m \ll 1$).

$$m = 1.0\, Ca^{\frac{1}{2}} \qquad Ca < 0.09 \tag{2.3a}$$

$$\xi = 0.5\, Ca^{\frac{1}{2}} \qquad Ca < 0.09\ . \tag{2.3b}$$

When the experiments were extended to values of Ca up to 1.9, Taylor found that m approached an asymptotic value of 0.55. Cox (1963) showed experimentally that when the Ca is increased to values larger than 10, the value of m approaches 0.6 ($\xi \approx 0.368$) . Marchessault and Mason (1960) and Goldsmith and Mason (1963) also verified the correlation given by Equation (2.3a)

Bretherton (1961) has given a theoretical treatment of flowing inviscid bubbles valid for $Ca < 3 \times 10^{-3}$. Assuming a film of constant thickness and that the flow could be described by the lubrication approximation, the following expressions were given for m and ξ

$$m = 1.29(3\, Ca)^{\frac{2}{3}} \tag{2.4a}$$

$$\xi = .643(3\, Ca)^{\frac{2}{3}}\ . \tag{2.4b}$$

The discrepancy between Equations 2.3 and 2.4 is larger for very small Ca values.

Hammond (1983) suggested that this is due to Bretherton's usage of a first-order rather than a second-order lubrication theory analysis.

Although the foregoing results allow good predictions for the thickness of the lubrication film in straight capillaries, they do not address the question of converging-diverging tubes which characterize porous media. At present there are no data on the lubrication film thickness on capillaries of varying cross section. A theoretical analysis by Hammond (1983) suggests that the film thickness in such cases depends not only on the system parameters but also on position and time as well, making it a more difficult subject to treat.

Another important topic is the problem of the lubrication film stability. The collapsing of an unstable film leads to the formation of a contact line and the re-establishment of consecutive flow. Hall, Collins and Melrose (1983) have recently analyzed the conditions for the existence and stability of a wetting film interposed between a solid boundary and stationary non-wetting phase. Chen and Slattery (1982) treated the problem of rupture of the thinning dimpled film formed as a drop or a bubble approaches a solid boundary. In both works the London-van der Waals effect are taken into account. Hammond (1983) solved the problem of the adjustment of a thread of viscous fluid surrounded by a thin lubrication film in a straight capillary, up to the point where London-van der Waals forces become important. A synthesis of these works is still pending.

2.3.3 Pinch-off, Snap-off and Dynamic Breakup

During a waterflood in a porous medium initially saturated with oil, the displacing water often surrounds a region of oil and disconnects it from the body of

continuous oil. Thus, the process by which an initially continuous region of oil becomes disconnected is of great importance in deciding the amount and form of the residual oil. Three major classes of local events leading to the formation of an oil ganglion can be identified: Pinch-off, snap-off and dynamic breakup (Payatakes, 1982; Payatakes and Dias, 1984).

Pinch-off results from the collapse of an unstable thread within a single throat or chamber. The instability of a fluid thread residing in another fluid has been the object of several studies. Plateau (1864) and Rayleigh (1879, 1892) solved the problem of the stability of a long cylindrical thread of a viscous fluid omitting the effect of the surrounding fluid. They found that if the thread is slightly deformed, this deformation is stable or unstable according to whether the wavelength of the varicosity is less than or greater than $2\pi r$, where r is the tube radius. A deformation of any wavelength exceeding $2\pi r$ increases exponentially with time. The value of the wavelength of maximum instability was found to be equal to $9.02r$. The effect of the surrounding fluid was studied experimentally by Taylor (1934) and theoretically by Tomotika (1935, 1936). They found that the value of the wavelength of maximum instability depends not only on r, but also on the viscosity ratio, κ. Taylor observed that, while the surrounding fluid kept drawing on an elongated drop by flowing parallel to its long axis, the drop remained stable for a substantial period of time before rupturing into small droplets. Tomotika (1936) and latter Mikami, Cox and Mason (1975) performed a theoretical analysis of this stabilization effect.

Meseguer (1983) introduced the effect of the presence of a solid boundary by investigating numerically the breakup of axisymmetric inviscid liquid bridges that were supported by two parallel disks. Goldsmith and Mason observed that the

lubrication films formed around the non-wetting fluid during drainage experiments were stable while the flow lasted but became unstable when the flow was stopped. At this point, the film breaks up by developing capillary disturbances which travel inwards from the bubble ends. Bubbles with length smaller than *ca* $8r$ did not rupture. The rupture of very long bubbles created a series of small, nearly uniform bubbles that did not break further. Values of the wavelength of maximum instability determined from the size of the small bubbles seemed to be in good agreement with theoretical predictions by Goren (1962) and with observations made by Blake, Everett and Haynes (1969).

During a displacement process, pinch-off may occur if, during the retraction of an oil microfinger, its velocity becomes small for a sufficient length of time.

Another breakup phenomenon, termed *snap-off*, was pointed out by Pickell, Swanson and Hickerman (1966). In this process, as an oil drop moves through a throat into a chamber filled with the aqueous phase, part of the oil drop snaps off into a smaller droplet and moves ahead of the primary drop. Roof (1970) analyzed this process for the case in which the throat has the shape of a torus. For this geometry Roof found that, before snap-off can occur, the oil drop must advance beyond the throat for a distance of at least seven times the throat radius. Experiments conducted in static systems in which the wetting phase was not flowing seemed to support the model qualitatively. The formation of a "collar" of water around the oil in the throat seemed to be necessary before snap-off could occur. In circular cross section constrictions, the snap-off occurred very slowly because a path for flow of the water into the collar was not readily available. The snap-off rate is enhanced in noncircular cross sections since the water can by-pass the oil drop and

thus forms collar readily. More recently Arriola, Willhite and Green (1983) reported snap-off occurrence in the presence of a flowing wetting phase using capillary and constriction systems with geometry resembling that of pores in reservoir rocks.

Wardlaw (1982) concluded from his experiments and theoretical analysis that snap-off occurs due to the capillary instability in the exit throat caused by the interface moving to maintain equal curvature at all points. From Wardlaw's work it can be concluded that snap-off can be very important in porous media with large chamber-to-throat diameter ratios.

It is clear that both the pinch-off and the snap-off processes result from the collapse of an unstable neck of non-wetting fluid surrounded by the wetting fluid. Using lubrication theory, Hammond (1983, 1984) analyzed the problem of non-linear adjustment of a thread of viscous fluid surrounded by another within a circular cylindrical pipe and within an axisymmetric constricted pipe. He points out that in order for the lubrication film to rupture, it is not only necessary for the film to become unstable but there must also be a sufficient amount of wetting fluid in the film near the throat to form a lenticular bridge across the tube. Hammond estimated that in an axisymmetric tube rupture is impossible if $\xi < \pi/12$, where ξ is the dimensionless film thickness, and that breakup will occur if $\xi > \pi/6$. Hammond also analyzed the time scale of growth of a perturbation large enough to cause rupture of a stationary thread. From this analysis it is possible to conclude that, when Ca is small, moving threads may not spend enough time in a constriction to rupture. This agrees with the observation of Legait (1981b), namely that when droplets are forced to flow through axisymmetric constrictions, there is a critical capillary number below which rupture does not occur. In the same work, Legait observes

that the breaking up of the non-wetting phase passing through a constriction is not dependent on the geometry of the constriction or on viscosity of the wetting fluid as long as $\kappa \gg 1$.

Dynamic breakup is a fundamentally different breakup mechanism that usually occurs at relatively high capillary number values. It was first reported by Payatakes (1982) based on observations of ganglion displacement experiments filmed by Rapin (1980) and Hinkley (1982). It results from the simultaneous advancement of two or more interfaces through different channels of the porous medium. Details of this type of breakup will be discussed in detail in Sections 2.5.2 and 4.2 and 4.4.

2.3.4 Trapping and Mobilization of Oil Droplets and Ganglia

During the displacement of oil in a reservoir rock by advancing water, some of the displaced phase becomes disconnected and trapped. Once entrapment occurs, the removal of this oil is achieved only with great difficulty.

Analysis of trapping and mobilization of oil droplets in single pore-throat pairs was done, among others, by Wardlaw (1982) and Arriola, Willhite and Green (1983).

Pore doublet analysis was developed in order to predict the conditions under which oil droplets are trapped both in large and small pores. Moore and Slobod (1956), Rose and Witherspoon (1956), Slobod (1957) and Rose and Cleary (1958) carried out a theoretical analysis of immiscible displacement in pore doublets and concluded that, if both pores of the pore doublet are nearly of the same size or if they are of considerably different sizes, the residual oil will be nearly zero. They also found that trapping is favored by a high viscosity ratio and that the imposition of a backpressure causes both pores of the doublet to empty simultaneously so that zero

residual oil results. Finally, they observed that, in the absence of a backpressure, maximum recovery in water-wet systems is obtained when capillary forces alone bring in the displacing wetting phase, namely, a low ΔP driving force.

Ehrlich and Crane (1969) treated the case where the two fluids are of different viscosities taking into consideration the role of the inlet and the outlet, but restricted their treatment to balancing the capillary pressures. Chatzis and Dullien (1983) performed a theoretical and experimental analysis of dynamic drainage and imbibition displacement mechanisms in pore doublets considering unequal viscosities. More recently, Laidlaw and Wardlaw (1983) provided a detailed analysis of a pore doublet with a finite source and sink containing two fluids with unequal viscosities and subject to an adjustable external pressure.

As it has been pointed out before (Rose and Witherspoon, 1956; Payatakes and Dias, 1984), the use of doublet models does not give a definitive answer to the trapping problem, since they do not take into account the topology of the pore network or the conditions of the invasion.

The conditions for mobilization of a single ganglion in conduits of varying cross section were studied by Slattery (1974), Stegemeier (1977) and Singhal and Dranchuk (1980). Batycky (1981) and Batycky and Singhal (1978) studied the conditions for ganglion mobilization in a model porous medium consisting of spheres arrayed in a single cubic geometry and aligned parallel to the applied force field. Payatakes, Ng and Flumerfelt (1980) developed a mobilization criterion for a single ganglion in a network of constricted unit cells. A description of this criterion and its major conclusions will be given in Section 2.5.1

2.3.5 Motion of Oil Droplets and Ganglia in Capillary Tubes

Although this topic is of great importance for the analysis of immiscible displacement of two fluids in porous media and particularly for the mathematical modeling of such processes there are very few studies of this type.

Singhal and Dranchuk (1980) performed an analysis of the motion of a single oil-droplet through a periodically constricted tube filled with water. This study was restricted by the assumptions that the two fluids had vanishingly small viscosity.

Legait (1981a) performed an experimental and theoretical study of the motion of a non-wetting droplet through a single constriction in a glass tube filled by a wetting fluid, taking into account inertial, viscous and capillary forces. Based on this analysis, he calculated the pressure drop required in order to force the droplet through the constriction as a function of the droplet velocity before it reaches the constriction and reported good agreement with his experiments. Legait and Jacquin (1982) studied the conditions under which a non-wetting droplet can pass through a constriction of square cross section in an otherwise straight capillary tube filled with wetting fluid. They concluded that the critical capillary number depends on the tube shape and the viscosity ratio. In two recent works Legait, Sourieau and Combarnous (1983) and Legait (1983) concluded that the pressure drop necessary to force a dynamic droplet through the throat of a constricted capillary depends on the ratio of the Reynolds number to the capillary number. This dependence was such that the pressure drop becomes independent of the wettability, of the droplet size, and of the inertia forces if the Reynolds number is small compared with the capillary number. If on the other hand, the Reynolds number is large compared to the capillary number, the pressure drop necessary to force a dynamic

droplet through the throat of a constricted capillary decreases as the Reynolds number increases, and theoretically may reach zero. Furthermore, a non-wetting droplet trapped in a capillary tube of nonuniform square cross-section can be forced through the tube if the ratio of the viscosity forces to the interfacial forces is greater than a critical value. This critical value depends on the viscosity ratio and on the contact angle.

Olbritch and Leal (1982) examined the creeping motion of liquid drops through a circular tube of comparable diameter. One of their main conclusions was that even small density differences between the two fluids can produce eccentricity of the drops and affect their velocity substantially. In a follow-up study Olbritch and Leal (1983) studied experimentally the shapes of non-wetting lubricated drops passing through sinusoidal tubes and measured the associated pressure differences and velocities. Their experiments were performed with Ca values of the order of 10^{-2} and higher. The data provide valuable information on the phenomenon but need to be extended to smaller Ca values so as to apply to immiscible displacement in porous media.

2.3.6 Coalescence of Oil Droplets and Ganglia

Recent studies reveal that the reconnection of oil ganglia plays an important role in the formation of an oil bank once the immiscible mode of displacement during chemical flooding is established (Wasan *et al* 1978a, 1978b, 1979; Ng and Payatakes, 1980; Payatakes, 1982).

Reconnection of oil ganglia occurs through collision followed by coalescence. When two droplets of oil collide with each other, a thin film of continuous water phase is trapped between the two drops. If this film is drained to such an extent

that hydrodynamic disturbances and interfacial attractive forces eventually cause the film to collapse, coalescence occurs (McKay and Mason, 1963; Hartland, 1967).

Jeffreys and Davis (1971) identified five stages for a typical coalescence process between two droplets. First the drops approach one another under the influence of some external force. Then, a lendular film of the continuous phase is formed between the two drops. As time passes the film drains slowly until it ruptures. The process ends with the rapid combination of the contents of the two drops. The film drainage step tends to be rate limiting.

Among the numerous models presented for the film drainage, the one developed by Barber and Hartland (1976) is of great importance since it includes dynamic interfacial effects such as interfacial tension gradients and interface viscosities, and analytical solutions are obtainable. Flumerfelt, Catalano and Tong (1981) used the Barber and Hartland model to analyze the results of coalescence experiments done with a spinning drop interfacial tensiometer. Flumerfelt, Oppenheim and Son (1982) incorporated London Van der Waal's forces in the Barber and Hartland model. Oppenheim (1983) developed a number of mathematical models to address the effects of interfacial tension, interfacial viscosity and short-range dispersion and electrical double layer forces on the coalescence process.

Coalescence of oil-in-water suspensions by flow through porous media has been studied by Spielman and Goren (1970, 1972a, 1972b) and Spielman and Su (1977).

2.4 Immiscible Displacement. Formation of Ganglia

The mechanism of displacement of one fluid by another fluid, immiscible with

the first, in porous media is the object of study of the microscopic modelling approach. This approach consists in associating a description of the fluid behavior at the pore scale with the representation of the structure of the porous medium using an interconnected pore network.

The fluid behavior at the pore scale has been described both theoretically and experimentally by the use of single capillaries and pore-doublets (see Section 2.3). As was pointed out, neither single capillaries nor pore-doublets describe the complexity of porous media adequately. Lack of interconnectivity is often the major flaw of such descriptions. Imbibition and drainage experiments have been carried out in artificial model porous media in order to study the effect of interconnectivity (see for example, Lenormand and Bories, 1980; Wardlaw and McKellar, 1981; Lenormand, Zarcone and Sarr, 1983; Chatzis, Morrow and Lim, 1983).

The complexity of most porous media makes it impossible to formulate an exact description of their geometrical structure. In order to obviate this problem, idealizations of the porous space, called *porous media models* are often adopted. Any such model should incorporate the most relevant characteristics of the prototype porous medium, taking into account the nature of the particular process under study.

Interconnectivity has long been identified as one of the most important characteristics of porous media. The idea of using networks of uniform capillary tubes to analyze flow in porous media was first introduced by Fatt (1956a, 1956b, 1956c) and Josselin de Jong (1958). This class of models fails to provide a satisfactory treatment of immiscible displacement, mainly because the converging-diverging character of the porous structure is not taken into account. A good review of such models was

given by van Brakel (1975).

Two types of modeling methods have been introduced recently: percolation models and networks of converging-diverging tubes. Because of their importance in the study of immiscible displacement in porous media, a brief description of these two methods and the relevant works is given below.

2.4.1 Percolation Models

Percolation models make use of *percolation theory* in conjunction with lattices consisting of sites (i.e. chambers) and bonds (i.e. throats). The theory of percolation was first stated by Broadbent and Hammersley (1957) as the theory of the properties of particles interacting with a random network. Good reviews of percolation theory are provided by Frisch and Hammersley (1963), Shante and Kirkpatrick (1971) and Essam (1980). Extensions of percolation theory to treat transport were described by Kirkpatrick (1973). More recent studies of Monte Carlo tests of percolation methods include the ones by Sur *et al* (1976) and Blumberg, Shlifer and Stanley (1980).

The applicability of percolation theory to the study of disconnection and entrapment in porous media was suggested independently by several research groups (Melrose and Brandner, 1974; Larson, Scriven and Davis, 1977; de Gennes and Guyon, 1978). Following de Gennes and Guyon, Lenormand and Bories (1980) used percolation theory to model the percolation threshold (i.e. breakthrough) for drainage in porous media.

Larson, Scriven and Davis (1981) and Larson, Davis and Scriven (1981) proposed a percolation model to study drainage in porous media and to calculate the

dependence of the residual non-wetting saturation on the capillary number. A critical review of these two works can be found in Payatakes and Dias (1984). Other percolation models have been proposed that, not only take into account the compressibility of the non-wetting phase, but also account for a certain sequence of events.

Chandler *et al* (1982) proposed a different method to simulate the displacement of an incompressible fluid (oil) from a network of bonds and sites by a second immiscible and incompressible fluid (water). This method can be used in both water-wet and oil-wet conditions. In the first case, water will spontaneously be imbibed, while in the second case, an external pressure head across the lattice is applied, and then the capillary pressure will provide a variable resisting force. The lattice is initially filled with oil, and water is allowed to enter along one edge in the presence of the capillary pressure differences across the interface. Each interface throat is assigned a random ranking in the interval $[0,1]$. The simulation is done in a discrete, stepwise process where, at each step, the oil-water interface moves through exactly one element of the lattice. The chosen element has the lowest ranking along the interface, i.e., it corresponds to the interface throat of smallest size. The newly created interfaces are assigned random sizes and the simulation proceeds until all throats that can be invaded for a given pressure difference are invaded, provided that their turn comes up. It is possible that throats with the proper size are not invaded because the interface never reached them. Ganglia formed during the invasion are stranded as soon as they are formed and invasion of pores corresponding to these ganglia is not allowed in view of the incompressibility of the oil. As pointed out by the authors, this simulation method differs from the

classical percolation problem. The simulation consists of a sequence of motions in which each step is determined by the results of the previous one, while classic percolation provides a static configuration. Nevertheless, the final state of the oil seemed to be qualitatively similar to a percolation cluster which can be treated with classic percolation analysis.

Wilkinson and Willemsen (1983) proposed a simulation method that applies to quasistatic imbibition and which they termed *invasion percolation.* A lattice composed of chambers and throats is initially filled with oil. Each chamber is assigned a random size ranking in the interval [0.1]. Water is brought into contact with the oil forming a set of menisci occupying throats near the entrance to the lattice. Each of the menisci is assumed to be near the entrance into the next chamber. A backpressure P_b is applied in order to attain quasistatic imbibition (see Section 2.2). The smallest interface chamber is selected and is flooded by water, provided that the equivalent diameter of the chamber is smaller than D_b, the chamber diameter (for a given contact angle) corresponding to P_b. All the throats connected to this newly invaded chamber get invaded at this point, and the chambers into which these throats lead are now included among the interface chambers. The process is repeated until no more interface chambers with diameter less than D_b are found. For relatively small values of D_b, the invasion stops before the water reaches the other end of the lattice. As D_b increases the amount of displaced oil increases. For a critical value of D_{bc}, the water just reaches the other end of the lattice. The corresponding pressure, P_{bc}, is called the *percolation threshold.* It is often observed that, when this method is applied to non-planar networks show that at the percolation threshold, the oil is still mostly connected. The same effect is

not observed in planar media, because of the difference in topology. In non-planar lattices breakthrough can take place while both fluids are still connected. As the value of D_b increases beyond D_{bc} more oil is displaced, and the residual oil becomes progressively more disconnected. Once a ganglion is formed, it is assumed to be stranded immediately and the simulation is modified by specifying that any chamber that is occupied by a part of a ganglion cannot be invaded. This modification takes into account the incompressibility of the oleic phase . The simulation continues until all the residual oil is disconnected.

Based on percolation theory analysis, Wilkinson and Willemsen (1983) proposed that the ganglia size distribution of the ganglia is given by

$$f(s) = f_o s^{-\gamma} , \tag{2.5}$$

where s is the number of chambers (i.e. sites) occupied by the ganlion, $f(s)$ is the frequency distribution of s, f_o is the extrapolated value of $f(s)$ at $s = 1$ and γ is an exponent, the value of which was found to be $\gamma \approx 2.07$. Equation 2.5 is a theoretical result that can be expected to apply to relatively large values of s. It means that, although small ganglia are more numerous than larger ones, some large ganglia are also formed, and even very large ganglia (with size comparable to that of the network) have finite probability of being formed. There exist no experimental data that have been obtained under strictly quasistatic imbibition conditions with which to compare Equation 2.5. It is accepted, however, that ganglia generated during waterflooding of oil reservoirs ($Ca \approx 10^{-8}$ to 10^{-6}) range in size from 1 to 15 chambers, and that the smaller ones predominate.

This work models a clearly defined flow regime of immiscible displacement, taking into account most of the relevant physical aspects of the process. It gen-

erates a unique (for given conditions) sequence of invasion steps that is in accord with quasistatic imbibition. Since it does not consider the rates of advancement of the menisci, it is not expected to apply for Ca values large enough to give significant viscous effects. On the other hand, it produces results with much smaller computational effort than converging-diverging tubes network simulations.

Wilkinson (1984) generalized the invasion percolation model to include buoyancy forces. This model assumes that at any given instant the system is in mechanical equilibrium in the vertical sense, so that the capillary pressure depends linearly on height, and a jump potential for each pore is defined as the threshold pressure minus the capillary pressure. The pore which fills is now the one with the largest jump potential rather than simply that with the largest threshold pressure. In the presence of this vertical bias the system shows now a well developed transition zone, below which the oil is completely disconnected. Wilkinson also suggests that this analysis can be extended to the case of pressure fields created by viscous forces rather than buoyancy effects.

2.4.2 Networks of Converging-Diverging Tubes

Simulators of this nature are more powerful than percolation models. They apply to every situation in which percolation models can be used, whereas the reverse is not true. They take into account the rates with which interfaces advance and the effect of the viscosity ratio, which may become important for moderate and high Ca values (percolation models are restricted to very low Ca values displacements). Their main disadvantage is that they require substantially more extensive computations than percolation models.

This class of models represents the porous medium as either *sphere-and-capillary networks* or *constricted unit cells networks*, and, together with a detailed analysis of the motion of both fluids, they model a wide variety of flow phenomena.

Sphere-and-capillary networks have been proposed by Singhal and Somerton (1977), Mohanty and Salter (1982), Koplik and Lasseter (1982) and Koplik (1982). Koplik and Lasseter considered a 2-D non-planar network consisting of randomly sized spherical chambers connected to neighbors through throats that are straight capillaries of random length and diameter. The coordination number is also random. The two fluids are assumed to be Newtonian and incompressible. The viscosity ratio value is assumed to be $\kappa = 1$ in order to simplify the calculation. This is a key feature of the model, since for $\kappa = 1$ the hydraulic conductance of any network element is independent of which fluid is present there. The flow is solved with standard electrical network analysis, recognizing the analogy between pressure difference and potential difference, hydraulic conductance and electrical conductance, flow rate and current, and capillary pressure and electromotive force. At each step the system of linear equations is solved for the pressure field. The pressure field values are, in turn, used to calculate the instantaneous flow rates in the pores and the corresponding velocities of the menisci. Assuming these velocities to be constant over a small time interval Δt, new positions for the menisci at the end of the time step Δt can be calculated. Not all menisci are allowed to move during a time increment Δt. Due to the existence of wall discontinuities at the cross sections where the cylindrical throats are connected to the spherical chambers, many menisci are "constrained" (i.e. stuck at such cross sections while the corresponding pressure differences are within certain limits). Others that are free to move, may

become constrained when they reach cross sections with wall discontinuity. Thus, the computational algorithm has to keep track of which menisci are constrained, which ones become constrained, which ones get free, and how these events affect each other. This simulator can be used to study microdisplacement in a variety of consolidated porous media. One serious short-coming is the assumption that the viscosities of the two fluids are equal, a situation that is rarely encountered outside of the laboratory. The authors also report computational difficulties that stem from the fact that many menisci in the network are, or may become, constrained. This complication worsens rapidly as the lattice size increases, since the number of possibilities for constraints is at least of order $O(2^N)$, where N is the number of chambers. The computational effort becomes prohibitive very rapidly, as N increases. The method was used to calculate the distribution of the water saturation S_w as a function of time for several Ca values. It was also used to obtain ganglion size distributions for various Ca values and average coordination numbers.

In the present work, a simulation method based on the *constricted unit cell network* proposed by Payatakes, Ng and Flumerfelt (1980) is developed. This type of simulation has the advantage of not producing the constraint problem encountered by Koplik and Lasseter (1983). It can be used with any value of the viscosity ratio, and it can be applied to unconsolidated sands ad consolidated rocks, with relatively simple changes in the formulation of the unit cell shape.

2.5 Ganglion Dynamics

2.5.1 Mobilization and Quasistatic Displacement of a Solitary Ganglion

Consider an oil ganglion stranded in a porous medium. If the macroscopic pressure gradient is nil, $-\nabla P = 0$, both the aqueous phase and the ganglion are immobile, and both P_o and P_w, the pressure values in the oil and the aqueous phases, respectively, are constant.

The condition for quasistatic equilibrium at each point of an oil-water interface is given by

$$P_o - P_w = \sigma_{ow} J \ . \tag{2.6}$$

and for the solid-oil-water contact line the equilibrium is given by Young's equation (Young, 1805),

$$\sigma_{ow} \cos\theta_e = \sigma_{os} - \sigma_{ws} \ . \tag{2.7}$$

Here, J is the Gaussian curvature of the interface, θ_e is the equilibrium contact angle, σ_{ow} is the interfacial tension between the oil and the water, σ_{os} is the interfacial tension between the oil and the solid and σ_{ws} is the interfacial tension between the water and the solid.

From equations (2.6) and (2.7), neglecting gravitational effects, it follows that the curvature, J, of each interface of the ganglion is the same, irrespective of the sizes and the shapes of the pores in which they reside (Figure 2.1a).

If the macroscopic pressure gradient is increased to a non-zero ($-\nabla P > 0$) but small value (below the value required to induce mobilization), the pressure in the

water decreases along the ganglion, while the pressure P_o in the oil phase remains virtually uniform. The pressure drop $(P_o - P_w)$ across each downstream interface is now larger than the pressure drop across each upstream interface. In order to retain an equilibrium position, the ganglion responds as follows. The downstream interfaces advance in their respective throats, increasing their curvatures, and the upstream interfaces recede in the corresponding throats, so that their curvatures decrease (Figure 2.1b). Due to the roughness of most prototype porous media, the contact angle may present hysteresis effects, as was discussed in Section 2.3.1. This being the case, at the same time as the downstream interfaces advance, the contact angle decreases tending to the limiting value of θ_r at zero velocity θ_r^o, and, similarly, the contact angle for the upstream interfaces tends to θ_a^o. Equation (2.7) becomes

$$\sigma_{ow} \cos \theta_r^o = \sigma_{os} - \sigma_{ws} \ , \tag{2.8a}$$

$$\sigma_{ow} \cos \theta_a^o = \sigma_{os} - \sigma_{ws} \ , \tag{2.8b}$$

for the downstream and upstream interfaces respectively.

At this new position, Equations (2.8a) and (2.8b), together with Equation (2.6), are satisfied. This position can be considered as an equilibrium position between viscous and capillary forces, since the resulting capillary pressure imbalance tends to move the ganglion backwards, whereas the external pressure difference caused by viscous dissipation in the aqueous phase tends to move it forward.

The macroscopic pressure gradient may be increased even further and the ganglion rearranges and remains in an equilibrium position as long as all interfaces of the ganglion are stable. Melrose (1970) and Melrose and Brandner (1974) developed a criterion for the stability of a single interface in a water-wet system. In essence

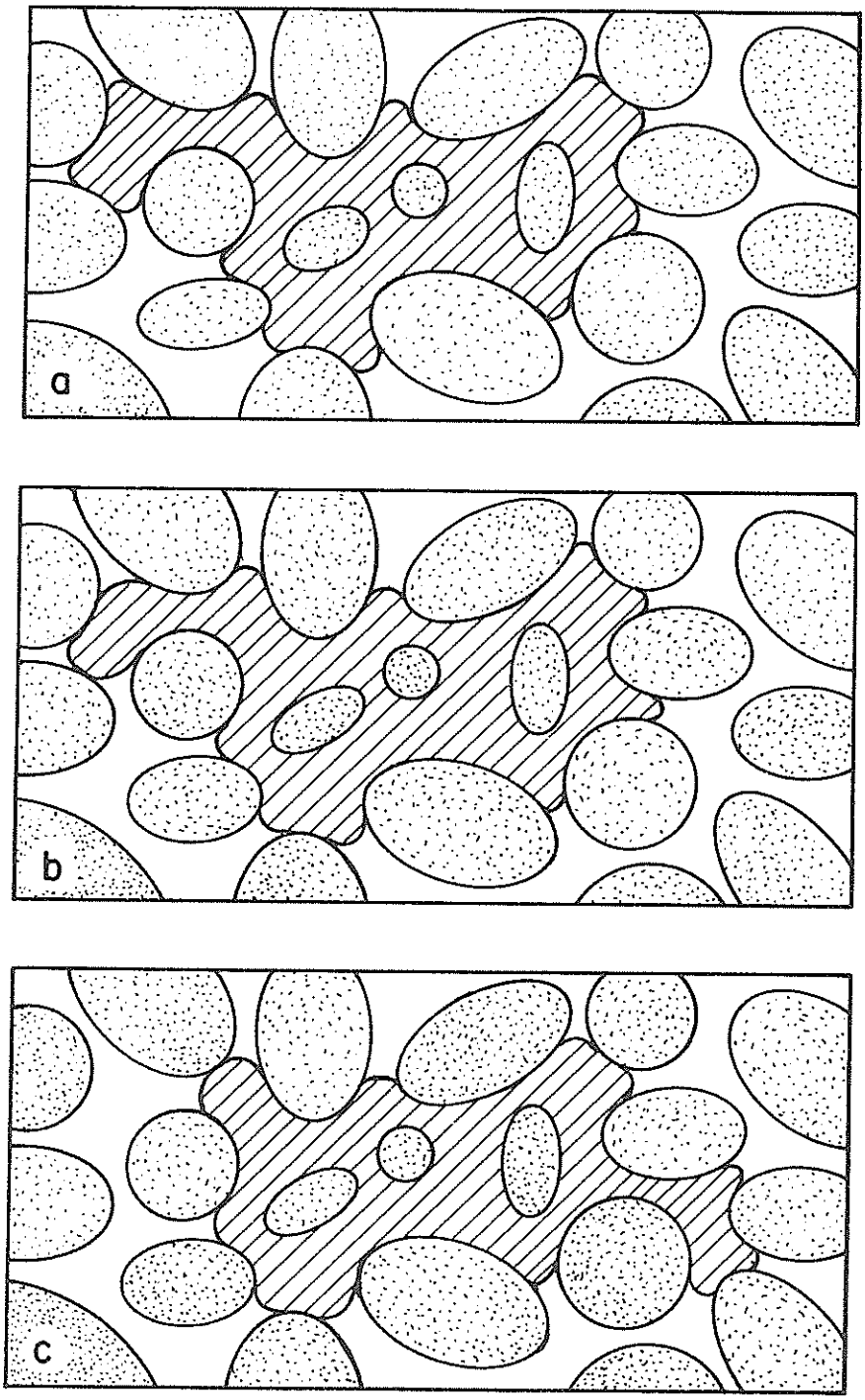


Figure 2.1

Mobilization of a ganglion. a) No Flow; ganglion at equilibrium. b) The non-wetting phase flows from left to right with pressure gradient less than the critical value required for mobilization. c) If the pressure gradient exceeds the critical value for mobilization, a rheon takes place. From Payatakes, 1982.

this criterion says that an interface is stable as long as its curvature is within the range $J_{imb} \leq J \leq J_{dr}$, where J_{imb} is the minimum stable curvature (imbibition curvature) and J_{dr} is the maximum stable curvature (drainage curvature). Both J_{imb} and J_{dr} are functions of the contact angle, of the local geometry and of the volume of oil. A generalized version of the Melrose and Brandner criterion that determines not only whether, but also how a ganglion becomes mobilized was developed by Payatakes, Ng and Flumerfelt (1980) and Ng and Payatakes (1980).

Assume now that the macroscopic pressure gradient is increased to exceed a critical value ($|\nabla P| \geq |\nabla P_{cr}|$ or $Ca \geq Ca_{cr}$) at which the curvature of one of the downstream interfaces exceeds its critical drainage curvature J_{dr} . The ganglion becomes unstable and it moves. The oil invades one of the downstream chambers (this event is called a *xeron*) and the aqueous phase invades one (maybe two or more if the xeron occurs in an unusually large chamber) of the upstream chambers that used to be occupied by the oil (a *hygron*). This motion is a relatively fast one and was first called a *rheon* by Heller (1968) and Melrose and Brandner (1974) (Figure 2.1c).

If the macroscopic pressure gradient is kept constant, the ganglion may continue to move through a series of rheons and hygrons until it breaks in two daughter ganglia or it finds a new equilibrium position and gets stranded again.

This type of displacement where only one of the downstream interfaces of the ganglion advances while one or maybe two upstream interfaces retract is called *quasistatic displacement of ganglia* (Payatakes, 1982; Payatakes and Dias, 1984). It occurs when the applied macroscopic pressure gradient $|\nabla P|$ is slightly larger than the value required to cause mobilization.

Ng and Payatakes (1980) developed a criterion for the quasistatic mobilization of ganglia. This criterion is based on the one developed by Melrose and Brandner (1974), but it is capable of determining not only whether mobilization occurs, but also through which pair of throats (one for the xeron and one for the hygron) the rheon is going to occur. This is an important question affecting the fate of a mobilized ganglion, and the validity of the aforementioned criterion will be checked against results given by the model developed in the present work. Also, in Chapter 5, this criterion will be used to determine the fate of ganglia formed under imbibition and dynamic invasion of oil by water. A short description of this criterion is given below.

Consider the ganglion in a square network represented in Figure 2.2 (for details on the porous medium model and network formulation see Chapter 3). Assign indices to all unit cells containing interfaces (gate unit cells). For each pair of gate unit cells, one downstream with index i and one upstream with index k , there is a critical pressure gradient for which mobilization will occur. Repeating the calculation of this critical pressure gradient for all possible pairs of gate unit cells, it is possible to identify the particular pair ($i \quad I$, $k = K$) for which the required pressure gradient is minimum. Mobilization (if it occurs at all) will proceed through the I^{th} and K^{th} gate unit cells. Ng and Payatakes (1980) determined that this analysis is equivalent to identifying the indices I and K for which the *appendix mobility factor* becomes a maximum, namely

$$\beta_{KI} = \frac{\Delta L_{KI} \cos\theta_{KI}}{J_{dr,I}(\theta_r^o) - J_{lb,K}(\theta_a^o)} \ . \tag{2.9}$$

Here, ΔL_{KI} is the distance between throats with indices K and I, θ_{KI} is the angle between the line connecting the throats K and I and the macroscopic flow direction,

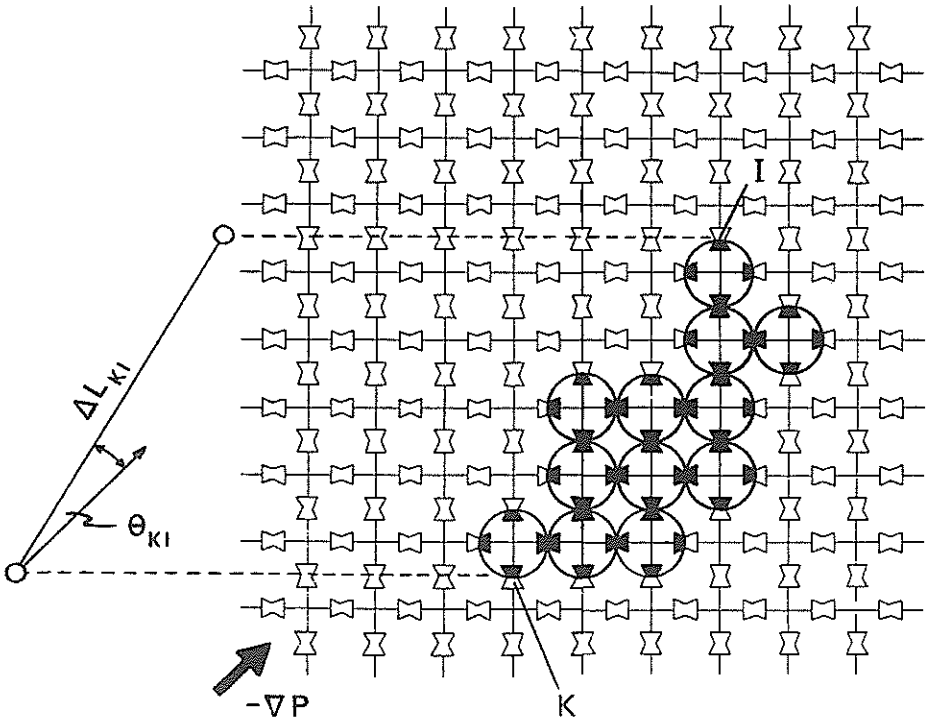


Figure 2.2

Concepts involved in the quasistatic criterion for mobilization.

$J_{dr,I}$ is the drainage curvature of the gate unit cell with index I, and $J_{lb,K}$ is the lower bound of the imbibition curvature. The values of $J_{dr,I}$ and $J_{lb,K}$ depend on the geometry of the corresponding unit cells. For the unit cells used by Ng and Payatakes (1980) and in the present work (see Section 3.2), $J_{dr,I} \approx 4\cos\theta_r^o/d_I$ and $J_{lb,K} \approx 4\cos\theta_a^o/a_k$, where d_I is the throat diameter of the unit cell with index I and a_K is the maximum diameter of the unit cell with index K.

This criterion may be expressed in terms of the *ganglion mobilization number*, Gm (Payatakes and Dias, 1983),

$$\begin{cases} Gm = \dfrac{|\nabla P|\beta_{KI}}{\sigma_{ow}} \geq 1 & \text{the ganglion gets mobilized} \\ Gm = \dfrac{|\nabla P|\beta_{KI}}{\sigma_{ow}} < 1 & \text{the ganglion remains stranded ,} \end{cases} \tag{2.10}$$

or expressed in terms of the capillary number as follows.

$$\begin{cases} Ca = \dfrac{\mu_w v_f}{\sigma_{ow}} \geq \dfrac{k_{rw}k}{\beta_{KI}} & \text{the ganglion gets mobilized} \\ Ca = \dfrac{\mu_w v_f}{\sigma_{ow}} < \dfrac{k_{rw}k}{\beta_{KI}} & \text{the ganglion remains stranded ,} \end{cases} \tag{2.11}$$

where μ_w is the viscosity of the aqueous phase, v_f its superficial velocity, k_{rw} the relative permeability to water and k the absolute permeability.

Ng and Payatakes (1980) and Payatakes, Ng and Flumerfelt (1980) developed a stochastic simulation model of the fate of a solitary oil ganglion undergoing quasistatic displacement. This stochastic simulation is based on a porous medium model formulation (see Section 3.2) and on the above criterion. Typical simulations of the fate of a solitary ganglion are given in these two publications as well as in Ng (1980). Their main conclusions were the following:

- As it moves, a ganglion tends to become elongated and to be aligned with the macroscopic pressure gradient direction.

- After undergoing a few rheons the ganglion breaks into smaller ganglia - *quasistatic breakup of ganglia.*
- The breakup of a ganglion undergoing quasistatic displacement usually produces two daughter ganglia of unequal size.
- The smaller daughter ganglion usually gets stranded, unless the capillary number exceeds its critical value for mobilization, Ca_{cr}.
- The larger daughter ganglion may in turn get stranded, or if it continues to move, it eventually breaks into smaller ganglia that become stranded.

The quantification of these observations was done by calculating the probabilities of stranding S, of mobilization M, and of breakup B per-rheon for a given ganglion size and for various capillary numbers. The effects of stranding and fissioning on oil ganglion dynamics were conveniently expressed in terms of the *stranding coefficient* λ and of the *breakup coefficient* ϕ, which are expressed by

$$\left.\frac{\partial n}{\partial z}\right|_{\text{due to stranding}} = -\lambda n \ , \tag{2.12}$$

$$\left.\frac{\partial n}{\partial z}\right|_{\text{due to breakup}} = -\varphi n \ , \tag{2.13}$$

where $n(z,t;v)\Delta v$ is the number of moving v-ganglia (ganglia with volume in the range v to $v+\Delta v$) per unit porous medium volume, at position z.

Systematic calculations of $\lambda\ell$ and of $\phi\ell$, where ℓ is the length of periodicity of the porous medium (see Chapter 3), were performed by Ng and Payatakes (1980) using the stochastic simulation referred above. Experimentally, Payatakes, Woodham and Ng (1981) examined the effects of ganglion elongation on $\lambda\ell$ and on $\phi\ell$, and Rapin (1980) made systematic calculations of random-shape and cruising values of

$\lambda\ell$. These observations will be compared in Chapter 4 with the results obtained by the present model.

An interesting, if somewhat extreme, example of quasistatic displacement of oil ganglia is seen in Figure 2.3, which shows a sequence of photographs taken from Hinkley's (1982) movie films. The model porous medium consisted of a monolayer of uniformly sized glass spheres (diameter equal to 3 mm), organized in a square configuration and held between two glass plates. The 8-pore ganglion is subjected to a flood with a capillary number just above its critical value for mobilization. The direction of the flow is from left to right. The mobilized ganglion takes a series of steps that leads to a zig-zag configuration with its long dimension parallel to the macroscopic flow direction. From this point on, the ganglion retains its configuration by taking one step to the front and left, then one step to the front and right, and so on, being able to travel indefinitely without breaking away. It should be noted that this is only possible in a regular porous medium. In a random porous medium, the ganglion would eventually get stranded by encountering a stable position or break into smaller daughter ganglia.

2.5.2 Dynamic Displacement of Ganglia. Experimental Observations

Experimental observations by Rapin (1980) and Hinkley (1982) show that, when the flood driving the ganglion has a capillary number that substantially exceeds the critical value for mobilization Ca_{cr}, the ganglion behaves somewhat differently from the way predicted by quasistatic displacement. The most important observation is that the ganglion can and does advance at more than one interface at the time. This type of displacement has been called (Payatakes, 1982; Payatakes

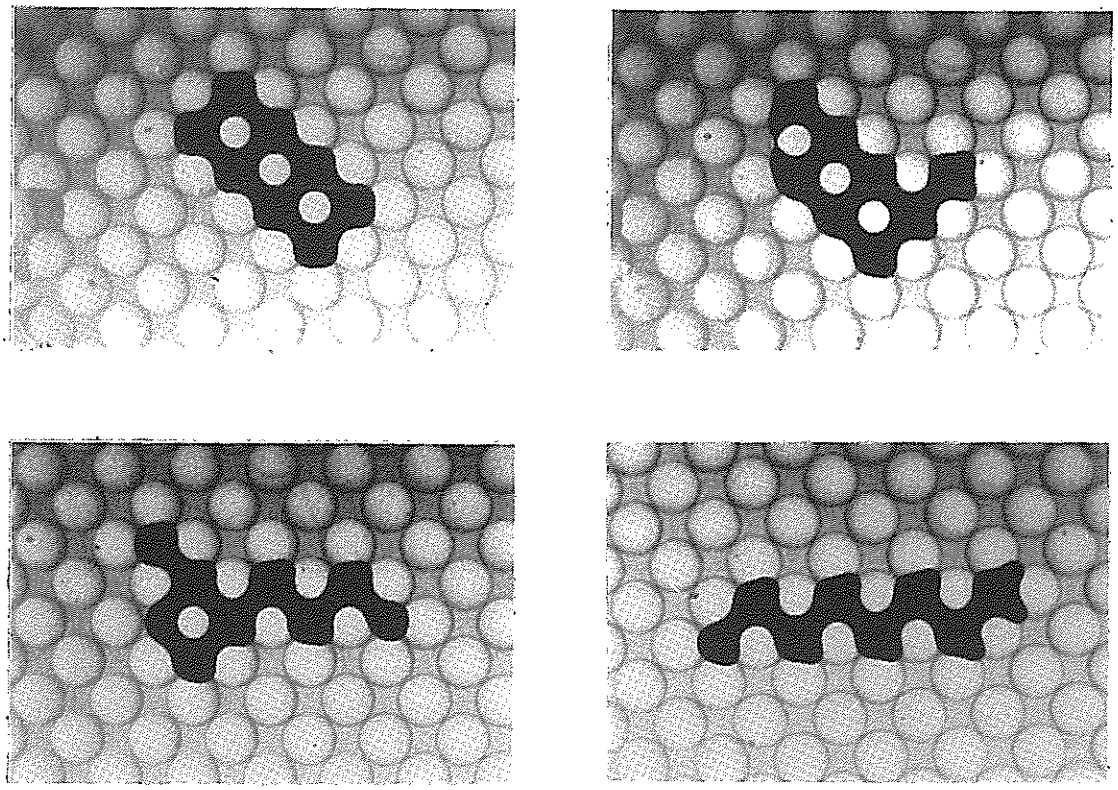


Figure 2.3

Evolution of an 8-pore ganglion undergoing quasistatic displacement for $Ca = 4.8 \times 10^{-4}$ and $\kappa = 7.0$. From Hinkley, 1983.

and Dias, 1984) *dynamic displacement of ganglia*. The consequences of dynamic displacement are significant and play an important role on the fate of moving ganglia.

As Figure 2.3 shows, when the capillary number is close to Ca_{cr}, the ganglion is capable of retaining its integrity by adopting a zig-zag shape along the macroscopic flow direction. Figure 2.4 shows the effect of an increase of the capillary number well above Ca_{cr}. The ganglion moves simultaneously at several interfaces, and, doing so, it soon disintegrates into many small daughter ganglia. This type of breakup, resulting directly from the advancement of the ganglion through more than one interface, is called *dynamic breakup*.

Figure 2.5 shows another example of this type of event. The experimental apparatus consists of a monolayer of randomly arrayed glass beads, with diameters in the range 1.0 ± 0.2 mm, held between two glass plates (Rapin, 1980). The downstream end of the ganglion has encountered a set of narrow throats and slows down at the same time as it grows another branch (Figure 2.5a). The ganglion takes a U shape (Figure 2.5b), which in turn leads to breakup at the base of the U (Figures 2.5c and 2.5d). The two daughter ganglia created have comparable sizes contrary to what usually occurs upon quasistatic breakup. Yet another example of dynamic breakup is given in Figure 2.6, taken from one of Hinkley's (1982) movies. Initially the ganglion occupies two adjacent tracks. Simultaneous advancement of both frontal interfaces leads to the formation of two prongs that, although in some points nearly touch, they fail to coalesce and the ganglion eventually breaks into similar daughter ganglia.

Since a ganglion undergoing dynamic displacement is also subject to quasistatic

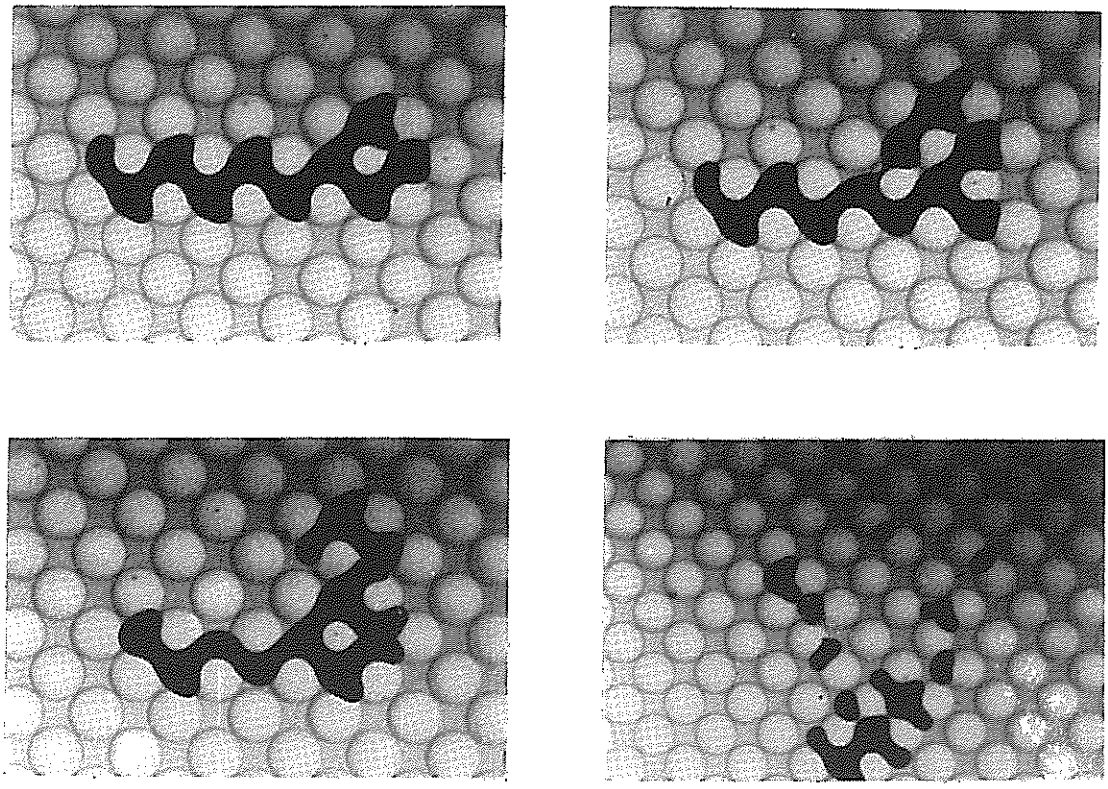


Figure 2.4

Evolution and breakup of the 8-pore ganglion of Figure 2.3 when subject to dynamic displacement for $Ca = 1.5 \times 10^{-3}$ and $\kappa = 7.0$. From Hinkley, 1983.

breakup (pinch-off), it can be said, in general, that the rate of breakup under dynamic displacement conditions is higher due to the added mechanism of dynamic breakup.

2.5.3 Dynamics of Ganglion Populations

The success or failure of a chemical flood depends, in part, on the formation and maintenance of an oil-bank. It is commonly assumed that an oil-bank is composed of blobs large enough to be immune to stranding. These superganglia are formed through collision-coalescence of residual ganglia during immiscible displacement (Payatakes, Ng and Flumerfelt, 1980; Payatakes, 1982).

Consider an immiscible flood of a given capillary number large enough so that at least a subpopulation of ganglia becomes mobilized. In principle it would be possible to follow the fate of mobilized and stranded ganglia with the simulation method described in the present work, together with a good coalescence criterion. However, considering the very large populations required for a meaningful study, the computational effort involved would be very high.

Payatakes *et al* (1980) developed a method, analytical in nature, that considers ganglia as a large interacting population, for which balance equations of the birth-death type apply. Let $n(z,t;v)$ be the number concentration of moving v-ganglia and $\sigma(z,t;v)$ the number concentration of stranded v-ganglia (a v-ganglion has volume in the range v to $v + \Delta v$). The interactions between ganglia belonging to each one of the two populations and between different moving ganglia may be

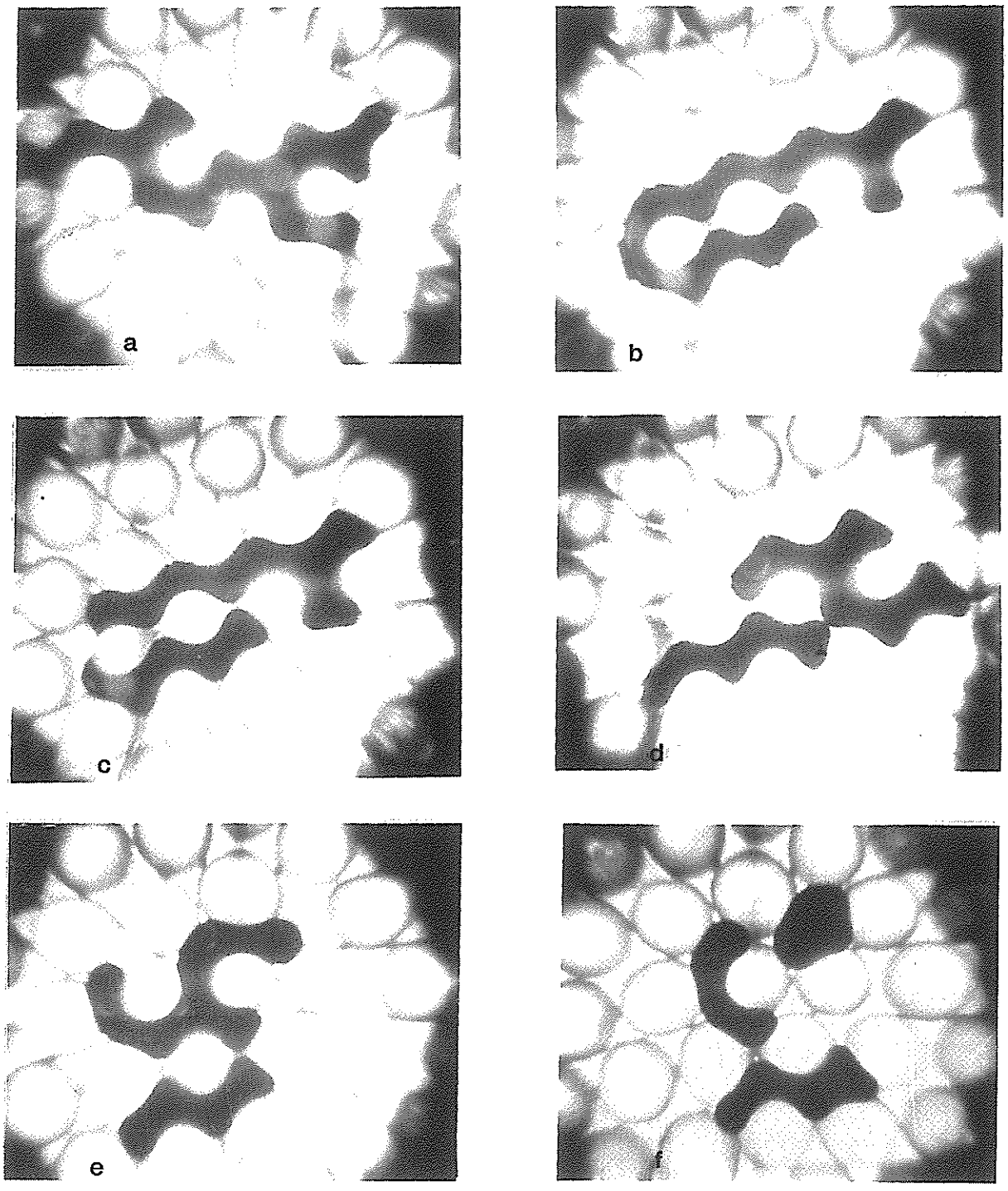


Figure 2.5

Evolution and breakup of an oil ganglion undergoing dynamic displacement. From Rapin, 1980.

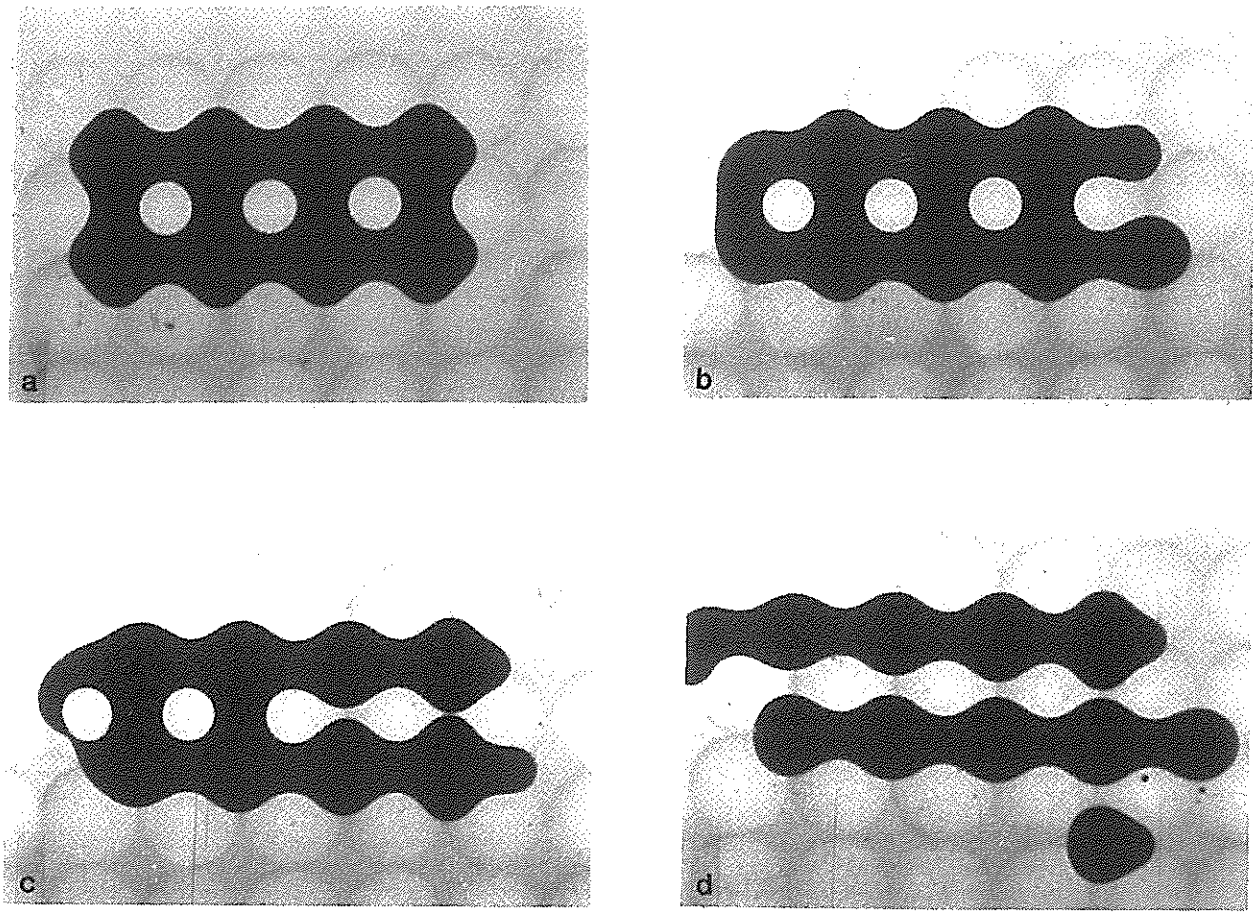


Figure 2.6

Evolution and breakup of an 8-pore oil ganglion undergoing dynamic displacement. From Hinkley, 1983.

described by two integro-differential equations.

$$\begin{aligned}
\frac{\partial n(z,t;v)}{\partial t} + \bar{u}_z(v;\underline{a}_1)\frac{\partial n(z,t;v)}{\partial z} = \\
- n(z,t;v)\left\{\bar{u}_z(v;\underline{a}_1)\,[\lambda(v;\underline{a}_2)+\phi(v;\underline{a}_2)]\right. \\
+ \int_0^\infty K_{11}(w,v;\underline{a}_4)\,n(z,t;w)\,dw \\
\left. + \int_0^\infty K_{01}(w,v;\underline{a}_4)\,\sigma(z,t;w)\,dw\right\} \\
+ \frac{1}{2}\int_0^v K_{11}(w,v-w;\underline{a}_4)\,n(z,t;w)\,n(z,t;v-w)\,dw \\
+ [1-S(v;\underline{a}_2)]\left[\int_0^v K_{10}(w,v-w;\underline{a}_4)\,n(z,t;w)\,\sigma(z,t;v-w)\,dw\right. \\
\left. - \int_v^\infty \bar{u}_z(w;\underline{a}_1)\,\phi(w;\underline{a}_2)\,W(w,v)\,n(z,t;w)\,dw\right] ,
\end{aligned} \tag{2.14}$$

and

$$\begin{aligned}
\frac{\partial \sigma(z,t;v)}{\partial t} = [\bar{u}_z(v;\underline{a}_1)\,\lambda(v;\underline{a}_2)]\,n(z,t;v) \\
+ S(v;\underline{a}_2)\left[\int_0^v K_{10}(w,v-w;\underline{a}_4)\,n(z,t;w)\,\sigma(z,t;v-w)\,dw\right. \\
\left. - \int_v^\infty \bar{u}_z(w;\underline{a}_1)\,\phi(w;\underline{a}_2)\,W(w,v)\,n(z,t;w)\,dw\right] \\
- \sigma(z,t;v)\int_0^\infty K_{10}(w,v;\underline{a}_4)\,n(z,t;w)\,dw ,
\end{aligned} \tag{2.15}$$

Here, $\bar{u}_z$ is the time-averaged velocity of the ganglion in the direction of the flood, λ and ϕ are the stranding and the breakup coefficients defined by Equations (2.12) and (2.13) respectively. K_{ij} are the *collision-coalescence kernels* and are given by

$$K_{ij}(w,v;\underline{a}_4) = R_{ij}(w,v;\underline{a}_1)C_{ij}(w,v;\underline{a}_3) , \tag{2.16}$$

where $R_{ij}(w,v;\underline{a}_1)$ is the rate of collisions between w-ganglia and v-ganglia and $C_{ij}(w,v;\underline{a}_3)$ is the probability of coalescence given a collision. The index i is set

equal to 1 or 0 depending on whether the w-ganglion is moving or not (the index j pertains to the v-ganglia). Usually collisions between a moving ganglion and a stranded one are much more likely to result in coalescence than collisions between two moving ganglia ($C_{10}, C_{01} \gg C_{11}$). The variables $\underline{a}_1$, $\underline{a}_2$, $\underline{a}_3$ and $\underline{a}_4$ are parameter vectors (such as Ca, v^*, κ, θ_r^o, θ_a^o, dimensionless geometric groups, etc).

The physical meanings of the terms appearing in Equation (2.14) are as follows (from left to right): (a) rate of accumulation of moving v-ganglia; (b) net efflux of v-ganglia due to convection: (c) rate of loss of moving v-ganglia due to stranding, breakup, collision-coalescence with other moving ganglia, and collision-coalescence with stranded ganglia; (d) rate of generation of moving v-ganglia through collision-coalescence of appropriately sized smaller moving ganglia; (e) rate of generation of moving v-ganglia through collision-coalescence of smaller moving ganglia with stranded ones, and through fission of larger ganglia.

The physical meanings of the terms appearing in Equation (2.15) are as follows (from left to right): (a) rate of accumulation of stranded v-ganglia; (b) rate of stranding of mobilized v-ganglia; (c) rate of generation of stranded v-ganglia through collision-coalescence of smaller ganglia, one of which is stranded, and through stranding of v-ganglia formed by breakup of larger ganglia; (d) rate of loss of stranded v-ganglia by collision-coalescence with oncoming ganglia.

Equations (2.14) and (2.15) together with appropriate initial and boundary conditions were solved by Ng (1980), for unfavorable viscosity ratio using a collocation method and his main conclusions may be found in Payatakes and Dias (1984). It becomes clear from Ng's work that the parameters λ, ϕ and $\overline{u}_z$ play an important role. These parameters may be obtained by simulation of the fate of a solitary

ganglion in a porous medium (see Chapter 4). The coefficients C_{ij} may also be obtained with a simulation method similar to the one developed in this work together with a good coalescence criterion. Finally, Ng's results also indicate that the value of the residual oil saturation S_{or} is also of great importance to the outcome of these processes. In Chapter 5, a model is developed that will determine not only S_{or} for various flooding conditions but also the size and volume distribution of the ganglion population.

Chapter 3

Modeling of Oil Ganglion Motion

3.1 Introduction

As was discussed in Sections 2.4 and 2.5, networks of pores of converging-diverging geometry seem to be well suited to represent porous media. Of these, networks of constricted unit cells such as the one developed by Payatakes, Ng and Flumerfelt (1980) seem to have some advantages over the other types of networks discussed. Constricted unit cell networks can deal with different values for the viscosity of each fluid, and do not develop the constraint of the menisci that appears in the case of sphere-and-capillary networks.

Payatakes, Ng and Flumerfelt (1980) formulated a network model of randomly sized constricted unit cells which is capable of identifying the size, shape, orientation and position of an oil ganglion as well as the local topology of the porous medium. The stochastic simulation model for ganglion motion developed by Ng

and Payatakes is based on this model together with the mobilization criterion described in Section 2.5. This approach offers a relatively simple and fast simulation algorithm. however, it also has some short-comings which are listed bellow.

- The pressure field outside the ganglion is approximated by Darcy's law and the pressure field inside the ganglion is uniform. In reality, the internal and external flow fields are coupled.
- The presence of a uniform pressure inside the ganglion results in a null flow field inside the blob which, in turn, prevents the study of the effect of viscosity differences between the two phases.
- Time, as an independent and explicit variable, is absent. Hence, calculation of important, time dependent features of ganglion motion, such as estimation of ganglion velocity, are not possible.
- The simultaneous advancement of several interfaces is not allowed due to the assumption of one rheon at a time. This is an important feature of ganglion motion when Ca is much larger than the critical value for mobilization (dynamic displacement, see Sections 2.5 and 4.3).

The model presented in this work uses *network analysis methods* to simulate the fate of a solitary oil ganglion in a porous medium. Network analysis methods make use of standard electric network analysis to solve the network flow field, recognizing the analogy between flow rate and current, pressure drop and voltage, hydraulic conductance and electric conductance. and capillary pressure drop and voltage source. The pressure fields for both the aqueous and the oleic phases are solved simultaneously, and viscosity differences between the two phases are taken into account. Time appears as an independent variable, and the continuous motion

of the ganglion allows for the simultaneous advancement of several interfaces and the occurrence of dynamic breakup.

Ng (1980) used network analysis to determine the permeability of a porous medium model consisting of a network of constricted unit cells and performed some preliminary work on oil ganglion motion. In the present work, an extension of the method used by Ng is developed, taking advantage of the numerical band-symmetric features of the problem and elaborating on motion rules and criteria for interface rupture and ganglion breakup.

3.2 Network Model

For the sake of clarity, certain definitions of idealized elements of the porous medium void space will be stated first. Following Payatakes,Tien and Turian (1973), Payatakes and Neira (1977) and Payatakes, Ng and Flumerfelt (1980), the pore space in porous media is composed of relatively large chambers connected through narrow throats with adjacent chambers. The void space comprised of a chamber and its satellite throats will be denoted as an *elemental void space* (EVS). It will be assumed that each throat is characterized by the diameter of its narrowest cross section d and each chamber characterized by its effective chamber diameter (diameter of the sphere with equivalent volume), D. In most porous media of interest such as sandpacks or sandstones, both d and D are random variables. The probability distribution function for the throat diameter d and the chamber diameter D will be herein referred to as *throat size distribution* and *chamber size distribution* respectively, as suggested by Payatakes and Dias (1984). Note that in the two original

papers referenced above these distribution functions were called respectively "constriction size distribution" and "pore size distribution", the former nomenclature preferred, so that pore will refer to the void space comprised by a chamber and its satellite throats.

Consider a finite, three dimensional cubic network of interconnected unit cells of the constricted tube type, called a unit block. The size of a unit block is given by the number of unit cells along each axis. $N_x \times N_y \times N_z$, its step is the length of periodicity, ℓ, and each branch is occupied by a *unit cell* (UC). Each unit cell has axial symmetry, and its wall profile is a sinusoidal function, Figure 3.1 (Payatakes, Ng and Flumerfelt, 1980). The distance of the wall from the axis at some position z is given by

$$r_w(z) = \frac{1}{4}\left[(a+d) - (a-d)\cos\left(\frac{2\pi z}{h}\right)\right] . \qquad (3.1)$$

where a and d are the maximum and minimum diameters of the sinusoidal function and h is its wavelength.

According to the P-T-T (Payatakes, Tien and Turian, 1973) porous media model, the unit cell dimensions are set so that

$$a = c_1 d \quad ; \quad h = c_2 d . \qquad (3.2)$$

Payatakes, Ng and Flumerfelt (1980) found that in order to keep these realistic unit cell dimensions, to properly account for the chamber interconnectivity and to preserve the volume and porosity of the prototype as well as the number of constrictions per unit volume, this formulation had to be modified. The unit cell in this *modified P-T-T* porous media model is comprised within the segment corresponding to $(-h'/2 \leq z \leq h'/2)$ in Figure 3.1 , where h' is the unit cell length $(h' < h)$ and

calculated so that

$$h' = c_2 c_3 d \, . \tag{3.3}$$

Constants c_1, c_2 and c_3 are dependent on the particular porous medium, and are calculated based on experimental measurements of the porosity, the initial drainage curve and the grain size distribution as described by Payatakes, Tien and Turian (1973) and Payatakes, Ng and Flumerfelt (1980). The segment corresponding to $(-h/2 \leq z \leq h/2)$, called an *extended unit cell* (EUC), is left as part of the model and it will be useful in the specification of motion rules as is discussed in Section 3.7.

This model applies to non-consolidated porous media such as sand or bead packs. For consolidated porous structures such as the ones occurring in oil reservoirs (sandstones, limestones, etc.), the sinusoidal shape of the unit cell and the relations between its minimum and maximum diameters and length should be relaxed and their size distributions calculated independently by pore cast analysis and/or porosimetry and imbibition/drainage curves.

A two-dimensional representation of a random cubic network of constricted unit cells is given in Figure 3.2. This depiction and the nomenclature used are similar to the ones used in Payatakes, Ng and Flumerfelt (1980). Each node is connected to six unit cells (the pair normal to the paper plane is not shown). Unit cells are represented by *bow-tie* symbols whose sizes are proportional to the actual size of each unit cell. One node and the adjacent six-half unit cells comprise a *conceptual elemental void space* (CEVS), the network equivalent to an EVS. According to the model, when a CEVS is occupied by oil, the oil fills part of the six unit cells associated with the CEVS under consideration. Note that in this particular repre-

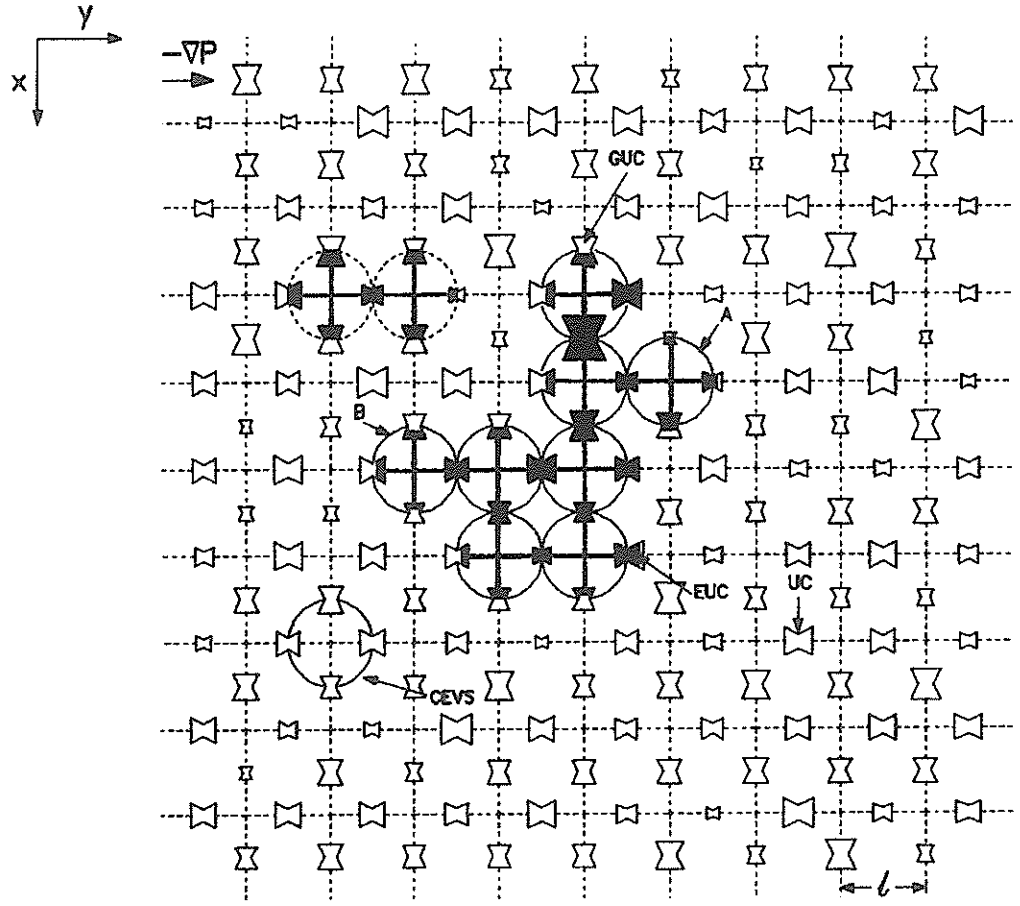


Figure 3.2

Two dimensional depiction of a cubic network of unit cells. A CEVS, a UC and an EUC are identified, as well as an 8-CEVS ganglion (solid line circles) and a 2-CEVS ganglion (dashed line circles).

sentation, unlike the one used by Payatakes, Ng and Flumerfelt (1980), the volume of oil associated with a particular CEVS may be larger (CEVS A, Figure 3.2) or smaller (CEVS B, Figure 3.2) than the CEVS volume. This occurs because in the network analysis oil (or water) is allowed to move slowly along each unit cell until it finally enters the next CEVS. The representation of an oil ganglion occupying several adjacent pores is made in a similar way, filling the unit cells of the appropriate CEVS's according to the volume of oil held by each unit cell. A unit cell occupied by an oil-water interface will be denoted as a *gate unit cell*, GUC or as an EUC if it temporarily takes the form of an extended unit cell (see Section 3.7). When a ganglion breaks to give two daughter ganglia, the different ganglia will be distinguished by the use of solid and dashed lines to circle the CEVS's of each ganglion as is also shown in Figure 3.2.

The simulations and results presented in this work were obtained in a two-dimensional version of the cubic lattices as shown in Figure 3.2. The error introduced by omitting the third dimension is expected to be significant only for relatively large ganglia, say ganglia occupying 20 or more elemental void spaces. It must be noted that, in the case of the two-dimensional network, the value of c_3 has to be modified to satisfy the porosity equality requirement.

3.3 Analogy Concepts

For simplicity consider a $N_x \times N_y = 6 \times 7$ network such as the one represented in Figure 3.3. The network nodes are numbered as shown in the same figure starting with the node at the upper-left-hand corner and proceeding downwards and from

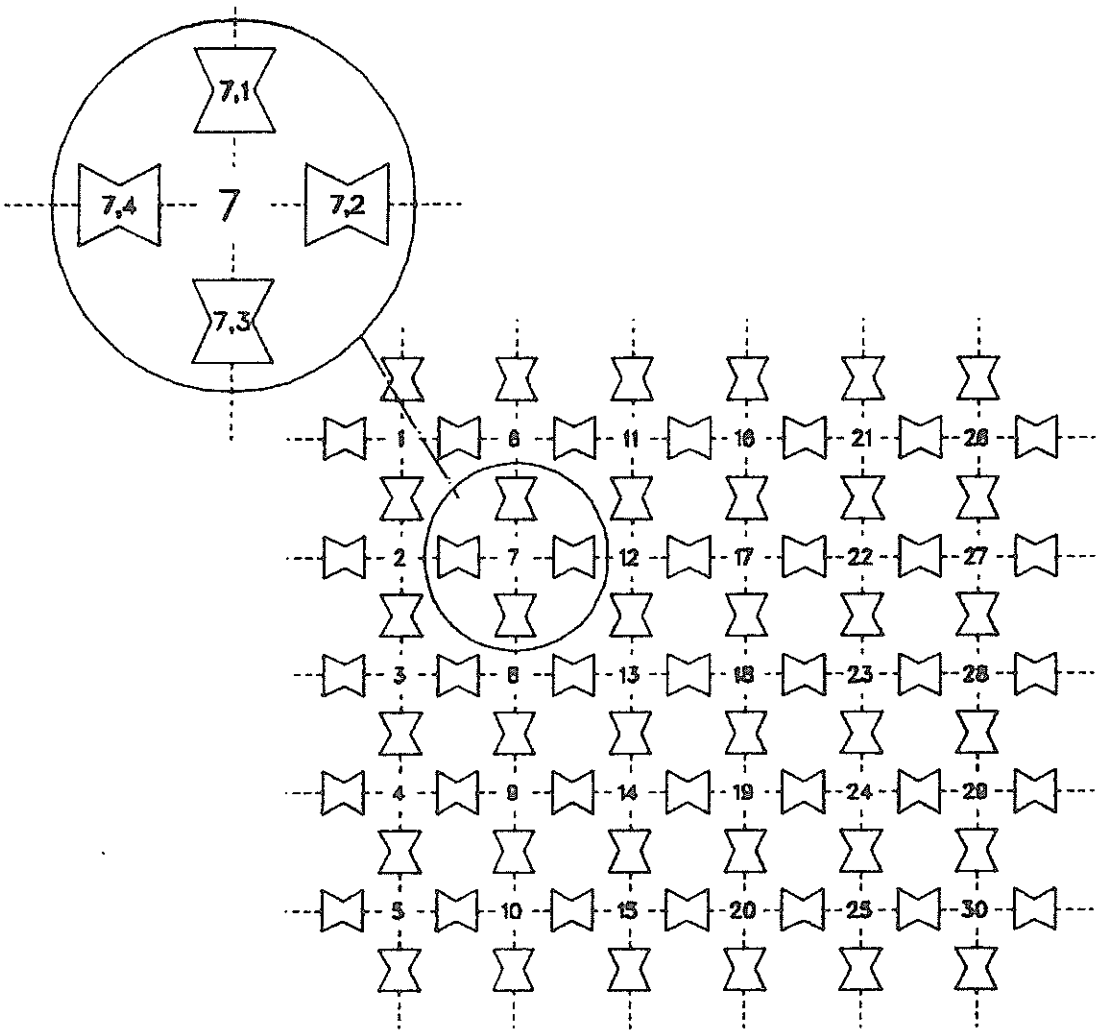


Figure 3.3

Depiction of a $N_x \times N_y = 6 \times 7$ cubic network showing the nodes numbering system and in the inset the branches numbering system.

left to right. Each branch of the network corresponding to a unit cell is numbered with relation to the node to which it is connected. Considering then node k, the four branches connected to it are numbered (j,k), $j = 1,2,3,4$, starting with the upper branch and proceeding clockwise around the node (see inset in Figure 3.3). This numbering system results in duplication of addresses for some unit cells. For example $(3,k)$ and $(1,k+1)$ refer to the same unit cell and similarly $(2,k)$ and $(4,k+N_x-1)$ also refer to the same unit cell. For relatively small networks (up to 900 nodes) this duplication does not create severe problems in memory requirements and, on the other hand, results in a simpler algorithm that can easily be adapted to other network lattices such as tetrahedric, rhombohedric or even random.

Such a network can be regarded as an electric network of resistors, each resistor corresponding to a unit cell with an associated *conductance* value, G. The flow rate through each unit cell, q_{uc}, corresponds to the *branch current*, q and the pressure drop along a unit cell, ΔP_{uc}, to the *branch voltage* (also called branch potential), v_p. For each gate unit cell, its resistance is taken as the sum of the resistance corresponding to the segment of the unit cell containing water, plus the resistance corresponding to the oil part.

The pressure drop across an oil-water interface for each GUC, ΔP_i, is taken as a *voltage source* (or electromotive force), v_s. Finally the pressure at each boundary node, resulting from the applied macroscopic pressure gradient, is represented as an additional voltage source, v_s^*. These and other pertinent analogies are condensed in Table 3.1, where subscripts k and j pertain to nodes and branches respectively.

A 7-CEVS oil ganglion in the same (6×7) network is represented in Figure 3.4a with the corresponding electric analog shown in Figure 3.4b. In the latter repre-

Table 3.1

Analogies between the Hydraulic and the Electric Networks

HYDRAULIC PROTOTYPE		ELECTRIC ANALOG	
Physical Variable	Symbol	Physical Variable	Symbol
hydraulic conductance	G	electric conductance	g_{kk}
flow rate through UC	q_{uc}	branch current	q_j
pressure at CEVS center	P	node voltage	p_k
pressure drop along UC	ΔP_{uc}	branch voltage	v_{b_j}
pressure drop across interface	ΔP_i	voltage source	v_{s_j}
pressure drop along boundary UC's	ΔP_{uc}^*	boundary voltage source	$v_{s_j}^*$

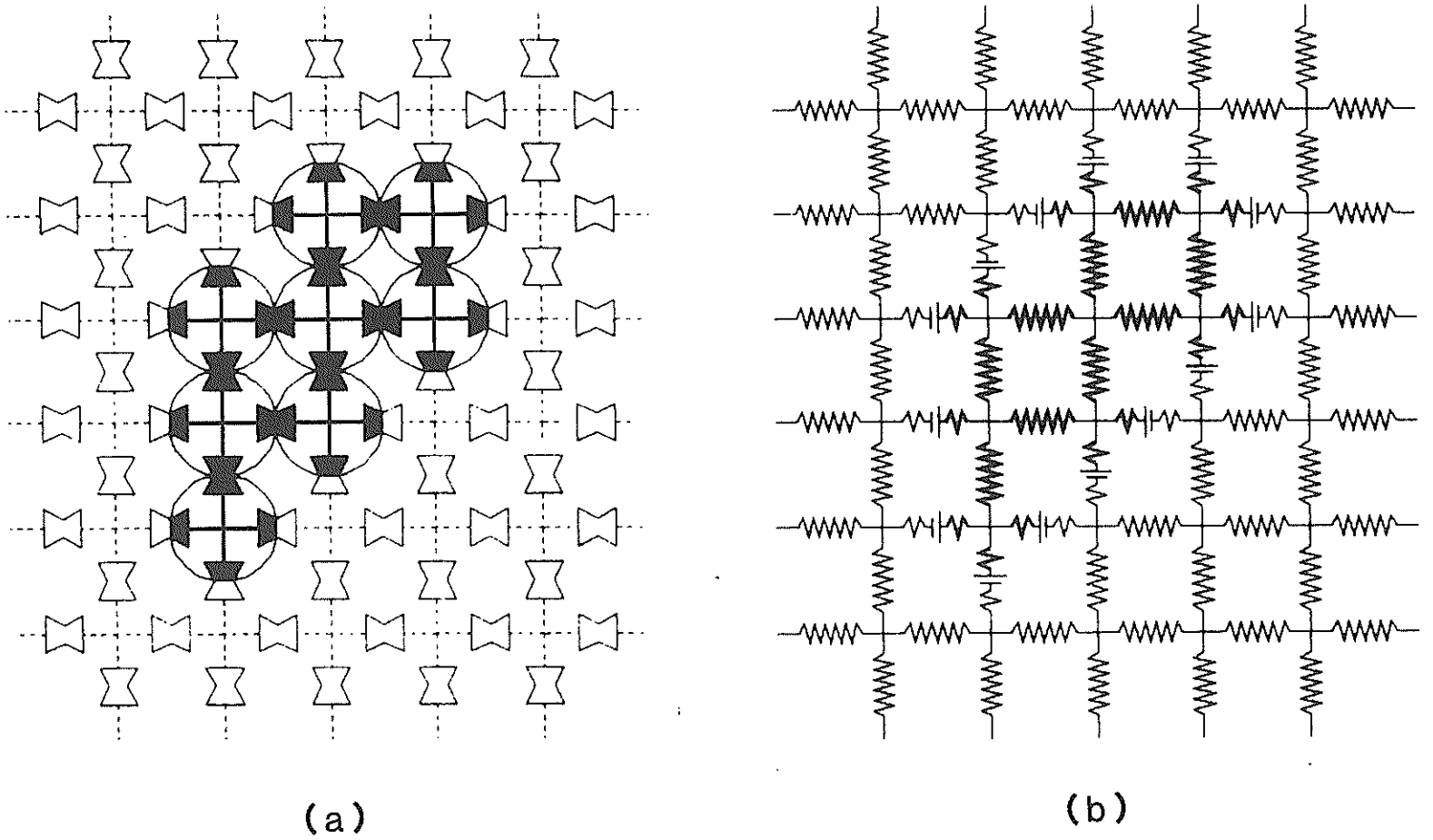


Figure 3.4

(a) Depiction of a 7-CEVS ganglion on a two-dimensional square network and (b) its electric network

sentation, unit cells filled with water are shown as thin line resistors, whereas unit cells filled with oil are shown as thick line resistors. Gate unit cells are shown as part thin line resistors corresponding to the water, and part thick line resistors corresponding to the oil, separated by a voltage source corresponding to the oil-water interface.

In order to use network analysis efficiently, it is necessary to express the network variables in vector form.

The *branch conductance matrix*, $\underline{\underline{G}}$, is an $N_b \times N_b$ diagonal matrix where

$$N_b = (2N_x - 1)(N_y - 1) + (N_x - 1) \ , \tag{3.4}$$

is the total number of branches in the network. Each element, g_{lk} , of matrix $\underline{\underline{G}}$ is given by:

$$\begin{cases} g_{kk} = \text{conductance of branch } k \\ g_{lk} = 0, \qquad \text{if} \quad l \neq k \ . \end{cases} \tag{3.5}$$

Voltage sources resulting from oil-water interfaces and/or from the pressure values applied to the boundary nodes are taken in a single vector $\underline{v}_s$. This vector has dimension N_b , and its elements are null everywhere except for the ones corresponding to the branches at the network boundaries or branches containing an oil-water interface. Using circuit theory it can be shown that

$$\underline{q}_s = \underline{\underline{G}}\, \underline{v}_s \ . \tag{3.6}$$

An element q_{s_k} of the vector $\underline{q}_s$, called the *node current source vector*, can be interpreted as the algebraic sum of all source currents entering node k. Its dimension is equal to the total number of nodes in the network given by

$$N_p = (N_x - 1)(N_y - 1) \ , \tag{3.7}$$

Using standard electric network analysis. this problem can be treated as a linear, pure resistitive network (see for example Desoer and Huh, 1969). For fixed time it can be reduced to

$$\underline{\underline{Y}}\ \underline{p} = \underline{q}_s \ , \tag{3.8}$$

where $\underline{\underline{Y}}$, the *node conductance matrix*, is constructed as follows.

1. y_{kk} , called the *self-admittance of node* k , is the sum of the conductances of all branches connected to node k .
2. y_{lk} , the *mutual admitance between nodes* l *and* k , is the negative of the sum of the conductances of all branches connecting nodes l and k .

Equation 3.8 is to be solved for $\underline{p}$ the *node voltage vector*, by inversion or decomposition of matrix $\underline{\underline{Y}}$. It is important to take advantage of the band-symmetric form of this matrix and use this feature conveniently in order to reduce computation time.

The vector $\underline{p}$, has dimension N_p and represents the voltage at each node, that is, in hydrodynamic terms, the pressure at the center of each CEVS. The pressure drop along a unit cell or, in electric analog notation, the branch voltage may be calculated as

$$\underline{v}_b = \underline{\underline{A}}\ \underline{p} \ . \tag{3.9}$$

The *reduced incidence matrix*, $\underline{\underline{A}}$, has dimensions $N_p \times N_b$, and it defines how the branches are connected. Its components are set so that,

$$a_{jk} = \begin{cases} 1 & \text{flow in branch } j \text{ away from incident node } k \\ -1 & \text{flow in branch } j \text{ towards incident node } k \\ 0 & \text{branch } j \text{ is not incident with node } k \ . \end{cases} \tag{3.10}$$

Finally vector $\underline{q}$ corresponding to the branch current or the flow rate through each unit cell is given by

$$\underline{q} = \underline{\underline{G}} \, (\underline{v}_b - \underline{v}_s) \; . \tag{3.11}$$

3.4 Permeability and Network Isotropy

The permeability of a specified network of randomly sized unit cells can be calculated by applying the analysis described in the previous sections to single phase flow as is explained in detail by Ng (1980). Imposing a constant macroscopic pressure gradient and averaging the calculated permeability values obtained from a number of realizations for each one of which a different random unit cell size distribution is chosen, a good estimation of the permeability value may be obtained. The question may arise as to whether this value is dependent on the macroscopic pressure gradient direction, that is, whether the network is isotropic or anisotropic. In the case of packings (sandpacks or beadpacks), the permeability in the plane of bedding is isotropic and only slightly larger than the permeability normal to it (Fontugne, 1969 ; Rice *et al* , 1970). Hence, granular packings are usually considered as isotropic. This is not usually the case whit reservoir rocks.

Darcy's law for isotropic and anisotropic porous media may be expressed as

$$\underline{v} = \frac{1}{\mu} \underline{\underline{k}} \bullet (-\nabla P) \; , \tag{3.12}$$

where $\underline{v}$ is the velocity vector, μ is the fluid viscosity, $\underline{\underline{k}}$ is the permeability tensor of porous media, and $(-\nabla P)$ is the pressure gradient. The permeability tensor is a second order, symmetric tensor with components k_{ij} (Scheidegger, 1957). It follows

that it has (at least) one set of three orthogonal principal axes, and, if the pressure gradient is parallel to any of these axes, then the velocity is also in that direction.

Consider, then, a three dimensional cubic network of unit cells. The size of each unit cell is chosen randomly according to some distribution function and independently for each of the three network planes. Apply a constant pressure gradient along one of the network axes, taking the boundary conditions on the remaining sides to be, for example, periodic and repeat for all three network axes. In each case the resultant average flow has the same direction as the macroscopic pressure gradient; that is to say that the three principal axes are coincident with the network axes. Since all three network planes were constructed independently, randomly and following the same distribution function, it follows that the calculated permeability values will have the same value independently of the direction. Using a well known theorem in tensor analysis (see for example Bear, 1972), which states that, if all three principal axes are equal, any direction of space is a principal direction and any set of orthogonal axes is a set of principal axes. it follows that

$$k_{ij} = k\delta_{ij} \ , \tag{3.13}$$

where k is the absolute permeability of the isotropic medium and δ_{ij} are the components of the Kronecker $\underline{\underline{\delta}}$. Darcy's law, for the model under consideration, may now be expressed as

$$\begin{aligned} \underline{v} &= \frac{1}{\mu}\, k\, \underline{\underline{\delta}} \bullet (-\nabla P) \\ &= \frac{1}{\mu}\, k\, (-\nabla P) \ , \end{aligned} \tag{3.14}$$

and the model is shown to be isotropic.

In order to numerically verify the statement that the network represents indeed an isotropic medium, simulations at different macroscopic pressure gradient

directions including directions not coincident with any of the network axes were performed both in the present work and by Ng (1980) and in fact the average permeability value is found to be independent of the macroscopic pressure gradient direction.

3.5 Macroscopic Pressure Gradient and Boundary Conditions

Given the capillary number

$$Ca \equiv \frac{\mu_w v_f}{\sigma_{ow}} , \tag{3.15}$$

where μ_w is the viscosity of the aqueous phase, v_f is its superficial velocity and σ_{ow} is the interfacial tension between the two fluids, and taking the absolute permeability value calculated as described in the previous section, the magnitude of the corresponding macroscopic pressure gradient is given by

$$-\nabla P = \frac{Ca\sigma_{ow}}{k} . \tag{3.16}$$

This approximation is valid as long as the oil ganglion is small when compared with the network size so that the network itself can be considered infinite and the presence of the oil ganglion is not perceived at the network boundaries. When simulating imbibition or drainage processes this is clearly not true, since now the oleic phase may occupy most of the network up to and including its boundaries. This situation and how to deal with it will be discussed in detail in Chapter 5.

The flow configuration is then determined by choosing:

1. The macroscopic pressure gradient direction given by ϕ' defined as the angle between the x-axis and the direction of the macroscopic pressure gradient.

2. The unit block size (N_x and N_y)

Take two planes normal to the macroscopic pressure gradient direction and located as shown in Figure 3.5. The pressure drop along the network is then determined by

$$P_1 - P_0 = (-\nabla P)\,\ell\, D_{xy}\ , \tag{3.17}$$

where

$$D_{xy} = N_y \sin\phi' + N_x \cos\phi'\ , \tag{3.18}$$

and P_1 and P_0 represent respectively the pressures at planes 1 and 0 in Figure 3.5. For simplicity, P_0 is given the value zero. The pressures at each boundary node can easily be derived using geometrical considerations. For example, the pressures at locations I, J, M and N in Figure 3.5 are given respectively by

$$P_I = (-\nabla P)\,\ell\,(D_{xy} - N_I \sin\phi')\ , \tag{3.19a}$$

$$P_J = (-\nabla P)\,\ell\,(D_{xy} - N_J \cos\phi'\ , \tag{3.19b}$$

$$P_M = (-\nabla P)\,\ell\,(D_{xy} - N_y \sin\phi' - N_M \cos\phi')\ , \tag{3.19c}$$

$$P_N = (-\nabla P)\,\ell\,(D_{xy} - N_x \cos\phi' - N_N \sin\phi')\ , \tag{3.19d}$$

where N_I and N_N are the number of branches along the y-axis up to the locations I and N, respectively, and N_J and N_M are the number of branches along the x-axis up to the locations J and M, respectively.

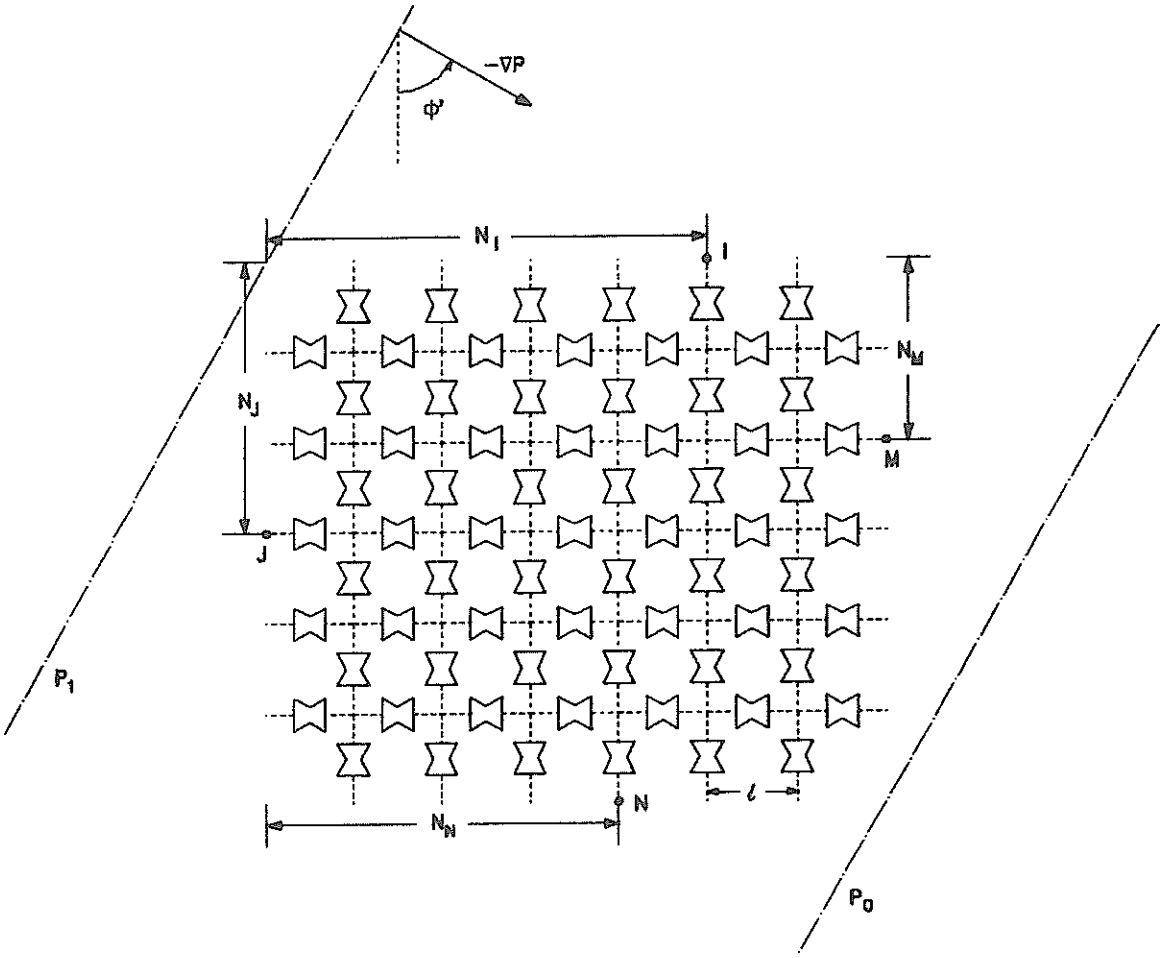


Figure 3.5

Flow configuration calculation example. The direction of the macroscopic pressure gradient is at an angle ϕ'.

3.6 Conductance and Pressure Drop Across an Interface

3.6.1 Single Phase Flow Conductance

Single phase flow through constricted tubes has been the object of extensive study. The problem of laminar Newtonian flow through periodically constricted tubes was solved by Payatakes *et al* (1973) using a finite-difference method of the stream function-vorticity type. This method presents the advantages of being applicable to tubes of arbitrary shape and of retaining the non-linear terms of the equation of motion. It has the disadvantage of requiring large memory to achieve satisfactory accuracy, and it renders a solution in matrix form. Chow and Soda (1972) have solved this problem analytically over a limited range of parameters, namely for small amplitudes in the periodic function describing the tube wall. More recently Deiber and Schowalter (1979) solved numerically the problem of flow through tubes with sinusoidal axial variations in diameter using an iteration technique. Again, this solution is limited to a range of the wall diameter not exceeding 60% of the mean diameter, and it yields a solution in matrix form Fedkiw and Newman (1977) used a collocation method for the same geometry in the creeping flow regime. In fact, it is in the domain of creeping flow (Reynolds number < 1) that displacement of oil by water occurs in most cases of interest. Collocation solutions of creeping newtonian flow through periodically constricted tubes with piecewise continuous wall profile and through sinusoidal tubes were also obtained by Neira and Payatakes (1978 and 1979 respectively). Recently Tilton and Payatakes (1984) noted that the solution given by Neira and Payatakes (1979) resulted in a velocity singularity along the

tube axis. After correcting this mistake they found that the value of the pressure drop along a unit cell agreed quite closely with those originally reported by Neira and Payatakes (1979), due to the fact that very little viscous dissipation takes place along and near the axis of the tube.

This latter solution is here adopted in order to calculate the conductance of a unit cell filled with a single fluid. The pressure drop along a unit cell ΔP_{uc} and the flow rate through the unit cell q_{uc} are related by

$$q_{uc} = \frac{\pi c_2 d^3}{4\mu\left(-\Delta P_1^*\right)} \Delta P_{uc} \ , \tag{3.20}$$

where ΔP_1^* is the dimensionless pressure drop along an extended unit cell at Reynolds number equal to unity ($Re = 1$), that is

$$\Delta P_1^* = Re\, \Delta P^* \ , \tag{3.21}$$

$$\Delta P^* = \frac{\Delta P_{uc}}{\rho v_o^2} \ , \tag{3.22}$$

$$Re \equiv \frac{h v_o}{\nu} \ . \tag{3.23}$$

ρ is the fluid density, v_o is the mean velocity at the cross section of minimum radius and ν is the fluid kinematic viscosity. ΔP_1^* is a function of the minimum and the maximum radius of the sinusoidal tube, that is in our case of c_1, c_2 and c_3, and its value may be estimated following the procedure used by Neira and Payatakes (1979), and Tilton and Payatakes (1984).

3.6.2 Two Phase Flow Conductance

Two-phase flow through constricted tubes has also been studied extensively mainly in what refers to motion, snap-off, pinch-off and breakup of drops, long

bubbles and small ganglia (see Section 2.3). However, complexity of the subject, there is not, at the moment, a complete solution for two-phase creeping flow in a constricted tube. In order to overcome this difficulty, in the present study an approximation based on lubrication theory as described below will be used.

Sheffield and Metzner (1976) used lubrication theory to obtain an approximate solution to single phase flow through a sinusoidal tube

$$-\frac{\partial P}{\partial z} = \frac{8\mu}{\pi \left(r_w(z)\right)^4} q_{uc} \ . \tag{3.24}$$

This result was obtained by approximating the sinusoidal tube as a series of infinitely short cylindrical tubes whose diameter varies sinusoidally with axial position. Prasad (1978) obtained similar results by approximating the sinusoidal tube as a series of cones of infinitesimal length. In his study, Prasad found the Sheffield and Metzner method to be sufficiently accurate and within 20% error of the collocation solution obtained by Neira and Payatakes (1979). For reasons of simplicity Equation (3.24) will be here taken as the basis to calculate conductances of gate unit cells.

Integrating Equation (3.24), the pressure drop between any two points, z_1 and z_2 , is obtained

$$\Delta P(z_1, z_2) = \frac{2^{10} \mu c_2}{\pi^2 d^3 (c_1 + 1)} \Psi(z_1, z_2)\, q_{uc} \ , \tag{3.25}$$

where

$$\begin{aligned}\Psi(z_1, z_2) = & \frac{b}{3(1-b^2)}\left[\frac{\sin x}{(1-b\cos x)^3}\right]_{x(z_1)}^{x(z_2)} \\ & + \frac{5b}{6(1-b^2)^2}\left[\frac{\sin x}{(1-b\cos x)^2}\right]_{x(z_1)}^{x(z_2)} \\ & + \frac{b(11+4b^2)}{6(1-b^2)^3}\left[\frac{\sin x}{(1-b\cos x)}\right]_{x(z_1)}^{x(z_2)} \\ & - \frac{2+3b^2}{(1-b^2)^{7/2}}\tan^{-1}\left[\frac{(1-b^2)^{1/2}\tan(x/2)}{(1-b)}\right]_{x(z_1)}^{x(z_2)},\end{aligned} \tag{3.26}$$

$$b = \frac{c_1 - 1}{c_1 + 1}, \tag{3.27}$$

and

$$x = \frac{2\pi z}{c_2 d}. \tag{3.28}$$

For a gate unit cell, assuming the interface to be at some position z_i

$$\Delta P(z_i) = \Delta P\left(-\frac{h'}{2}, z_i\right) + \Delta P\left(z_i, \frac{h'}{2}\right), \tag{3.29}$$

and the conductance becomes

$$G(z_i) = \left\{\frac{2^{10}\mu_w c_2}{\pi^2 d^3 (c_1+1)^4}\left[\Psi\left(-\frac{h'}{2}, z_i\right) + \kappa\Psi\left(z_i, \frac{h'}{2}\right)\right]\right\}^{-1}, \tag{3.30}$$

where $\kappa = \mu_o/\mu_w$ is the viscosity ratio.

3.6.3 Pressure Drop Across an Interface

Using a Washburn (1921) type approximation, that is, assuming that the effect of capillary forces is to introduce a pressure drop across the oil-water interface which

is equal to that which would be present if the fluids were stationary, and following Oh and Slattery (1970), it can be shown from geometrical considerations and the Young and Laplace equation that

$$\Delta P_i(z_j) = 2\,\sigma_{ow}\,\frac{\cos\beta}{r_w(z)}\bigg|_{z=z_j}\,, \tag{3.31}$$

where z_j is the axial position of the solid-oil-water contact line,

$$\cos\beta = \frac{\cos\theta + \sin\theta\tan\alpha}{\left(1+\tan^2\alpha\right)^{1/2}}\,. \tag{3.24}$$

$$\tan\alpha = \frac{d\left(r_w(z)\right)}{dz} = \frac{\pi}{2c_2}(c_1-1)\sin\left(\frac{2\pi z}{c_2 d}\right)\,, \tag{3.33}$$

and θ is the contact angle.

3.6.4 Effective Conductance and Effective Pressure Drop Across an Interface

It is clear from Equations (3.30) and (3.31) that both the conductance and the pressure drop across an interface for a gate unit cell depend on the position of the interface. It is possible to calculate the exact values of the conductance and of the pressure drop across an interface knowing the position of the interface, but since the interfaces are constantly moving this would result in a large computational effort without a significant improvement in accuracy or overall behavior.

In order to reduce the computational effort, each gate unit cell is divided into several compartments. For simplicity the compartments are equally spaced, that is, $z'_k - z'_{k-1} = z'_{k+1} - z'_k$, where z'_k is the axial position of the division corresponding to compartment k taken from the end of the unit cell ($z = -h'/2$, $z' = 0$). The extended unit cell is also divided into equally spaced compartments. Figure 3.6

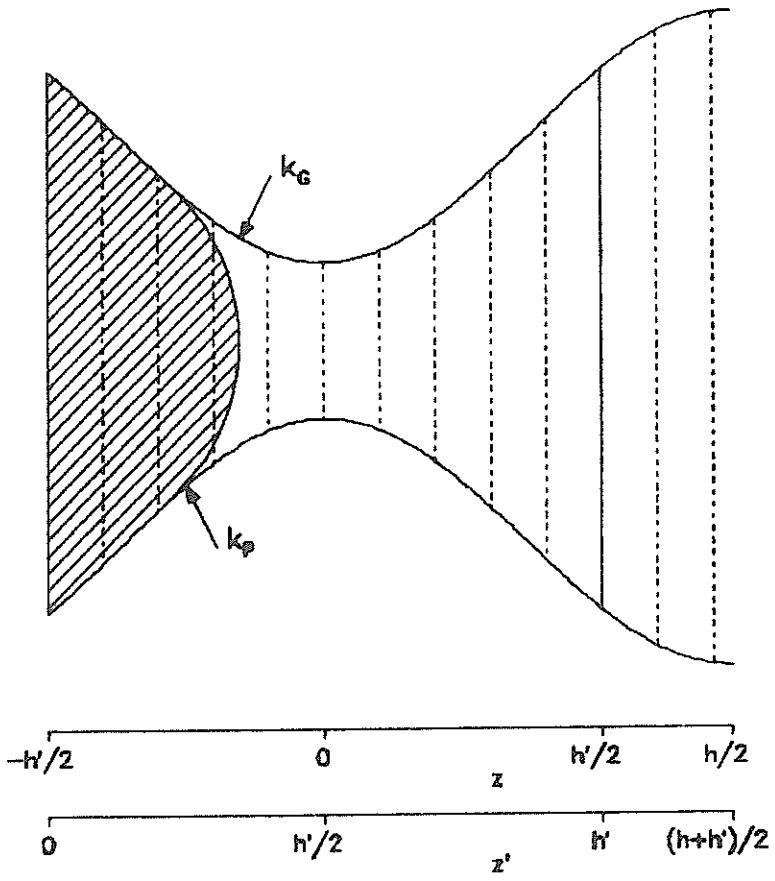


Figure 3.6

Representation of a gate unit cell divided into ten compartments showing compartments k_G and k_P used to calculate the effective conductance and the effective pressure drop respectively.

shows an example of a unit cell divided into ten equally spaced compartments as well as the corresponding extended unit cell.

The volume of the compartments located at or near the throat is smaller than the volume of those compartments at either end of the unit cell. This is a precaution designed to provide for the fact that both the pressure drop across an interface and the conductance change more rapidly in the throat region for a given change in the volume of oil.

The effective conductance G_{eff} is estimated as follows. Take V_g to be the volume of oil contained in the gate unit cell at a given instant of time. There is a compartment number, k_G, for which $V_{k_G-1} < V_g \leq V_{k_G}$, where V_{k_G-1} and V_{k_G} are the volumes of the part of the constricted tube up to z'_{k_G-1} and z'_{k_G}, respectively. G_{eff} is estimated to be equal to the conductance that would be obtained if the pseudo-interface were situated at the plane bisecting compartment k_G, that is at $z'_G = (z'_{k_G} - z'_{k_G-1})/2$.

In the calculation of G_{eff} the shape of the meniscus and the actual position of the solid-oil-water contact line are not taken into account, since Equation (3.30) was derived assuming a flat interface. On the other hand, the calculation of the pressure drop across an interface using Equations (3.31) through (3.33) assumes a spherical shape for the interface, and the actual position of the contact line for a given volume of oil is dependent on the contact angle. The compartment number k_P, where the contact line is located is calculated given the contact angle θ, the volume of oil in the gate unit cell V_g and assuming a spherical shape for the meniscus. The effective pressure drop ΔP_{eff} is taken as the one that would be obtained if the interface were situated at the bisector of this compartment, that is, $z'_P = (z'_{k_P} + z'_{k_P-1})/2$, where

z'_{k_P} and z'_{k_P-1} are the axial positions of the divisions at both ends of compartment k_P.

Figure 3.6 shows the position of k_G and k_P for a given volume of oil in a typical unit cell and perfect wetting conditions, $\theta_e = 0^\circ$.

3.7 Motion Rules and Interface Rupture Mechanisms

Due to the converging-diverging geometry of the unit cells and the randomness of their sizes, it is clear that the flow field will change constantly as the oil progresses in the gate unit cells. Using network analysis, the flow field at each instant can be calculated if the position and volume of oil in each gate unit cell is known. Assuming pseudosteady-state conditions, a time step can be calculated so that during this time the flow field, and particularly the flow rate through each gate unit cell, is taken as constant. As was described in Section 3.6.4, each gate unit cell is to be divided into a certain number of compartments, and the time increment is chosen so that each interface is allowed to move at the most to the next compartment. The number of compartments, N_c, required to ensure pseudosteady-state conditions will be determined by analyzing qualitatively as well as quantitatively the oil ganglion motion for several values of N_c.

Once the proper time increment is determined, the volume of oil in all GUC's is updated according to their respective flow rates and the total time elapsed recorded. This process is repeated until one of following occurs.

1. A gate unit cell fills with oil.
2. A gate unit cell becomes emptied of oil.

3. The ganglion fissions in two daughter ganglia (breakup).

Upon the occurrence of one of the first two events, motion rules have to be applied in order to determine the fate of the ganglion at this particular instant. If the ganglion breaks, the simulation is stopped and the position and volume of the two daughter ganglia recorded.

3.7.1 Treatment of Xerons

3.7.1.1 General Case

Consider the 6-CEVS ganglion represented in Figure 3.7a and concentrate on the downstream most gate unit cell A. Under the applied pressure gradient, the oil in this particular gate unit cell will advance according to the criterion described above (Figure 3.7b). If the time increment calculated using this criterion leads to an updated volume of oil in the unit cell which is greater than the volume of the unit cell in question, the time increment is adjusted so that the interface now lies at the end of the unit cell and the unit cell is now filled with oil (Figure 3.7c).

Before continuing to the next step, it is necessary to decide what configuration to assign to the interface. A first and simple minded approach leads to the placement of three new interfaces with associated infinitesimally small amounts of oil at the three downstream unit cells belonging to the same CEVS (unit cells B, C and D, Figure 3.7c). This solution presents the following problem. On the next step the flow rate through one of these three unit cells is likely to be negative; that is, the volume of oil in this unit cell will decrease, but since its volume was very

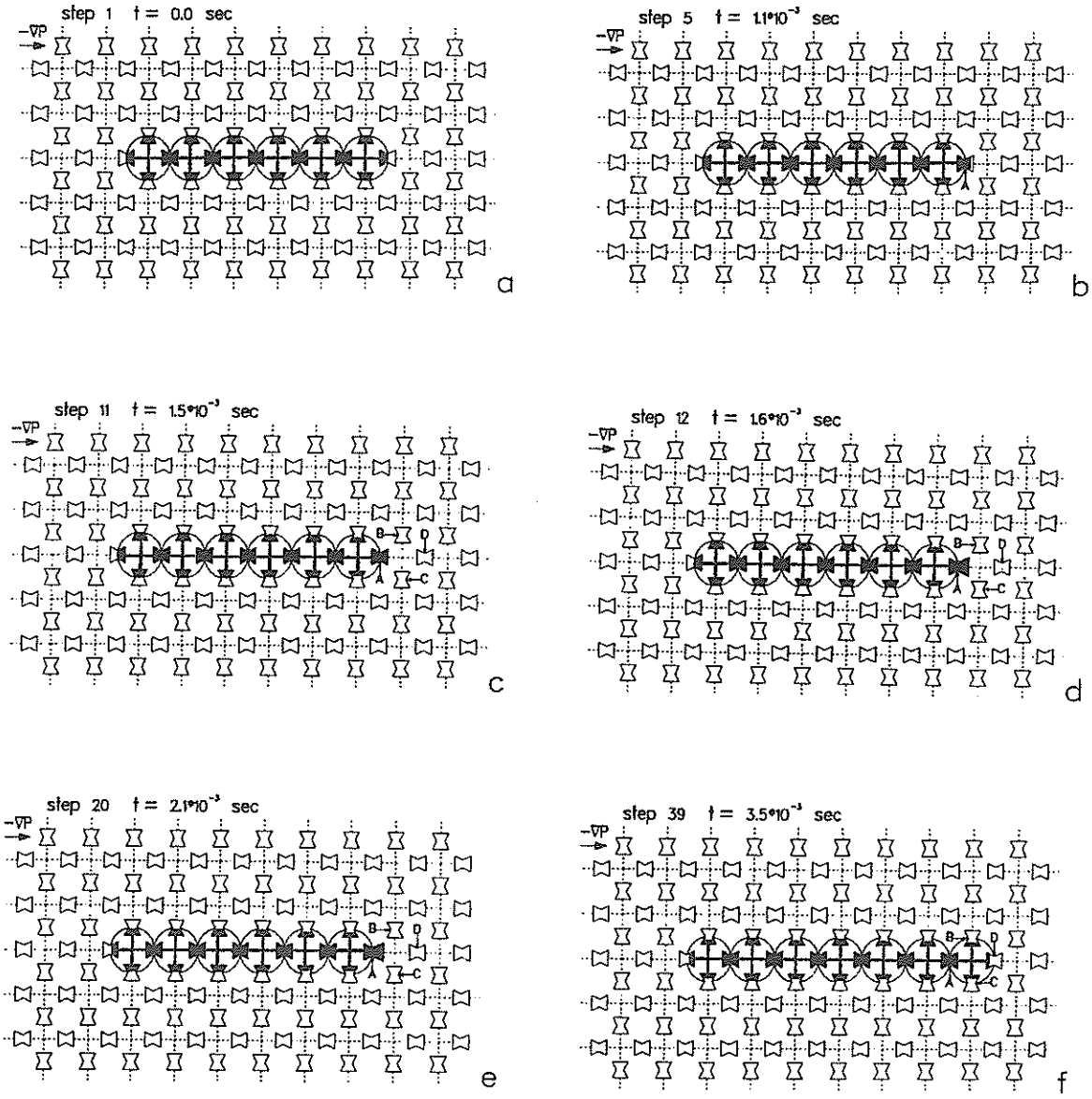


Figure 3.7

Stages of a 6-CEVS ganglion motion simulation. Occurrence of a xeron.

small, this gives rise to negative volumes of oil in a unit cell, which of course is bothersome.

In order to find a more sound solution for this situation, it is helpful to look at actual laboratory studies of oil-ganglion motion. Figure 3.8 shows a sequence of photographs taken from movies made by Hinkley (1982). The experimental apparatus used by Hinkley consisted of a single layer of uniformly sized glass spheres organized in a square configuration and held between two glass plates. In Figure 3.8 a 6-pore rectilinear oil-ganglion moving from left to right is pictured. It can be observed that the downstream-most oil-water interface is advancing and, in Figure 3.8c, about to invade the adjacent pore (pore G). Looking now at subsequent photographs, this interface is actually invading pore G but not touching either one of the two spheres located downstream. The interface proceeds in this way for some time (Figures 3.8d and 3.8e), until finally the volume of oil in this pore is sufficiently large so that all four spheres come in contact with oil (Figure 3.8f).

In the simulation algorithm this series of events is represented by allowing unit cell A to take an extended unit cell configuration ($-h'/2 \leq z < h/2$) (Figure 3.7d). The oil fills part of this extended unit cell depending on the volume of the unit cells downstream (Figure 3.7e). At the point where there exists enough oil in the extended unit cell to fill 15% of each the three downstream unit cells (roughly corresponding to the situation of Figure 3.8f), the adjoining pore chamber is considered to have been invaded by this excess oil. New interfaces are then placed simultaneously at the downstream unit cells B, C and D (Figure 3.7f), dividing among them the excess oil, in proportion to their respective volumes. At the same time, unit cell A regains its usual shape and size ($-h'/2 \leq z \leq h'/2$) and a *xeron* is said to have

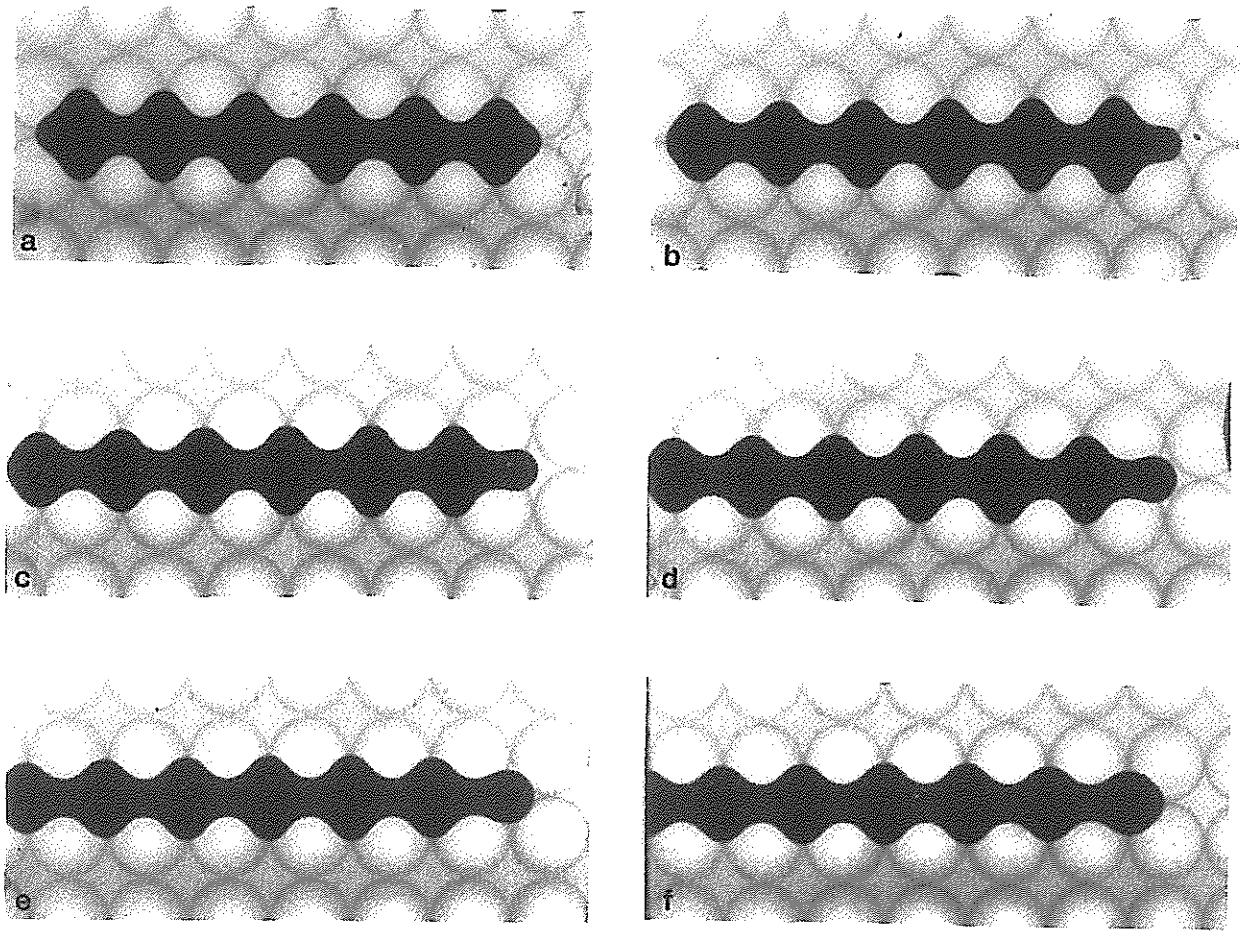


Figure 3.8

Sequential pictures of a moving 6-pore oil ganglion. Demonstration of a xeron. From Hinkley (1983).

occurred. It should be stressed here that a similar situation occurs if the unit cells were of different sizes. The use of monosized unit cells in this analysis (as well as in the next section) is due only to the fact that the experimental work was performed using monosized glass spheres in a square pack, resulting in equally sized pores.

3.7.1.2 Simultaneous Xerons into CEVS's sharing the same UC

Figure 3.9 shows a simple example of the occurrence of simultaneous xerons. Here an 8-CEVS ganglion is introduced in a monosized network in two parallel tracks following the same direction as the macroscopic pressure gradient (Figure 3.9a). Gate unit cells A and B advance at practically the same rate. When each one of them fills with oil (Figure 3.9b), each takes an EUC form, and the simulation allowed to proceed (Figure 3.9c). After some time two xerons occur, and, since the downstream nodes corresponding to unit cells A and B share a common unit cell (C, Figure 3.9d), two interfaces are placed in opposite sides of this gate unit cell.

It should be noted here that in the present work, coalescence *is not* allowed. The water trapped between two interfaces in a unit cell has no passage to escape. Interfaces belonging to a same gate unit cell are still allowed to move, but they will move in tandem. In essence, this assumption is equivalent to assuming no coalescence given a collision ($C_{ij} = 0$). Experimental work by Rapin (1980) and Hinkley (1982) show that coalescence and self-coalescence occur in certain situations. Then this assumption should be amended in future work. A modification of this algorithm that allows the water to escape by connecting the center of the unit cell with a sink has been proposed elsewhere (Leu, 1983).

On a later stage of the simulation (Figure 3.9e) another occurrence of simulta-

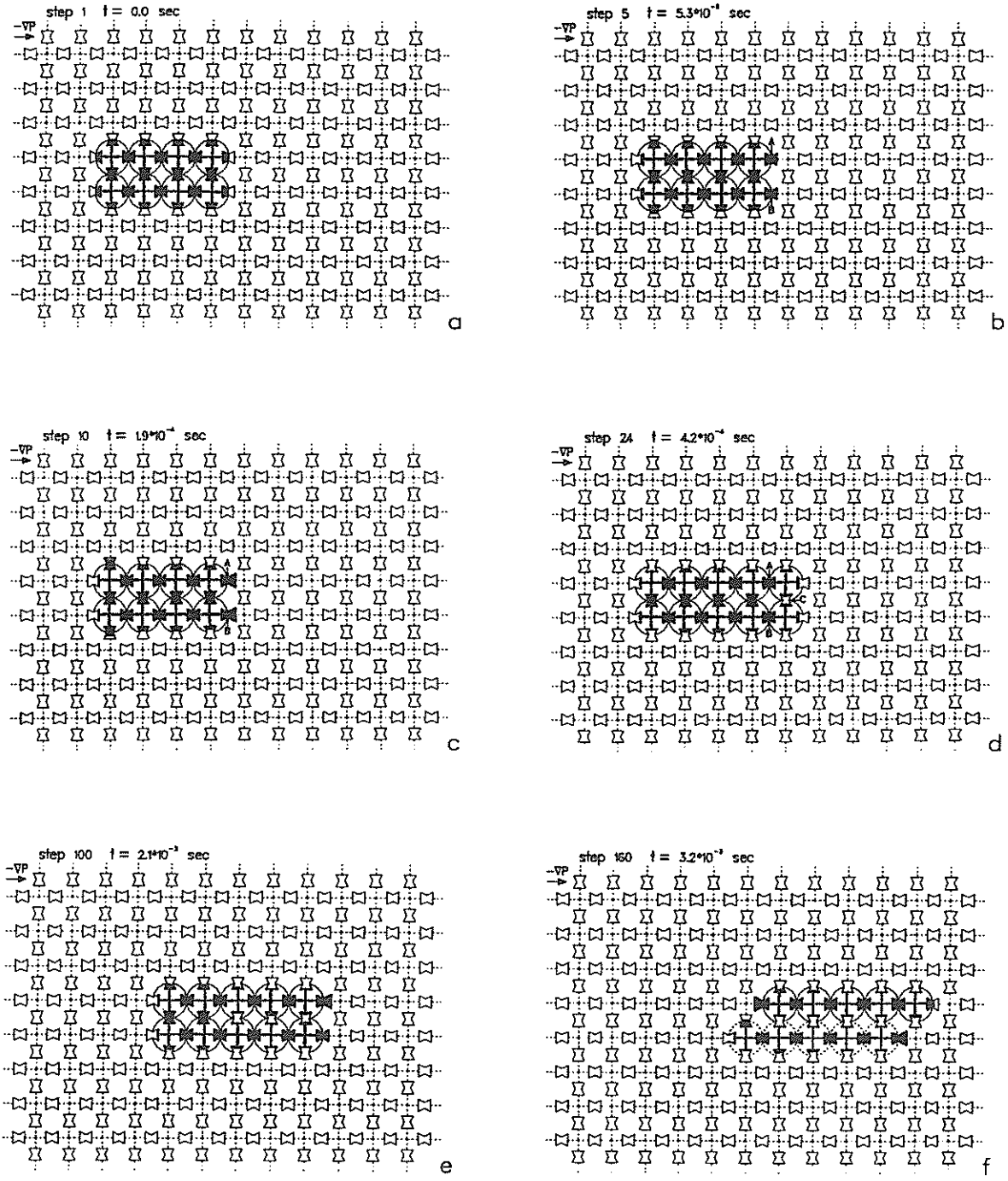


Figure 3.9

Stages of an 8-CEVS ganglion motion simulation. Occurrence of two simultaneous xerons into CEVS's sharing a same unit cell.

neous xerons and the formation of yet another gate unit cell with two interfaces can be seen. As will be discussed in Chapter 4, this process will lead to the eventual breakup of the ganglion into two similar daughter ganglia (Figure 3.9f).

3.7.1.3 Xeron into a CEVS sharing a GUC with another CEVS

Consider now the 9-CEVS ganglion pictured in Figure 3.10, and concentrate on unit cell A. Figure 3.10b. which is filling with oil according to the established motion rules. Later on this unit cell fills completely with oil (Figure 3.10c) and proceeds by considering the extended unit cell (Figure 3.10d). Because the immediately downstream CEVS shares a GUC (unit cell C, Figure 3.10c) with the adjoining CEVS, when the xeron occurs, this gate unit cell becomes a GUC with two interfaces, similarly to the case in Figure 3.9. Again, these two interfaces are not allowed to coalesce, and the ganglion proceeds forming new gate unit cells with two interfaces (Figure 3.10e) and eventually breaking-up (Figure 3.10f).

To be consistent with the non-coalescence criterion the following rule is assumed. The oil that goes into an already formed GUC by occurrence of a xeron is always calculated so that the two interfaces are at least one compartment apart. Since both interfaces always move in the same direction, this insures that they will never come closer to each other than one compartment; that is, collision of two menisci is not allowed.

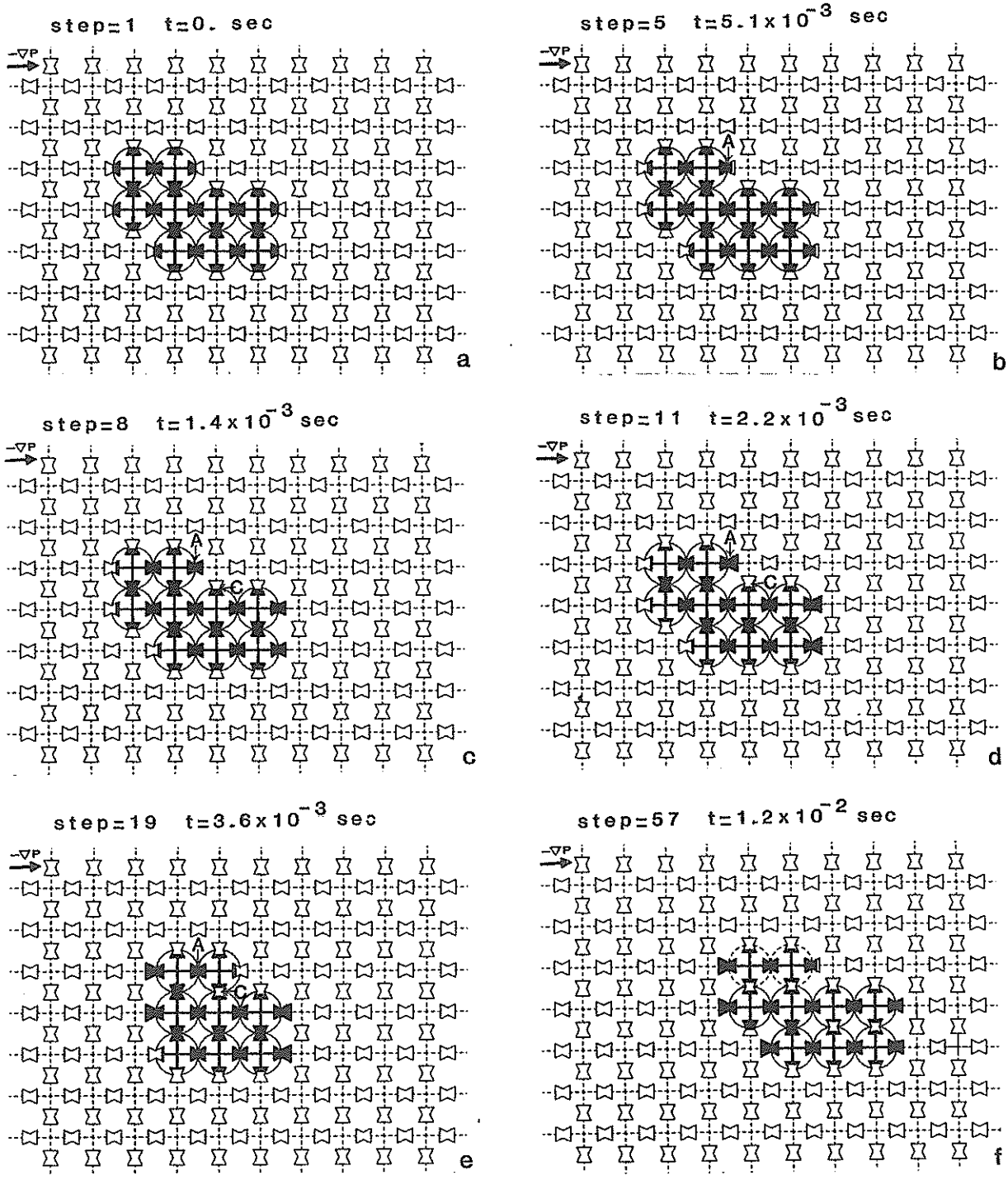


Figure 3.10

Stages of a 9-CEVS ganglion motion simulation. Occurrence of a xeron into a CEVS sharing a GUC with another CEVS.

3.7.2 Treatment of Hygrons. Interface Rupture Criterion

3.7.2.1 General Case

In order to decide on the fate of an oil-water interface when the gate unit cell becomes emptied of oil, a similar analysis of an actual laboratory experiment will be done. Consider the 2-CEVS oil-ganglion represented in Figure 3.11a and consider the upstream-most gate unit cell A. As is shown in subsequent Figure 3.11b, the oil in this gate unit cell is receding, that is, the volume of oil is decreasing. If this decrease leads to a negative volume of oil in the unit cell in question, the time increment is adjusted so that unit cell A is now filled with water, Figure 3.11c. At the same time, unit cells B and C, which belong to the same CEVS as unit cell A, still contain some oil.

An analogous situation is seen in Figure 3.12 taken from the experimental work of Hinkley (1982). This sequence of photographs shows a 2-pore oil ganglion for which the upstream-most interface is about to leave pore G (Figure 3.12c), but there is still some oil left in both lateral connections. In the following photograph (Figure 3.12d), it is seen that the interface has now detached itself from the walls of the two upstream spheres. It proceeds in this way for some time (Figures 3.12d and 3.12e), until finally it leaves pore G (Figure 3.12f) completely.

This series of events is recreated by the simulation algorithm by placing an interface at the end of the oil-filled unit cell which is adjacent to the common node. This unit cell takes the form of an extended unit cell (D, Figure 3.11d), and it is partially filled with the oil contained in unit cells B and C (Figure 3.11c). At this

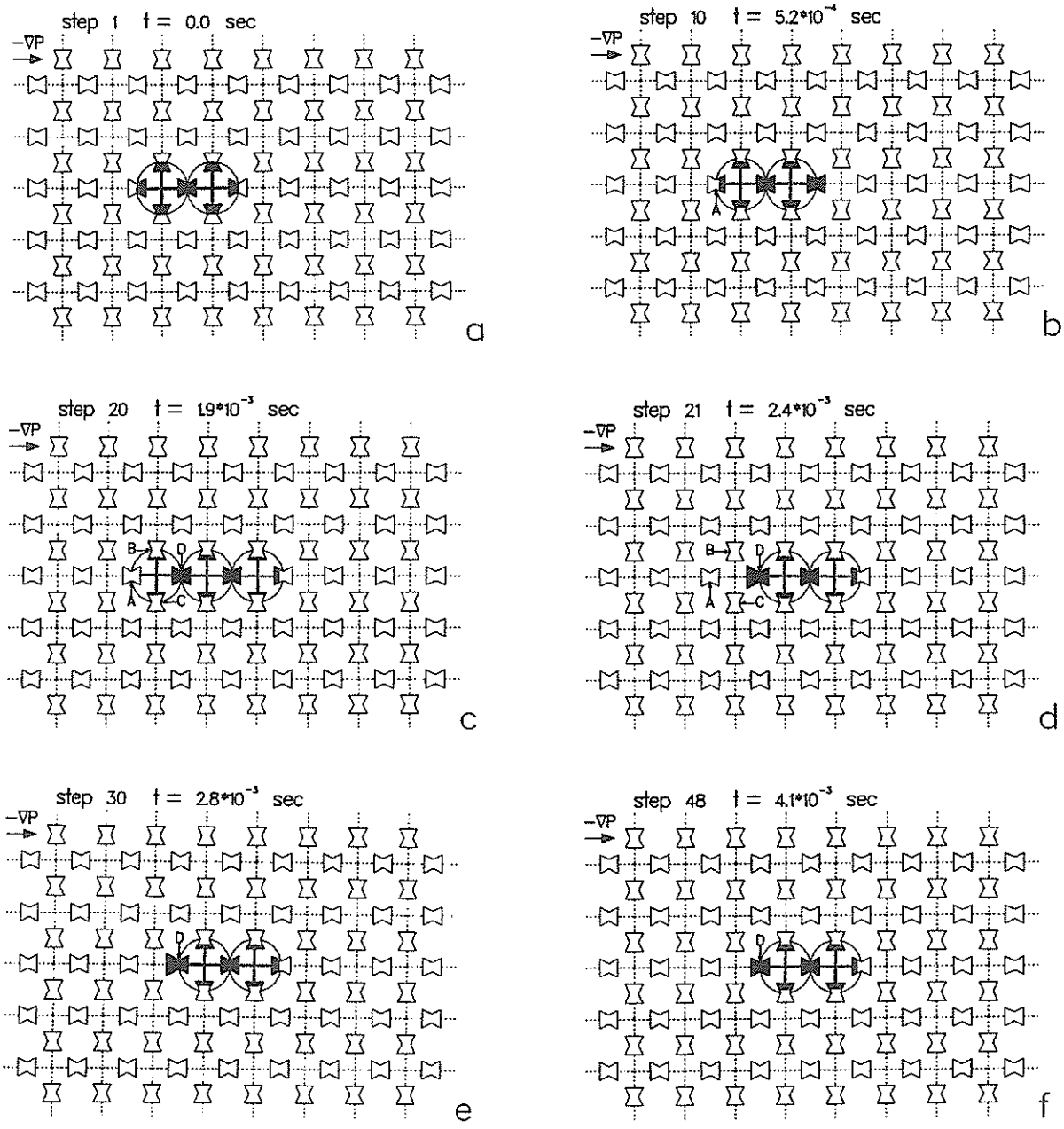


Figure 3.11

Stages of a 2-CEVS ganglion motion simulation. Occurrence of a hygron.

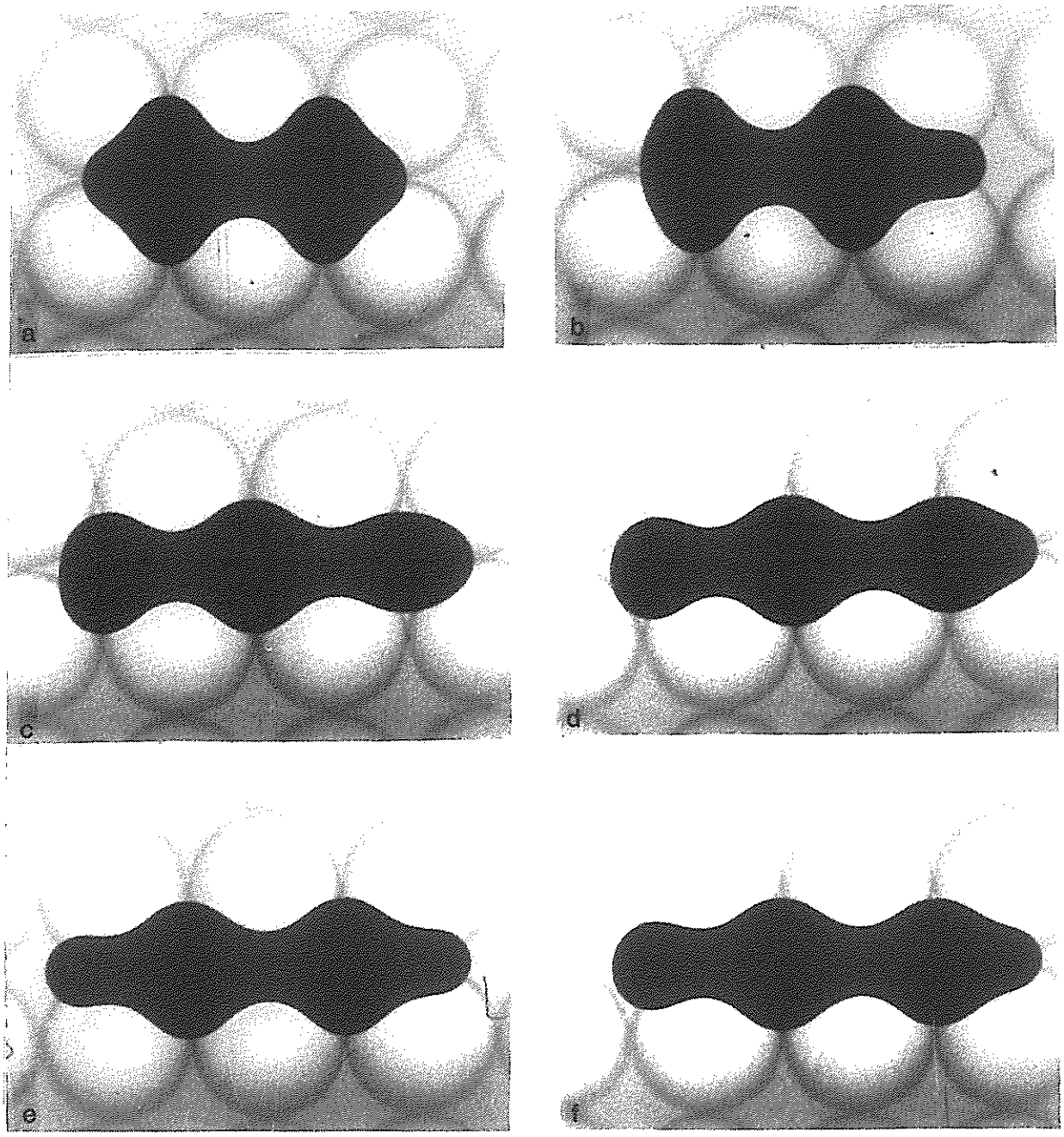


Figure 3.12

Sequential pictures of a moving 2-pore oil ganglion. Demonstration of a hygron. From Hinkley (1983).

point a *hygron* is said to have taken place. The simulation now proceeds as usual until finally the volume of oil in this unit cell is equal to or less than the volume of a regular unit cell, at which point the EUC shape is dropped (Figures 3.11e and 3.11f).

Figure 3.13 shows an example of a situation that commonly occurs for networks with random sized unit cells. Gate unit cell A fills with water (Figure 3.13b). The total volume of oil occupying unit cells B and C (Figure 3.13b) is larger than the excess volume corresponding to the EUC for unit cell D, so the hygron can not occur. This situation is solved by taking the total volume of oil contained in unit cells B and C and dividing it throughout all three unit cells A, B and C in proportion to their respective volumes (Figure 3.13c). The simulation proceeds, and later on, when unit cell A gets filled with water, the volume of oil occupying unit cells B and C is smaller than the excess volume corresponding to unit cell D (Figure 3.13e). At this point the hygron occurs (Figure 3.13f).

3.7.2.2 Criterion for Rupture of Oil Threads (Pinch-off)

Figures 3.14, 3.15, 3.16 and 3.17 illustrate some special cases where a gate unit cell becomes filled with water. In all four simulations the oil is receding in gate unit cell A (Figures 3.14b, 3.15b, 3.16b and 3.17b) until it finally gets filled with water (Figures 3.14c, 3.15c, 3.16c and 3.17c). Connected to the common CEVS there is only one other gate unit cell (unit cell B), and the other two unit cells are filled with oil and connected to the remainder of the ganglion (unit cells C and D). The oil in these two unit cells plus the oil remaining in gate unit cell B can be visualized as forming a thread connecting both parts of the oil ganglion. Figures 3.18 and 3.19

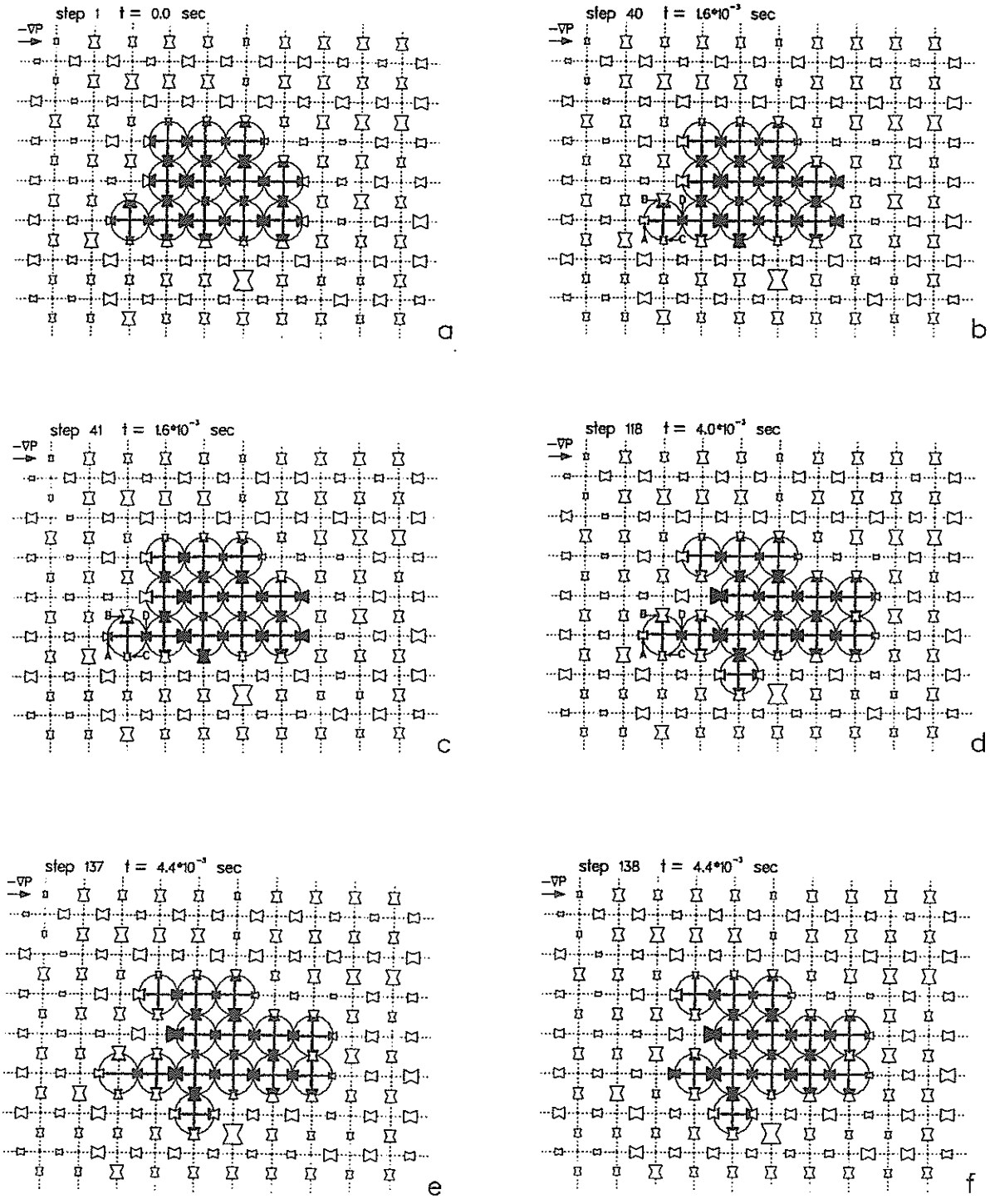


Figure 3.13

Stages of a 12-CEVS ganglion motion simulation. Occurrence of a hygron, after redistribution of oil.

show schematic representations of both situations in a porous medium. It is clear that at this point it has to be decided whether this thread of oil is going to rupture and two new interfaces form or whether the oil is going to "squeeze" through this thread.

Either one of these two events is likely to occur as is shown in Figures 3.20 and 3.21. These two figures show a sequence of photographs taken from movies made by Rapin (1980). The experimental apparatus consists of a single layer of glass beads of different sizes organized in a random configuration and held between two glass plates. In both figures, a thread of oil has been formed at the upstream side of the ganglion (Figures 3.20b and 3.21b), but in the first case this thread ruptures, resulting in breakup of the ganglion, whereas in the other case the oil retracts and follows the larger branch of the ganglion, thus avoiding breakup.

In order to determine the fate of this interface, a rough analysis of the local flow and pressure fields is done.

Consider Figures 3.18b and 3.19b, and determine the flow rates q_C and q_D for unit cells C and D. Two situations may occur. Either $q_C < 0$ and $q_D < 0$ (that is, the oil in both unit cells is flowing out of the common node) or $q_C < 0$ and $q_D > 0$ (conversely, $q_C > 0$ and $q_D < 0$) (that is, the flow in both unit cells is in the same direction). In the first case the interface ruptures, whereas in the second case an analysis of the local pressure field is necessary, in order to decide the issue. The analysis adopted is by needs approximate, based on the assumption of pseudostatic conditions.

The capillary pressure drop across the interface oil-water formed by the oil

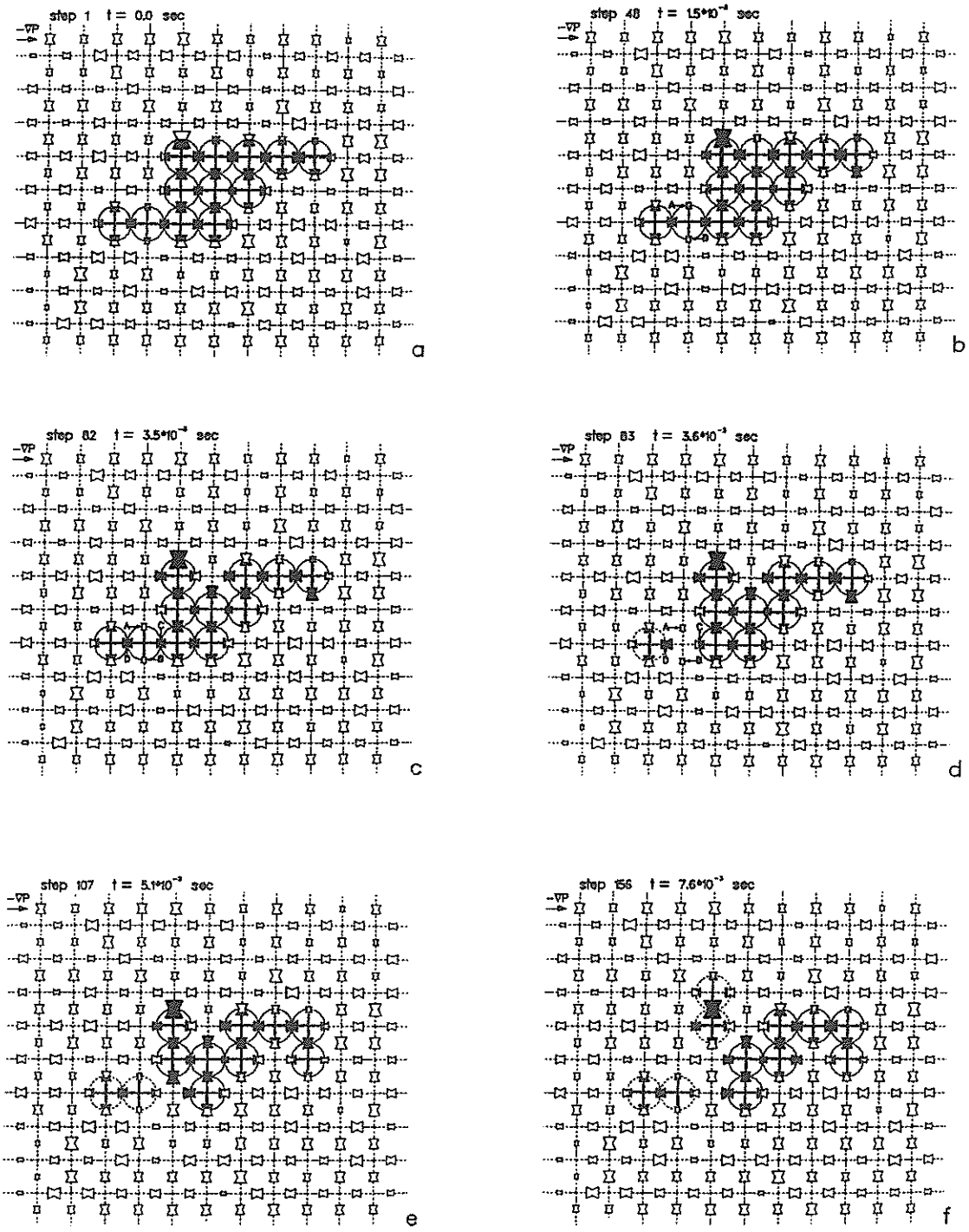


Figure 3.14

Stages of a 12-CEVS ganglion motion simulation. Formation of an oil thread with subsequent rupture of the interface.

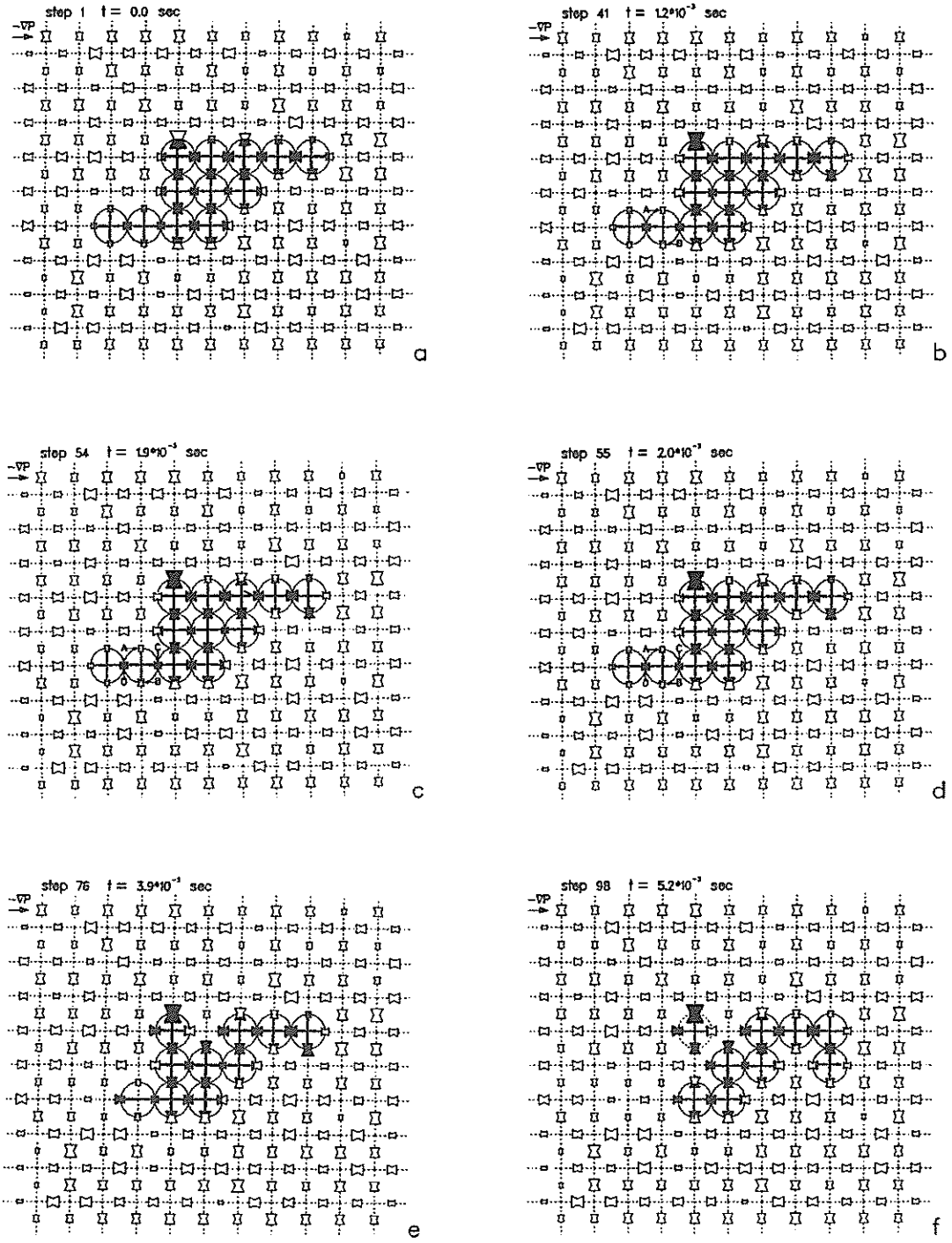


Figure 3.15

Stages of a 12-CEVS ganglion motion simulation. Formation of an oil thread without rupture of the interface.

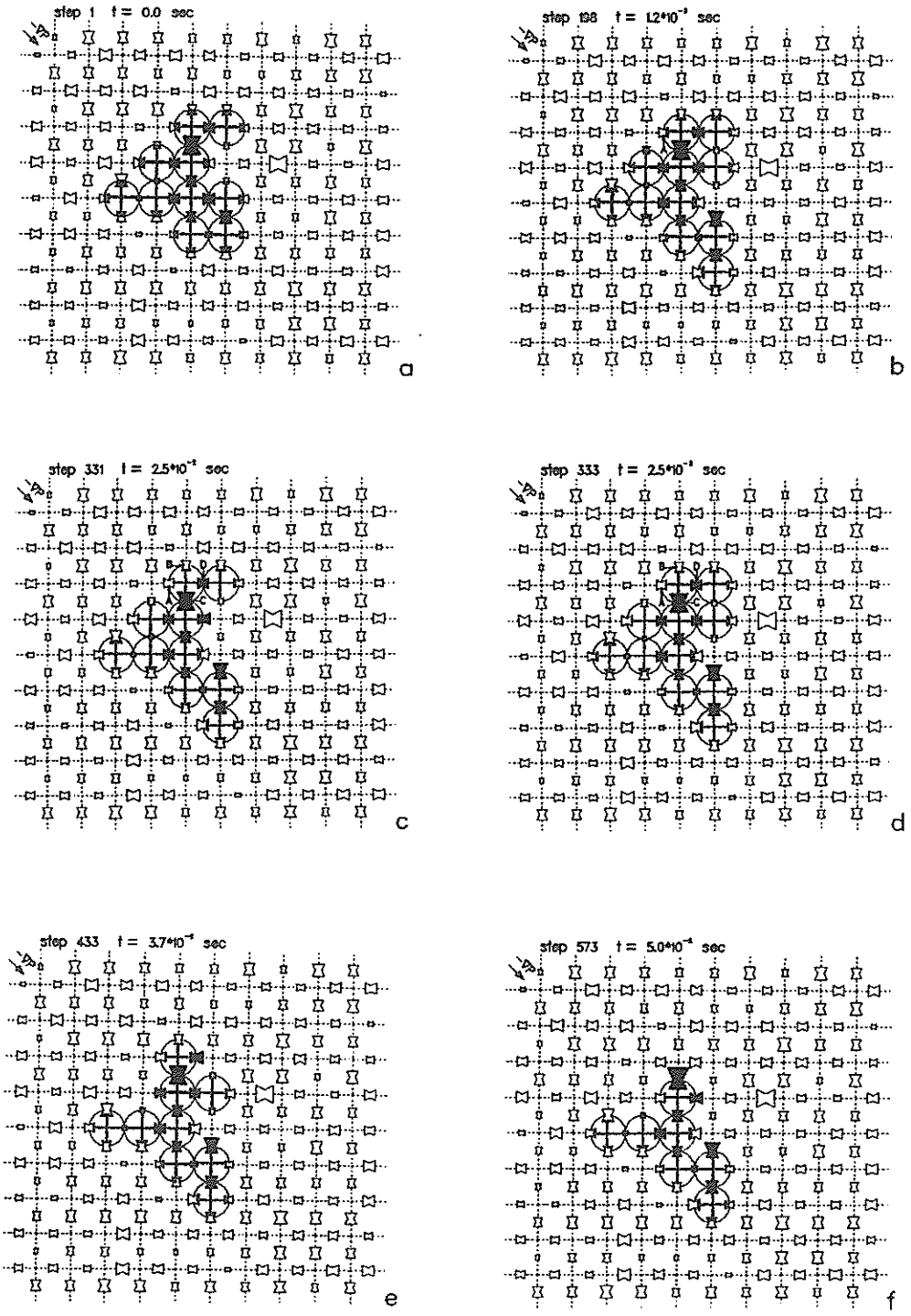


Figure 3.16

Stages of a 10-CEVS ganglion motion simulation. Formation of an oil thread surrounding a grain without rupture of the interface.

thread can be approximated by

$$\Delta P_c = \sigma_{ow} J_{neck} \ , \tag{3.34}$$

where,

$$J_{neck} = \left(\frac{1}{R_1} + \frac{1}{R_2} \right) \ , \tag{3.35}$$

and R_1 and R_2 denote the two principal radii of curvature for the interface.

Taking $\Delta P_{neck} = P_w - P_o$, where P_w and P_o are the local pressures of the aqueous and of the oleic phase respectively, then the thread ruptures if $\Delta P_{neck} > -\Delta P_c$, and if $\Delta P_{neck} \leq -\Delta P_c$, the oil squeezes through the thread. without breakup.

The criterion for thread rupture may be summarized as

$$\begin{cases} q_C < 0;\ q_D < 0 & \text{thread rupture occurs} \\ q_C < 0;\ q_D > 0;\ \Delta P_{neck} > -\Delta P_c & \text{thread rupture occurs} \\ q_C < 0;\ q_D > 0;\ \Delta P_{neck} \leq -\Delta P_c & \text{oil squeezes through thread.} \end{cases} \tag{3.36}$$

The two principal radii of curvature R_1 and R_2 may be estimated as follows. Consider first the case of Figure 3.18. Assume the oil thread to be a cylinder with diameter equal to the mean throat diameter between unit cells C and D. Then

$$\begin{cases} R_1 \to \infty \\ R_2 = \dfrac{1}{4}(d_C + d_D) \ , \end{cases} \tag{3.37}$$

where d_C and d_D are the throat diameters of unit cells C and D respectively.

In the second case, the oil thread is considered to have the shape of a cylinder curved around a grain of average diameter, $\langle d_g \rangle$. Then

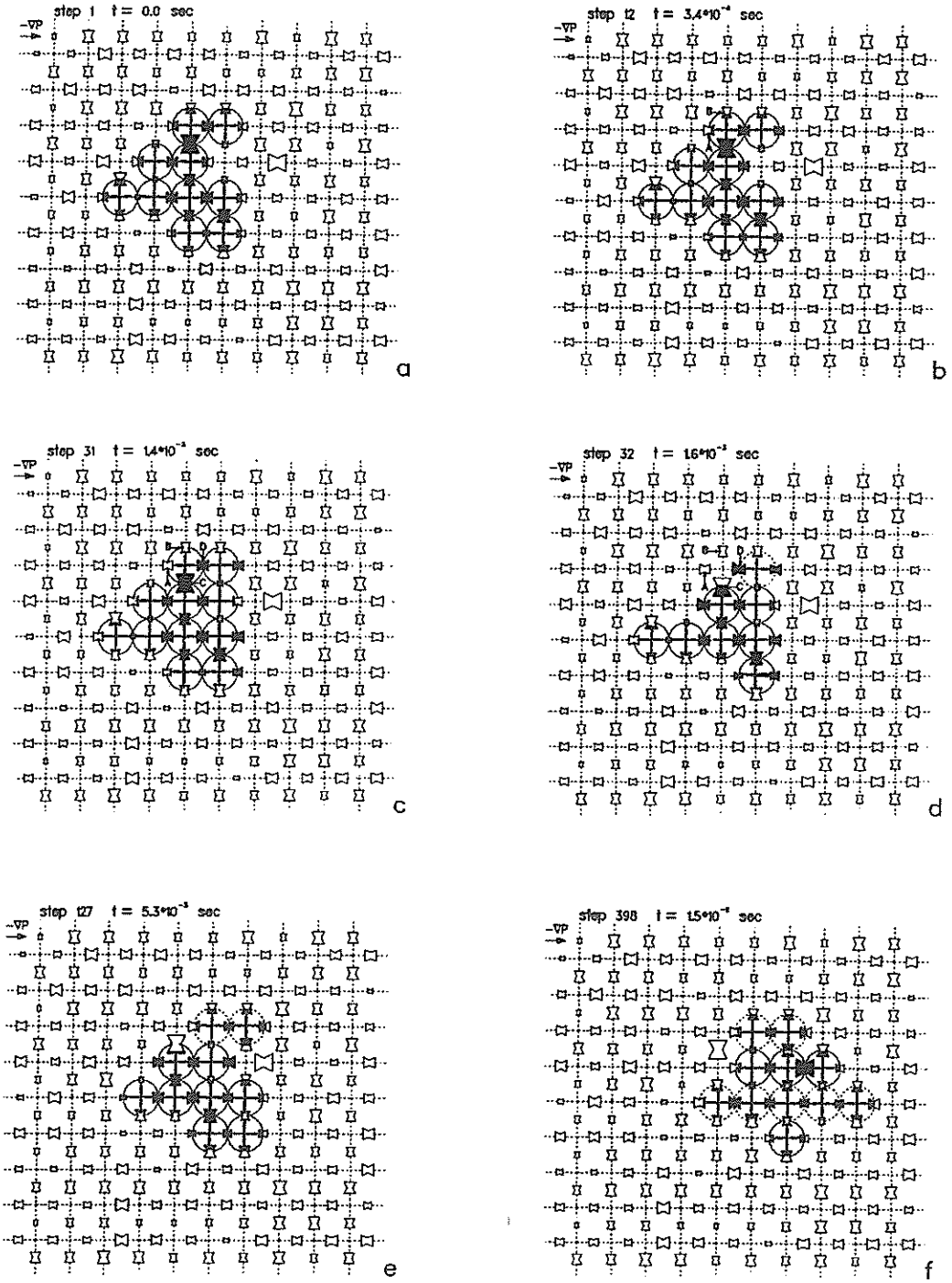


Figure 3.17

Stages of a 10-CEVS ganglion motion simulation. Formation of an oil thread surrounding a grain with subsequent rupture of the interface.

Figure 3.18

Schematic representation of an oil thread formed between two pores.

Figure 3.19

Schematic representation of an oil thread surrounding a grain.

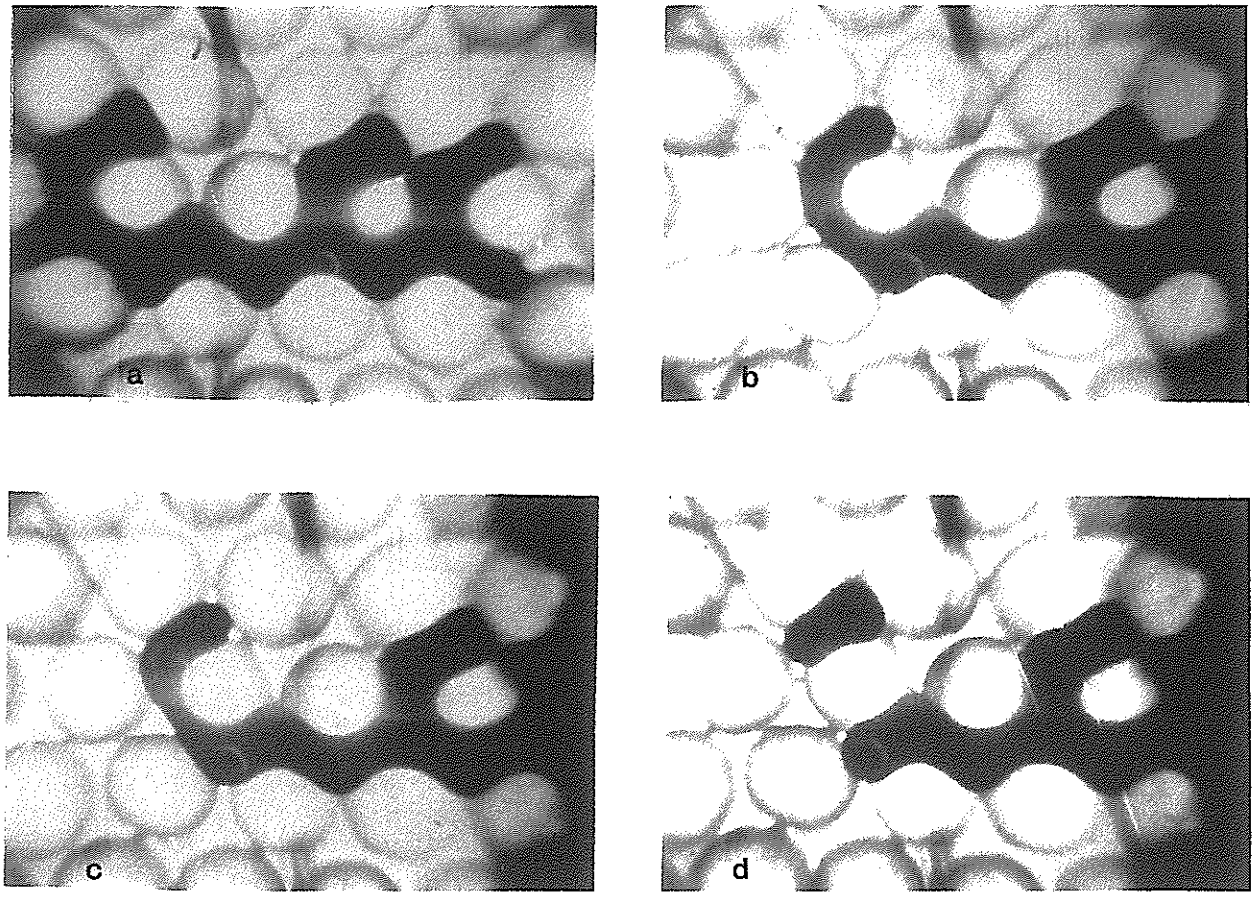


Figure 3.20

Sequential pictures of a moving oil ganglion. Demonstration of interface rupture with simultaneous breakup. From Rapin (1980).

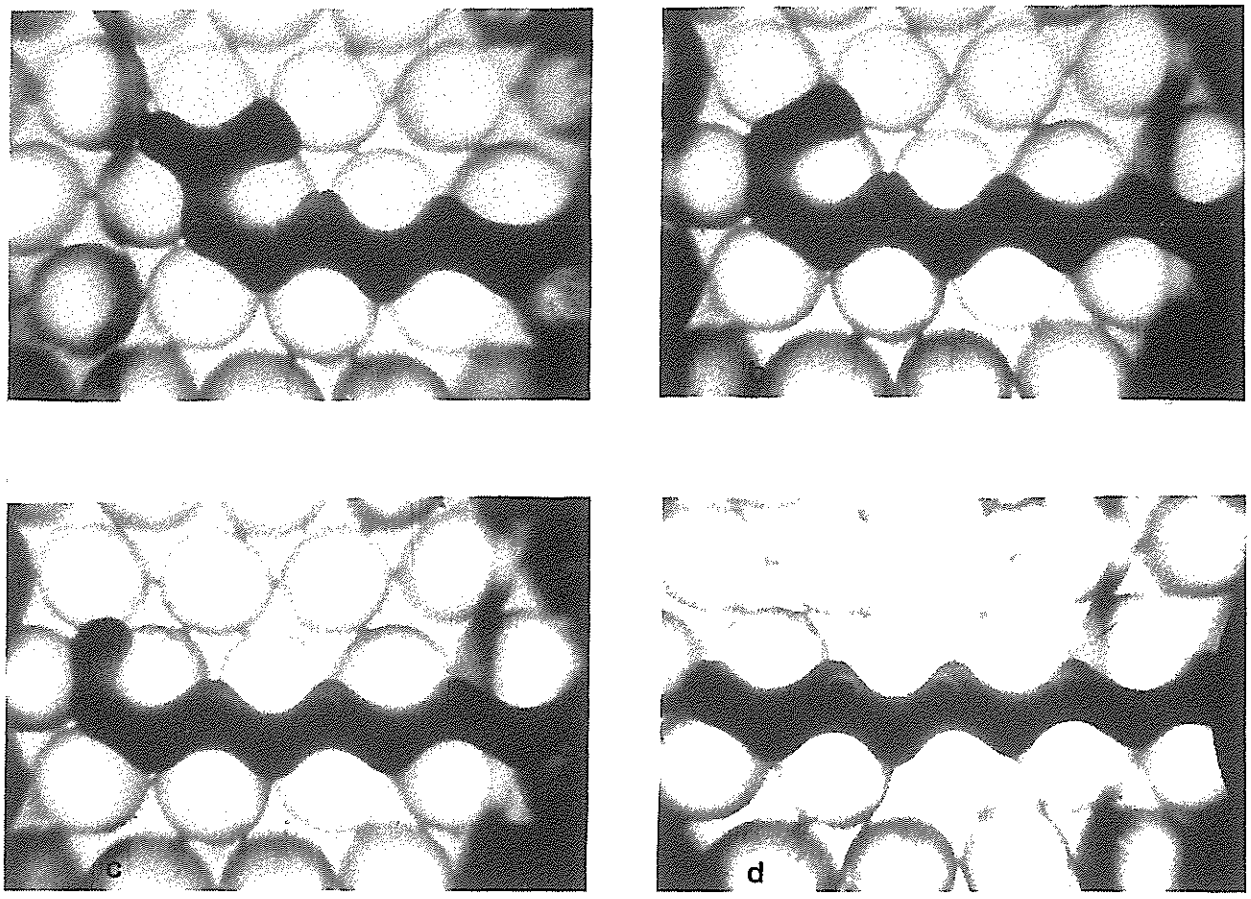


Figure 3.21

Sequential pictures of a moving oil ganglion. Demonstration of reconnection through an oil thread. From Rapin (1980).

$$\begin{cases} R_1 = \frac{1}{4}\left(d_C + d_D\right) \\ R_2 = \frac{1}{2}\left\langle d_g \right\rangle + \frac{1}{4}\left(d_C + d_D\right) . \end{cases} \tag{3.38}$$

Examples of all of the cases considered above are given in Figures 3.14 through 3.17.

The first one of these figures shows a 12-CEVS ganglion placed on a random network and moving subject to a macroscopic pressure gradient at a $\phi' = 90°$ angle from the x-axis. Figure 3.14b shows the ganglion some time after it started to move. Both gate unit cells A and B are filling with water. In Figure 3.14c, unit cell A has just been completely filled with water, and there is still some oil left in gate unit cell B. The oil in unit cell C is flowing out of the common node, while the flow in unit cell D is towards the common node, that is both flows have the same direction. When the quasistatic criterion is applied, it turns out that $-\Delta P_c < \Delta P_{neck}$, and the interface ruptures. Two new interfaces are placed at both unit cells C and D resulting (necessarily) in the formation of two daughter ganglia (Figure 3.14d). The smaller daughter ganglion rearranges its shape and, having found a stable configuration, becomes stranded (Figure 3.14e). The larger ganglion continues to progress in the porous medium and eventually breaks into smaller ganglia that in turn become stranded (Figure 3.14f).

Figure 3.15 shows a simulation under conditions similar to the previous case, except for a slight difference in the distribution of throat sizes. As the ganglion advances through the porous medium (Figures 3.15a and 3.15b), gate unit cells A and B get emptied of oil until gate unit cell A becomes filled with water (Figure 3.15c). Following the same procedure as before, it turns out that the flows in unit cells C

and D again have the same direction, but now the estimation of the capillary pressure across the thread results in $-\Delta P_c > \Delta P_{neck}$. At this point the volume of oil in gate unit cell B is redistributed through gate unit cells A and B (Figure 3.15d) and the simulation allowed to continue, until later the portion of oil downstream of the thread rejoins the main part of the ganglion (Figure 3.15e). Unfortunately, in this particular case the ganglion ends up breaking at another interface (Figure 3.15f).

A situation where an oil thread is formed surrounding a grain is shown in Figures 3.16 and 3.17. The motion of a 10-CEVS oil ganglion is followed in both figures. The ganglion is placed in a random network, in the first case the macroscopic pressure gradient direction is at $\phi' = 45^{\circ}$. and for the second one $\phi' = 90^{\circ}$. Gate unit A fills with water while gate unit cell B still contains some oil (Figures 3.16c and 3.17c). Again. the thread rupture criterion has to be applied.

In the case of Figure 3.16, it turns out that the flow in both unit cells C and D is in the same direction (towards the main part of the ganglion), and the second criterion results in $-\Delta P_c < \Delta P_{neck}$; that is, the thread does not rupture. The oil in gate unit cell B is then divided through gate unit cells A and B (Figure 3.16d), and the simulation continues. A few steps later the oil reconnects, thus avoiding breakup (Figures 3.16e and 3.36f).

The calculation of the flow rates through unit cells C and D in the case of Figure 3.17c leads to different directions of flow, and the interface ruptures. Two new interfaces are placed at unit cells C and D, and two new ganglia are formed (Figure 3.17d). The smaller ganglion undergoes another xeron after which it becomes stranded (Figure 3.17e), while the larger one continues to move until it finally breaks into other daughter ganglia (Figure 3.17f).

In the example of Figure 3.14 the formation and subsequent rupture of a thin thread resulted in the breakup of the ganglion. This is usually the case; that is, whenever a linear thread is formed and it ruptures, breakup usually occurs. In the case of the formation of a thread around a grain, rupture without ganglion breakup is often observed.

An example of thread rupture without breakup can be seen in Figure 3.22. In this case, the motion of a 10-CEVS ganglion through a uniform network is followed. Gate unit cell A becomes filled with water (Figure 3.22c) while some oil is still left in gate unit cell B. Using the interface rupture criterion, rupture results. Unit cells C and D take the form of extended unit cells, and the oil left in unit cell B is divided through them according to their respective sizes and instantaneous flow rates (Figure 3.22d). A hygron has taken place, and the simulation proceeds until the volume in these extended unit cells is equal to or less than the volume of the corresponding unit cell, at which point the EUC's are dropped (Figures 3.22e and 3.22f).

3.8 Computational Aspects

A summary of the simulation algorithm is presented below, followed by a block diagram of the structure of the computer code. A listing of the computer code written in FORTRAN 77 is given in Appendix A. Input variables and other variables considered important for the understanding of the program are described, together with a short explanation of each subprogram.

The size of the network, N_x and N_y , and the number of compartments, N_c ,

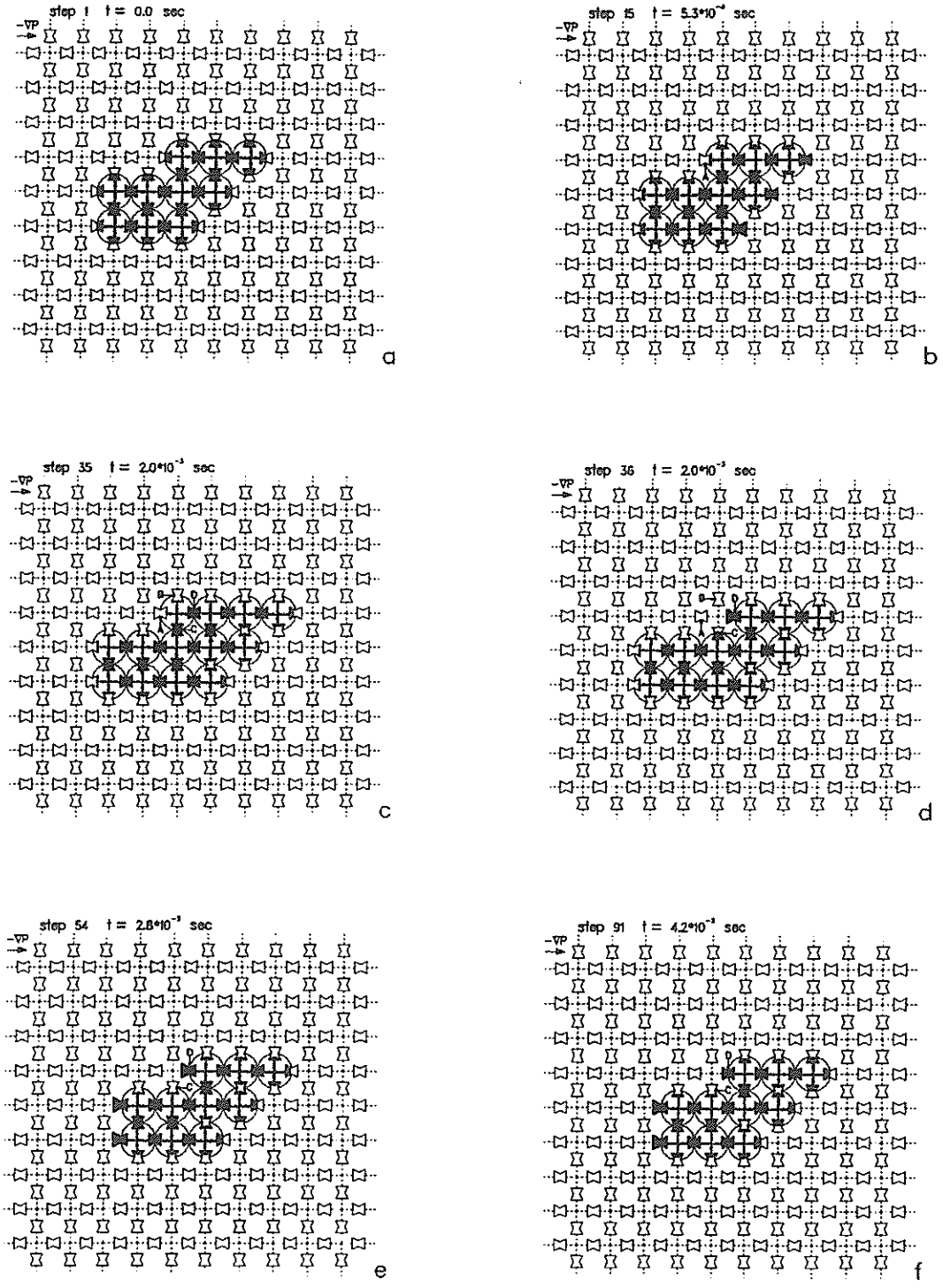


Figure 3.22

Stages of a 10-CEVS ganglion motion simulation. Example of reconnection through an oil thread.

in which each unit cell is divided, are of great importance in the determination of computation times. In Sections 3.8.3 and 3.8.4 these parameters will be discussed in order to determine the values that will give a good accuracy together with reasonable computation times.

3.8.1 Simulation Algorithm

1. Specify porous medium model constants and throat size distribution function.
2. Specify network size, number of compartments, macroscopic pressure gradient direction, random number generator seed, etc.
3. Specify equilibrium contact angle and parameters to calculate advancing and receding dynamic contact angles.
4. Assign sizes to all unit cell throats.
5. Partition unit cells in compartments and calculate volume, position and curvature of interface for each compartment. This is done for a dimensionless unit cell (see Appendix B).
6. Specify interfacial tension, viscosity of water and viscosity ratio and calculate conductances for a dimensionless unit cell filled with water and filled with oil and conductances for a dimensionless gate unit cell with the interface located at each compartment.
7. Specify the capillary number and the direction of the macroscopic pressure gradient.
8. Calculate single phase flow permeability and macroscopic pressure gradient magnitude.

9. Specify ganglion position and shape, as well as the volume of oil in each gate unit cell.
10. Determine conductances for all unit cells and the pressure drop across each interface for all GUC's.
11. Solve the network analysis equations to determine the voltage (pressure) at each node. Calculate the pressure drop along and the flow rate through each unit cell.
12. Calculate the time increment such that the interface in each gate unit cell advances or recedes, at most, to the next compartment.
13. Update the volume of oil in all GUC's, record the total time elapsed and calculate the coordinates of the ganglion center of gravity.
14. Apply breakup criterion and motion rules. If a unit cell is filled with or emptied of oil, apply motion rules. If a hygron or/and a xeron occurs update coordinates of ganglion. If breakup occurs, the simulation is usually stopped, unless the further behavior of the daughter ganglia is to be determined.
15. Iterate steps 10 through 14.

3.8.2 Block Diagram

Figure 3.23 shows a block diagram with the computer code structure without going into the details of the calculations or with the details pertaining to the various subprograms used. In order to facilitate the reading of this flow chart and its use with the FORTRAN code, identical labels are used in both listings, and some of the variables used in the code are also used in the block diagram. A full description

of these (and other) variables is given in Appendix A, but for convenience a short description is also given in Figure 3.23.

Two versions of the same program, one that calculates the average velocity of a ganglion and one that calculates the breakup coefficient, were also developed, and their listings are also given in Appendix A.

3.8.3 Choice of the Network Size

In the previous paragraphs it was seen that the node conductance matrix $\underline{\underline{Y}}$ (Equation 3.8), changes at each time step (the only exception being the case where $\kappa = 1$) along with the right-hand-side of Equation 3.8. the node current source vector, $\underline{q}_s$, thus making it necessary to invert or decompose matrix $\underline{\underline{Y}}$ at each step.

In Figure 3.24 is plotted the CPU time per step, t_{CPU}, (National Advanced Systems: AS/9000N computer) versus the total number of nodes N_p. A step corresponds to a change in position of the interface in each gate unit cell. As was expected, the computation time increases with N_p. For a given value of N_x, t_{CPU} changes linearly with N_p, and for a given N_p, the CPU time increases if N_x increases but decreases with an increase in N_y. This can be explained by the fact that the algebraic system of equations is to be solved in a band symmetric form with a band width equal to N_x. It becomes clear that if large networks (say $N_x > 20$, $N_y > 40$) are to be used the solution method should be improved, in order to reduce the computation time. The use of iterative solvers seems particularly well studied for this problem.

It is then apparent that the smallest possible network should be used, together with a small value for N_x. However, the network has to be considered of infinite

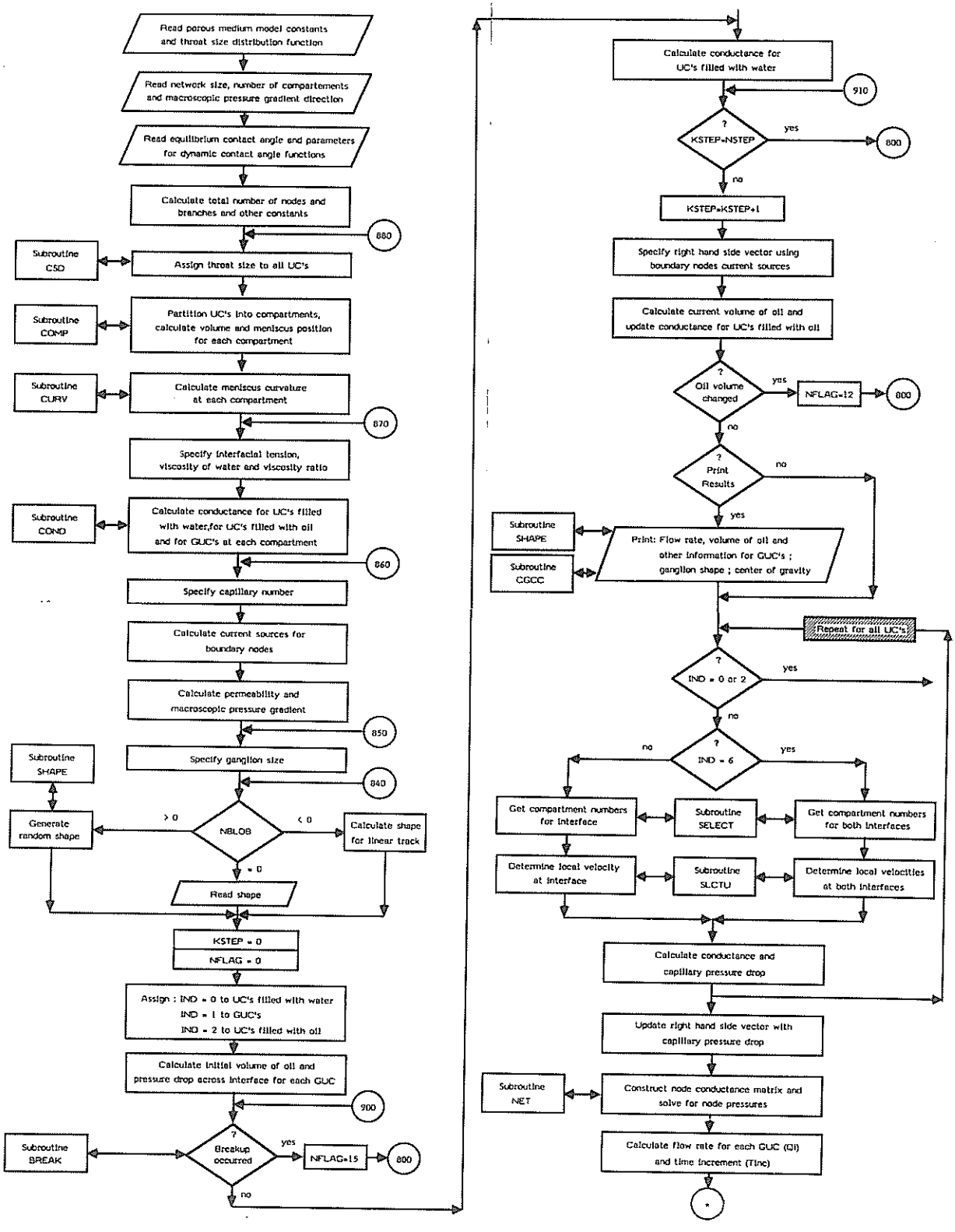


Figure 3.23

Block diagram of the ganglion dynamics simulation code.

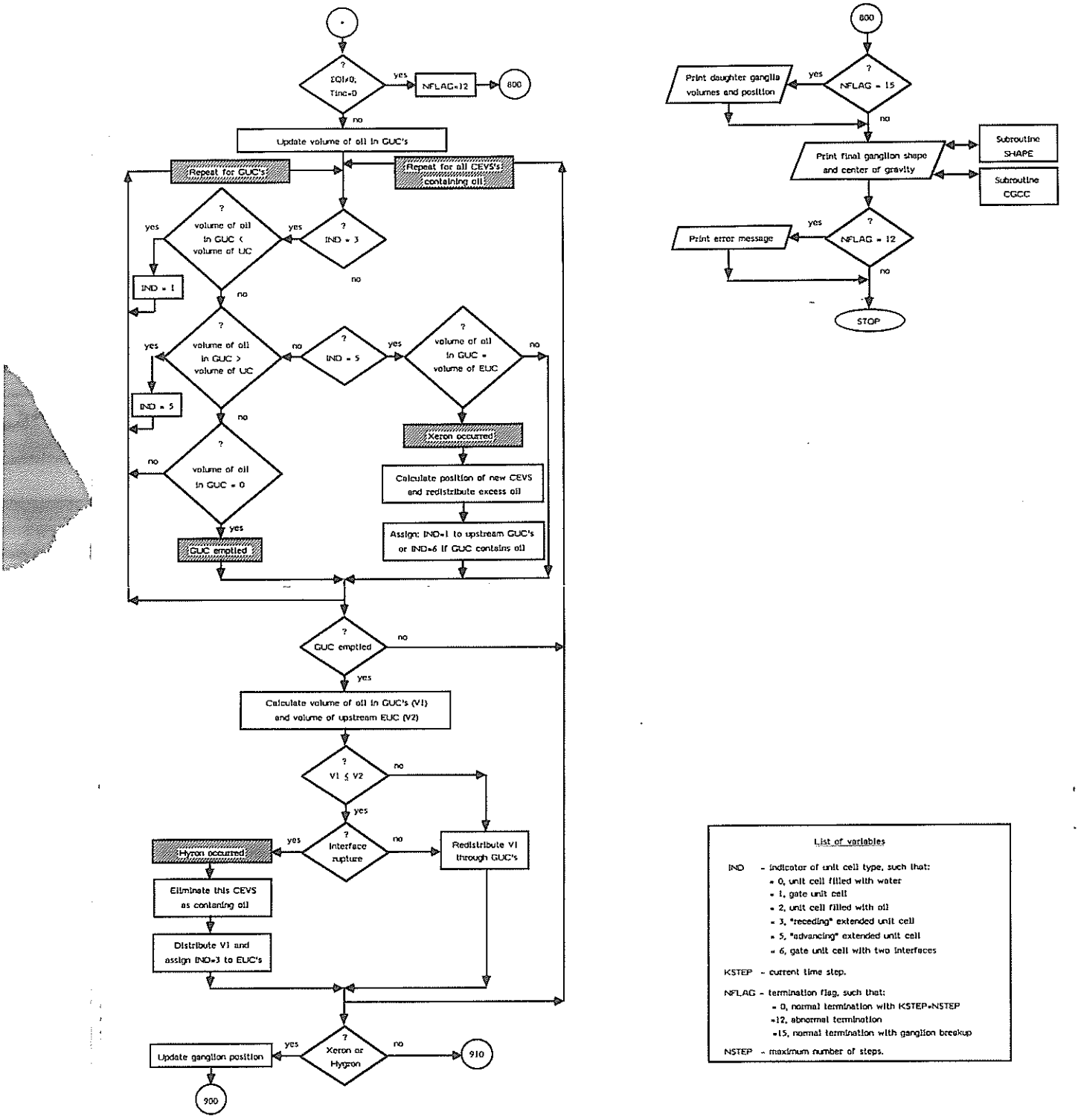


Figure 3.23 (continuation)

Block diagram of the ganglion dynamics simulation code.

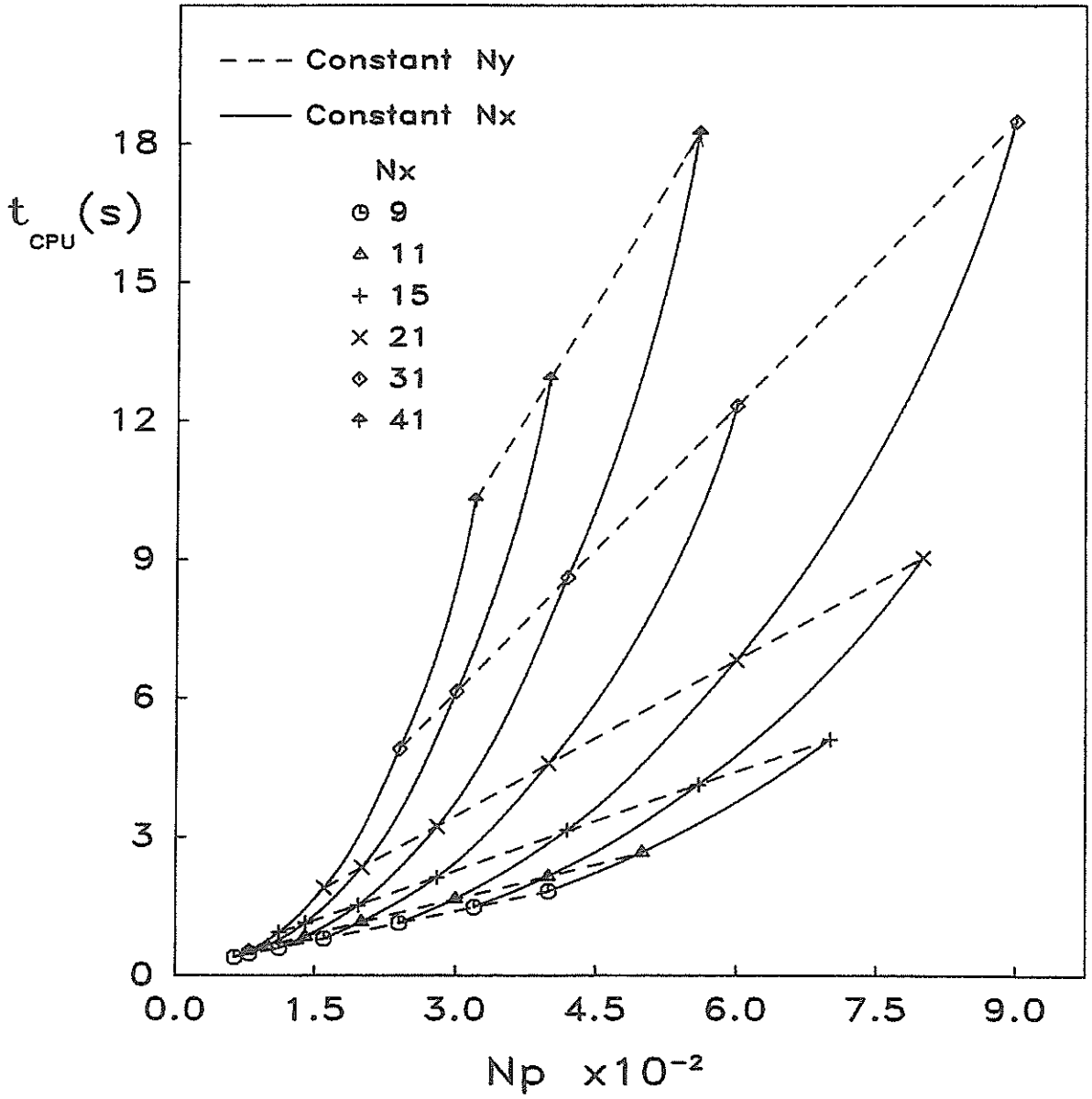


Figure 3.24

Plot of the CPU time per simulation step t_{CPU} *versus* the total number of nodes N_p.

dimension when compared with the size of an oil ganglion, so that its presence will not affect the network boundaries. The influence of an oil ganglion in the pressure field compared with the pressure field obtained with a single phase is shown in Figure 3.25. In this figure, ς is the reduced average radius of influence (normalized by ℓ, the length of periodicity of the network), and v^* is the reduced ganglion volume (ganglion volume v over v_{CEVS}, the average volume of a CEVS). The reduced average radius of influence was calculated by taking the maximum number of branches away from the centroid of the ganglion where its presence was no longer felt and averaging over several simulations with different ganglion shapes for a given ganglion size. As was expected, the radius of influence increases with the ganglion size, but in the range of sizes studied, this increase is not very pronounced. A good "rule of thumb" is to leave a margin of 5 to 6 branches from the ganglion to the boundaries.

3.8.4 Choice of the Number of Compartments

Because at each step an interface is allowed to move, at the most, up to the next compartment, it is obvious that the total number of steps in a particular simulation increases proportionally with the number of compartments, and so does the computation time. On the other hand, the quasi-steady-state assumption requires the pressure (flow) field to remain almost invariant from one step to the next, and this can only be assured if the number of compartments is large.

Figure 3.26 shows three simulations of an 8-CEVS ganglion placed in identical networks and initially with the same shape, carried out with different values of N_c. This is a typical situation in that it is seen that for $N_c < 10$ the qualitative behavior

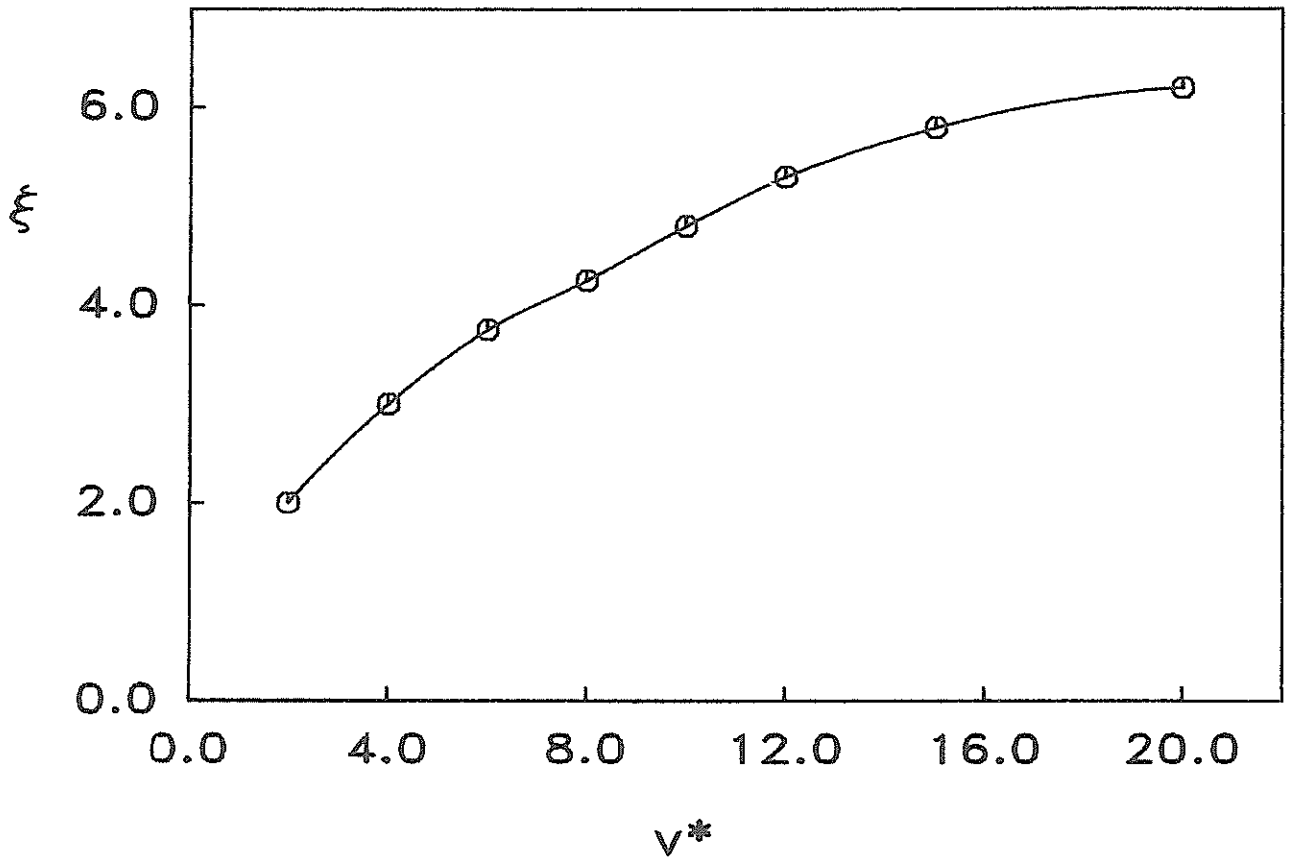


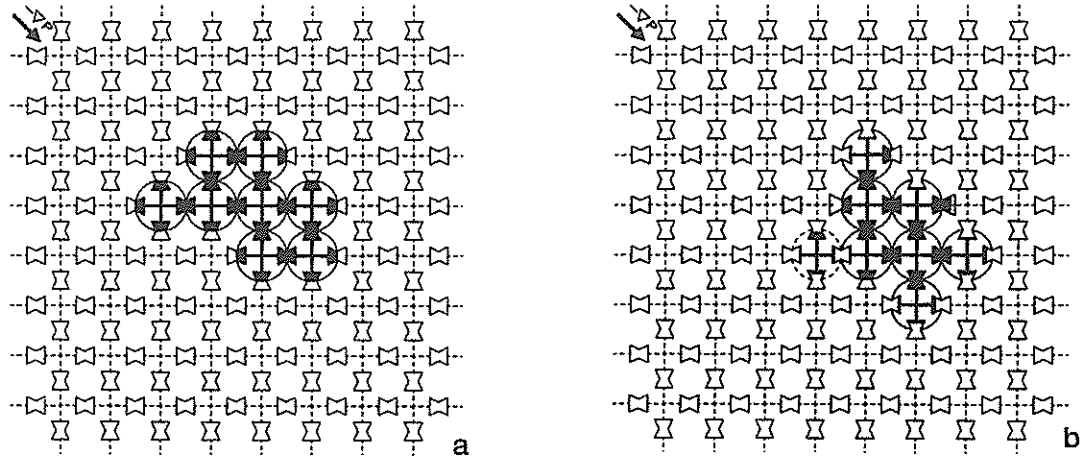
Figure 3.25

Plot of the normalized average radius of influence ς *versus* the reduced ganglion volume v^*.

of the ganglion changes somewhat from the one seen for $N_c \geq 10$.

The quantitative effect of the number of compartments can be seen in Figure 3.27. This figure plots the percent error in the reduced average velocity u^*, $E = (u^* - u^*_{40})/u^*_{40}$, ($u^* = \overline{u}_z/v_i$, where $\overline{u}_z$ is the time-averaged ganglion velocity and v_i is the mean interstitial velocity of the aqueous phase) relative to its value when $N_c = 40$, versus the number of compartments N_c for several values of the reduced ganglion volume v^* and $Ca = 10^{-4}$. The error comes to within 10% for $N_c = 10$ and within 1% when $N_c \geq 20$.

Based on the above verifications, in the present study a value of $N_c = 20$ was used for the calculation of u^*. For the calculation of the breakup coefficient ϕ (see Section 4.3), because it involves thousands of simulations and it is mostly dependent on the qualitative behavior of each ganglion, the number of compartments was set at $N_c = 10$.



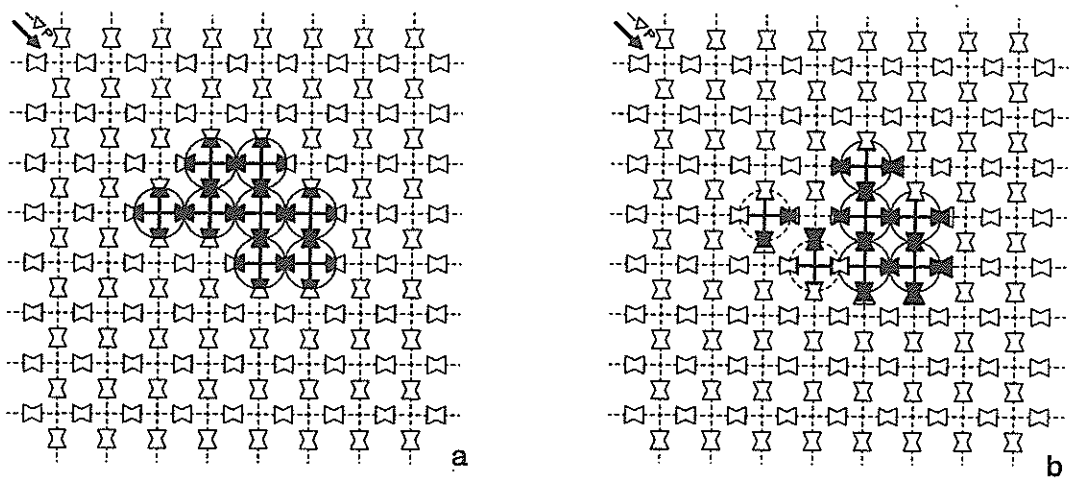


Figure 3.26

Example of influence of the number of compartments N_c on the qualitative behaviour of an 8-CEVS ganglion.

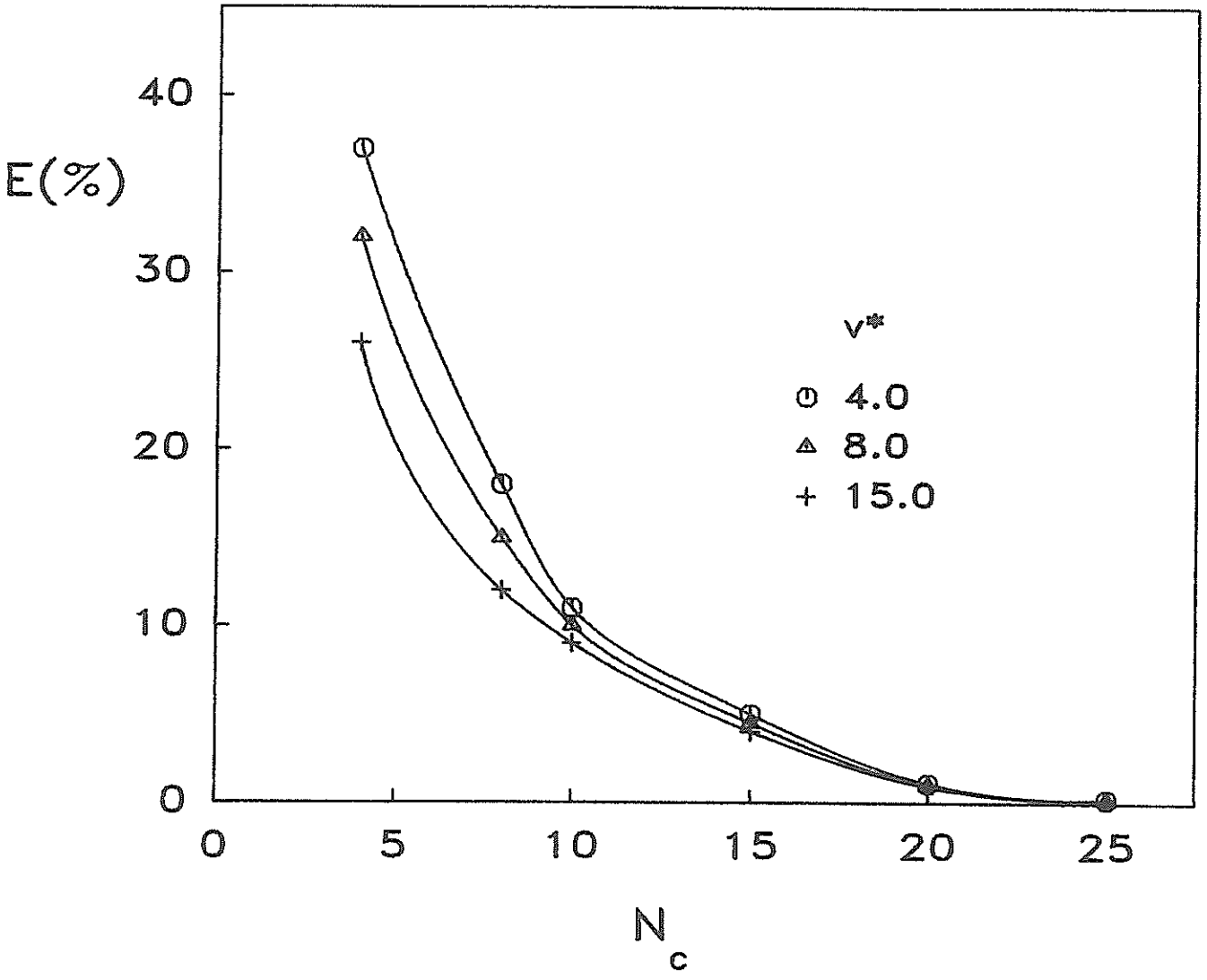


Figure 3.27

Plot of the percent error for u^*, $E = (u^* - u^*_{40})/u^*_{40}$, *versus* the number of compartments N_c for various values of v^* and $Ca = 10^{-4}$.

Chapter 4

Oil Ganglion Dynamics

4.1 Introduction

The study of the dynamics of individual oil ganglia provides information for the analysis of the collective behaviour of large populations of interacting ganglia (see Section 2.5).

The fate of a solitary oil ganglion can be simulated with the method developed in Chapter 3. Dimensional analysis shows that the mobilization (or stranding), the breakup, and the velocity of a solitary oil ganglion may depend on: the capillary number; the viscosity ratio; the size, shape and orientation of the ganglion; the contact angle; the local geometry of the porous medium: and the local value of the permeability.

In order to demonstrate the usefulness and applicability of the present model and in order to study both qualitatively and quantitatively the effect of each of the

variables listed above, simulations of the fate of a solitary oil ganglion in an infinite network were performed.

The effect of the geometry and the permeability of the porous medium value was investigated using two different networks.

The first represents a 100 × 200 sandpack as studied by Leverett(1941). The throat size distribution for this sandpack and other pertinent variables for the porous medium were obtained by Payatakes, Ng and Flumerfelt (1980), using the method developed in Payatakes, Tien and Turian (1973) and the data reported by Leverett (1941). The throat size probability distribution function for this porous medium is shown in Figure 4.1. Pertinent experimental and theoretical variables are given in Table 4.1. Note that the value of ΔP_1^* has taken from Tilton and Payatakes (1984). In this table is also reported the experimental absolute permeability, k, as well as its theoretical values as calculated by Payatakes, Ng and Flumerfelt (1980) and as calculated by the present model.

The second network is based on the two monolayer square beadpack apparatuses used by Hinkley (1982). Both apparatus consisted of a monolayer of spherical beads held in a square configuration between two glass plates. In one of the apparatus the flood direction was aligned with the longitudinal packing axis, whereas in the other one, the flood direction was parallel to the bisector of the angle of the packing axes. The porous medium constants were calculated based on geometrical considerations and data reported by Hinkley (1982) (see Appendix C), and are summarized in Table 4.2.

As is pointed out in Section 2.3.1, the complicated flow problem of moving contact lines is often treated in an approximate phenomenological way by considering

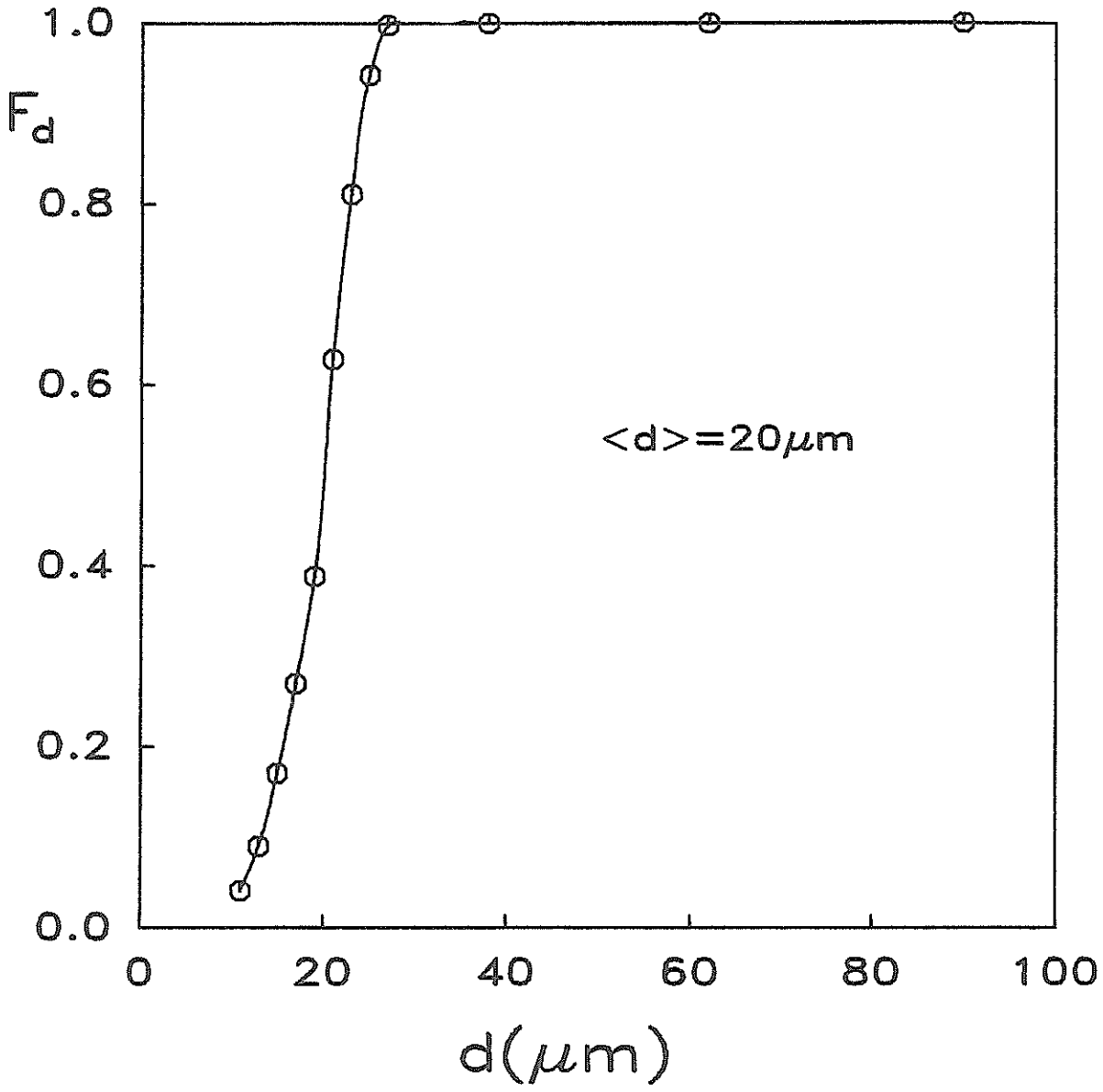


Figure 4.1

Plot of the throat size probability distribution function, $F_d(d)$. From Payatakes *et al* (1980).

Table 4.1

Experimental and theoretical analysis of a 100 × 200 sandpack. From Payatakes *et al* (1980).

Experimental		Theoretical	
ϵ	0.395		
microscopic analysis		unit cell geometry	
$\langle d_g \rangle, cm$	1.05×10^{-2}	c_1	4.16
$\langle d_g^3 \rangle, cm^3$	1.16×10^{-6}	c_2	5.25
		c_3	0.684
		ℓ, cm	0.010
initial drainage curve		collocation solution	
S_{wi}	0.09	r_1^*	0.095
$\langle d \rangle, cm$	2.00×10^{-3}	r_2^*	0.396
$\langle d^3 \rangle cm^3$	9.54×10^{-9}	$-\Delta P_1^*(r_1^*, r_2^*)$	194.26
k, cm^2	3.55×10^{-8}	k, cm^2 (Payatakes *et al*)	2.46×10^{-8}
		k, cm^2 (present work)	2.78×10^{-8}

Table 4.2

Experimental and theoretical analysis of the Monolayer Square Beadpack Apparatus used by Hinkley (1982).

Experimental		Theoretical	
ϵ	0.4764	c_1	2.16
$d_g\,, cm$	0.30	c_2	4.54
l, cm	0.30	c_3	0.50
S	0.22	$d\,, cm$	0.0979
		r_1^*	0.110
		r_2^*	0.238
		$-\Delta P_1^*(r_1^*, r_2^*)$	208.40
k, cm^2	1.0×10^{-4}	$k,\ cm^2$	8.9×10^{-5}
R_{min}	0.046	R_{min}	0.054
R_{max}	0.082	R_{max}	0.081

the motion of the interface as being controlled by the Young-Laplace equation,and by replacing θ by the apparent dynamic contact angle. The question may arise as to whether the rate-dependency of the dynamic contact angle and, furthermore, the hysteresis effect observed in the contact angle due to roughness of the solid wall, affect the fate of a solitary oil ganglion.

To investigate the effect of contact angle hysteresis, the advancing and receding contact angles for vanishingly small interface velocities, θ_a^o and θ_r^o respectively, are calculated based on the experimental work of Morrow (1975). Figure 4.2 shows the dependence of θ_a^o and θ_r^o on θ_e as reported by Morrow. Class I type behavior was obtained with a smooth surface for which the contact angle hysteresis was found to be extremely small. The behavior of Classes I and II was obtained with slightly roughened and well roughened surfaces, respectively.

Although the rate-dependency of the dynamic contact angle has been studied by several researchers, the experiments have been usually performed for liquid-gas systems rather than liquid-liquid systems as is the case in this work. Furthermore, these studies often contradict of each other in their findings and fail to provide a general correlation between the dynamic contact angle and the pertinent variables. A very careful set of experiments, including some liquid-liquid experiments, was obtained by Blake (1968). In this work, the following approach was taken. Figures 4.3 and 4.4 show examples of the dependency of the contact angle on the interface velocity, u_i , for two different values of the equilibrium contact angle, namely, $\theta_e = 10^\circ$ and $\theta_e = 30^\circ$. For each value of θ_e , four different cases are considered. In case (a) the contact angle is independent of the interfacial velocity and equal to its equilibrium value. Case (b) takes the advancing and receding contact angles to

be constant and equal to the hysteresis values as reported by Morrow for class II type behavior. Cases (c) and (d) take dynamic contact angles with different rates of dependency on the velocity of the interface, u_i. The maximum value for the contact angle is set at *ca* 47° so that, for the unit cell geometry corresponding to the 100 × 200 sandpack, it is ensured that the oil is the non-wetting phase.

Figure 4.5 shows the dynamic contact angle for an oil-brine system reproduced from Hinkley (1982) and used in conjunction with the simulations in the monolayer square beadpack network.

4.2 Individual Simulations. Motion and Fission

Various aspects of the behavior of mobilized oil ganglia can be obtained by averaging the results of a large number of simulations. In each simulation the initial shape of the ganglion is generated. There are no experimental data on the shape of oil ganglia at birth. Experimental and theoretical work (Ng, Davis and Scriven, 1978; Ng and Payatakes, 1980; Hinkley, 1982) show that although, during its short lifetime, each ganglion strives to acquire a preferred elongated configuration, at birth (through breakup of a large ganglia or coalescence of two smaller ones) its shape will be nearly arbitrary. Furthermore, it will be seen in Chapter 5 that ganglia created under dynamic displacement or imbibition conditions present various shapes.

In this work the initial ganglion shape is chosen randomly (unless otherwise indicated) by assigning oil to adjoining CEVS's at random, until a given volume of oil is obtained.

Of all factors affecting the fate of a solitary oil ganglion, the capillary number,

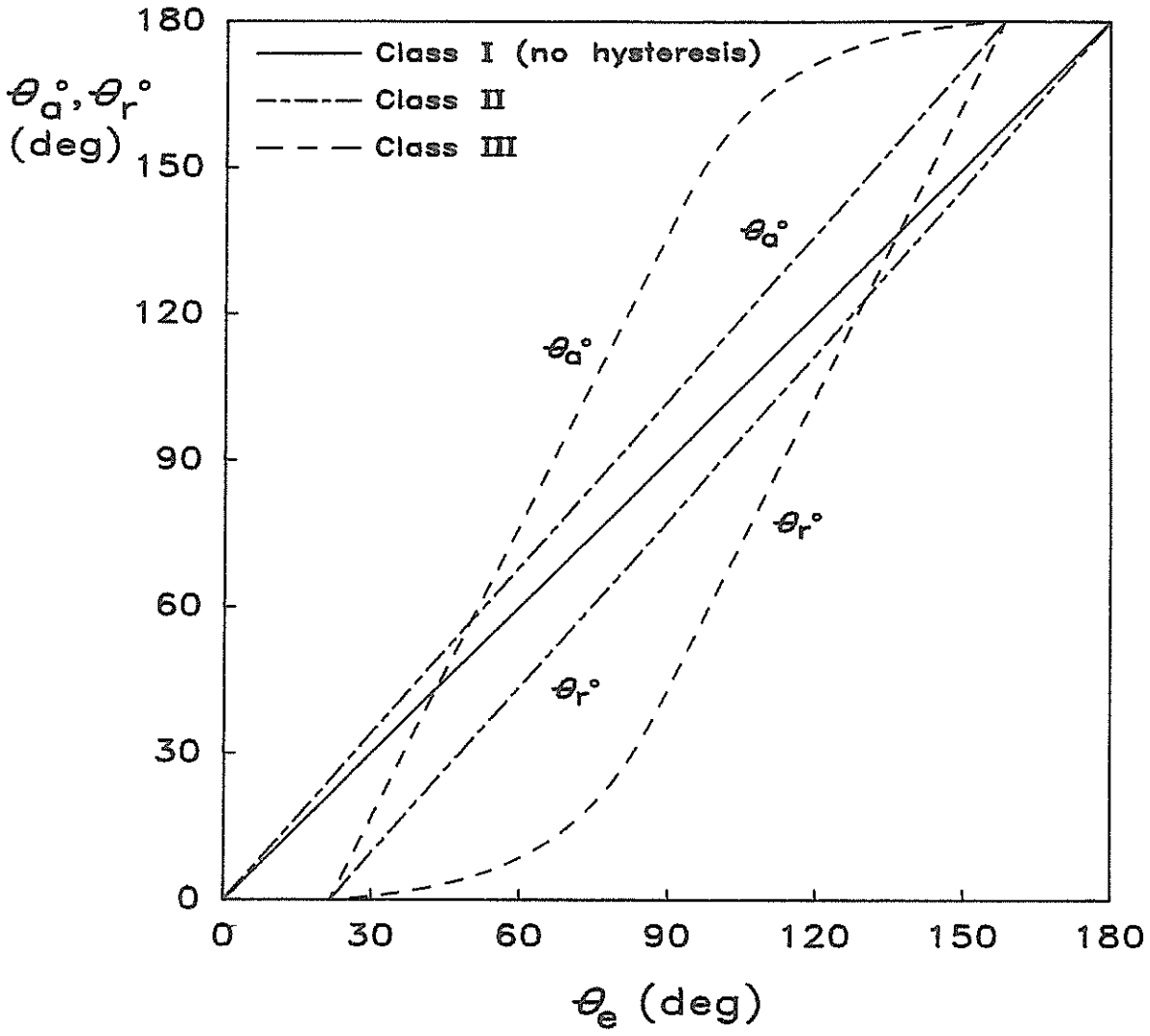


Figure 4.2

Dependence of the advancing contact angle, θ_a^o, and the receding contact angle, θ_r^o, on the equilibrium contact angle, θ_e, for various levels of surface roughness. From Morrow (1975).

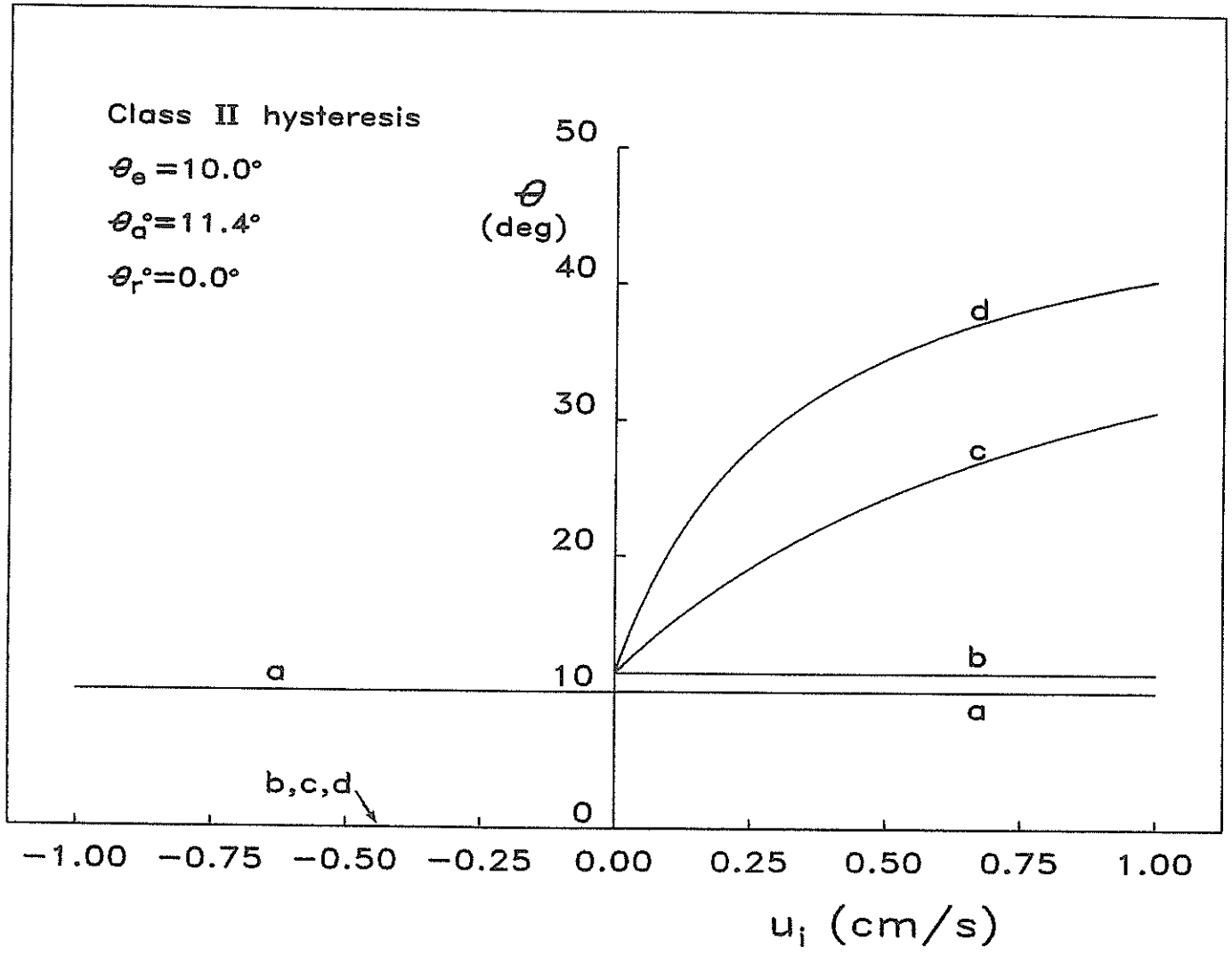


Figure 4.3

Dependence of the dynamic contact angle, θ, on the interfacial velocity, u_i, for $\theta_e = 10°$.

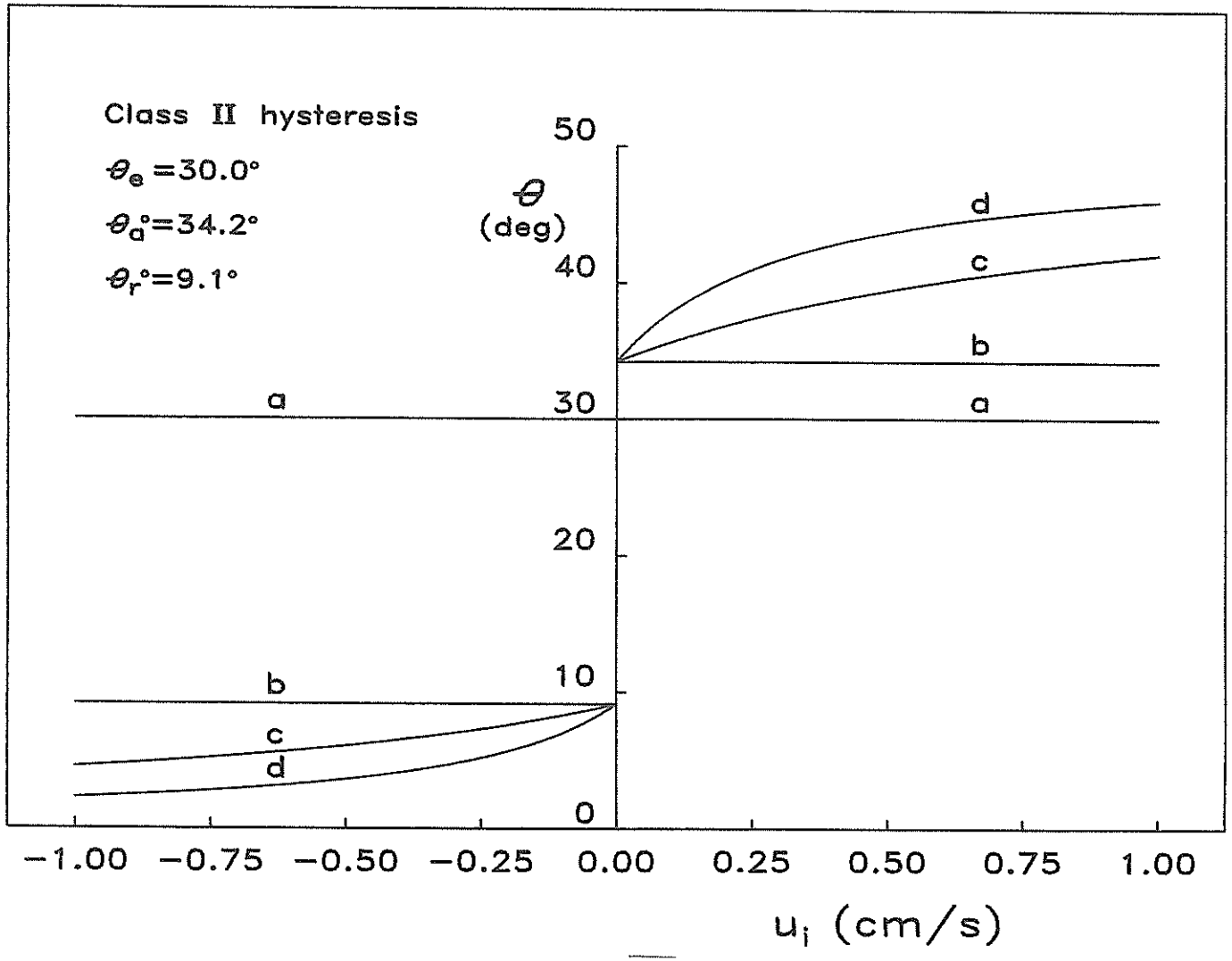


Figure 4.4

Dependence of the dynamic contact angle, θ, on the interfacial velocity, u_i, for $\theta_e = 30°$.

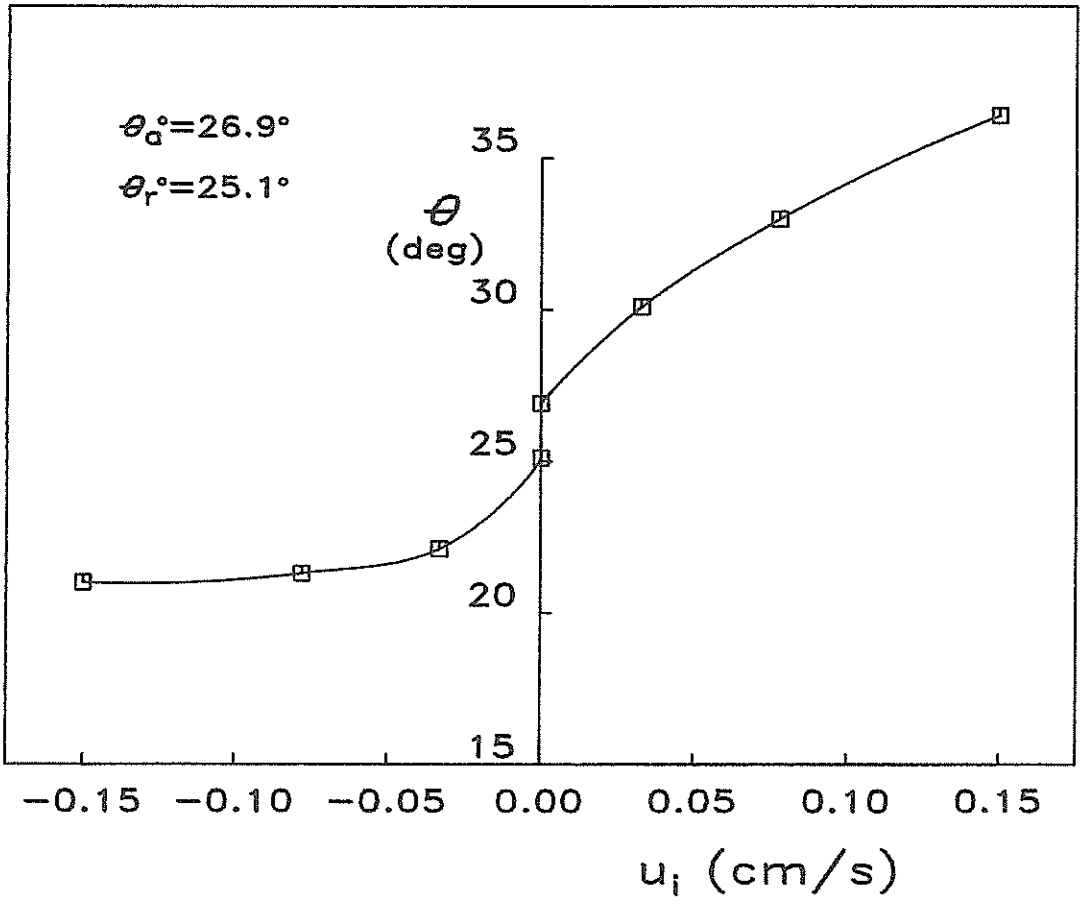


Figure 4.5

Dependence of the dynamic contact angle, θ, on the interfacial velocity, u_i, for an oil-brine system. From Hinkley (1983).

the viscosity ratio, the direction of the macroscopic pressure gradient, the topology of the porous medium and the contact angle influence the qualitative behavior of a solitary oil ganglion the most.

4.2.1 Influence of the Capillary Number

Consider the simulations shown in Figures 4.6 through 4.8. In order to isolate the effect of the capillary number, all three simulations were performed on the same random network, with a viscosity ratio of unity, perfect wetting conditions ($\theta_e = 0^\circ$), and the direction of the macroscopic pressure gradient set at 45°.

In Figure 4.6 the capillary number is set at a value just capable of inducing motion ($Ca \approx Ca_{cr}$). As it moves forward the ganglion elongates and aligns itself with the direction of the macroscopic pressure gradient. At a certain stage of the simulation, an oil thread is formed and the ganglion breaks in two daughter ganglia. The smaller ganglion gets stranded while the larger one continues to move forward. These observations are in close agreement with the characteristics of quasistatic displacement of ganglia stated by Ng and Payatakes (1980). This type of breakup, resulting solely from the rupture of an oil thread, is very common in quasistatic displacement, and so it is termed *quasistatic breakup*. It usually results in two differently sized daughter ganglia.

Figures 4.7 and 4.8 show the same ganglion subject now to dynamic displacement. In the simulation shown in Figure 4.7, the capillary number is set at a value roughly twice the critical value for mobilization. The ganglion now moves forward through two different interfaces simultaneously, forming two branches. Since coalescence is not allowed, this is an irreversible situation, and the ganglion eventually

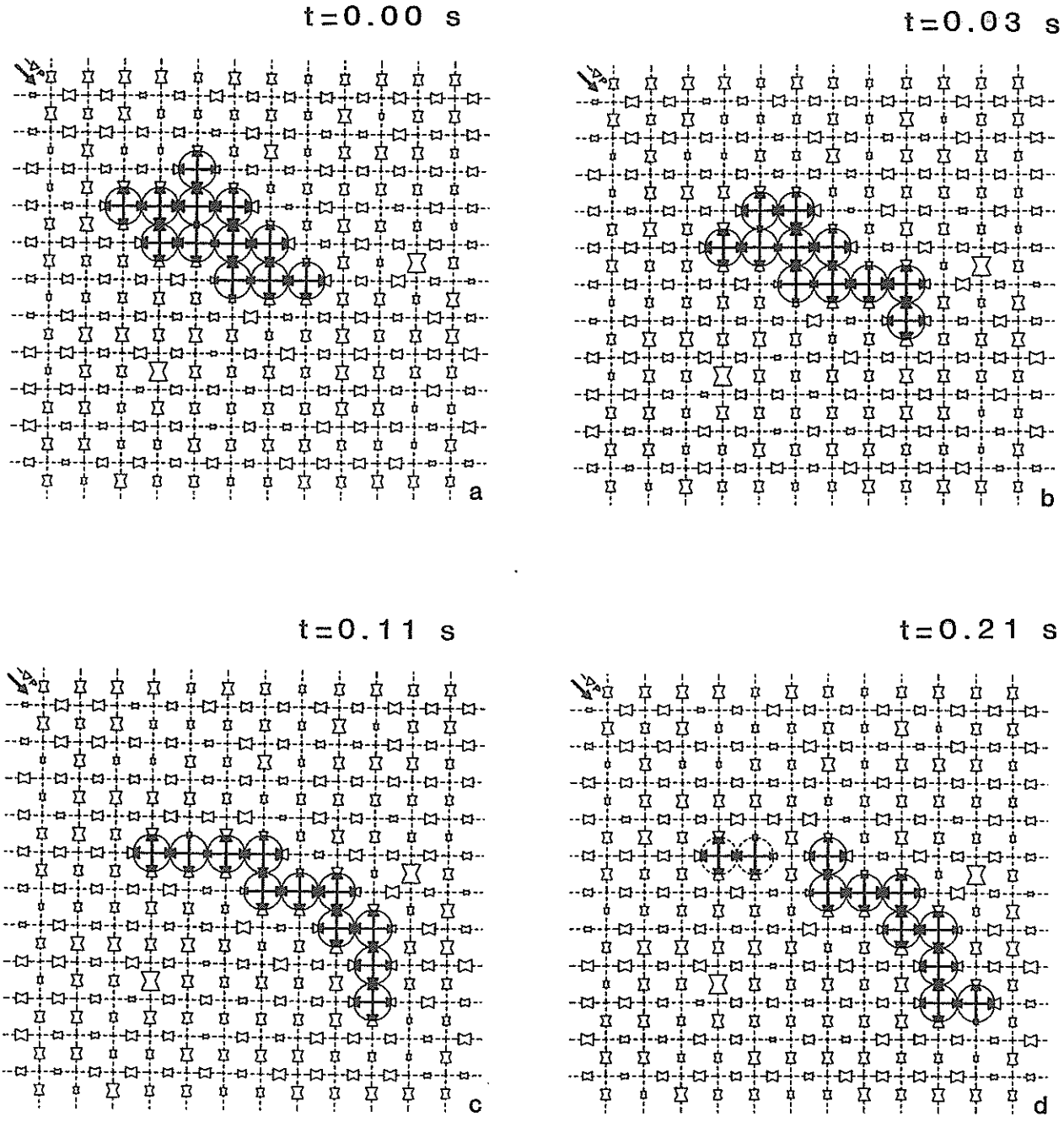


Figure 4.6

Stages of a 12-CEVS ganglion motion simulation in a network representing a 100×200 sandpack for $Ca = 2 \times 10^{-4}$, $\kappa = 1.0$, and $\phi' = 45°$.

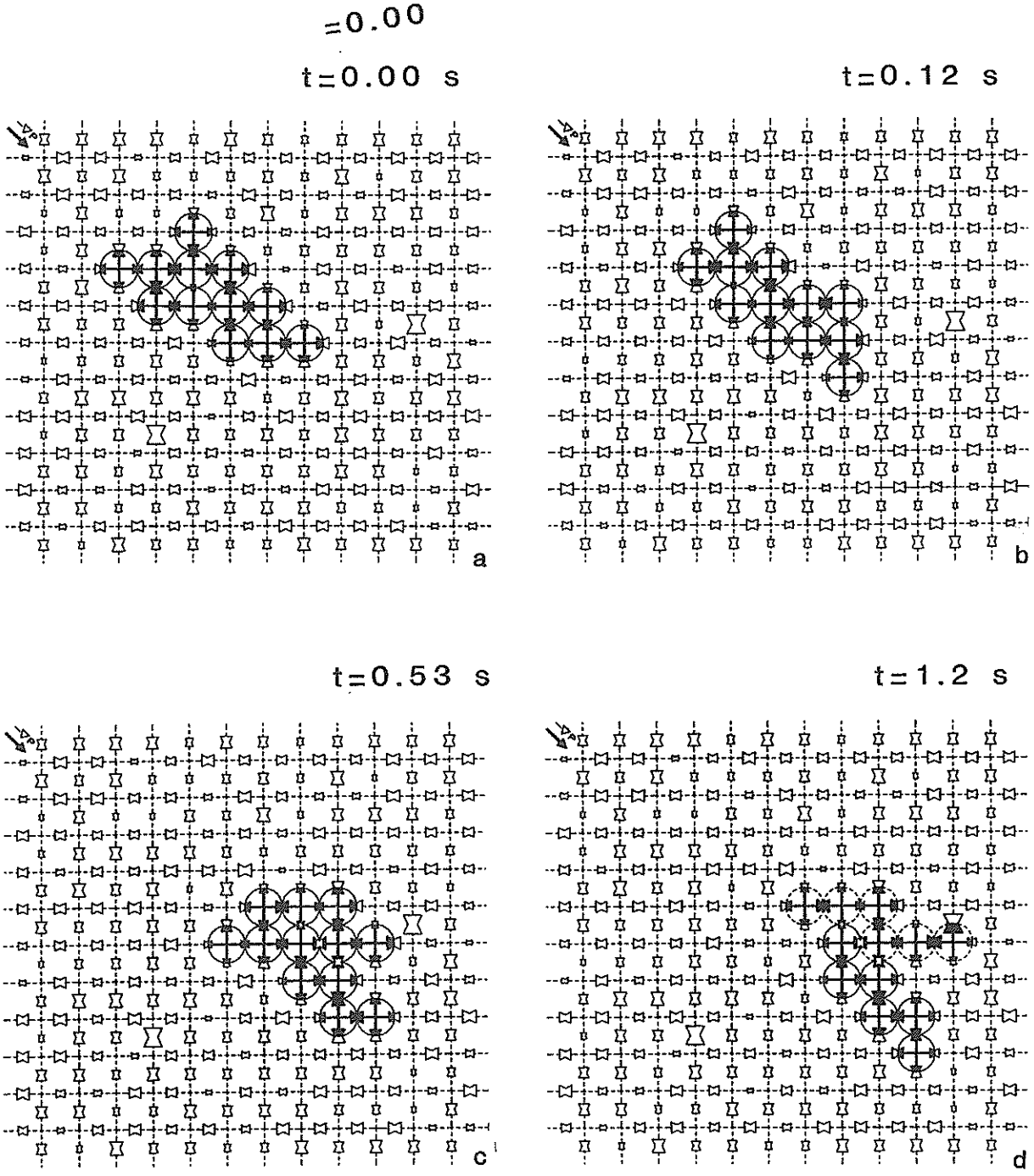


Figure 4.7

Stages of a 12-CEVS ganglion motion simulation in a network representing a 100×200 sandpack for $Ca = 4 \times 10^{-4}$, $\kappa = 1.0$, and $\phi' = 45°$.

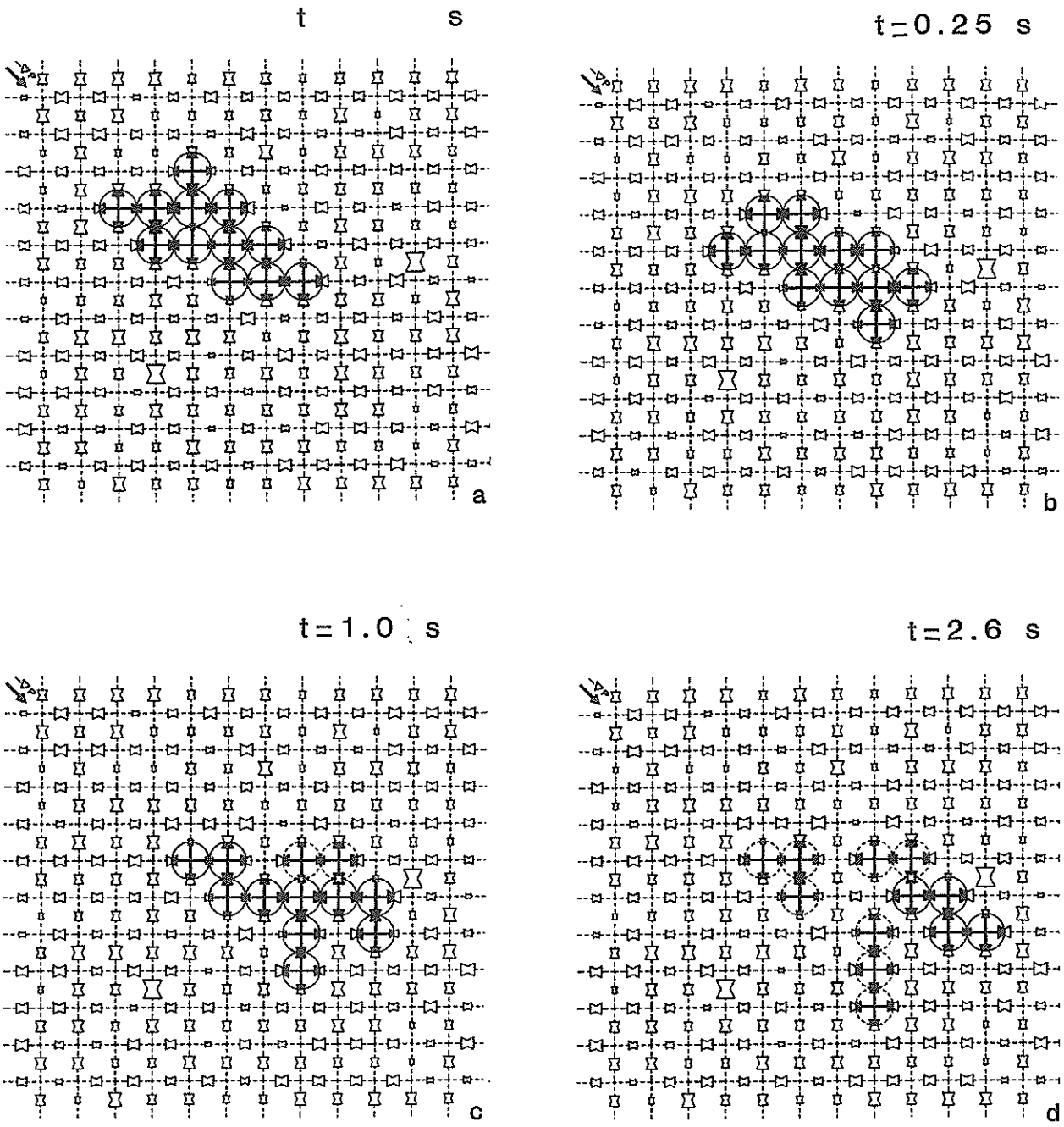


Figure 4.8

Stages of a 12-CEVS ganglion motion simulation in a network representing a 100×200 sandpack for $Ca = 10^{-3}$, $\kappa = 1.0$, and $\phi' = 45°$.

breaks in two similarly sized daughter ganglia. This type of breakup, resulting from the simultaneous advancement of two or more interfaces, and the formation of two branches, is a consequence of dynamic displacement and it is called *dynamic breakup*. An interesting note on this particular simulation is that, although the initial ganglion fissioned, the two resulting daughter ganglia had elongated forms and tried to keep their integrity in subsequent steps. An explanation for this behavior is that the capillary number, although sufficiently high to induce dynamic displacement to the large initial ganglion, is only inducing quasistatic displacement to the smaller daughter ganglia.

In the last case (Figure 4.8), Ca is set at a value much higher than Ca_{cr}. The ganglion now advances through several interfaces simultaneously and breaks into several daughter ganglia, some of which get stranded, while the others continue to move and, in turn, break into other ganglia. It should be noticed that, although most of the breakup results from the simultaneous advancement of more than one interface, some cases of quasistatic breakup (pinch-off) are also observed.

4.2.2 Influence of the Viscosity Ratio

Within the ranges of Ca and κ studied, the value of the viscosity ratio was found to have a small effect on the stranding and breakup of a solitary oil ganglion.

That the value of κ does not affect the value of Ca_{cr} is evident from the fact that at low Ca values the capillary forces dominate the viscous forces.

The lack of influence on the breakup by the viscosity ratio can also be explained by similar arguments. If the capillary number is small, the pathway chosen by the ganglion cannot be affected by κ , since it does not play an important role in

deciding the gate unit cells through which the ganglion moves (see Equation 2.9). For high values of Ca, the advancing interfaces will tend to choose the paths of least resistance, which are independent of the viscosity ratio.

As will be seen in Section 4.3, the major role of the viscosity ratio resides in the velocity achieved by the ganglion.

These finds are in disagreement with previous studies in capillary tubes with nonuniform cross-section (see for example, Legait (1983)), and further investigation is necessary.

4.2.3 Influence of the Macroscopic Pressure Gradient

In Section 3.4 it was shown that, for single phase flow, the network model used in this work is isotropic with respect to permeability. Clearly this is not true for a two phase flow system. Figures 4.9 through 4.11 demonstrate the effects of changing the direction of the macroscopic pressure gradient. A network of monosized unit cells is used in all three figures. The capillary number is set at $Ca = 10^{-3}$, and the viscosity ratio at $\kappa = 7.0$.

In Figure 4.9 the macroscopic pressure gradient is aligned with the longitudinal axis of the network, $\phi' = 90°$. Both frontal interfaces advance in tandem, and the ganglion divides into two prongs. Coalescence of the two prongs is not allowed (it would not occur anyway due to the lack of lateral driving force), so the ganglion eventually fissions into two similar ganglia (compare with Figure 2.6).

When $\phi' = 70°$ (Figure 4.10), the ganglion tends to elongate in the direction of the macroscopic pressure gradient; however, as it moves it finds itself in situations that cause pinch-off (quasistatic breakup) and dynamic breakup simultaneously.

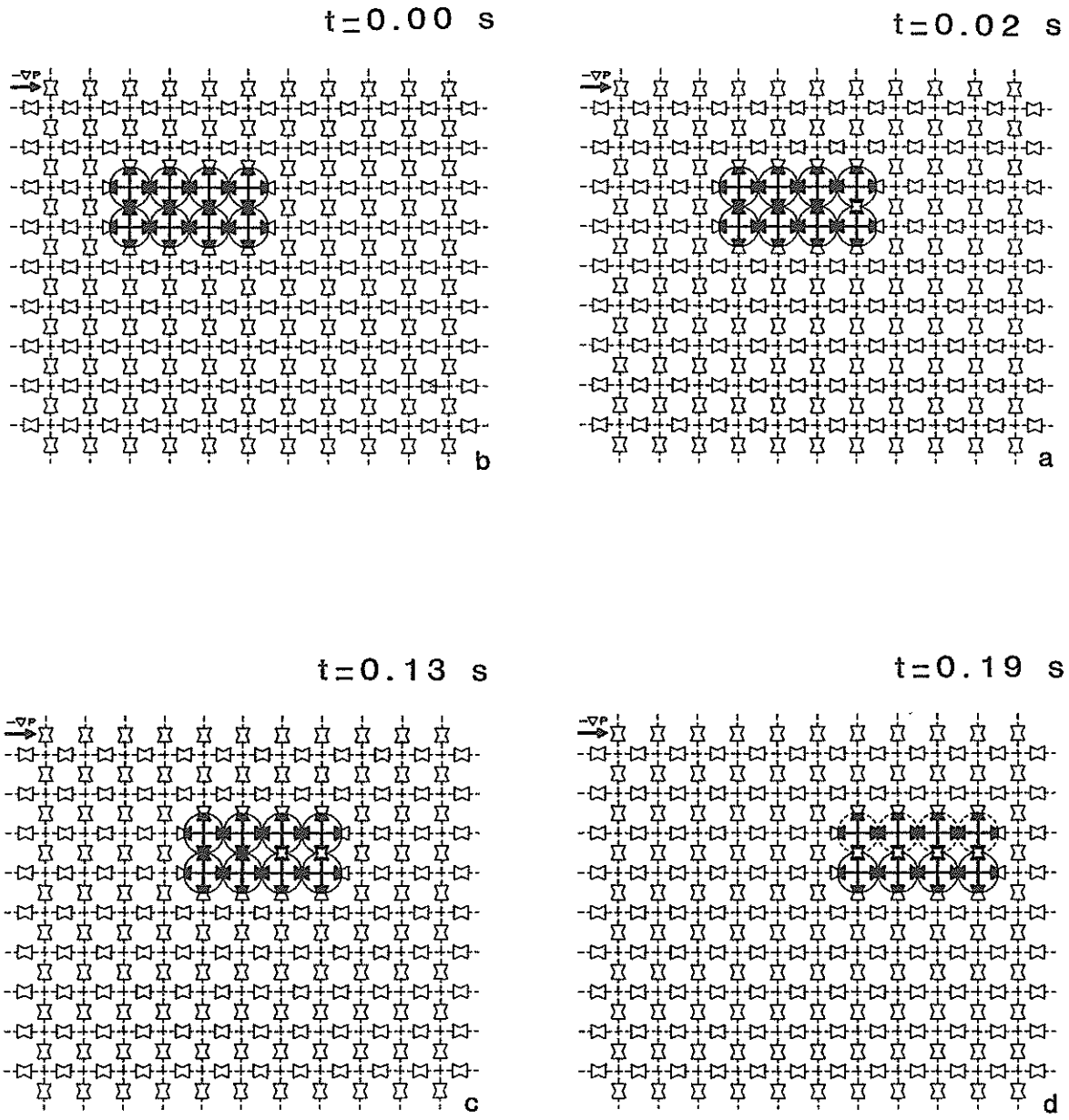


Figure 4.9

Stages of a 8-CEVS ganglion motion simulation in a network of monosized unit cells for $Ca = 10^{-3}$, $\kappa = 7.0$, and $\phi' = 90°$.

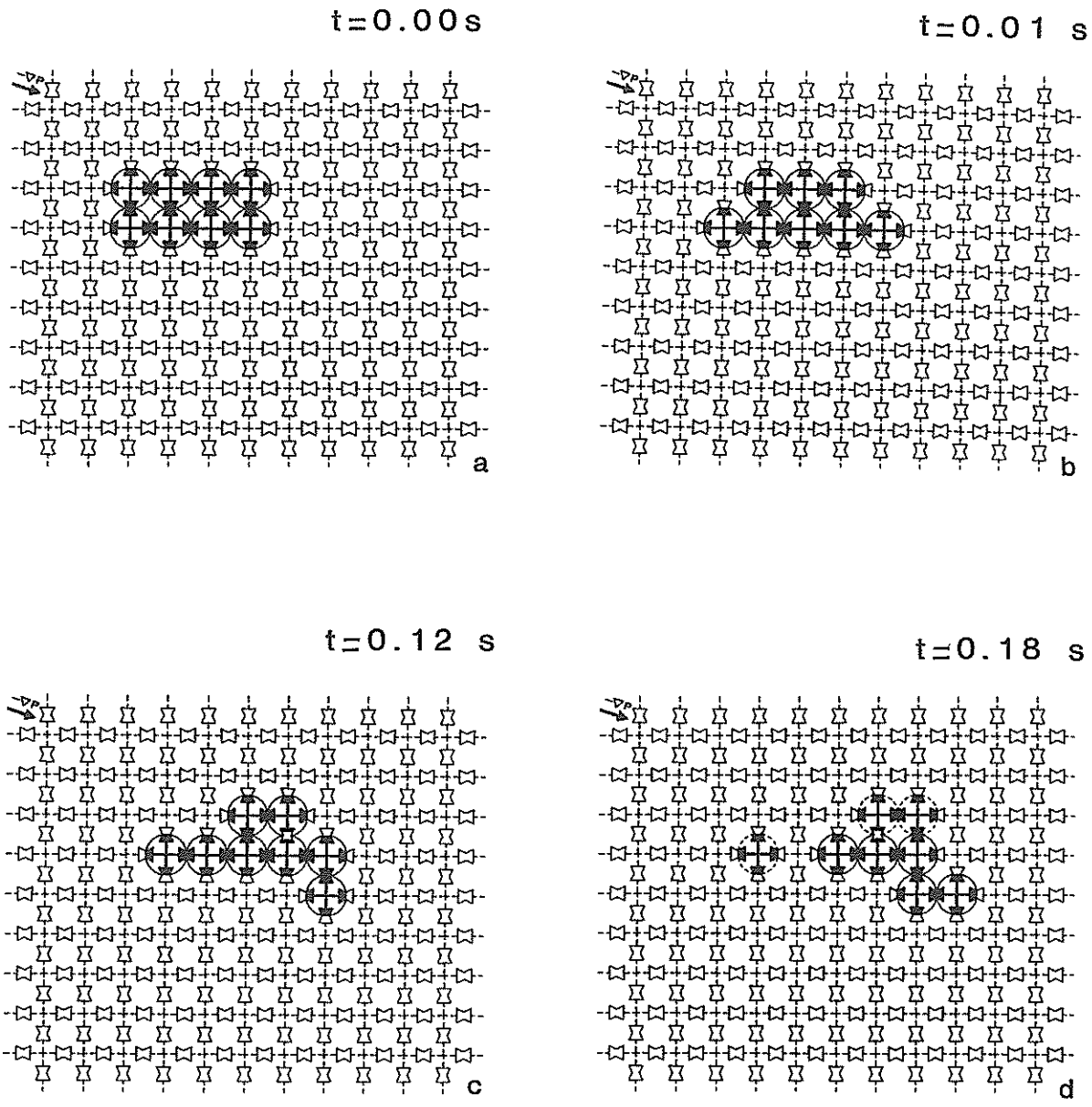


Figure 4.10

Stages of a 8-CEVS ganglion motion simulation in a network of monosized unit cells for $Ca = 10^{-3}$, $\kappa = 7.0$, and $\phi' = 70°$.

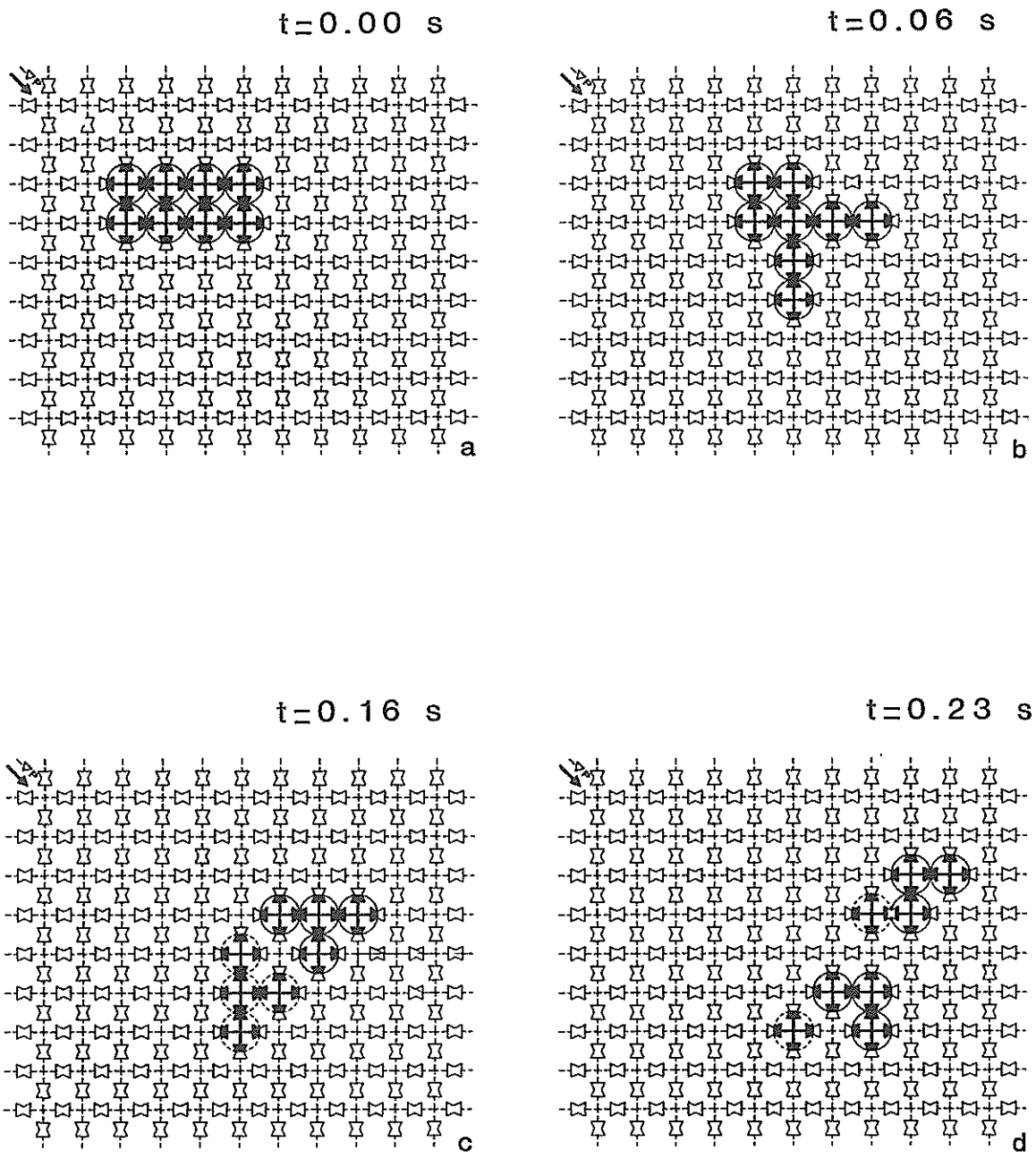


Figure 4.11

Stages of a 8-CEVS ganglion motion simulation in a network of monosized unit cells for $Ca = 10^{-3}$, $\kappa = 7.0$, and $\phi' = 45°$.

Finally, in Figure 4.11, the direction of the macroscopic pressure gradient is set at $\phi' = 45$. The ganglion advances through two interfaces simultaneously, and breaks into two daughter ganglia, which, in turn break again through dynamic breakup, and the resulting four ganglia get stranded.

4.2.4 Influence of Network Topology

From the simulation examples previously shown, it becomes clear that the local topology of the network influences the behavior of the ganglion. In Section 2.5.1, the quasistatic displacement of an oil ganglion in a monosized model porous medium was shown (see Figure 2.3). It was pointed out at the time that the behavior shown could only be achieved in a regular porous medium. Figures 4.12 through 4.14 demonstrate this fact very clearly.

In the first figure, the network is composed of monosized unit cells. The size of these unit cells was chosen so that the permeability of the regular network approaches closely the permeability of the random porous medium. The ganglion is subjected to a flood with a capillary number just above its critical value for mobilization. The ganglion advances through one interface at a time and takes a zig-zag configuration, much like the one taken by the oil ganglion in Figure 2.3.

The next two figures show the same ganglion subjected to the same flood conditions, but now, in each case, a different random network is shown. In Figure 4.13, the ganglion breaks into two daughter ganglia, while in the case of Figure 4.14, the ganglion gets stranded by encountering a set of very small unit cells upstream.

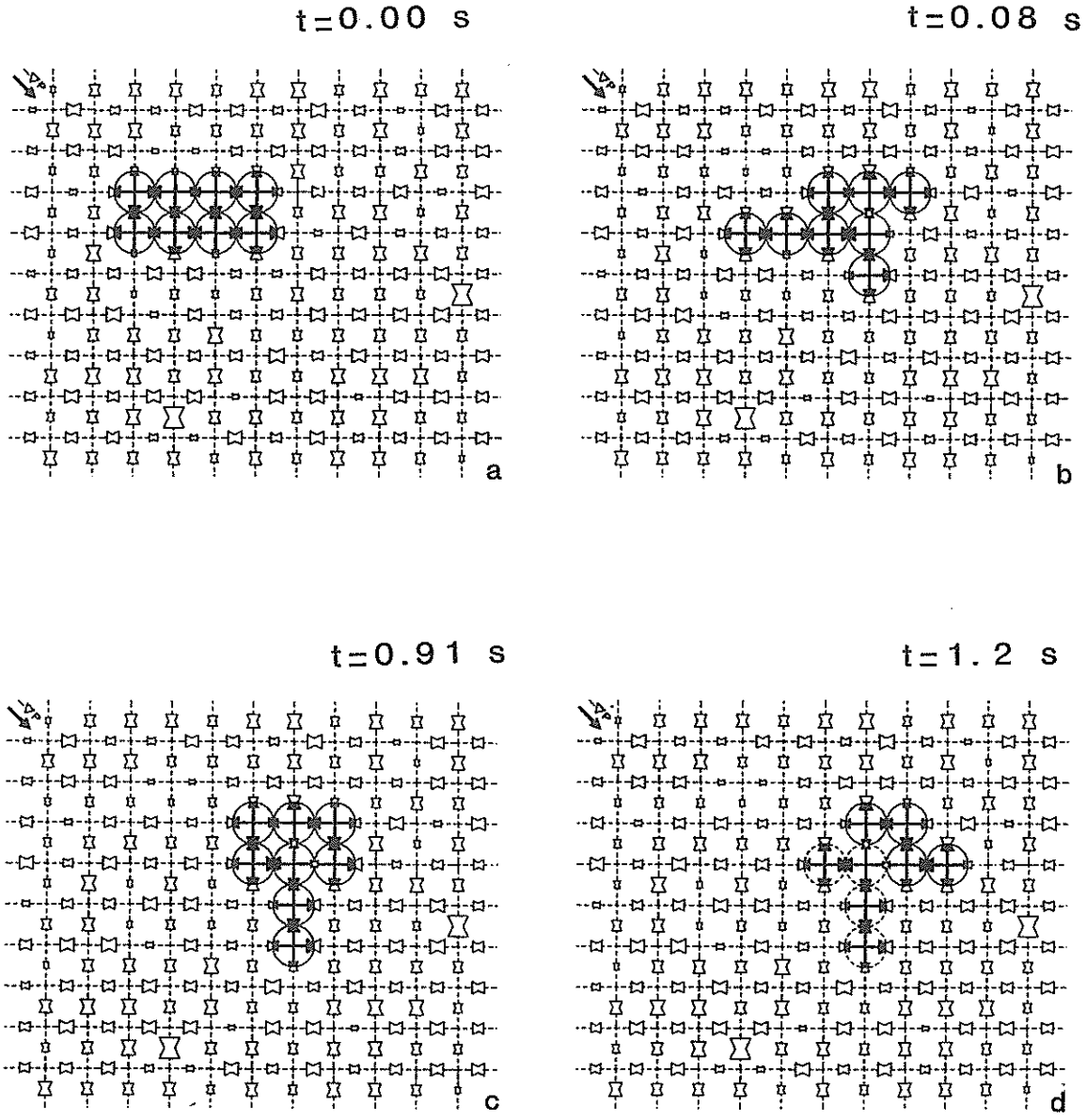


Figure 4.13

Stages of a 8-CEVS ganglion motion simulation in a network representing a 100 × 200 sandpack for $Ca = 5 \times 10^{-4}$, $\kappa = 7.0$, and $\phi' = 45°$.

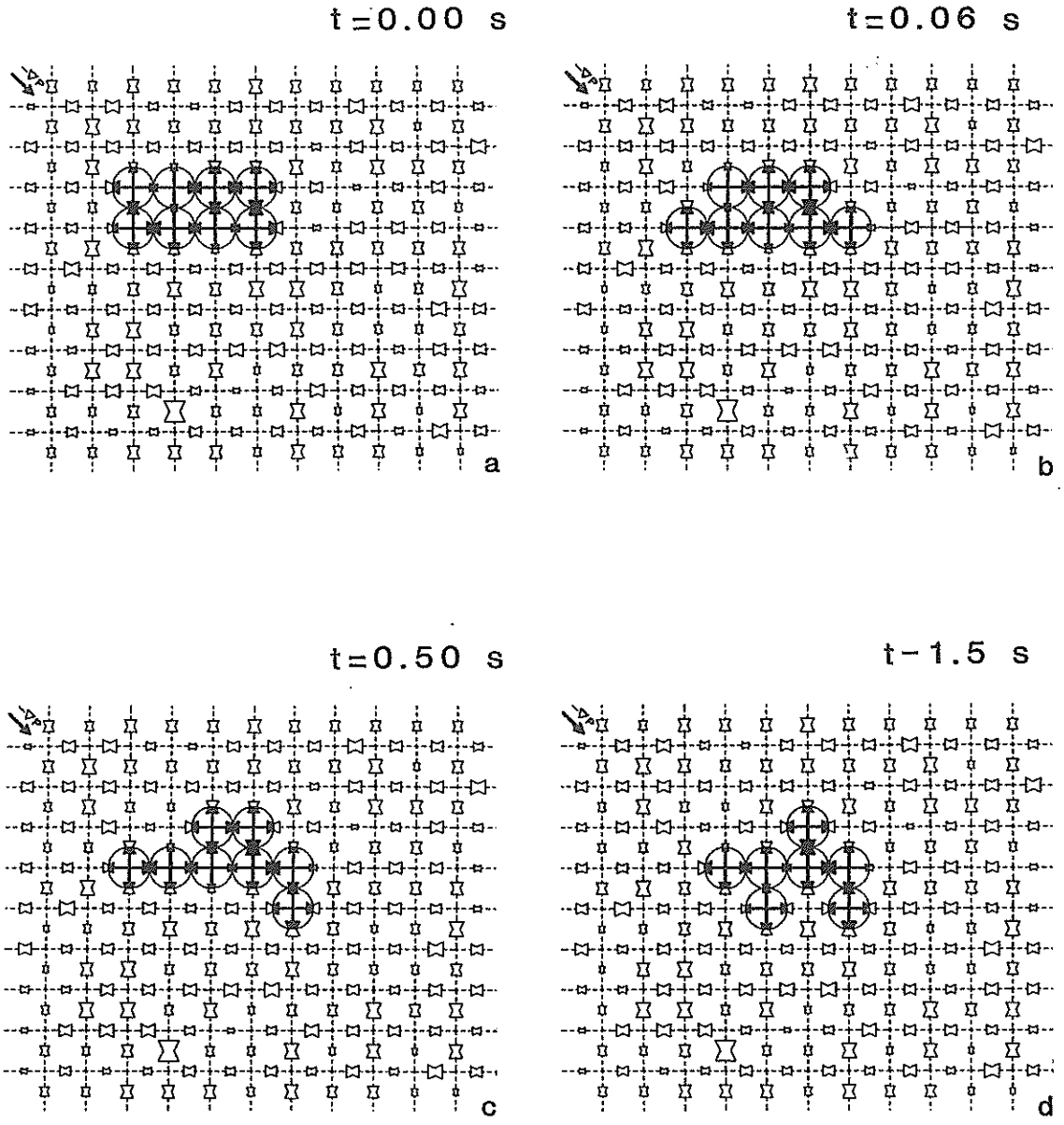


Figure 4.14

Stages of a 8-CEVS ganglion motion simulation in a network representing a 100 × 200 sandpack for $Ca = 5 \times 10^{-4}$, $\kappa = 7.0$, and $\phi' = 45°$.

4.3 Average Ganglion Velocity

One of the most important parameters in ganglion dynamics is the ganglion velocity, u_z (Payatakes, 1980). Due to the converging-diverging character and the randomness of the porous medium, the velocity of a ganglion is time dependent, even if the flooding conditions are kept constant. Hence, the ganglion velocity is measured in terms of the time-averaged velocity with which the centroid of the ganglion migrates downstream, $\overline{u}_z$.

to avoid the problem of frequent breakup under dynamic displacement conditions, in the calculation of ganglion velocities, the ganglia were placed in a rectilinear single track, and the macroscopic pressure gradient was applied in direction parallel to this track. A similar procedure was used experimentally by Hinkley (1982).

The ganglion velocity was calculated by dividing the distance traveled by the centroid of the ganglion by the elapsed time. Ganglia will tend to elongate until a cruising shape is attained. To ensure that this elongation effect did not affect the velocity calculations, each ganglion was allowed to travel a distance equal to twice its length, at which point the time was reset to zero, and the position of the centroid was recorded. From this point on, the ganglion velocity was calculated after the occurrence of each rheon, and its final value was taken when the last three measurements converged to the same average value.

In order to check the validity of the calculations, an idealized ganglion with the same viscosity as the aqueous phase and with a null ganglion-water interfacial tension was placed in the network. This is equivalent to track, experimentally, a ganglion of colored water being displaced by water. The average velocity of this ganglion was found to be the same as the interstitial velocity of the wetting phase

in a network free of the non-wetting phase, v_i , which can be expressed as $v_i = v_f/\epsilon$. Here, v_f is the superficial velocity of the flood, and ϵ is the porosity of the porous medium.

With the previous result in mind, the reduced time-averaged ganglion velocity is defined as $u^* = \overline{u}_z/v_i$. Under creeping flow conditions, u^* is a function of Ca, v^*, θ, and the geometric parameters defining the porous medium structure. Here, v^* is the reduced ganglion volume and is defined as $v^* = v/v_{CEVS}$, where v is the volume of the ganglion, and v_{CEVS} is the mean volume of the elemental void space.

Ganglion velocity calculations were performed in both networks as described in Section 4.1.

4.3.1 Ganglion Velocity in a Monolayer Square Beadpack

As was shown in Section 4.2, the model developed in Chapter 3 produces simulations that, at least from a qualitative point of view, approach very closely the few existing experimental observations. The question arises as to whether quantitative predictions of variables such as ganglion velocity are also accurate. To this end, the monolayer square beadpack network was considered and the predicted velocities compared with the experimental values reported by Hinkley (1982).

In Figures 4.15 and 4.16, the reduced time-averaged ganglion velocities as calculated by the present model and as obtained by Hinkley are plotted as functions of the reduced ganglion volume for various capillary numbers. The viscosity ratio values are $\kappa = 7.3$ and $\kappa = 0.56$, respectively. Good agreement between theoretical and experimental values is obtained for high capillary numbers. For low capillary numbers, the agreement is less satisfactory, especially for small ganglia. Finally,

the calculated values of Ca_{cr} for mobilization are, in general, higher than the ones reported by Hinkley.

In order to understand the cause of the observed discrepancies, it becomes necessary to analyze the forces involved in the mobilization and subsequent motion of an oil ganglion, and decide which of these forces are being estimated by the network model with reasonable accuracy and which ones are not. Three types of forces act on a ganglion placed in a porous medium and subjected to an immiscible flood: pressure forces; capillary forces; and viscous forces.

The pressure forces result from the applied macroscopic pressure gradient. For a given capillary number, the magnitude of the macroscopic pressure gradient is calculated using Equation 3.16 ($-\nabla P = Ca\sigma_{ow}/k$). The calculated and experimental values of k are within 10% of each other (see Table 4.2), so it can be assumed that the pressure forces are correctly estimated.

The capillary forces change as the interfaces move through the unit cells. The minimum and maximum radii of curvature in a unit cell are found at $z = 0$ and $z = h'/2$, respectively. Batycky (1981) showed that, for a geometry like the one used by Hinkley, the limits on the radii of curvature are given by

$$R_{min} = \frac{d_g}{2} \frac{\sqrt{\cos^2\theta_1 + 2\cos\theta_1\cos\theta_2 + 1} - \cos\theta_1 - \cos\theta_2}{\sin^2\theta_2} , \qquad (4.1)$$

$$R_{max} = \frac{d_g}{2} \frac{\sqrt{(\cos\theta_1 + \cos\theta_2) + 2\sin^2\theta_2} - \cos\theta_1 - \cos\theta_2}{\sin^2\theta_2} , \qquad (4.2)$$

where θ_1 is the contact angle occurring on the sphere surface, θ_2 is the contact angle at the overlying plate, and both θ_1 and θ_2 must reflect contact angle hysteresis. Assuming that $\theta_1 = \theta_2$ (experimental data by Batycky show this to be true), and taking into consideration that the minimum and the maximum values of the radii

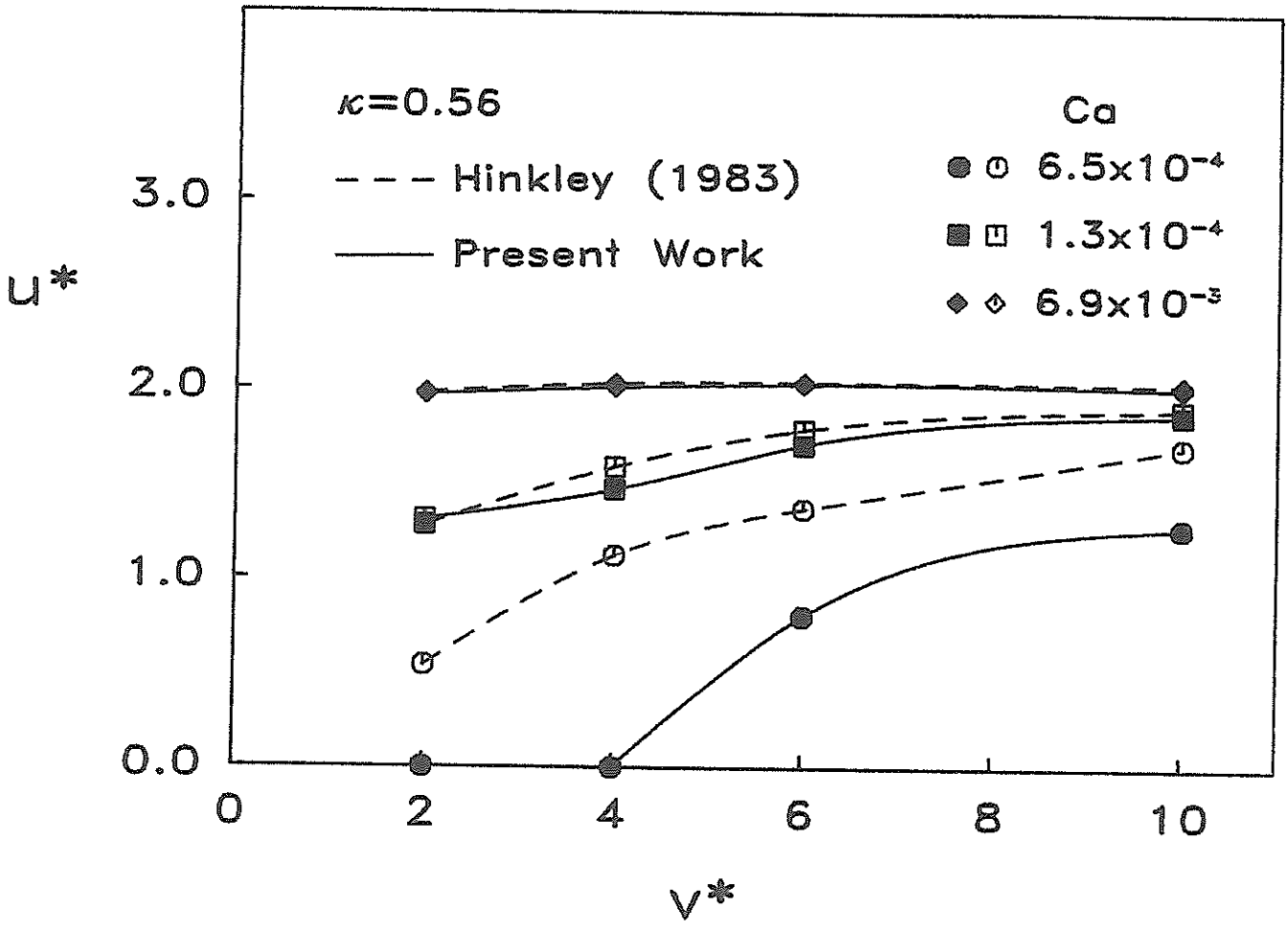


Figure 4.15

Comparison between experimental and theoretical values of the reduced time-averaged ganglion velocity, u^*, *versus* the reduced ganglion volume, v^*, for various Ca values and $\kappa = 0.56$.

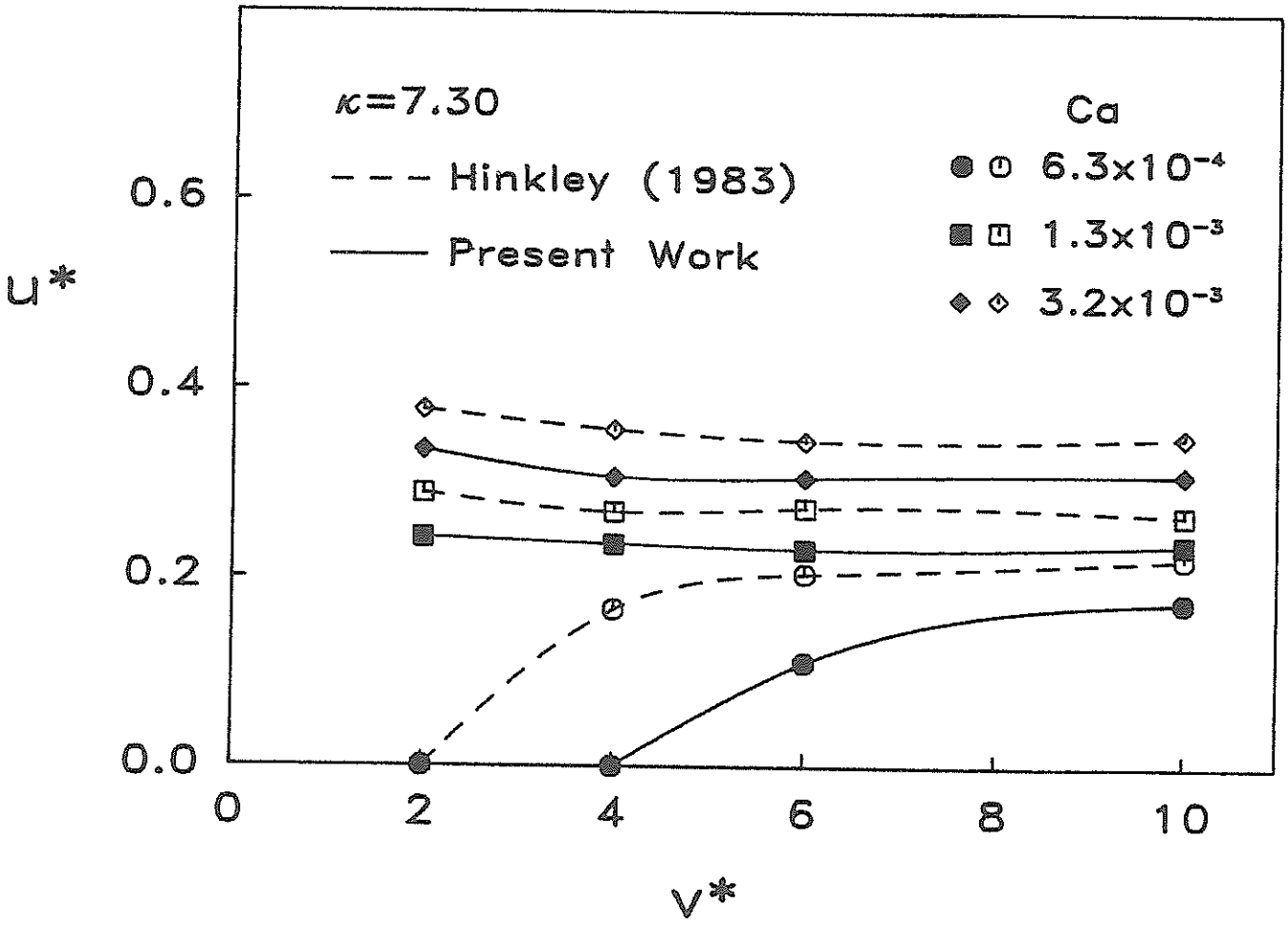


Figure 4.16

Comparison between experimental and theoretical values of the reduced time-averaged ganglion velocity, u^*, *versus* the reduced ganglion volume, v^*, for various Ca values and $\kappa = 7.3$.

of curvature occur for receding and advancing interfaces, respectively, the following expressions are obtained

$$R_{min} = \frac{d_g}{2} \frac{\sqrt{3\cos^2\theta_r^o + 1} - 2\cos\theta_r^o}{\sin^2\theta_r^o} , \tag{4.3}$$

$$R_{max} = \frac{d_g}{2} \frac{\sqrt{2\cos^2\theta_a^o + 2} - 2\cos\theta_a^o}{\sin^2\theta_a^o} . \tag{4.4}$$

The values of R_{min} and R_{max} as calculated using Equations 4.3 and 4.4 and calculated for the unit cells describing the porous medium model are reported in Table 4.2. It is clear that the agreement is within acceptable margins of error.

The viscous forces present in the experimental case are not easily calculated due to the unique geometrical configuration of the experimental apparatus. Visual observations by Hinkley showed that, due to the density difference between the oleic and the aqueous phases, the oil ganglion is contained in the space between the spheres and the overlying plate. It follows that while there exists contact displacement in the upper part of the ganglion, both with the overlying plate and the upper part of the spheres, the lower part of the ganglion moves, for the most part, in contact with water.

Consider, then, an oil ganglion placed in Hinkley's apparatus, in its static equilibrium position. Apply a small macroscopic pressure gradient so that the capillary number is smaller than its critical value for mobilization. As was described in Section 2.5.1, the ganglion will rearrange the position of its interfaces so that a new equilibrium position is obtained. At the same time, the lower part of the ganglion is in contact with moving water. In order to verify the non-slip condition at this oil-water interface, and so that, macroscopically, the ganglion remains immobilized, internal circulation of the oil inside the ganglion must take place. If the capillary

number is increased, a value will be reached, at which point the equilibrium between the pressure forces and the interfacial shear force at the lower part of the ganglion, on one hand, and the capillary forces, on the other hand, is no longer possible, and the ganglion will start to move. In the network model, the shear force resulting from the flow at the lower oil-water interface is not taken into account. In order to overcome the capillary forces, higher pressure forces have to be applied, and the calculated value of Ca_{cr} becomes higher.

The discrepancy observed on the velocities of small ganglia at low Ca values can be attributed to a similar effect of the interfacial shear force. However, the full understanding of this problem should involve the simultaneous solution of the equations of motion for the both phases, with the appropriate boundary conditions.

The question now arises as to whether the theoretical model will provide good estimates of ganglion velocities under reservoir conditions. Based on the above results and considerations, the answer is positive if gravity effects are not important and if the movement of the ganglion occurs under contact displacement conditions. In actual reservoirs and in laboratory experiments of immiscible displacement in sandstones, it has been verified that the gravity effects at the pore level are indeed negligible (see, e.g., Chatzis and Morrow, 1983). Contact displacement is favored by the roughness of the walls forming the porous stratum in reservoirs. In the case where a lubricating film of water surrounds the oleic phase, the present model needs to be modified to account for the effect of the film of water in the conductance of the unit cell and the presence of additional pathways for the water. Complete solutions of the flow problem of two immiscible fluids in converging-diverging tubes are required.

4.3.2 Ganglion Velocity in a 100 × 200 Sandpack

Calculated values of u^* in a 100 × 200 sandpack are shown in Figures 4.17 through 4.28. These figures illustrate the effect on the ganglion velocity of various parameters such as the capillary number, the viscosity ratio, the equilibrium contact angle, and the existence (or not) of contact angle hysteresis and of rate-dependent contact angles.

The influence of Ca, κ and v^* are shown in Figures 4.17 through 4.22. The contact angle is set at $\theta_e = \theta_a^o = \theta_r^o = 0.0°$. In the first three figures, u^* is plotted as a function of v^*, while in the next three figures, u^* is plotted as a function of Ca. The following is observed:

- For $\kappa > 1$, the reduced time-averaged ganglion velocity is smaller than unity, $u^* < 1$, Figure 4.17.
- For $\kappa < 1$ the reduced time-averaged ganglion velocity can be larger than unity, $u^* > 1$, Figure 4.19.
- For fixed values of the reduced time-averaged ganglion volume, v^*, the reduced ganglion velocity, u^*, increases with Ca. In the range of Ca values studied, for $\kappa \leq 1$, u^* seems to tend to an asymptotic value, which is independent of both Ca and κ, Figures 4.21 and 4.22. For $\kappa > 1$, there is no clear evidence that an asymptotic value is ever reached, Figure 4.20.
- For fixed values of Ca that are slightly higher than Ca_{cr}, u^* increases monotonically with v^*, reaching an asymptotic value for v^* ca 12 to 15.
- For fixed values of Ca that are substantially larger than Ca_{cr}, and for $\kappa \geq 1$, u^* may be slightly larger for 2-CEVS and 3-CEVS ganglia and then decreases and tends to an asymptotic value. This same effect is not observed for $\kappa < 1$,

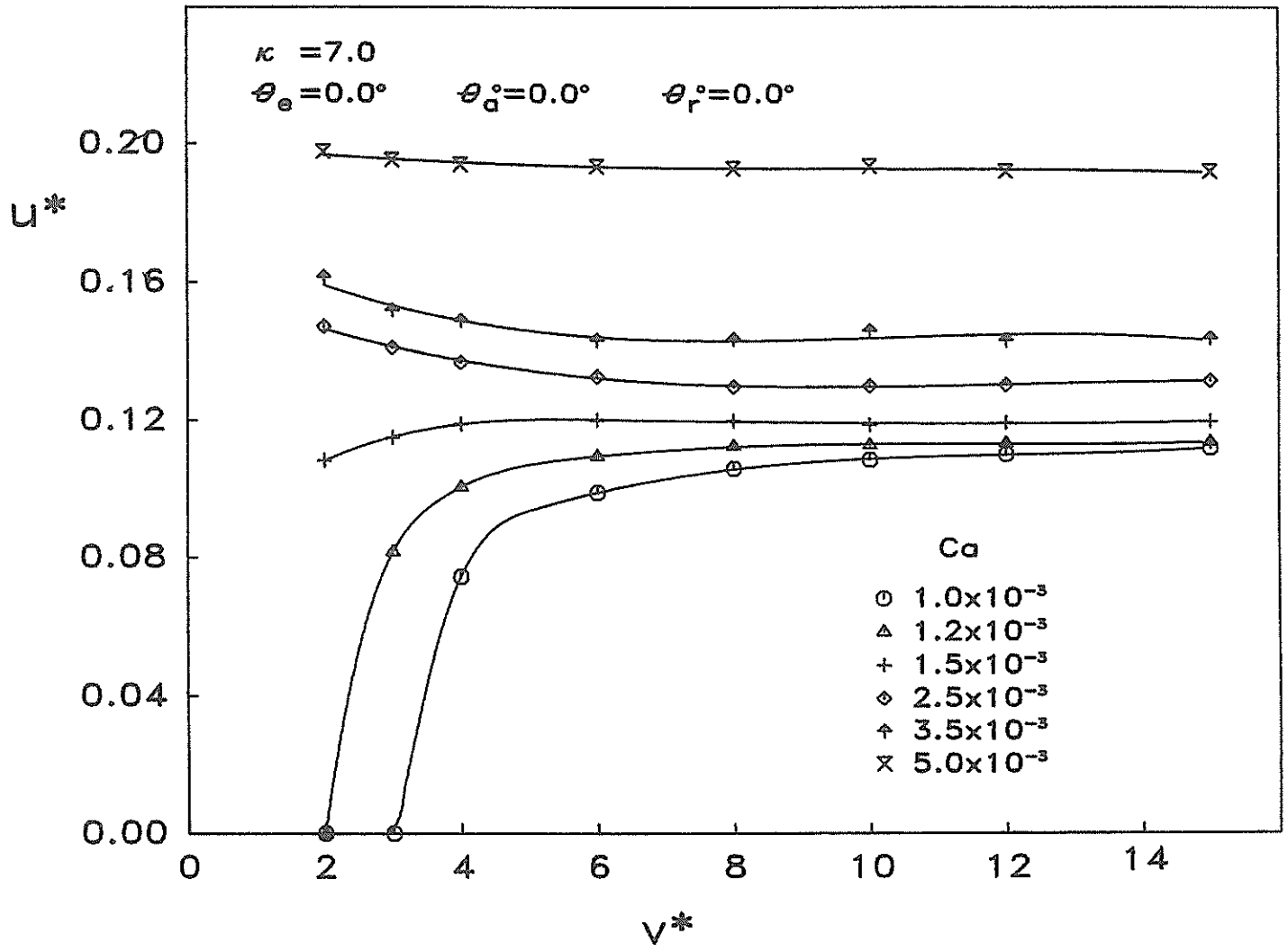


Figure 4.17

Plot of the reduced time-averaged ganglion velocity, u^*, *versus* the reduced ganglion volume, v^*, in a 100 × 200 sandpack for various Ca values. $\kappa = 7.0$, $\theta_e = 0°$.

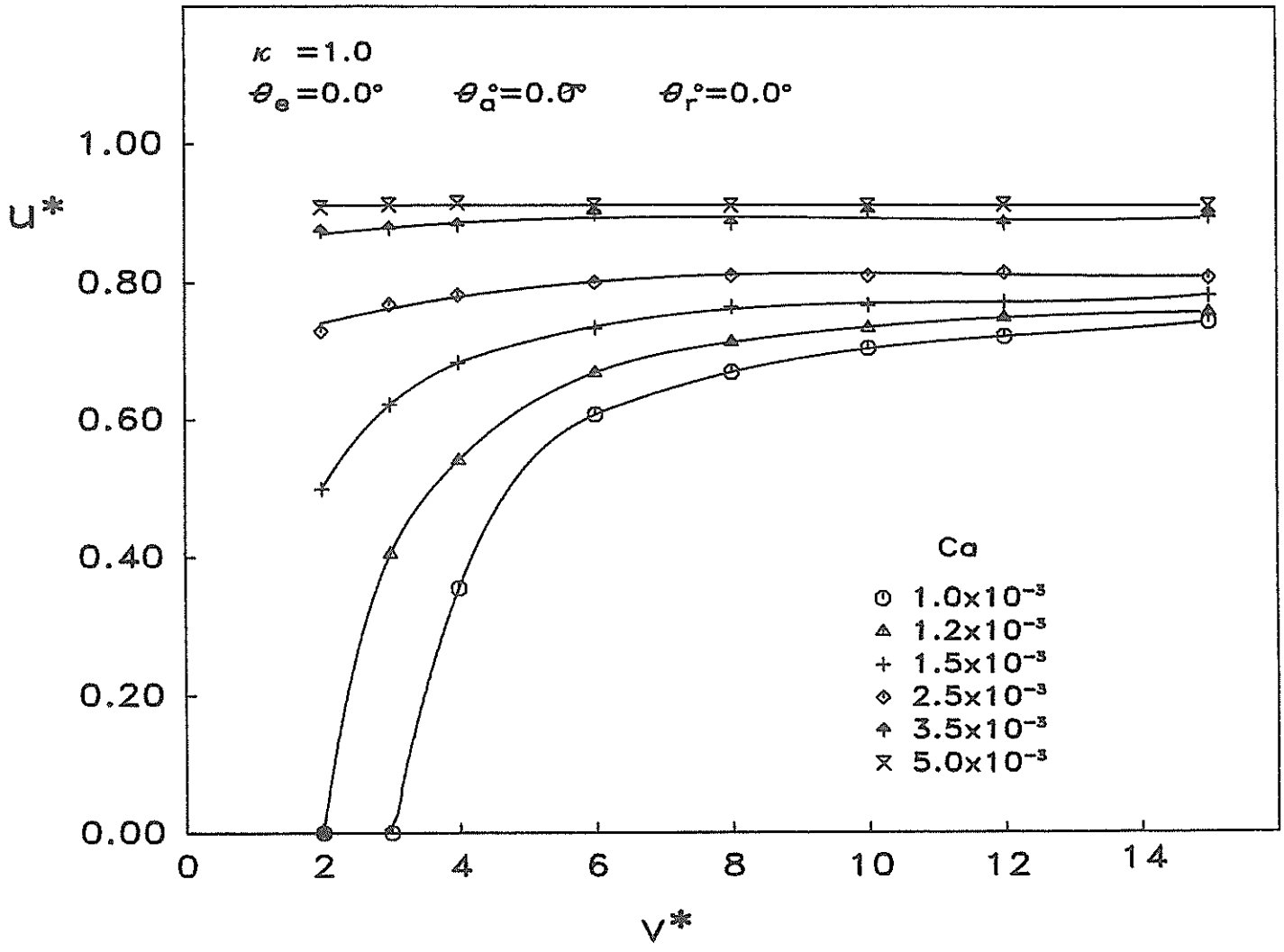


Figure 4.18

Plot of the reduced time-averaged ganglion velocity, u^*, *versus* the reduced ganglion volume, v^*, in a 100 × 200 sandpack for various Ca values. $\kappa = 1.0$, $\theta_e = 0°$.

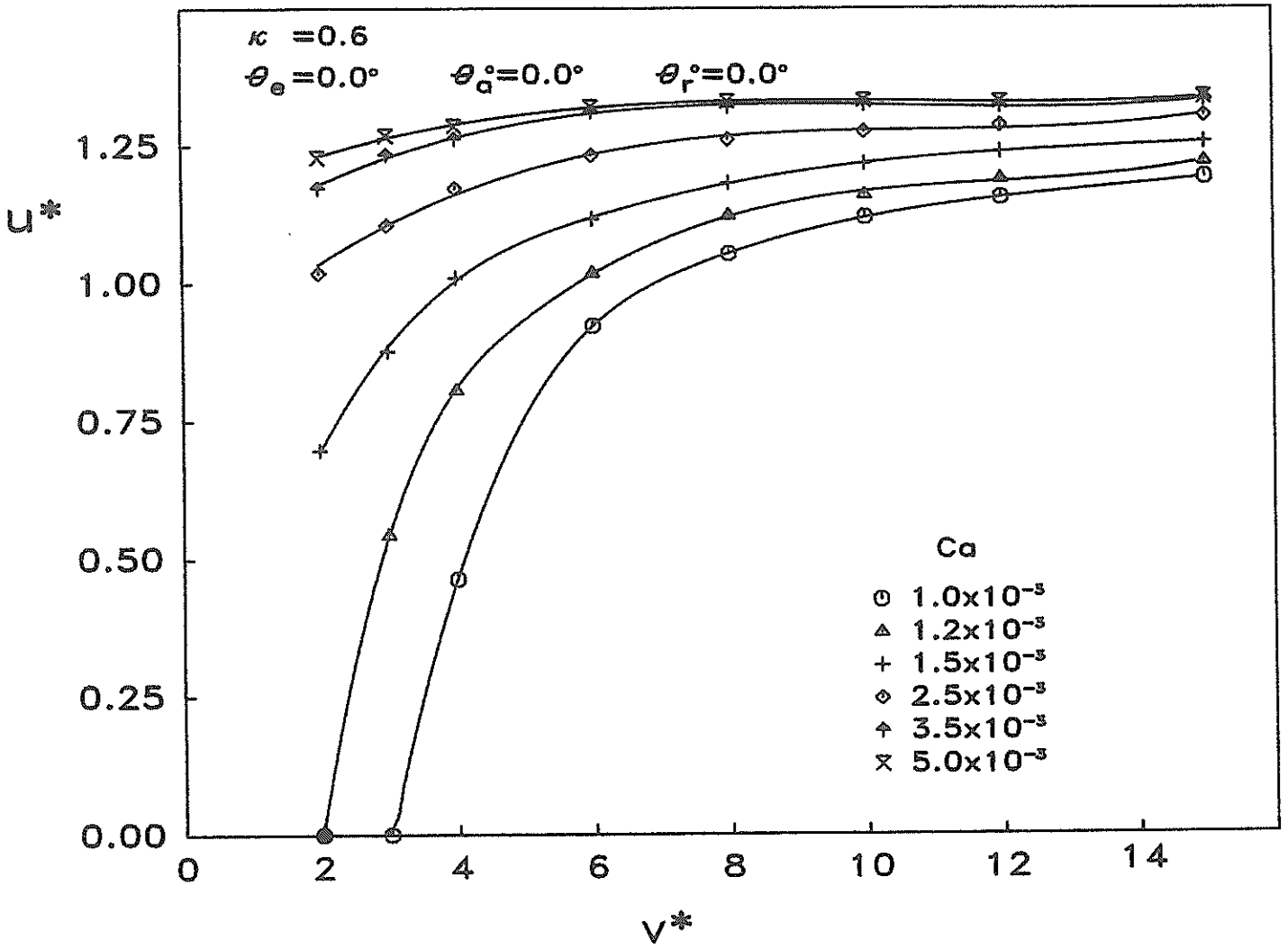


Figure 4.19

Plot of the reduced time-averaged ganglion velocity, u^*, *versus* the reduced ganglion volume, v^*, in a 100 × 200 sandpack for various Ca values. $\kappa = 0.6$, $\theta_e = 0°$.

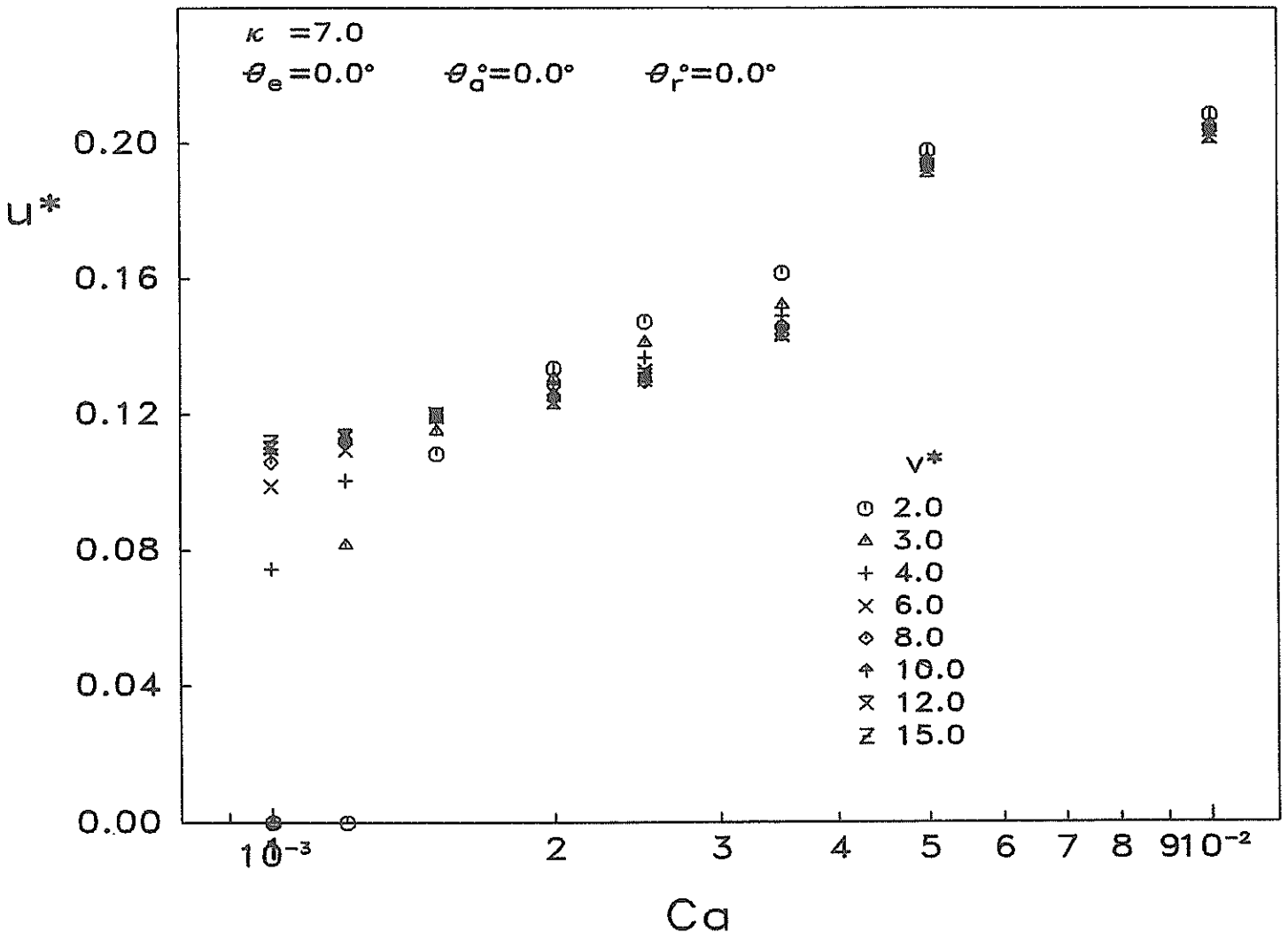


Figure 4.20

Plot of the reduced time-averaged ganglion velocity, u^*, *versus* the capillary number, Ca, in a 100 × 200 sandpack for various values of v^*. $\kappa = 7.0$, $\theta_e = 0°$.

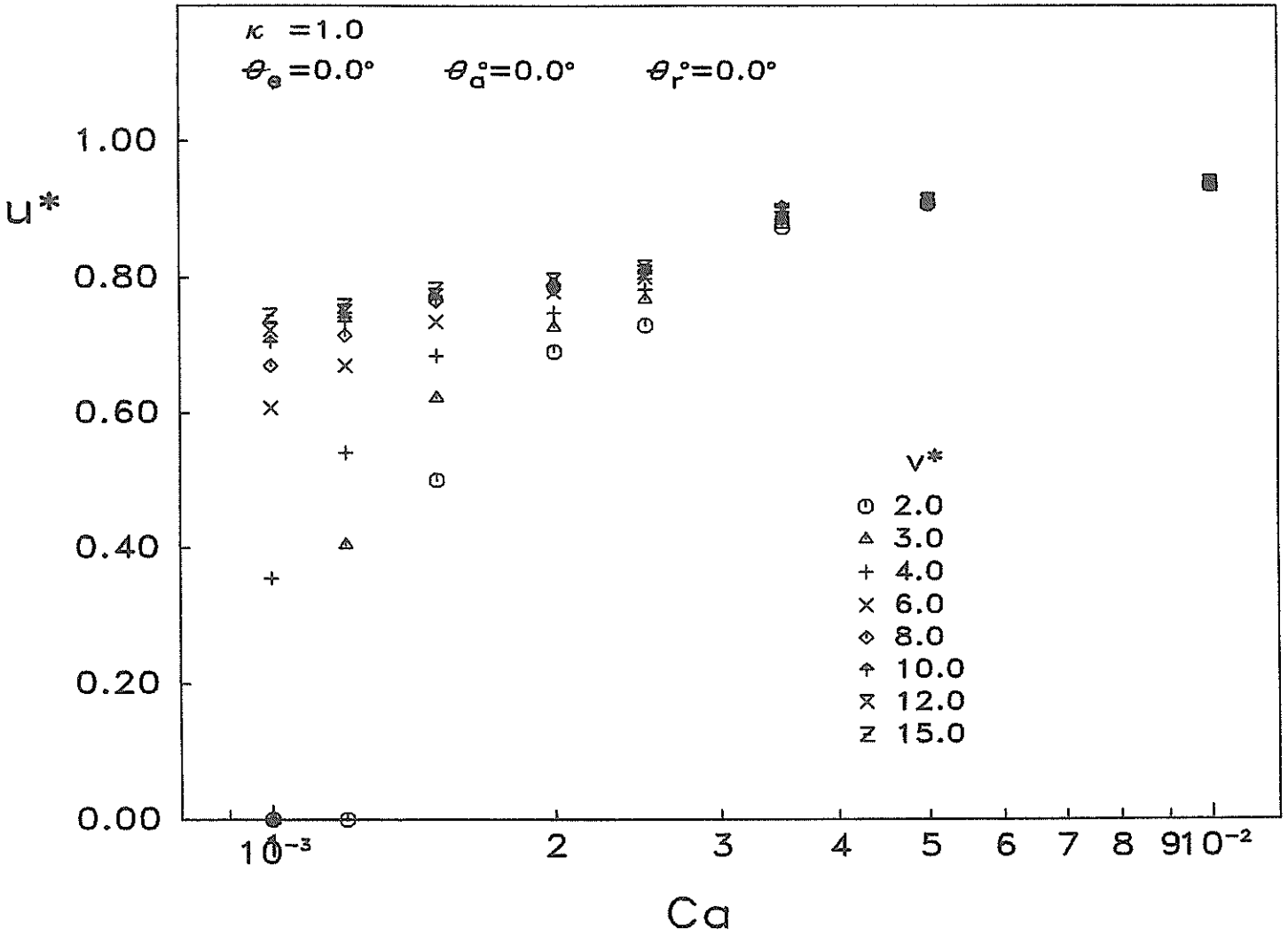


Figure 4.21

Plot of the reduced time-averaged ganglion velocity, u^*, *versus* the capillary number, Ca, in a 100 × 200 sandpack for various values of v^*. $\kappa = 1.0$, $\theta_e = 0°$.

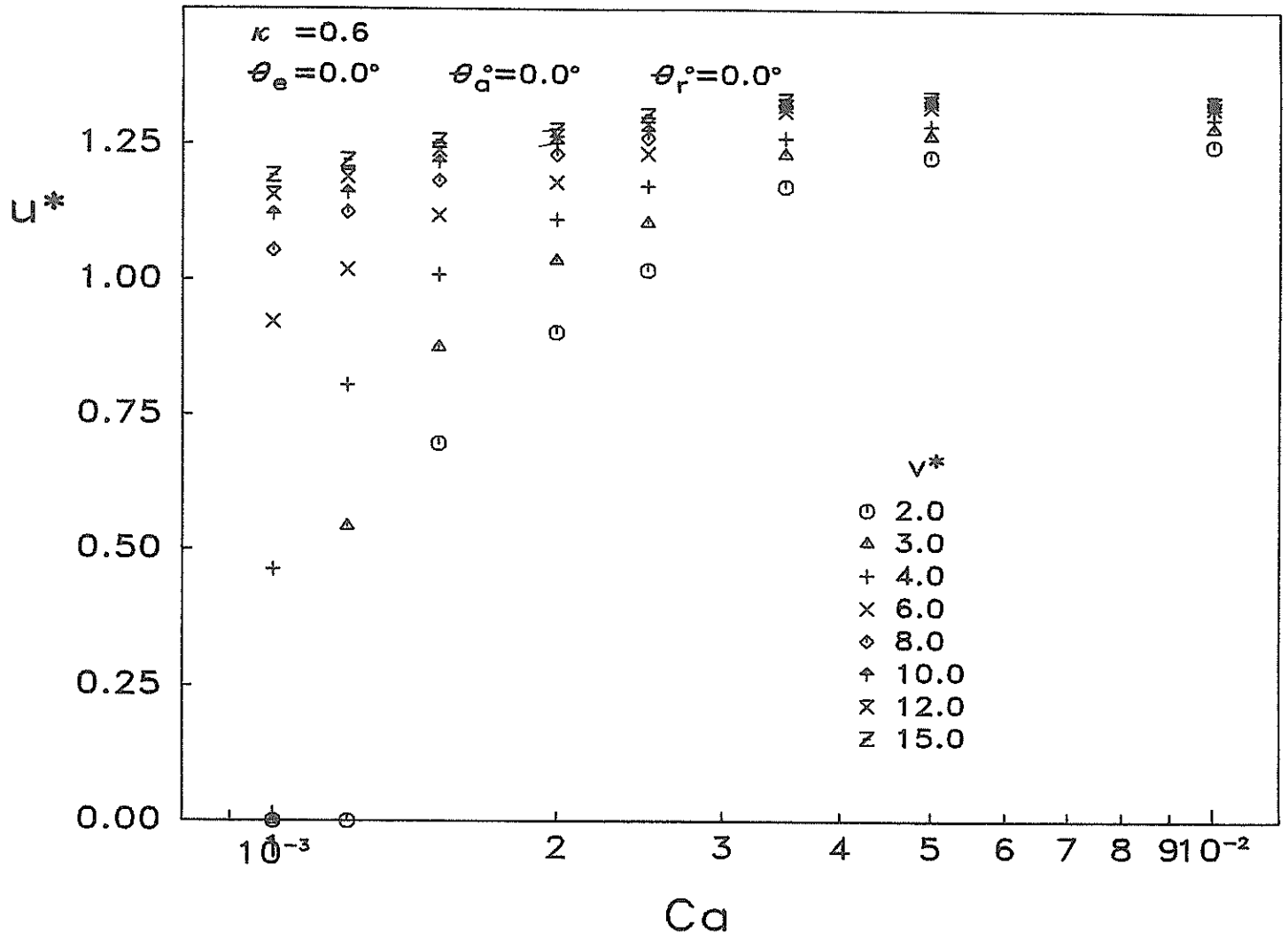


Figure 4.22

Plot of the reduced time-averaged ganglion velocity, u^*, *versus* the capillary number, Ca, in a 100 × 200 sandpack for various values of v^*. $\kappa = 0.6$, $\theta_e = 0°$.

and u^* increases monotonically with v^*.

At first glance, the observation that an oil ganglion having viscosity smaller than the viscosity of the aqueous phase that displaces it can move faster than the aqueous phase itself may seem strange. However, this can be explained by considering the role of the porous medium. The pressure difference in the wetting phase along a ganglion with projected length L_g, is of order $O(v_f \mu_w L_g/k)$. Note that the reduced ganglion length, L_g/ℓ, is equivalent to the reduced ganglion volume. The pressure drop inside the ganglion is of the order $O(\epsilon \bar{u}_z \mu_o L_g/k)$. Neglecting the effect of the capillary pressure, the two pressure differences are equal, from which it follows that $u^* = \epsilon\, \bar{u}_z/v_f = O(\mu_w/\mu_o) = O(1/\kappa)$, or $\kappa u^* = O(1)$. This argument is valid when Ca is substantially larger than Ca_{cr}. Closer to the critical Ca value, the capillary pressure cannot be neglected. Accounting for capillarity, $\kappa u^* = O(1) - O(k\sigma \Delta J/v_f \mu_w L_g)$, where ΔJ is a measure of the difference in curvature between the meniscus at the nose of the ganglion and the meniscus at the tail of the ganglion. When $O(k\sigma \Delta J/v_f \mu_w L_g \ll 1)$, this estimate reduces to $\kappa u^* = O(1)$.

Figures 4.23 and 4.24 show the effect of an intermediate wettability for the oleic phase. The viscosity ratio is set at $\kappa = 7.0$, and the receding and advancing contact angles are constant and equal to 10° and 30°, respectively. Comparing these two figures with Figure 4.17, the following conclusions can be drawn:

- The critical value for mobilization decreases as θ_e increases.
- For large values of Ca (say $Ca = 5.0 \times 10^{-3}$), the reduced ganglion velocity decreases as θ_e increases.
- As θ_e increases, the values of u^* for small ganglia (say 2 to 3 CEVS's) become larger than the values for large ganglia.

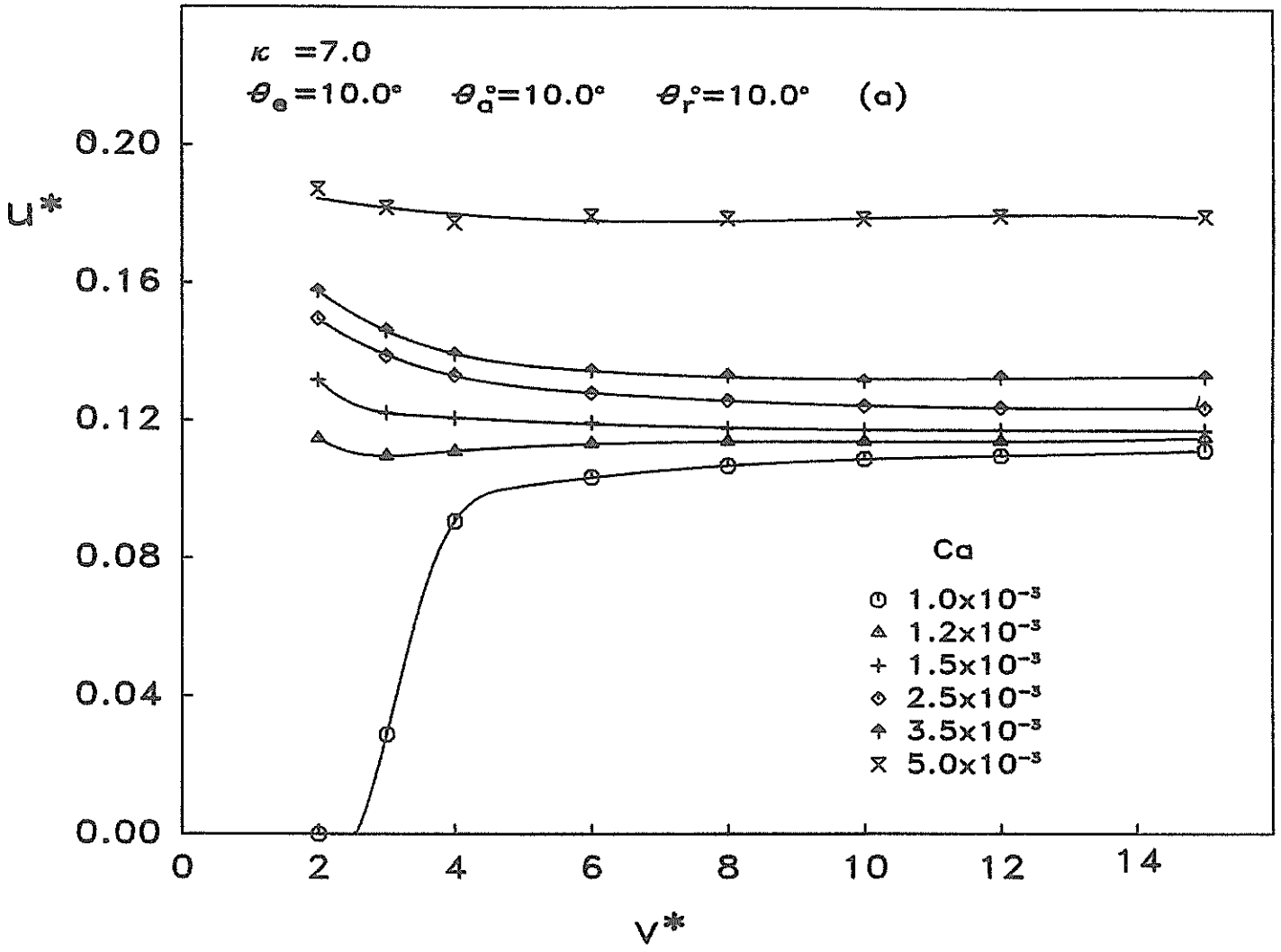


Figure 4.23

Plot of the reduced time-averaged ganglion velocity, u^*, *versus* the reduced ganglion volume, v^*, in a 100 × 200 sandpack for various Ca values. $\kappa = 7.0$, $\theta_e = \theta_a^o = \theta_r^o = 10°$.

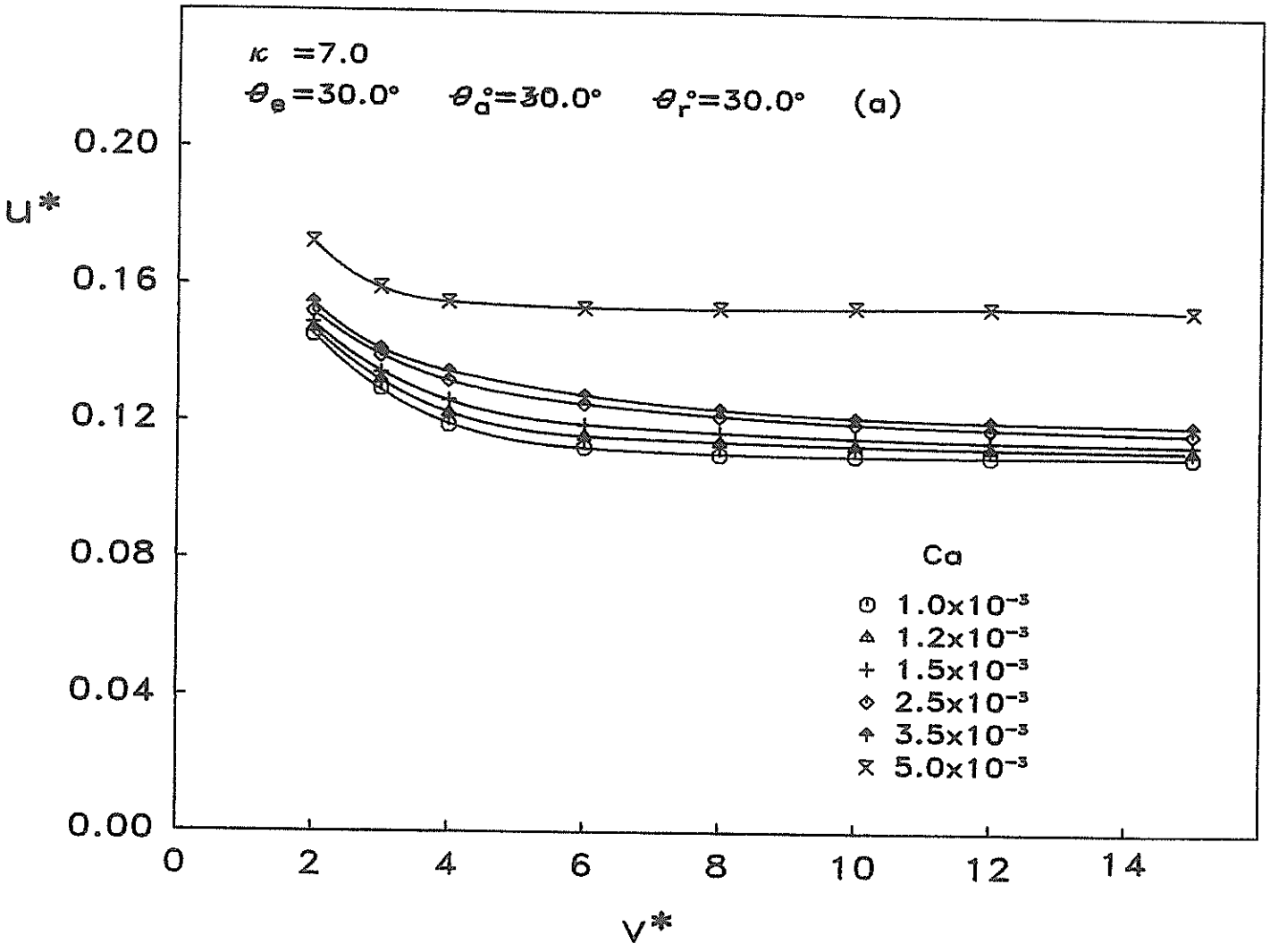


Figure 4.24

Plot of the reduced time-averaged ganglion velocity, u^*, *versus* the reduced ganglion volume, v^*, in a 100 × 200 sandpack for various Ca values. $\kappa = 7.0$, $\theta_e = \theta_a^o = \theta_r^o = 30°$.

Figures 4.25 and 4.26 show the effect of the contact angle hysteresis. The viscosity ratio is set at the same value as the previous two figures, $\kappa = 7.0$. In Figure 4.25, $\theta_e = 10°$, $\theta_a^o = 11.4°$ and $\theta_r^o = 0°$, and in Figure 4.26, $\theta_e = 30°$, $\theta_a^o = 34.2°$ and $\theta_r^o = 9.1°$. Finally, Figures 4.27 and 4.28 illustrate the effect of rate-dependent contact angles. In both figures, $\theta_e = 10°$, $\theta_a^o = 11.4°$, and $\theta_r^o = 0°$. The dependency of the contact angles, θ_a and θ_r , on u_i is given by curves (c) and (d) in Figure 4.3.

The overall conclusion drawn from this last set of figures, in comparison with Figures 4.23 and 4.24, is that the presence of contact angle hysteresis and rate-dependent contact angles does not affect substantially the values of u^*. However, it should be noted that the velocities of small ganglia may change significantly and may even become stranded for the same value of θ_e and different levels of contact angle hysteresis and rate-dependency. For accurate results, it becomes important to obtain complete information on the contact angles. To reinforce this statement it is noted that the results reported in the previous section were obtained using the experimental values for the dynamic contact angles reported by Hinkley (1982).

4.4 Fissioning and Break-up

4.4.1 The Breakup and the Stranding Coefficients.

Payatakes, Ng and Flumerfelt (1980) expressed the effects of stranding and breakup on oil ganglion dynamics (see Equations 2.14 and 2.15) in terms of the stranding coefficient, λ, and the breakup coefficient, ϕ.

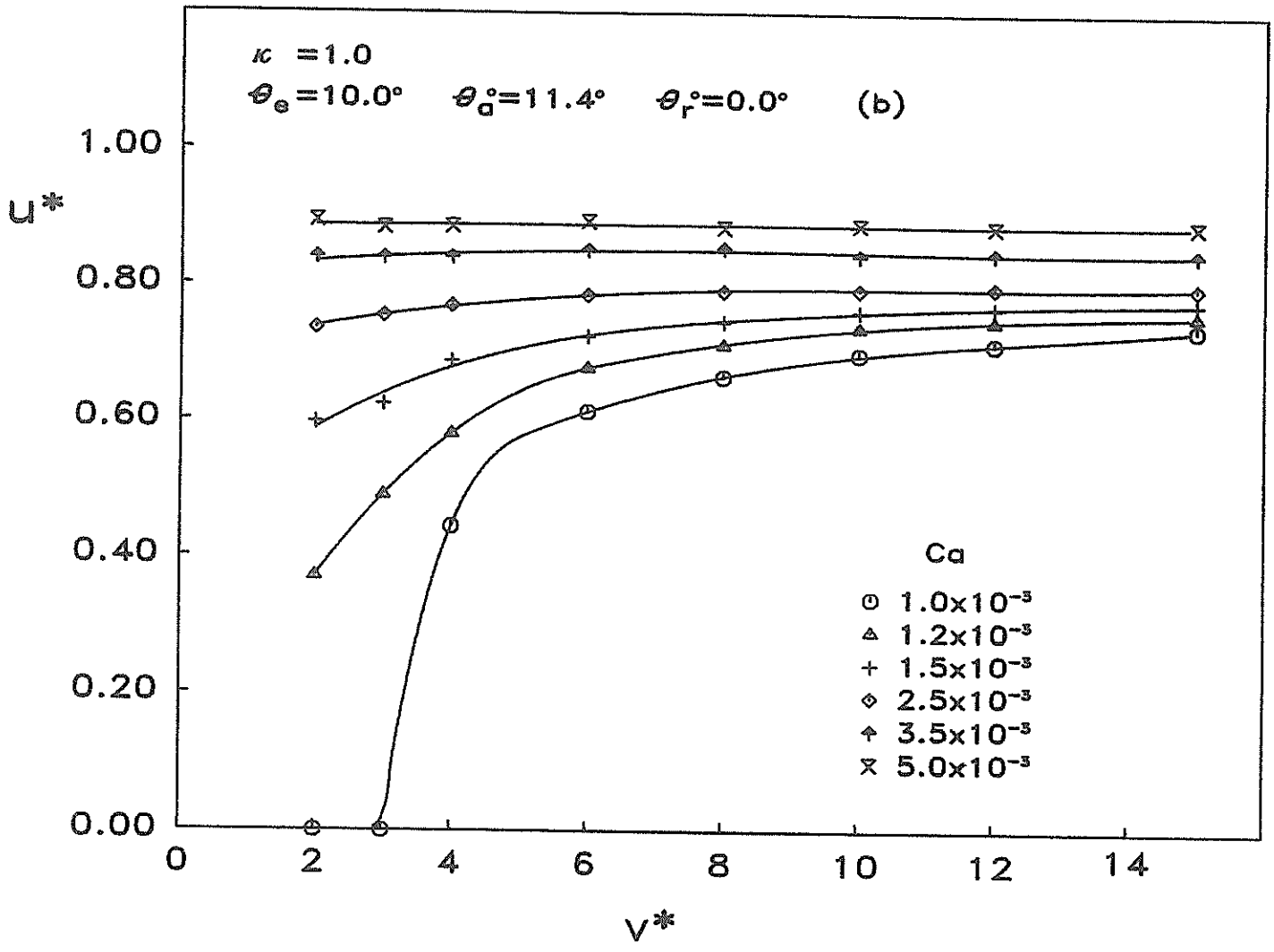


Figure 4.25

Plot of the reduced time-averaged ganglion velocity, u^*, *versus* the reduced ganglion volume, v^*, in a 100 × 200 sandpack for various Ca values. $\kappa = 7.0$, $\theta_e = 10°$, $\theta_a^o = 11.4°$, $\theta_r^o = 0°$.

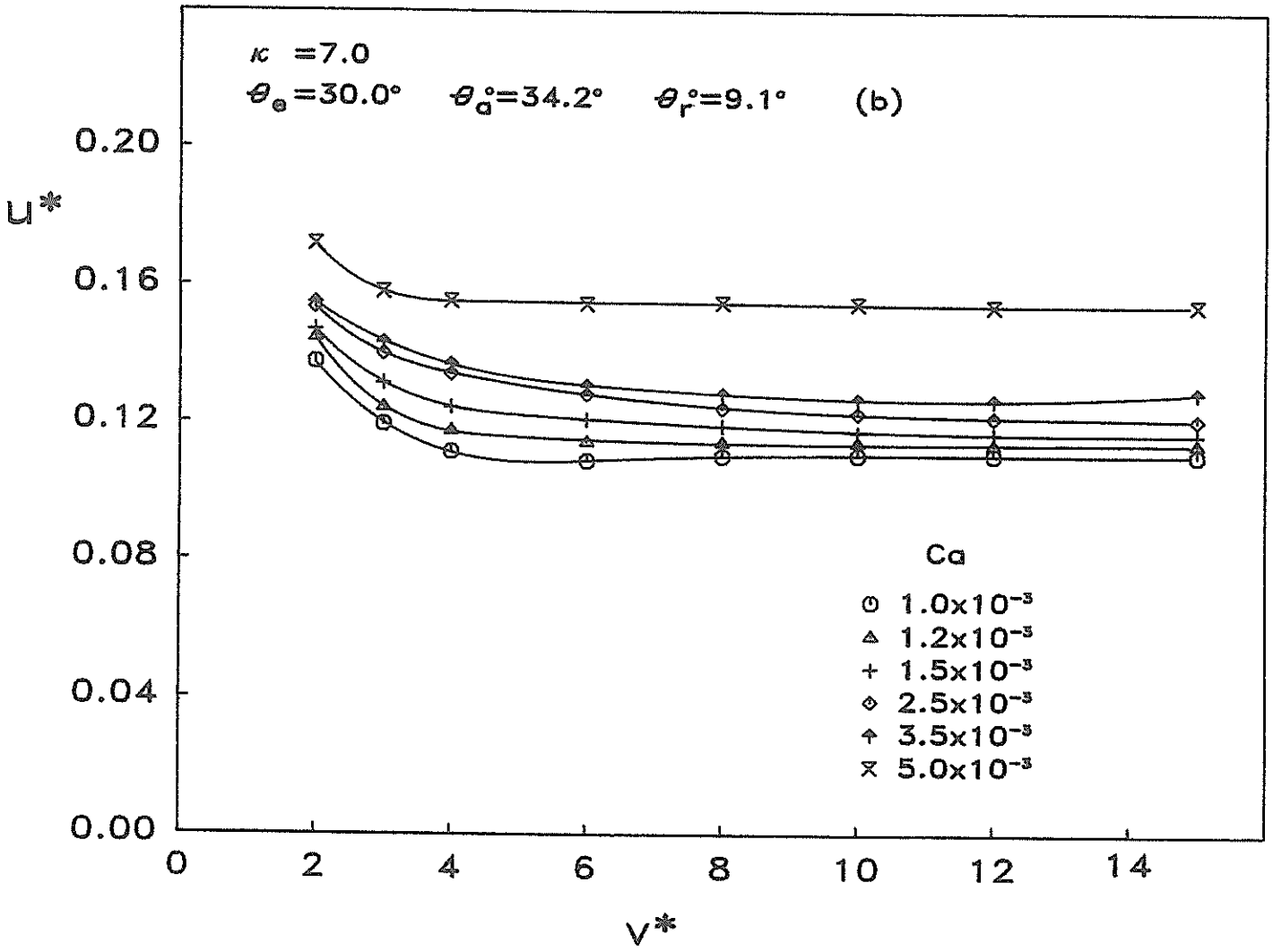


Figure 4.26

Plot of the reduced time-averaged ganglion velocity, u^*, *versus* the reduced ganglion volume, v^*, in a 100 × 200 sandpack for various Ca values. $\kappa = 7.0$, $\theta_e = 30°$, $\theta_a^o = 34.2°$, $\theta_r^o = 9.1°$.

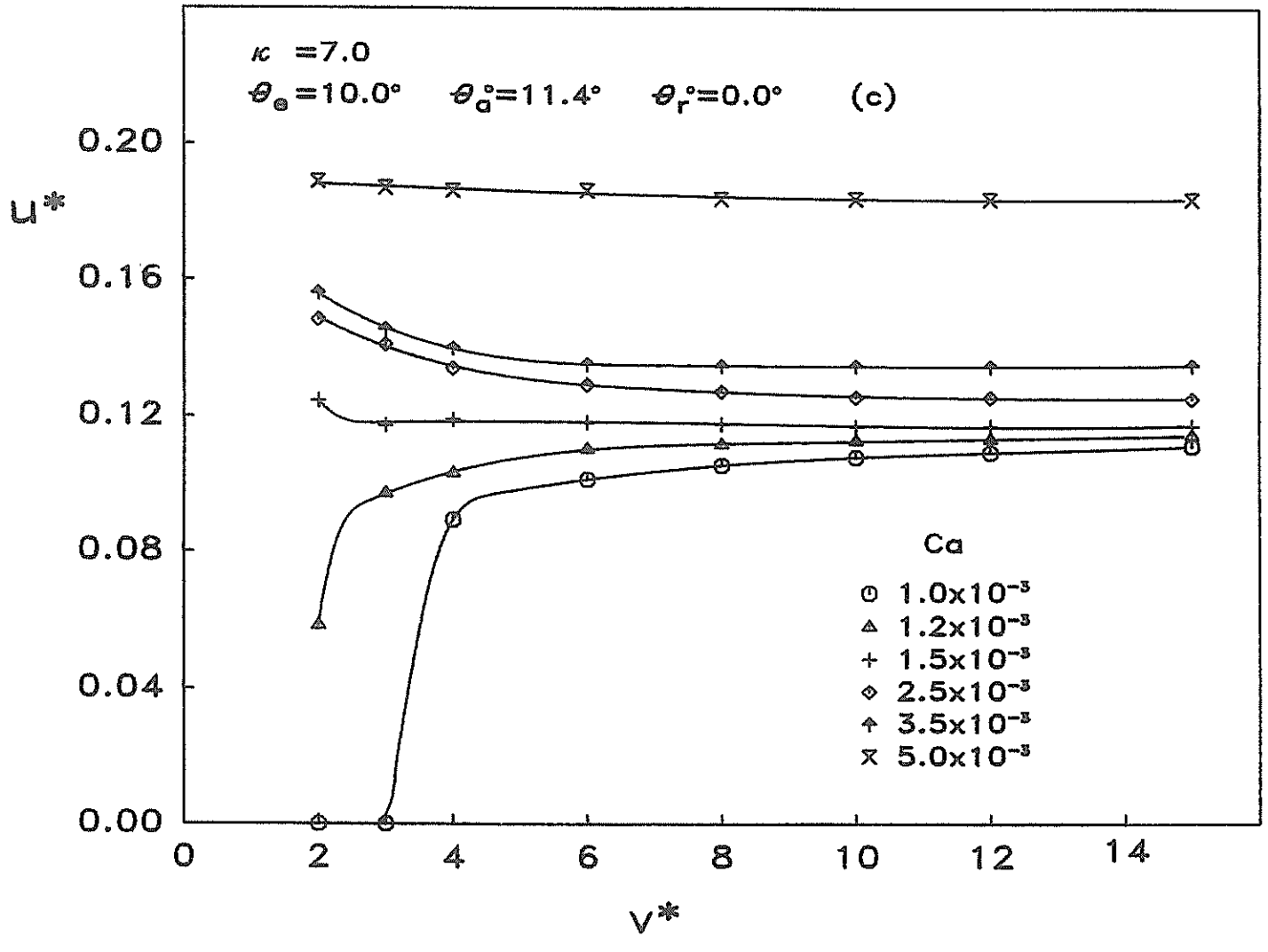


Figure 4.27

Plot of the reduced time-averaged ganglion velocity, u^*, *versus* the reduced ganglion volume, v^*, in a 100 × 200 sandpack for various Ca values. $\kappa = 7.0$, $\theta_e = 10°$, $\theta_a^o = 11.4°$, $\theta_r^o = 0°$. Rate-dependent contact angle as in curve (c), Figure 4.3.

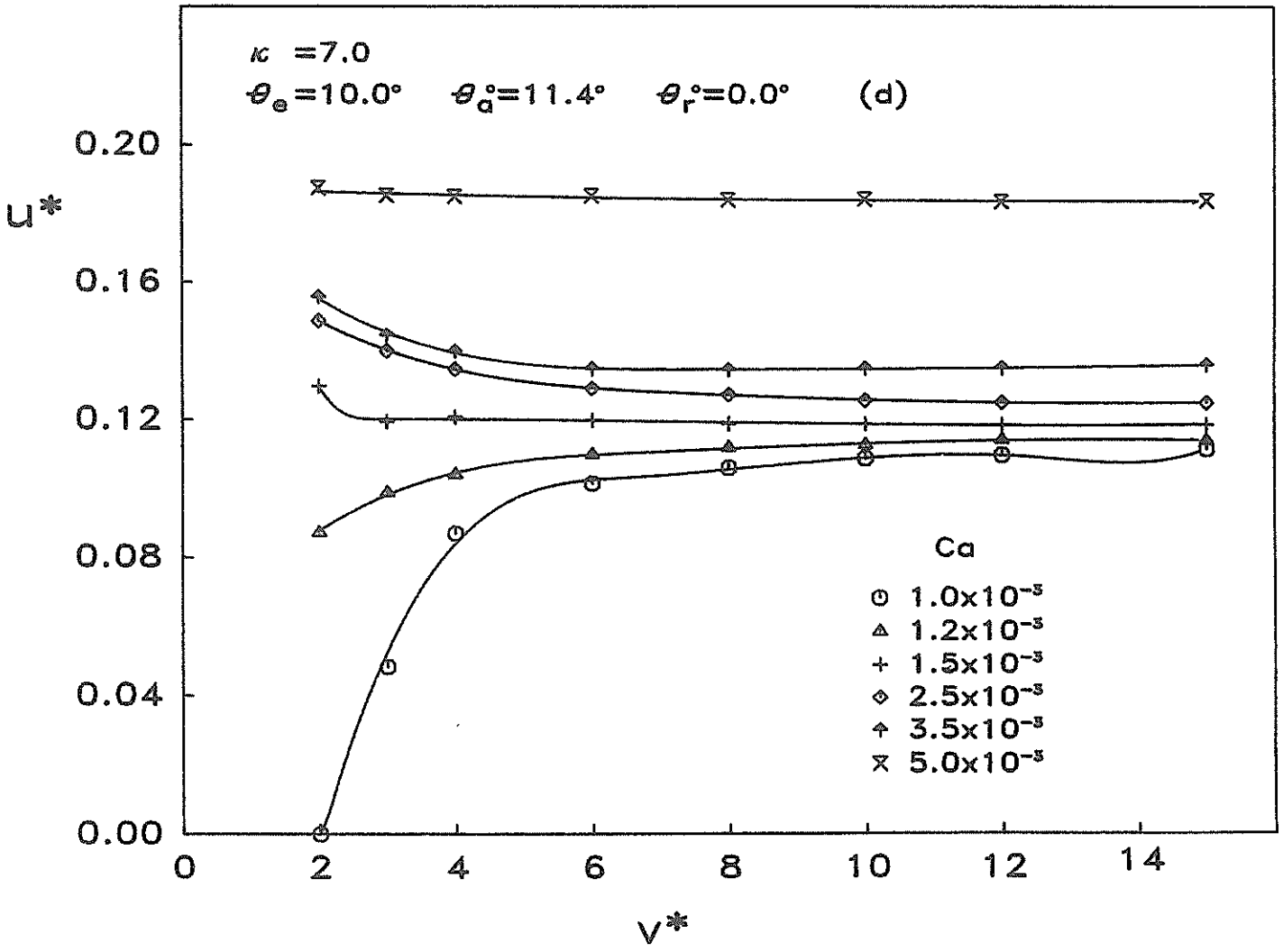


Figure 4.28

Plot of the reduced time-averaged ganglion velocity, u^*, *versus* the reduced ganglion volume, v^*, in a 100 × 200 sandpack for various Ca values. $\kappa = 7.0$, $\theta_e = 10°$, $\theta_a^o = 11.4°$, $\theta_r^o = 0°$. Rate-dependent contact angle as in curve (d), Figure 4.3.

Consider an initial population of v-ganglia (a v-ganglion is defined as one having volume between v and $v + \Delta v$) distributed between two planes which are normal to the main flow direction and are separated by a small distance δ. At time $t = 0$, an immiscible flood starts flowing past the oil ganglia. Neglecting axial dispersion and assuming that the ganglia population is sufficiently sparse that collisions between ganglia are unlikely, this slug of v-ganglia will begin to migrate downstream as a slug with velocity $\bar{u}_z(v; \underline{a}_1)$. As they move, the concentration of v-ganglia is reduced by either stranding or breakup.

Let $n(z, t; v)\Delta v$ be the number of moving v-ganglia at position z per unit porous medium volume. Ng and Payatakes (1980) showed that $n(z, t; v)$, as seen by an observer traveling with the slug, is given by

$$n(z, \tau; v) = n_0 \exp\left[-(\lambda + \phi)z\right] , \tag{4.5}$$

where n_0 is the initial value of $n(t, z; v)$ and τ is a transformed time variable defined as

$$\tau = t - \frac{z}{\bar{u}_z(v; \underline{a}_1)} . \tag{4.6}$$

λ and ϕ, the stranding and the breakup coefficients, respectively, are given by

$$\left.\frac{\partial n}{\partial z}\right|_{\text{due to stranding}} = -\lambda n , \tag{4.7}$$

$$\left.\frac{\partial n}{\partial z}\right|_{\text{due to breakup}} = -\phi n . \tag{4.8}$$

Similarly, the number of stranded v-ganglia at position z per unit porous medium volume, $\sigma(z, \tau; v)\Delta v$, and the number of v-ganglia that fissioned at position z per unit porous medium volume, $\beta(z, \tau; v)\Delta v$, are given by

$$\sigma(z, \tau; v) = \lambda \delta n_0 \exp\left[-(\lambda + \phi)z\right] , \tag{4.9}$$

$$\beta(z,\tau;v) = \phi\delta n_0 \exp\left[-(\lambda+\phi)z\right] . \tag{4.10}$$

Plotting $\ln(n/n_0)$ versus z/ℓ, a straight line with intercept unity and slope $-(\lambda+\phi)\ell$ is obtained. Similarly, plots of $\ln(\sigma\ell/\delta n_0)$ and $\ln(\beta\ell/\delta n_0)$ versus z/ℓ give straight lines with slope $-(\lambda+\phi)\ell$ and intercepts $\ln(\lambda\ell)$ and $\ln(\phi\ell)$, respectively. This linearity is a consequence of the assumption that λ and ϕ are not functions of z and have values which average over the ensemble of completely random shapes. However, if, as was seen before, a ganglion elongates as it moves, its probabilities of breakup and stranding are reduced, and λ and ϕ may very well be functions of z. It follows that the three curves $\ln(n/n_0)$ versus z/ℓ, $\ln(\sigma\ell/\delta n_0)$ versus z/ℓ, and $\ln(\beta\ell/\delta n_0)$ versus z/ℓ may actually deviate from linearity.

In order to calculate the values of λ and ϕ as functions of Ca, κ and v^* and to check for possible elongation effects, the simulation method developed in Chapter 3 can be used.

For a fixed ganglion volume and random initial shape, many simulations are undertaken with the same Ca and κ values, allowing in each simulation the ganglion to migrate until it either breaks or it gets stranded. Superimposing the starting planes of all simulations and considering the entire ensemble of results, values of (n/n_0), $(\sigma\ell/\delta n_0)$, and $(\beta\ell/\delta n_0)$ can be determined. To this end, consider several positions along z, count the number of moving v-ganglia at each position z, the number of stranded v-ganglia left in the interval $(z-\Delta z/2,\ z+\Delta z/2)$, and the number of fissions of v-ganglia in the same interval. The following variables are readily obtained:

$$\chi = \frac{\text{number of } v\text{-ganglia moving at position } z}{\text{initial number of } v\text{-ganglia}} \tag{4.11}$$

$$\psi = \frac{\text{number of } v\text{-ganglia stranded in the interval}(z \pm \Delta z/2)}{\text{initial number of } v\text{-ganglia}} \tag{4.12}$$

$$\omega = \frac{\text{number of } v\text{-ganglia fissioned in the interval}(z \pm \Delta z/2)}{\text{initial number of } v\text{-ganglia}} \tag{4.13}$$

Of course, these results are meaningful only if Δz is small, say $(\Delta z \ll \ell)$. In this way the values (n/n_0), $(\sigma\ell/\delta n_0)$, and $(\beta\ell/\delta n_0)$ correspond to χ, $(\psi\ell/\Delta z)$, and $(\omega\ell/\Delta z)$, respectively. Plotting $(\psi\ell/\Delta z)$ and $(\omega\ell/\Delta z)$ versus z/ℓ, the values of $\lambda\ell$ and $\phi\ell$ may be obtained by a simple linear fitting.

The results of this study for ganglia of various sizes are shown in Figures 4.29 through 4.37. In each figure, two plots at different Ca values are shown. Both curves, $(\psi\ell/\Delta z)$ versus z/ℓ and $(\omega\ell/\Delta z)$ versus z/ℓ, are plotted, except for the cases where too few ganglia were stranded and the curve $(\psi\ell/\Delta z)$ is omitted. Inspection of these figures leads to the following observations:

- Fewer and fewer ganglia get stranded as the capillary number and the ganglion size increase. For sufficiently large ganglia, $\lambda\ell$ becomes nil.
- On the contrary, high capillary numbers and large ganglion sizes favor the fissioning process.
- For small values of Ca and small ganglia ($v^* = 4$ to 7), the curves show a definite deviation from linearity, implying the presence of elongation effects.
- As the viscosity ratio increases, more and more ganglia get stranded while the rate of fissioning decreases. However, the rate at which ganglia get stranded increases more with κ than the rate of fissioning increases.

The first three observations are in accordance with previous observations (Ng, Payatakes, 1980; Rapin, 1980; Payatakes, Woodham and Ng, 1981) and with the ganglia velocity results reported in the previous section.

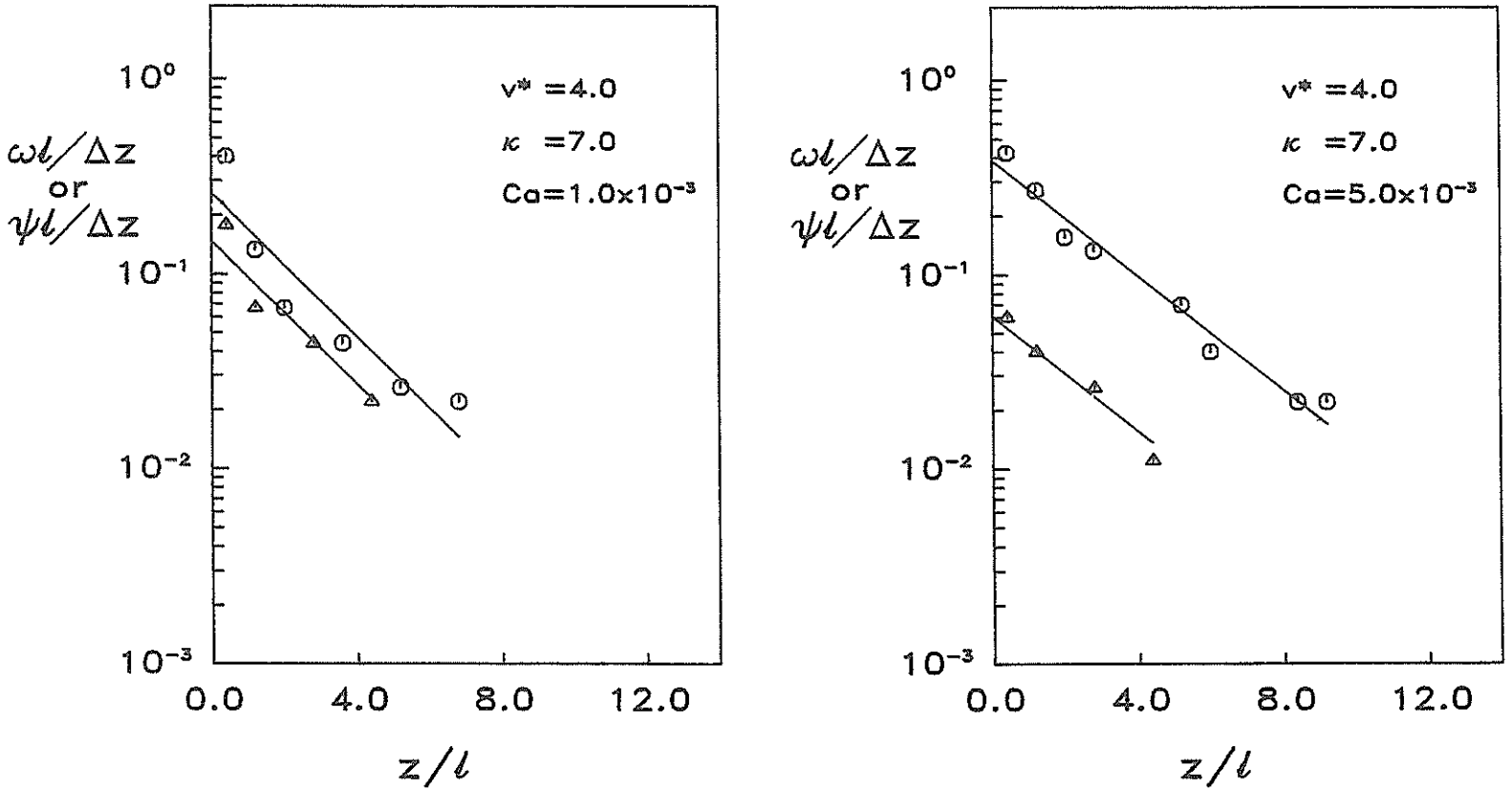


Figure 4.29

Plots of $(\omega\ell/\Delta z)$ and $(\psi\ell/\Delta z)$, *versus* the normalized length of migration, z/ℓ in a 100×200 sandpack, for a 4-CEVS ganglion, $\kappa = 7.0$ and a) $Ca = 10^{-3}$; b) $Ca = 5 \times 10^{-3}$.

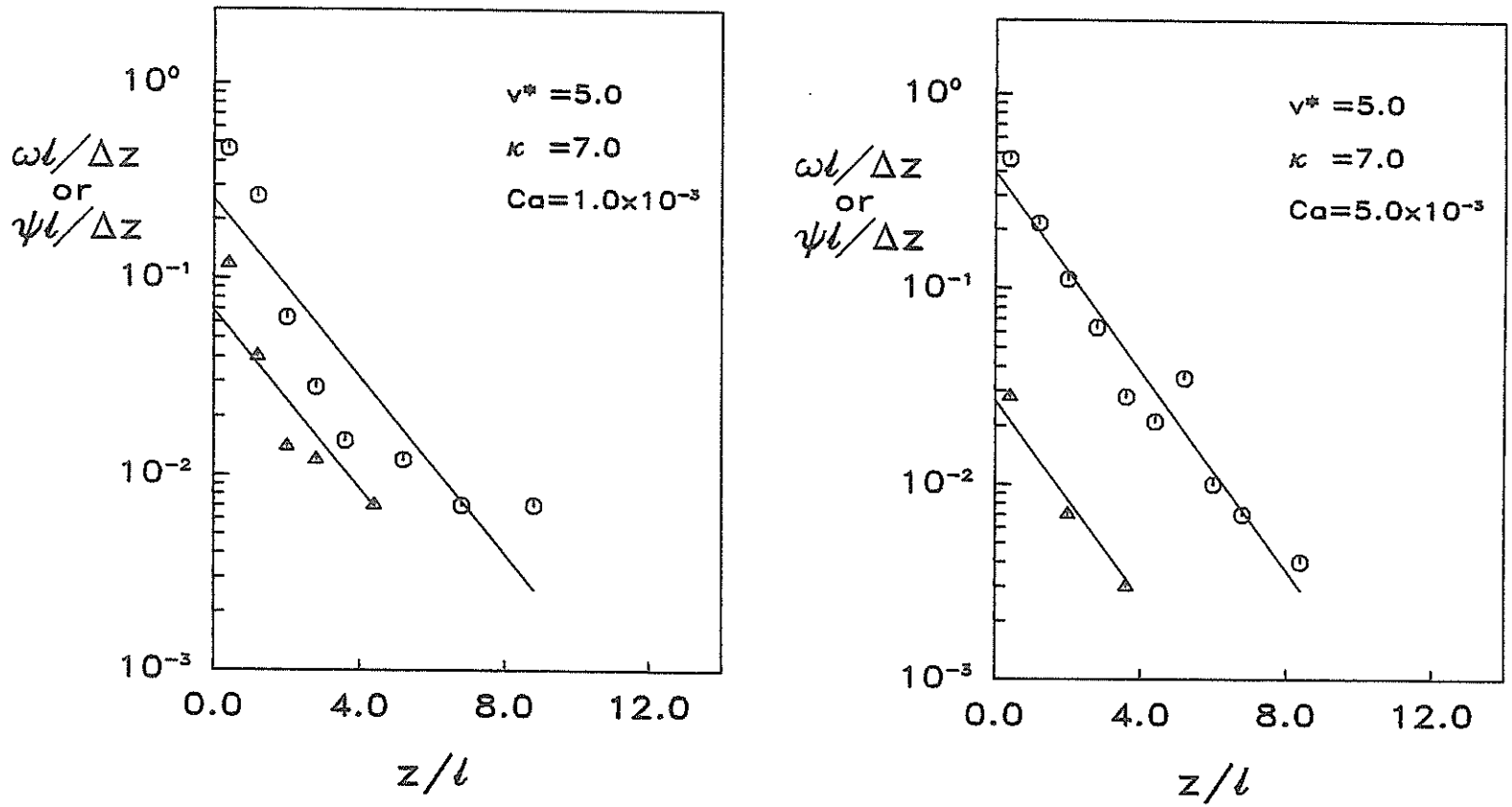


Figure 4.30

Plots of $(\omega\ell/\Delta z)$ and $(\psi\ell/\Delta z)$, *versus* the normalized length of migration, z/ℓ, in a 100 × 200 sandpack, for a 5-CEVS ganglion, $\kappa = 7.0$ and a) $Ca = 10^{-3}$; b) $Ca = 5 \times 10^{-3}$.

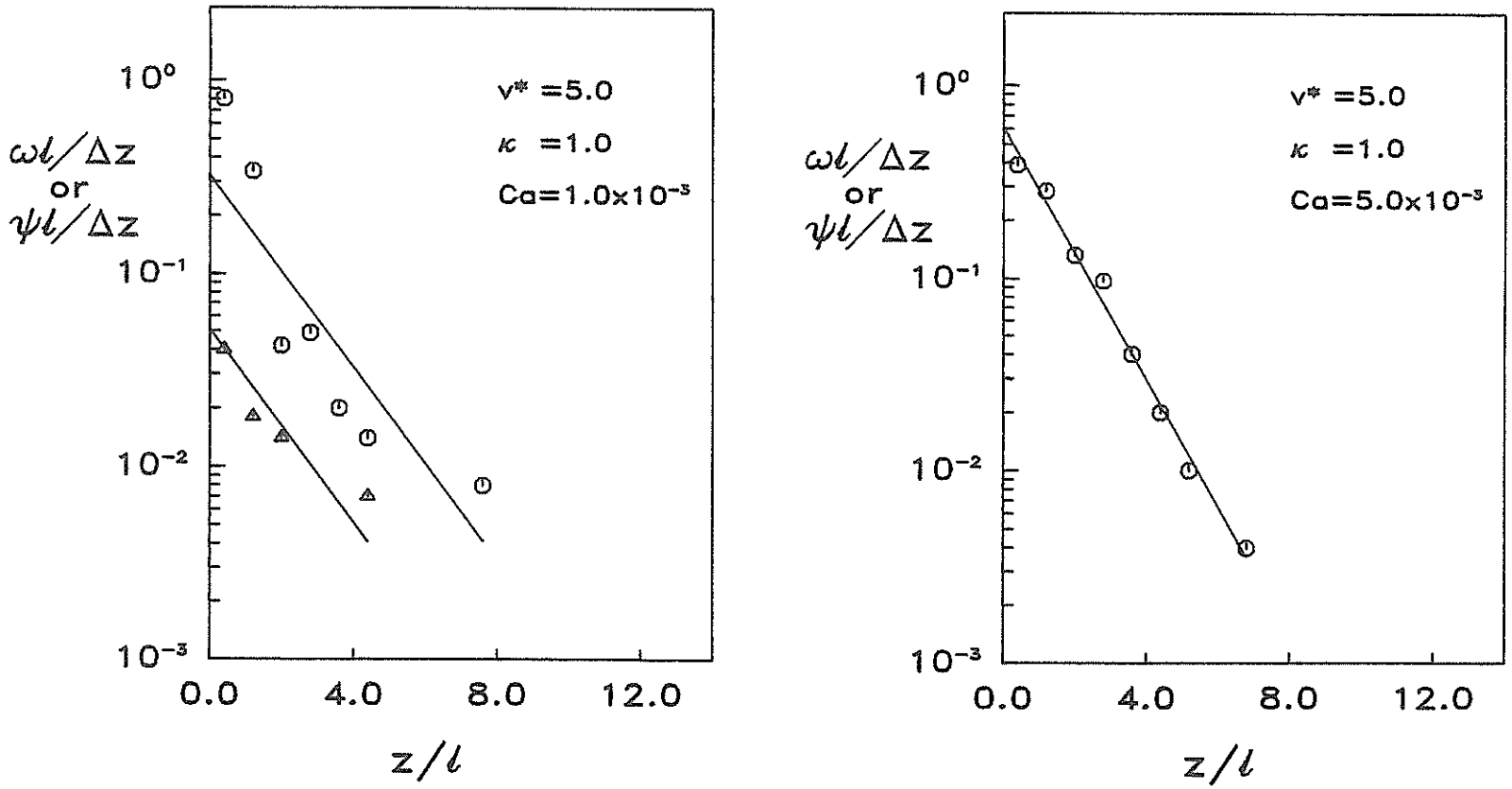


Figure 4.31

Plots of $(\omega\ell/\Delta z)$ and $(\psi\ell/\Delta z)$, *versus* the normalized length of migration, z/ℓ, in a 100×200 sandpack, for a 5-CEVS ganglion, $\kappa = 1.0$ and a) $Ca = 10^{-3}$; b) $Ca = 5 \times 10^{-3}$.

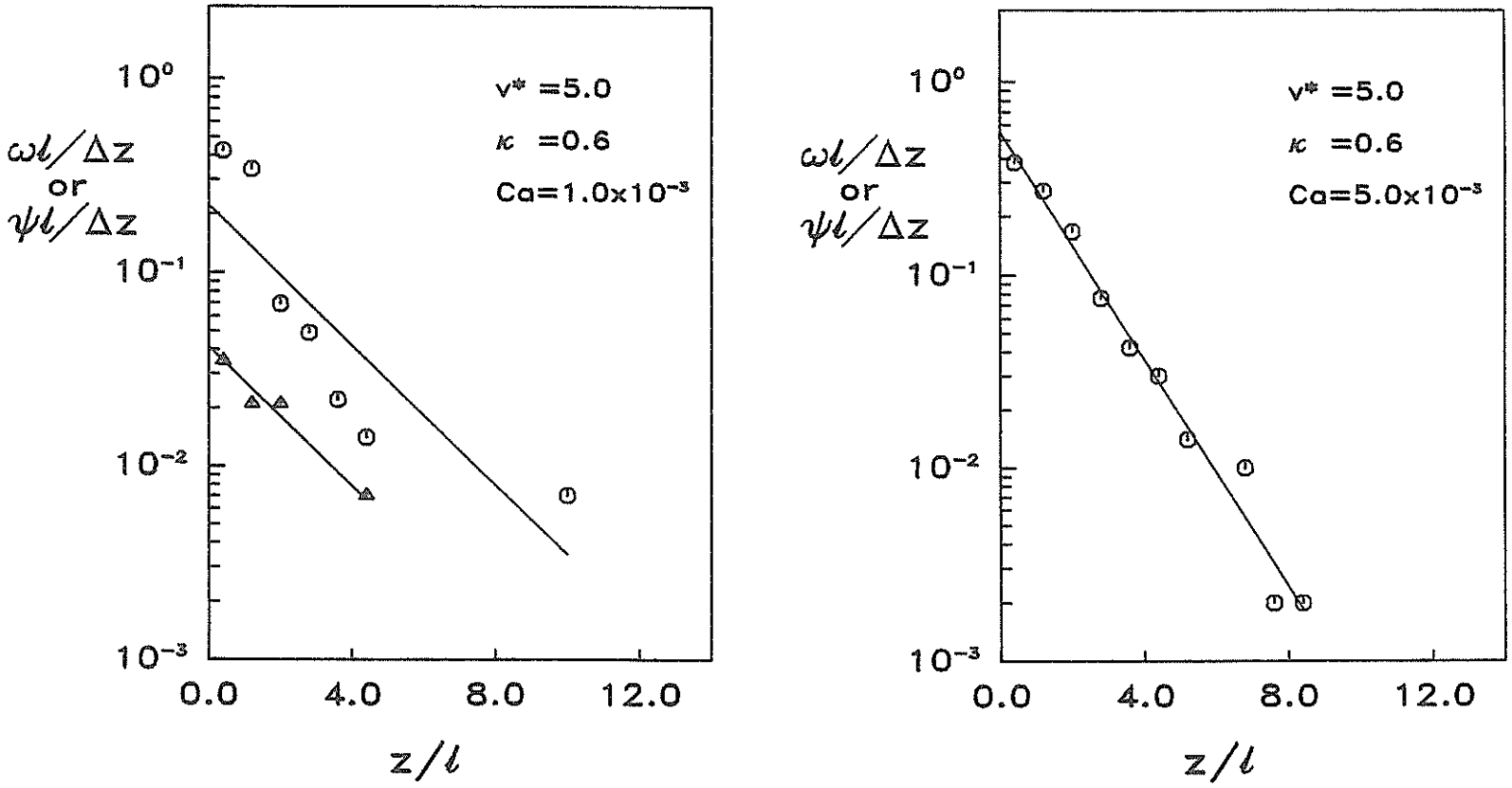


Figure 4.32

Plots of $(\omega\ell/\Delta z)$ and $(\psi\ell/\Delta z)$, *versus* the normalized length of migration, z/ℓ, in a 100×200 sandpack, for a 5-CEVS ganglion, $\kappa = 0.6$ and a) $Ca = 10^{-3}$; b) $Ca = 5 \times 10^{-3}$.

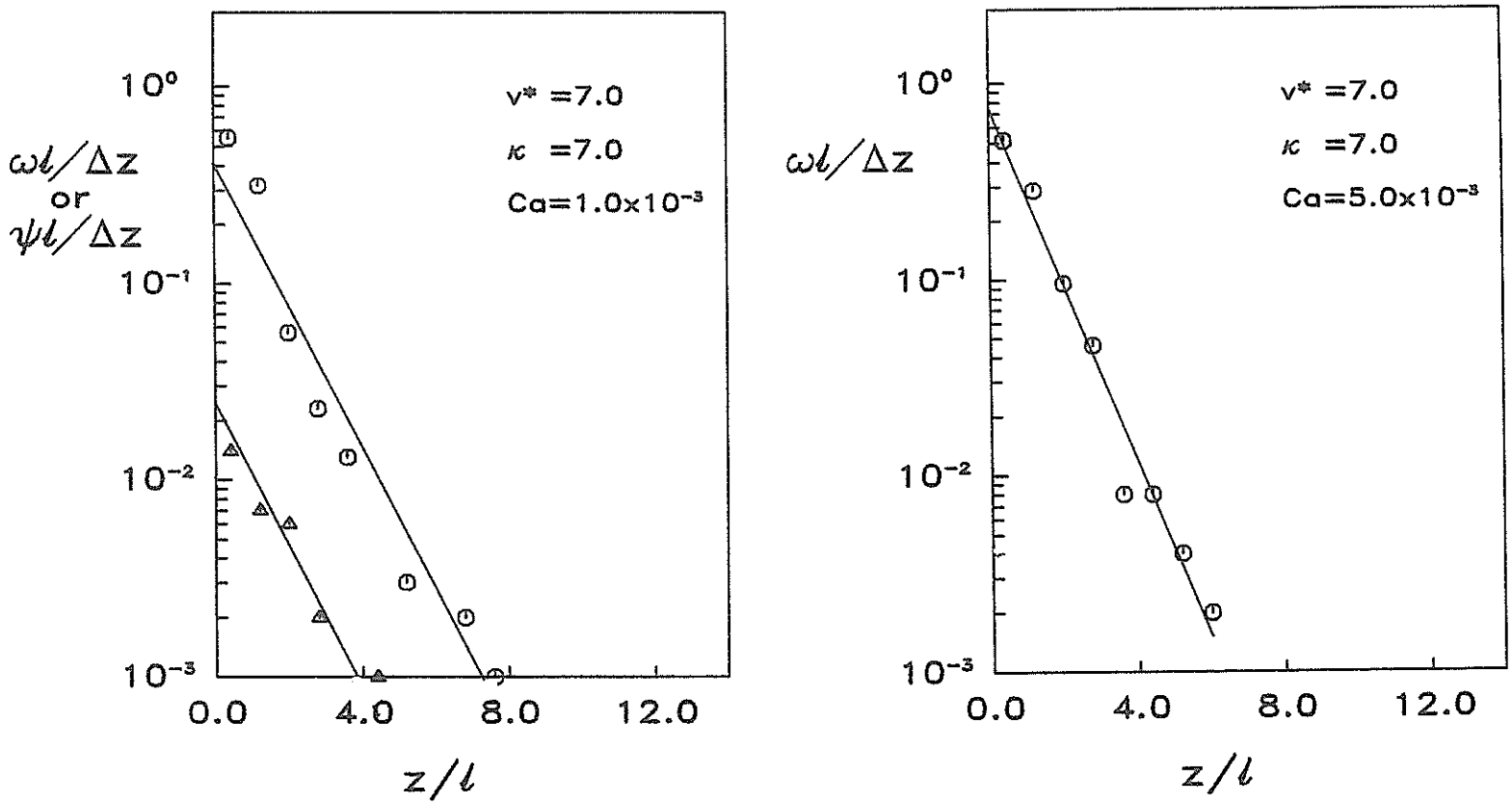


Figure 4.33

Plots of $(\omega\ell/\Delta z)$ and $(\psi\ell/\Delta z)$, *versus* the normalized length of migration, z/ℓ, in a 100 × 200 sandpack, for a 7-CEVS ganglion, $\kappa = 7.0$ and a) $Ca = 10^{-3}$; b) $Ca = 5 \times 10^{-3}$.

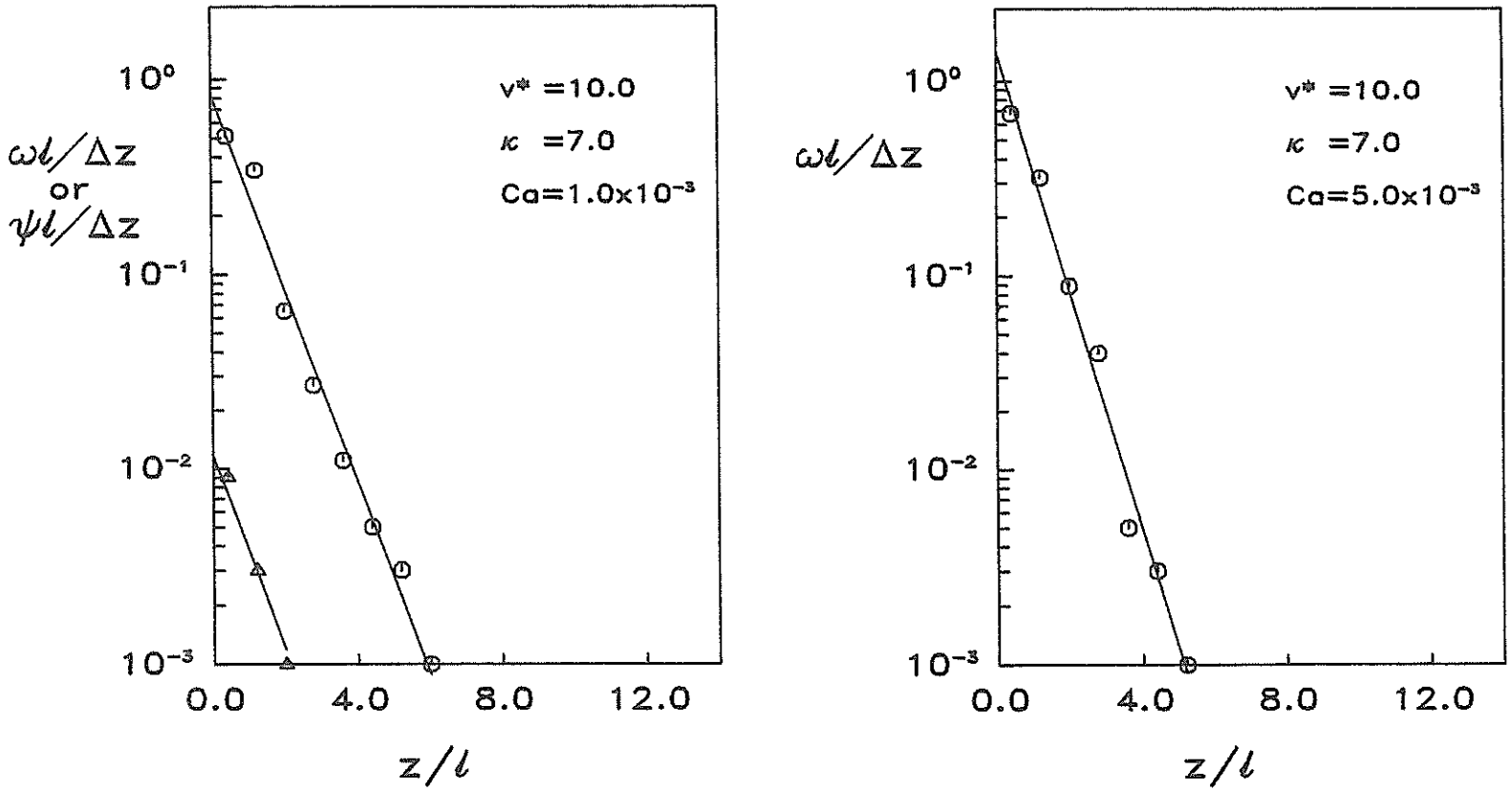


Figure 4.34

Plots of $(\omega\ell/\Delta z)$ and $(\psi\ell/\Delta z)$, *versus* the normalized length of migration, z/ℓ, in a 100×200 sandpack, for a 10-CEVS ganglion, $\kappa = 7.0$ and a) $Ca = 10^{-3}$; b) $Ca = 5 \times 10^{-3}$.

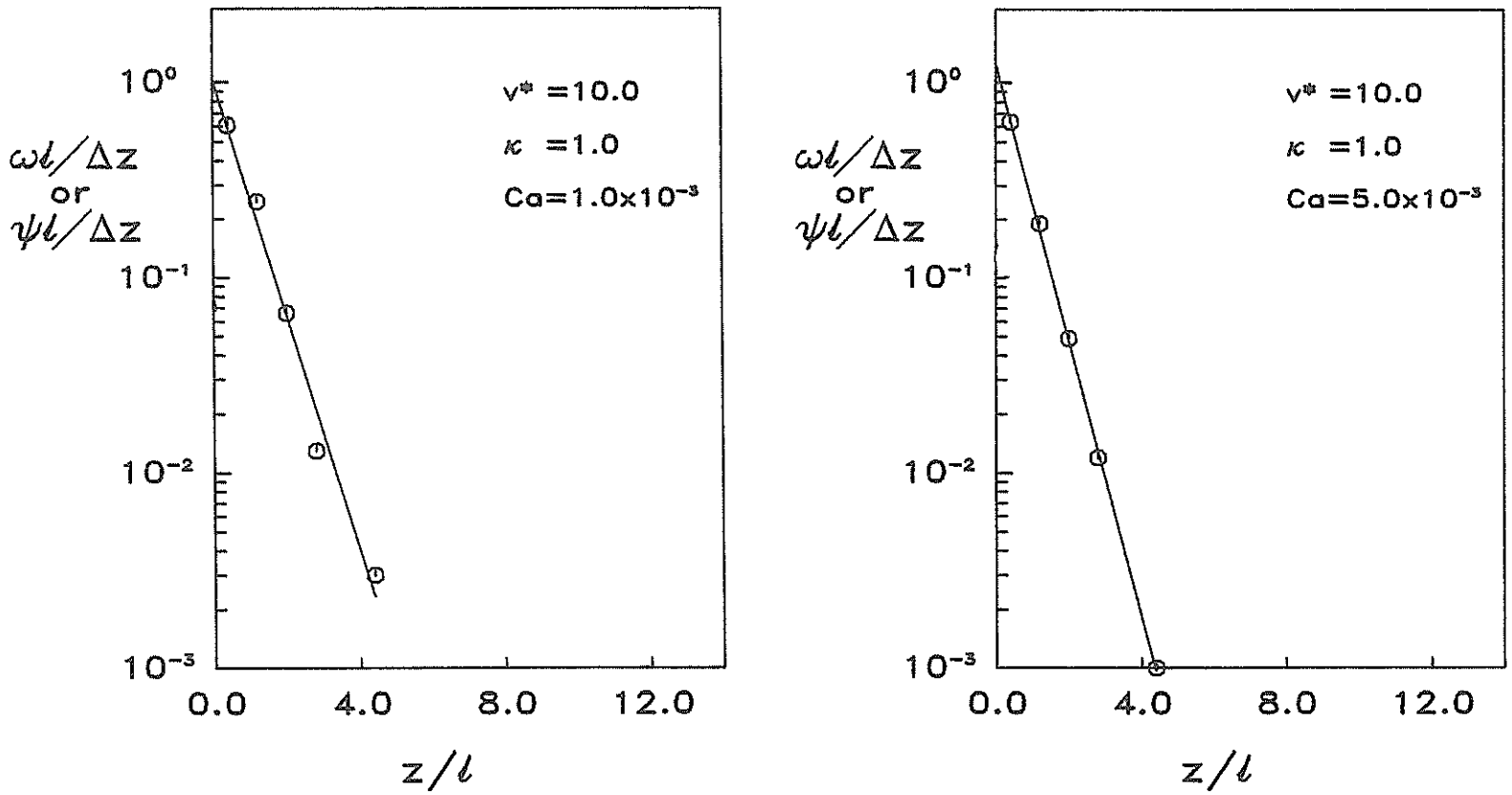


Figure 4.35

Plots of $(\omega\ell/\Delta z)$ and $(\psi\ell/\Delta z)$, *versus* the normalized length of migration, z/ℓ, in a 100×200 sandpack, for a 10-CEVS ganglion, $\kappa = 1.0$ and a) $Ca = 10^{-3}$; b) $Ca = 5 \times 10^{-3}$.

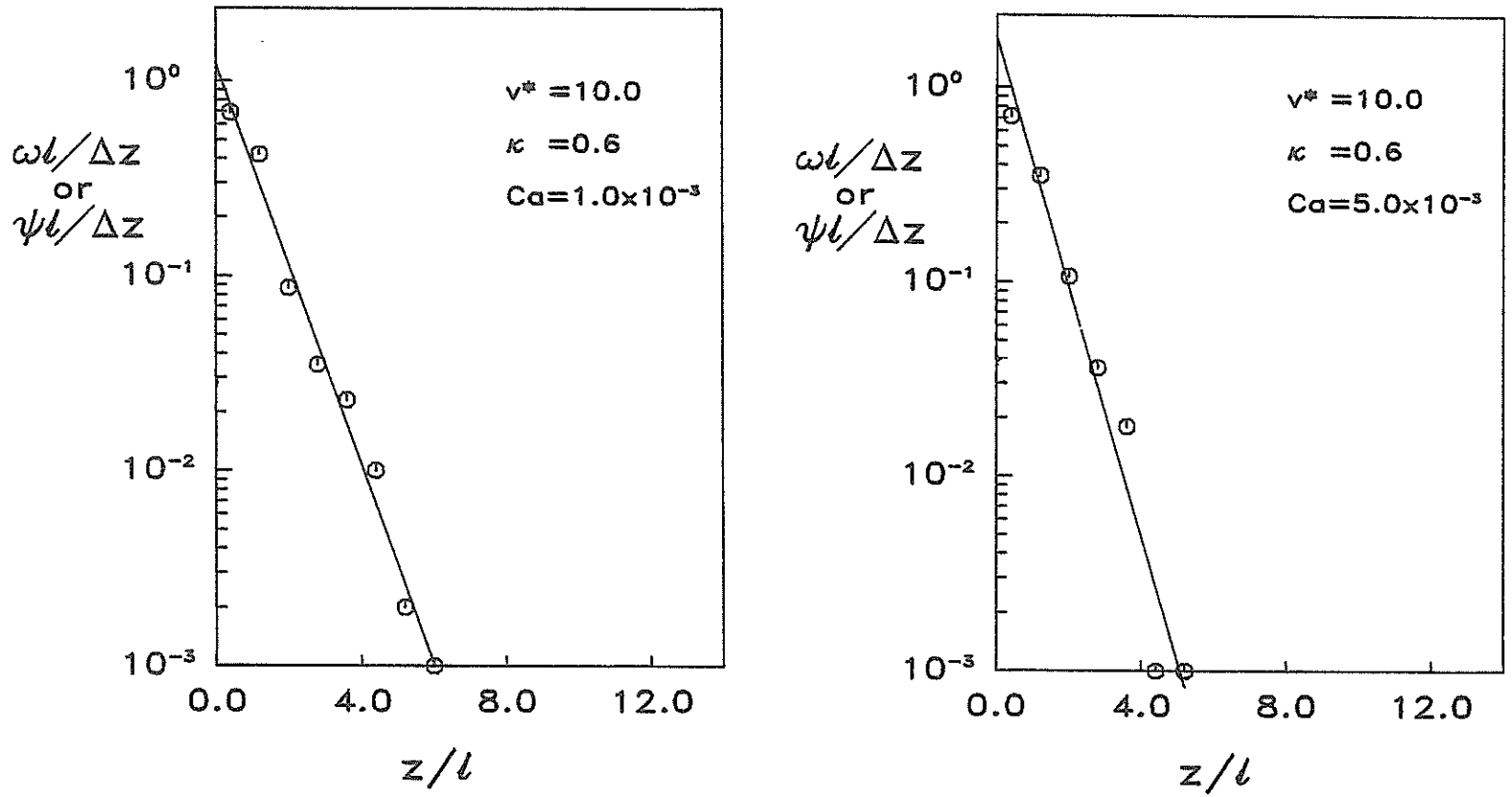


Figure 4.36

Plots of $(\omega\ell/\Delta z)$ and $(\psi\ell/\Delta z)$, *versus* the normalized length of migration, z/ℓ, in a 100×200 sandpack, for a 10-CEVS ganglion, $\kappa = 0.6$ and a) $Ca = 10^{-3}$; b) $Ca = 5 \times 10^{-3}$.

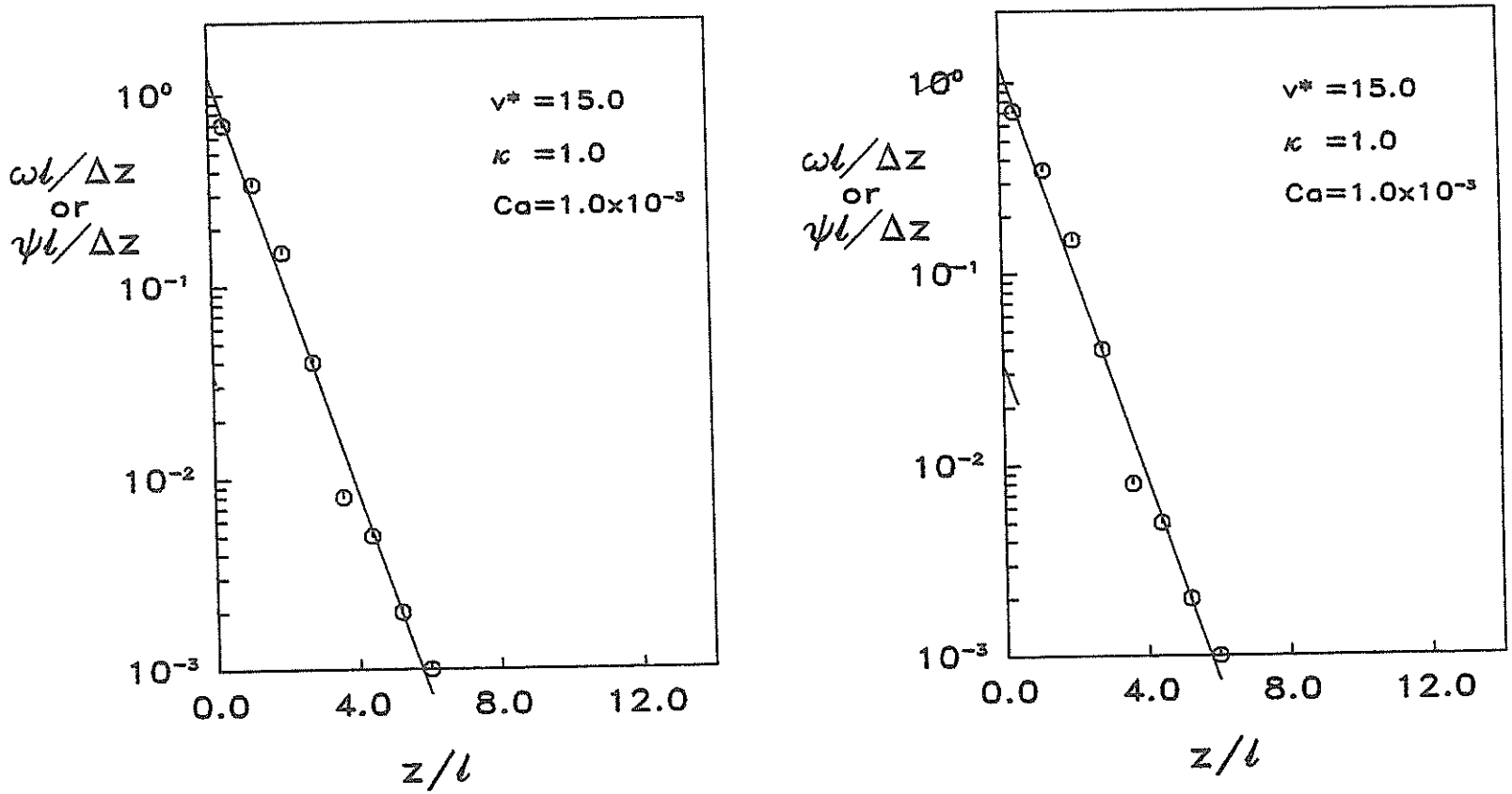


Figure 4.37

Plots of $(\omega\ell/\Delta z)$ and $(\psi\ell/\Delta z)$, *versus* the normalized length of migration, z/ℓ, in a 100×200 sandpack, for a 15-CEVS ganglion, $\kappa = 1.0$ and a) $Ca = 10^{-3}$; b) $Ca = 5 \times 10^{-3}$.

In order to verify the effects of elongation, the values of $\lambda\ell$ and $\phi\ell$ as calculated above may be compared with their values when calculated at each position z/ℓ. Following Payatakes, Woodham and Ng (1981), consider the conceptual slug experiment. A simple balance to the number of v-ganglia gives,

$$\sigma = -\delta\left[\frac{\partial n(z,\tau;v)}{\partial z}\right]_{\text{due only to stranding}} \tag{4.15}$$

$$\beta = -\delta\left[\frac{\partial n(z,\tau;v)}{\partial z}\right]_{\text{due only to break-up}} \tag{4.16}$$

Combining equations 4.7 and 4.15, and 4.8 and 4.16,

$$\lambda = \frac{\sigma(z,\tau;v)}{\delta n(z,\tau;z)} \tag{4.17}$$

$$\phi = \frac{\sigma(z,\tau;v)}{\delta n(z,\tau;z)}\ . \tag{4.18}$$

Recalling that the values of (n/n_0), $(\sigma\ell/\delta n_0)$, and $(\beta\ell/\delta n_0)$ are given by χ, $(\psi\ell/\Delta z)$, and $(\omega\ell/\Delta z)$, respectively, $\lambda\ell$ and $\phi\ell$ at various positions can be calculated as follows:

$$\lambda\ell = \frac{(\psi\ell/\Delta z)}{\chi} \qquad \text{(at fixed } z/\ell) \tag{4.19}$$

$$\phi\ell = \frac{(\omega\ell/\Delta z)}{\chi} \qquad \text{(at fixed } z/\ell)\ . \tag{4.20}$$

Values of $\lambda\ell$ and $\phi\ell$ versus z/ℓ for 4-CEVS, 5-CEVS and 7-CEVS ganglia at $Ca = 10^{-3}$ and $\kappa = 7.0$ are plotted in Figures 4.38 and 4.39. These plots confirm that there exists a strong dependency of both $\lambda\ell$ and $\phi\ell$ on z/ℓ, especially for small ganglia. These findings are in accordance with the results reported by Payatakes, Woodham and Ng (1981), except that in their case, the dependency of $\phi\ell$ on z/ℓ was not so strong and presented a much more erratic behavior. The elongation

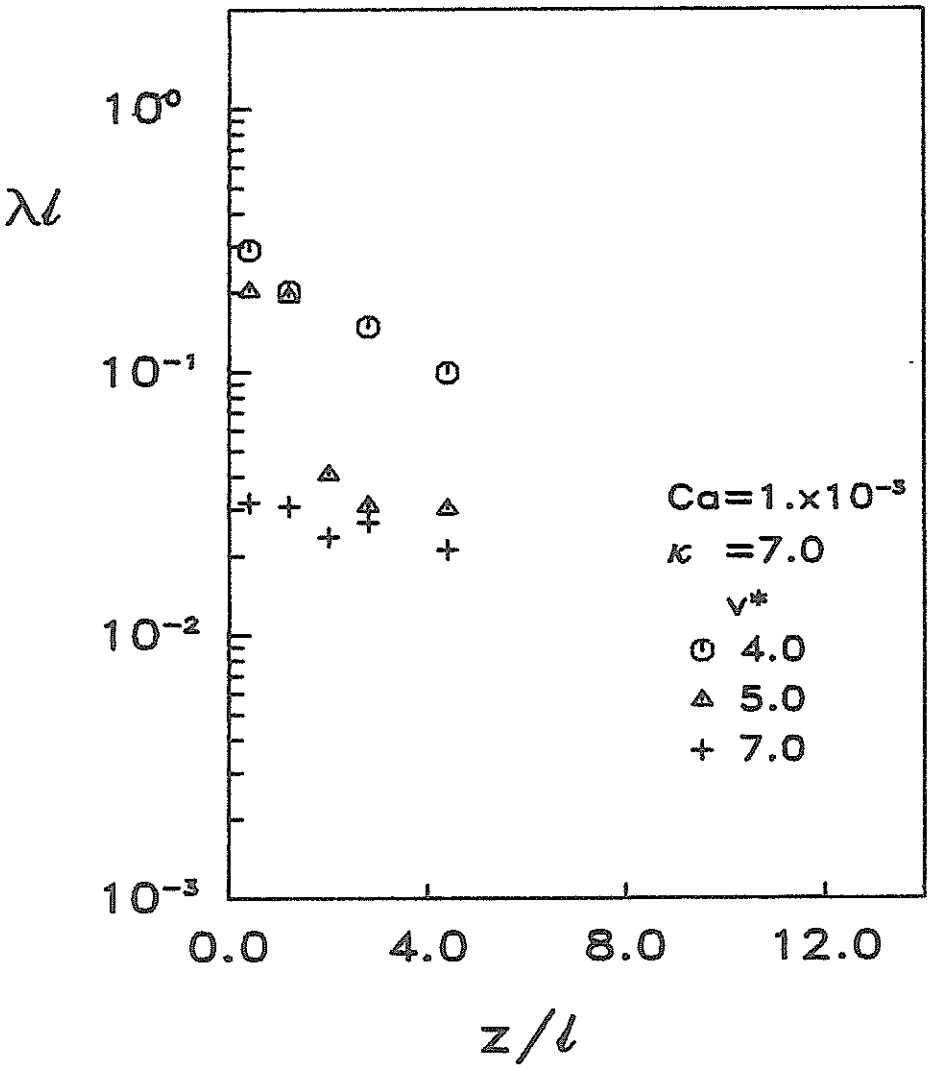


Figure 4.38

Plot of the normalized stranding coefficient, $\lambda\ell$, *versus* the normalized length of migration, z/ℓ, in a 100×200 sandpack, for 4, 5 and 7-CEVS ganglia, $\kappa = 7.0$ and $Ca = 10^{-3}$.

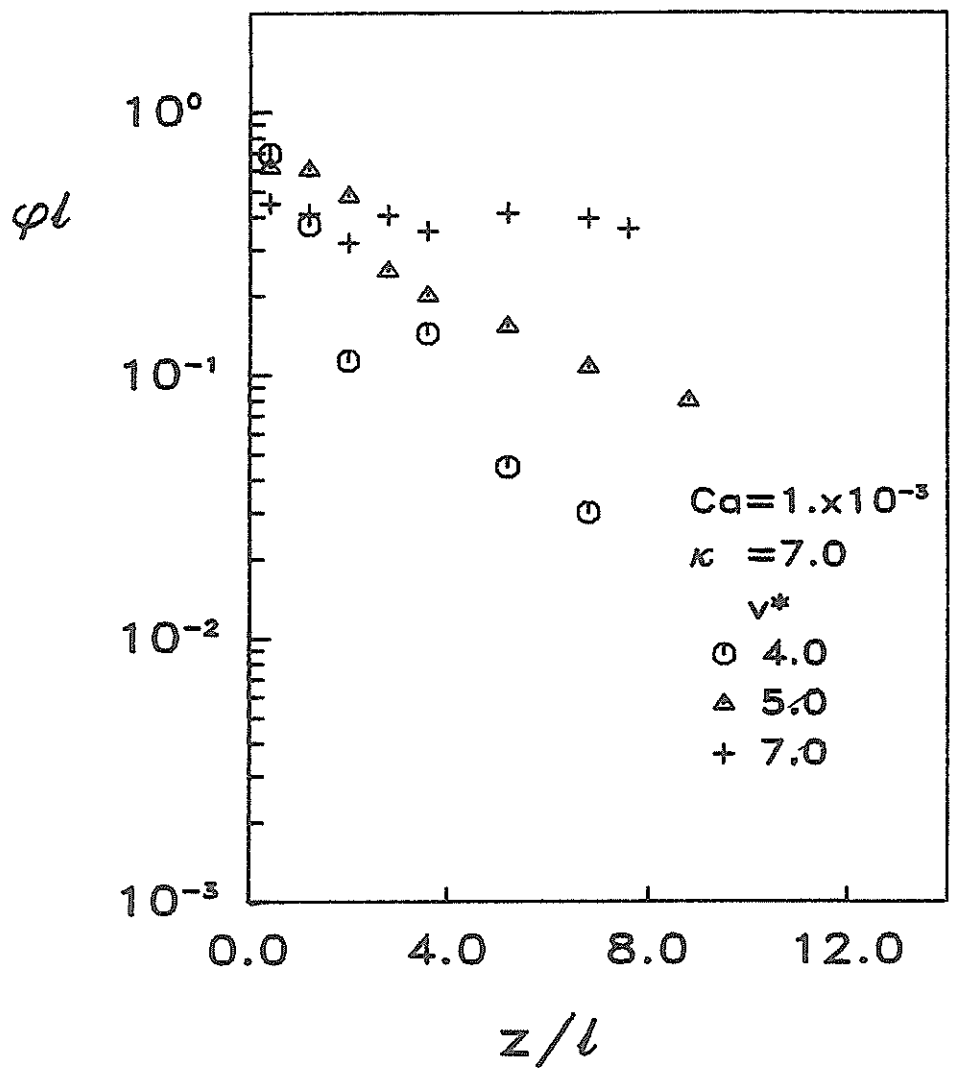


Figure 4.39

Plot of the normalized break-up coefficient, $\phi\ell$, *versus* the normalized length of migration, z/ℓ, in a 100 × 200 sandpack, for 4, 5 and 7-CEVS ganglia, $\kappa = 7.0$ and $Ca = 10^{-3}$.

effect is much more important in dynamic displacement since as it was observed in previous simulations (see, e.g. Figure 4.12), only by elongating, does a moving ganglion have any chance of surviving.

In order to compare and summarize these results, the break-up coefficient and the stranding coefficient are plotted versus the ganglion size for various capillary numbers in Figures 4.40 through 4.43. Due to the scarcity of data points in the other cases, only the case of $\kappa = 7.0$ is plotted for $\lambda\ell$. The role of the viscosity ratio in the break-up coefficient is not very clear or very strong. It seems that once a ganglion is mobilized, its chances of break-up are nearly the same, independently of its viscosity.

The capillary number plays an important role in the mobilization and break-up of small ganglia and a lesser, but still important, role for large ganglia. In general, an increase of the capillary number results in an increase of the break-up coefficient.

Finally, the ganglion size seems to be the single most important factor on break-up and stranding. The probability of break-up increases significantly with the ganglion size, while the probability of stranding decreases. It seems that every ganglion is destined to fission into smaller and smaller daughter ganglia, which in turn have a high probability of getting stranded.

4.4.2 Break-up Mode

Another important parameter in the dynamics of oil ganglion populations is the break-up mode probability, $W(w,v)\Delta v$, defined as the probability that a moving w-ganglion will break into two daughter ganglia, one of which is a v-ganglion.

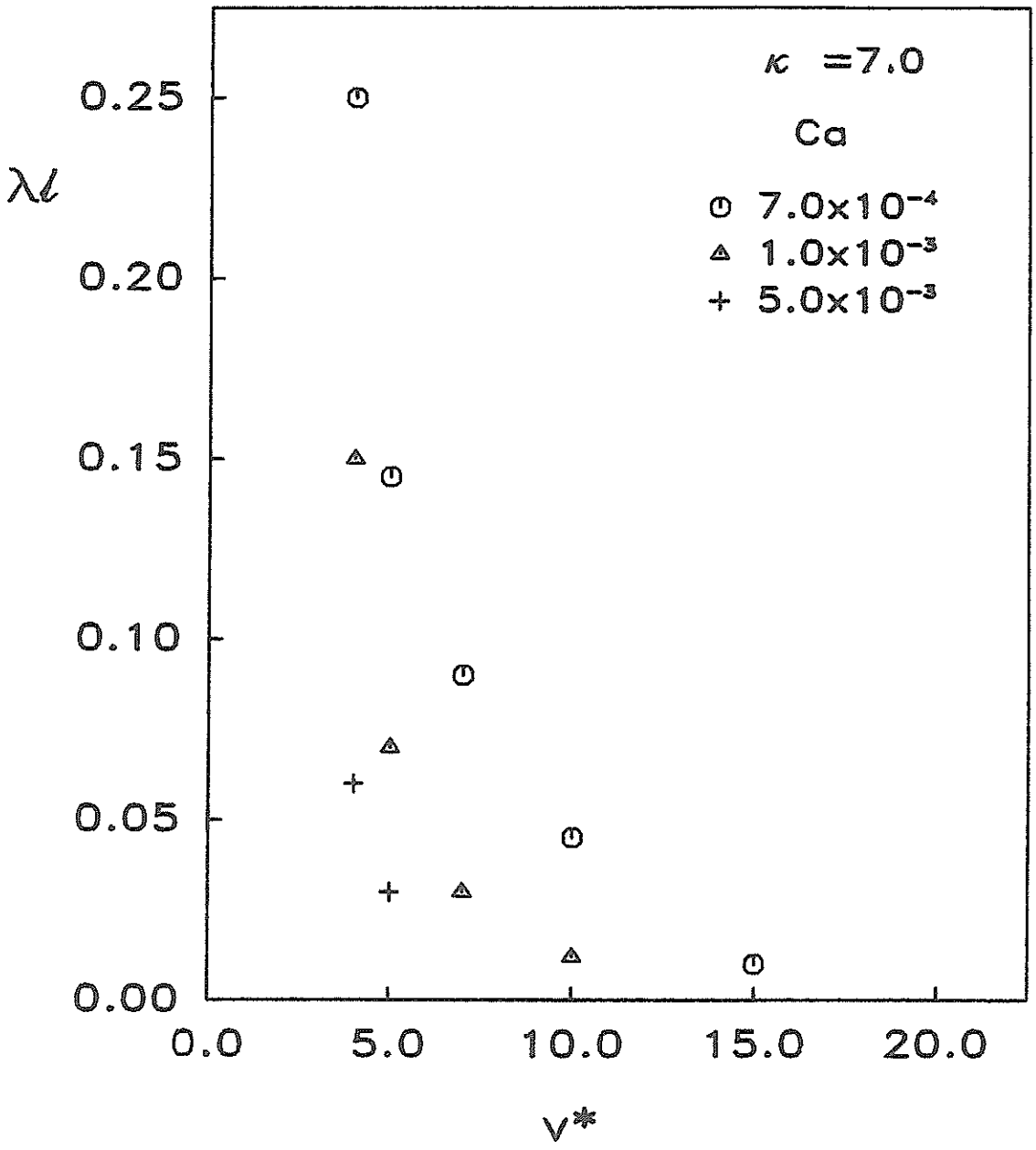


Figure 4.40

Plot of the normalized stranding coefficient, $\lambda\ell$, *versus* the reduced ganglion volume, v^*, in a 100 × 200 sandpack, for $\kappa = 7.0$ and various Ca values.

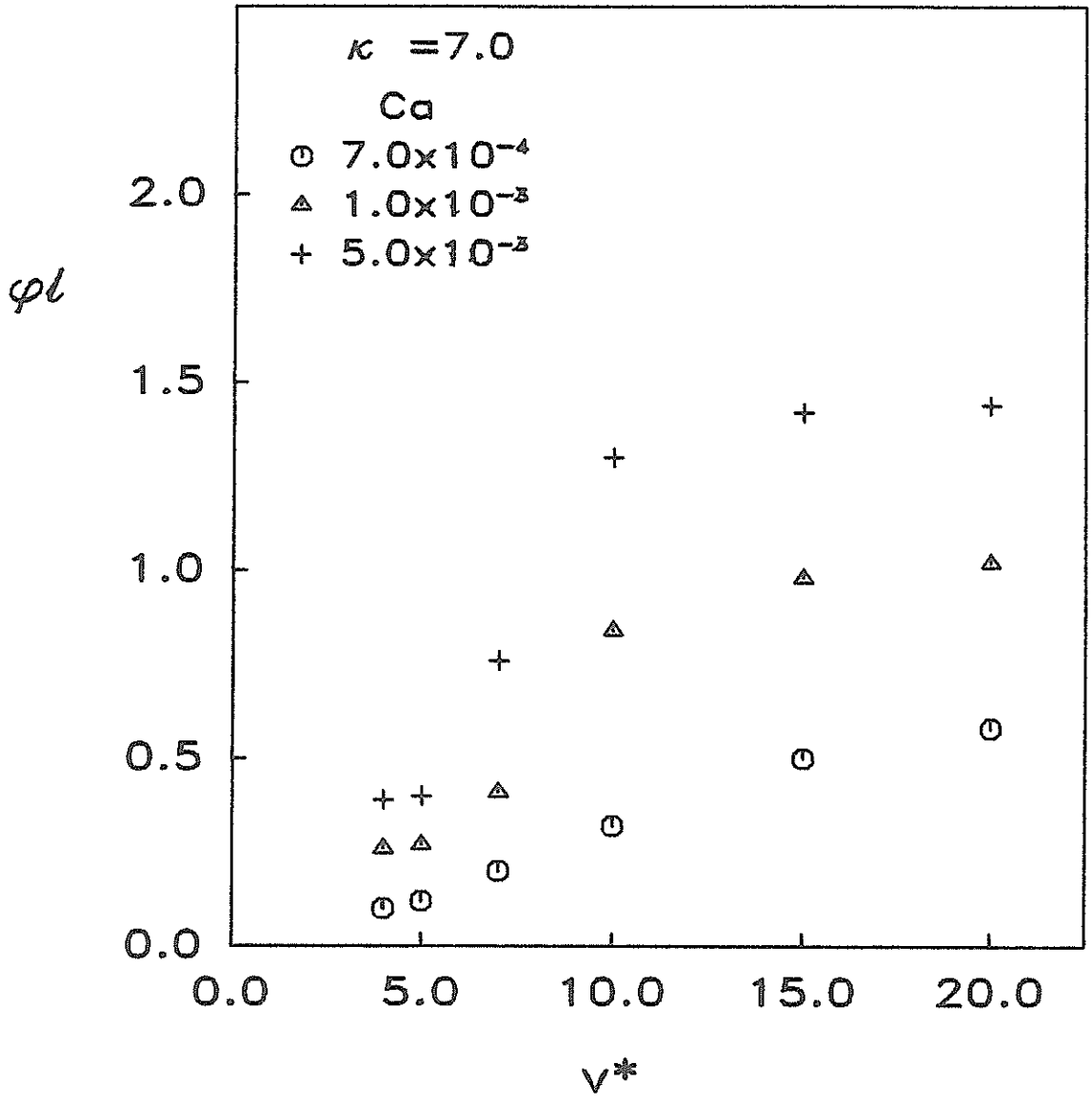


Figure 4.41

Plot of the normalized break-up coefficient, $\phi\ell$, *versus* the reduced ganglion volume, v^*, in a 100 × 200 sandpack, for $\kappa = 7.0$ and various Ca values.

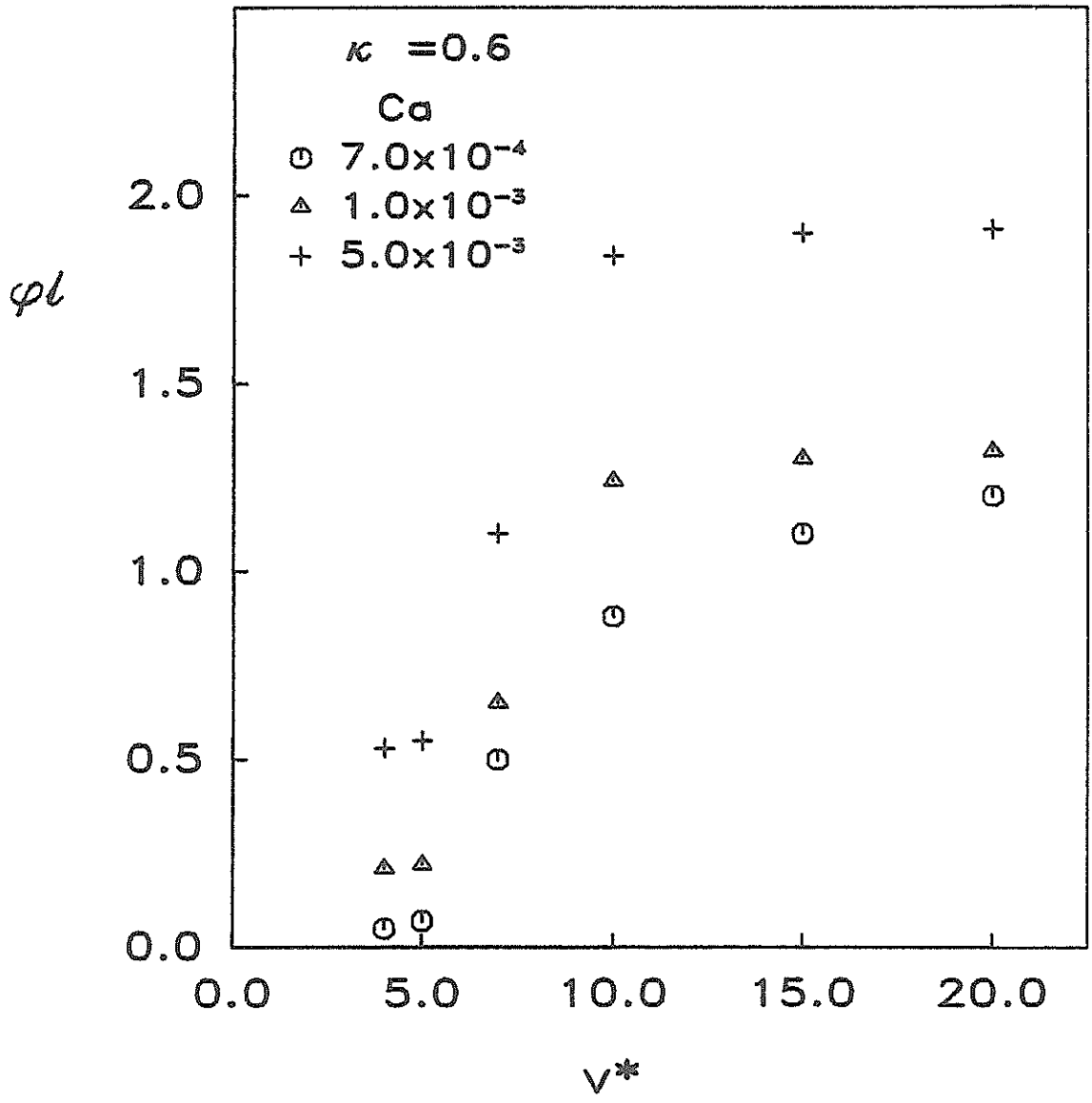


Figure 4.42

Plot of the normalized break-up coefficient, $\phi\ell$, *versus* the reduced ganglion volume, v^*, in a 100 × 200 sandpack, for $\kappa = 1.0$ and various Ca values.

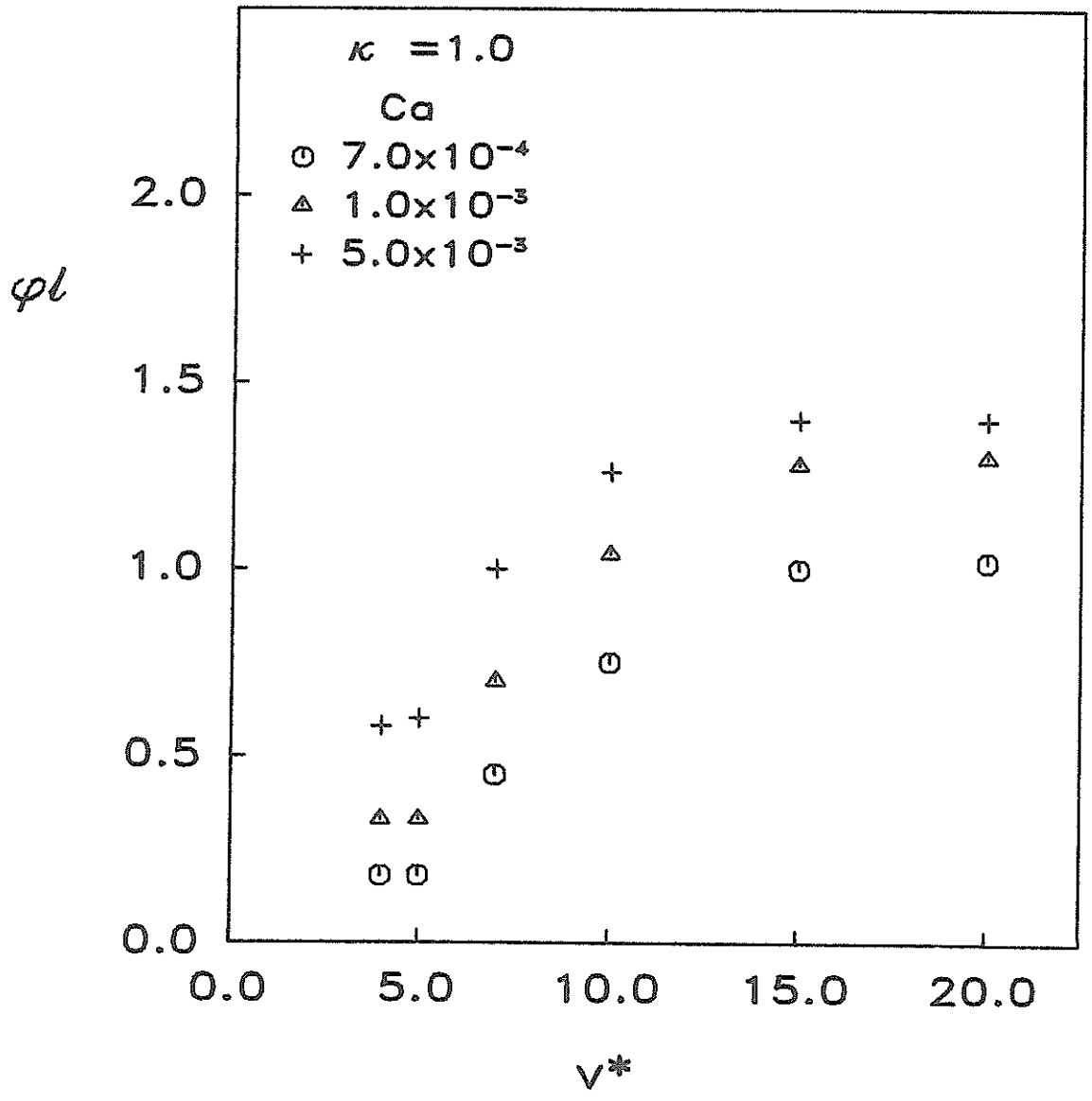


Figure 4.43

Plot of the normalized break-up coefficient, $\phi\ell$, *versus* the reduced ganglion volume, v^*, in a 100 × 200 sandpack, for $\kappa = 0.6$ and various Ca values.

The effect of the capillary number on $W(w,v)\Delta v$ is shown in Figures 4.44 through 4.46. The viscosity ratio did not seem to affect the outcome of this function in any systematic or appreciable way. The following is observed:

- In general, for a fixed v^*, $W(w,v)\Delta v$ decreases as the size of the mother ganglion increases.
- For low capillary numbers, $W(w,v)\Delta v$ decreases monotonically with v^*,
- As the capillary number increases the probability that a large ganglion will break into a 1 or 2-CEVS daughter ganglion decreases slightly with the capillary number. At the same time there is a slight increase in the probability that the break-up will result into two similarly sized daughter ganglia.
- For very large ganglia, $v^* \geq 15$, $W(w,v)\Delta v$ approaches a relatively small asymptotic value.

These observations lead to the conclusion that: a) quasistatic break-up, leading to the formation of differently sized daughter ganglia occurs for any value of the capillary number, large or small; b) dynamic break-up, leading to the formation of similarly sized daughter ganglia, and resulting from the advancement of two or more interfaces simultaneously, also occurs at any values of Ca, but it seems to be favored by high capillary numbers.

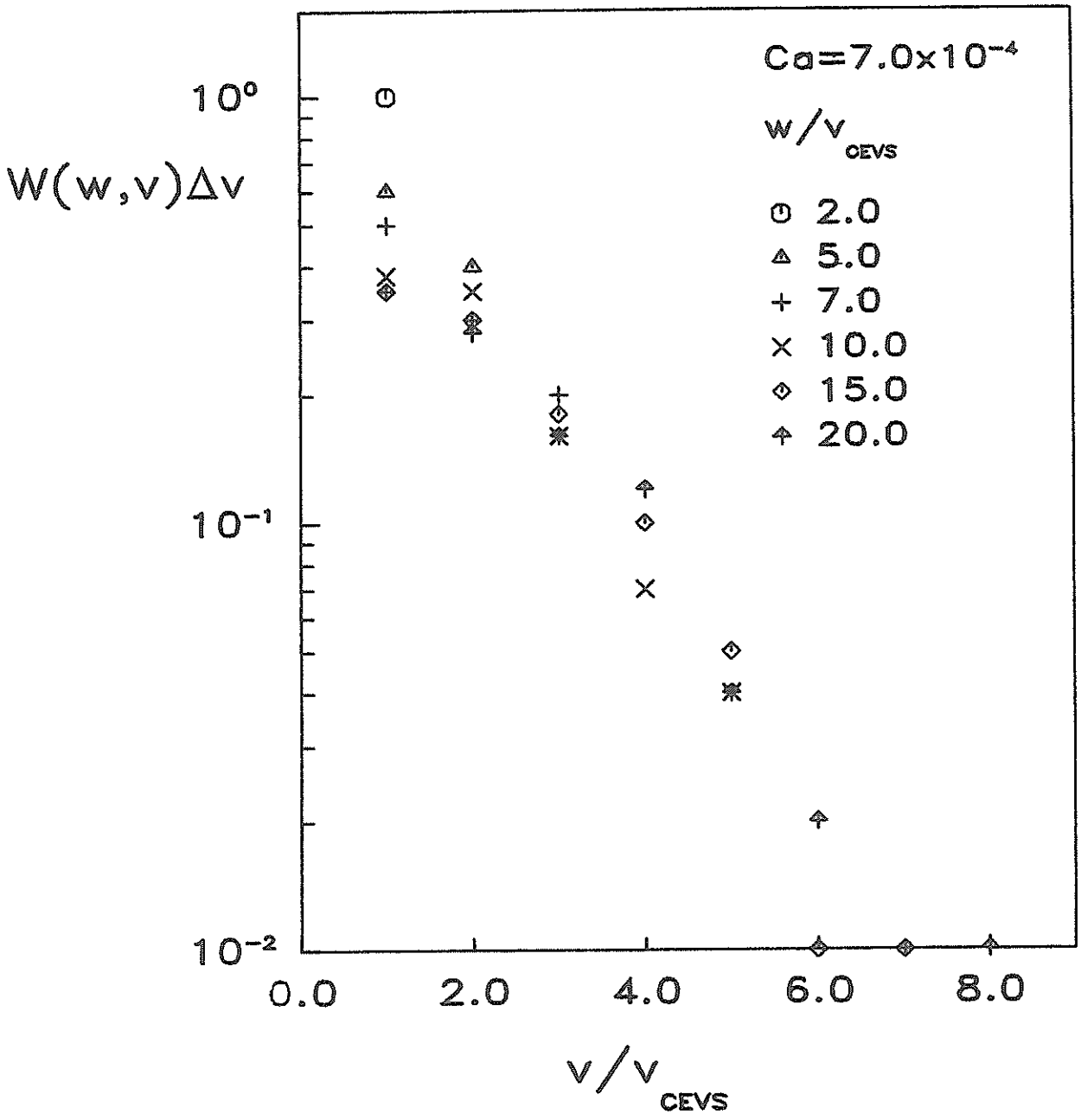


Figure 4.44

Plot of the break-up mode probability, $W(w,v)\Delta v$, *versus* the reduced ganglion volume, v^*, in a 100×200 sandpack, for $\kappa = 7.0$ and $Ca = 0.7 \times 10^{-3}$, with the mother ganglion reduced ganglion volume, w/v_{CEVS}, as a parameter. The symmetrical right half of the plot is not shown.

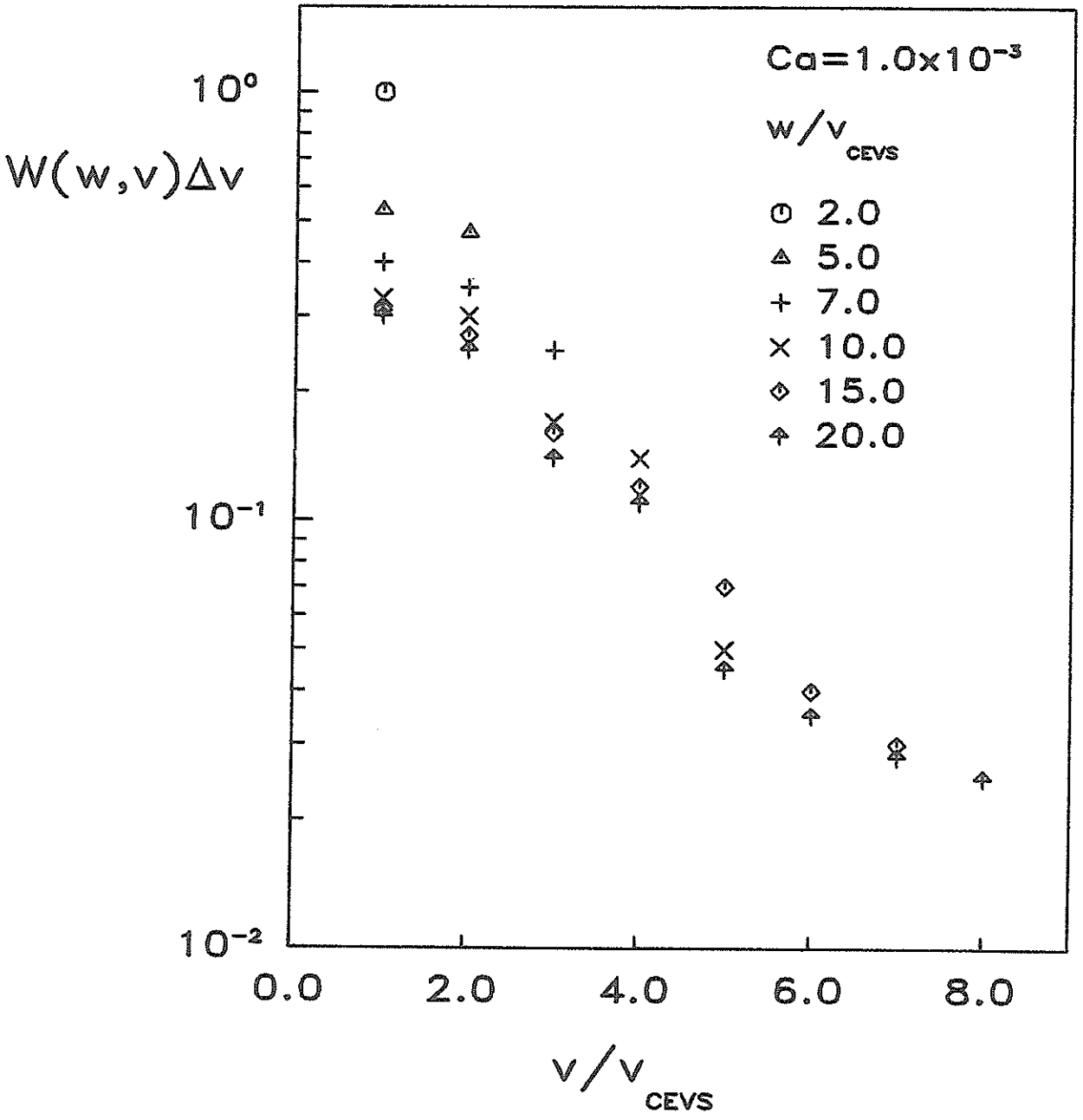


Figure 4.45

Plot of the break-up mode probability, $W(w,v)\Delta v$, *versus* the reduced ganglion volume, v^*, in a 100×200 sandpack, for $\kappa = 7.0$ and $Ca = 10^{-3}$, with the mother ganglion reduced ganglion volume, w/v_{CEVS}, as a parameter. The symmetrical right half of the plot is not shown.

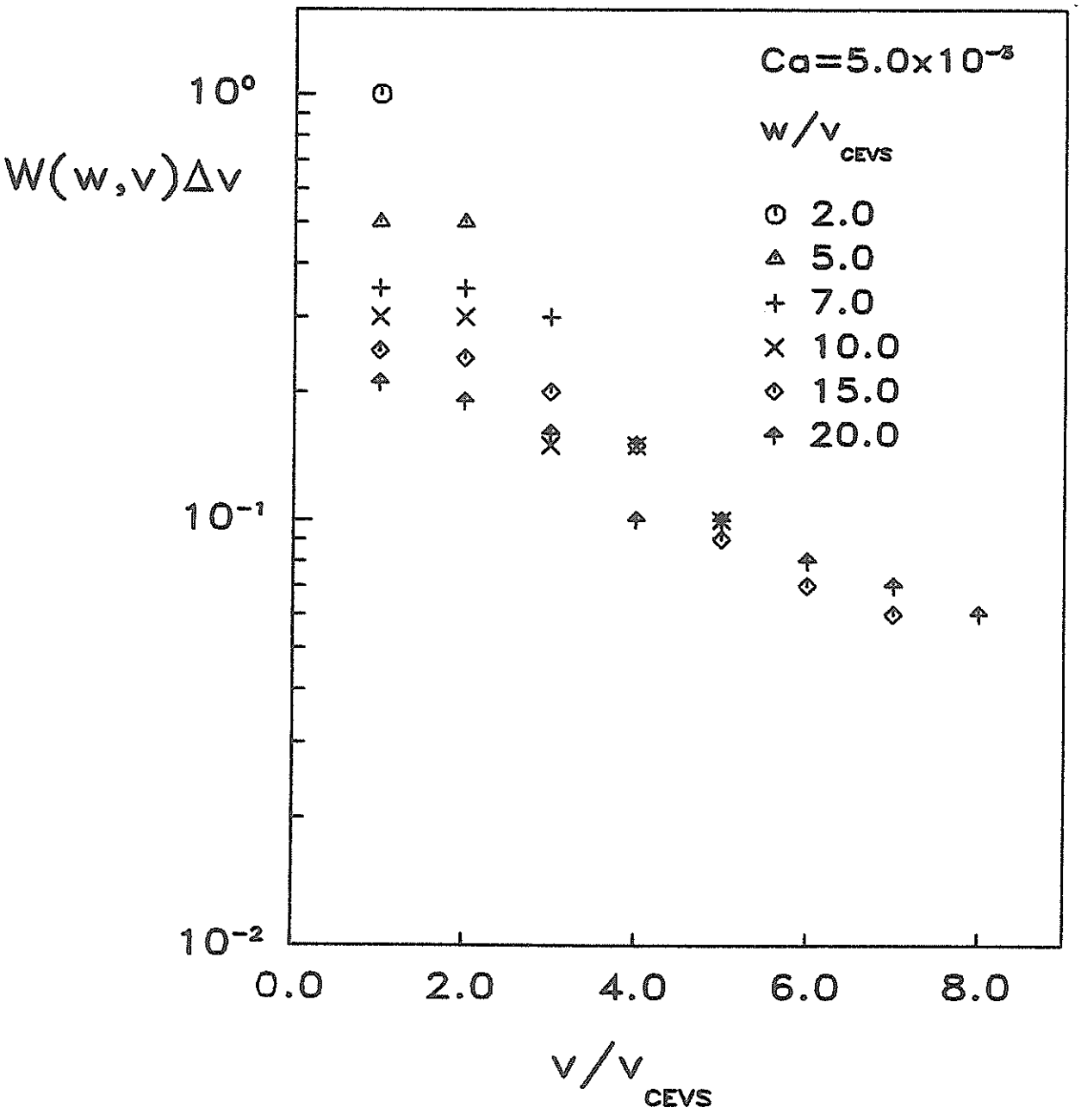


Figure 4.46

Plot of the break-up mode probability, $W(w,v)\Delta v$, *versus* the reduced ganglion volume, v^*, in a 100×200 sandpack, for $\kappa = 7.0$ and $Ca = 5 \times 10^{-3}$, with the mother ganglion reduced ganglion volume, w/v_{CEVS}, as a parameter. The symmetrical right half of the plot is not shown.

Chapter 5

Modeling of Imbibition and Dynamic Invasion Processes

5.1 Introduction

Ganglia are formed during the invasion by water of a porous medium initially saturated with oil, except, possibly, for small amounts of connate water. As the water advances in the porous formation, it tends to follow certain preferred pathways, and ganglia are formed as the oil is microscopically by-passed. Due to the low flow rates involved in most invasion processes, these ganglia usually get immediately stranded. If the flow rates are high or the ganglia are large enough, they may take a few steps and break into two or more daughter ganglia, which in turn get stranded. The remobilization of these stranded ganglia is the target of tertiary methods of oil recovery. It is then important to determine the conditions under which these ganglia were formed. The following questions arise from the analysis of this problem.

- What are the pathways followed by the water?

- At what rates does the water advance?
- Do these rates vary as more and more water fills the porous medium?
- How are ganglia formed?
- What is the final size distribution of ganglia?
- How much oil remains entrapped at the end of the invasion process?
- How are all the above variables affected by the pore system parameters (i.e., the porous medium topology, the physical properties of both fluids and the externally imposed pressure drop)?

These and other questions can be analysed by microscopic modelling of invasion processes.

The simulation method developed in Chapter 3 is here extended and adapted to model displacement of an initially connected phase by another fluid. As was described in Section 2.4, invasion processes have been studied before using percolation theory and sphere-and-capillary networks. Simulators using converging-diverging tubes present the advantage of being more powerful than percolation models in the sense that they take into account the rates with which interfaces advance. Furthermore, the present simulation method is capable of handling viscosity ratios different than unity, while previous works using sphere-and-capillary networks have been unable to do so, mostly due to computation time limitations.

5.2 Simulation Model

Consider the network of unit cells described in Chapter 3, initially saturated with the oleic phase. The connate water is taken into account from the outset,

since in the formulation of the porous medium model, the actual porosity of the network, that is, the fraction of the medium available to the oleic phase, is set equal to $\epsilon(1 - S_{wi})$, where S_{wi} is the irreducible water saturation during an initial drainage experiment (Payatakes, Tien and Turian, 1973; Payatakes and Neira, 1977; Payatakes, Ng and Flumerfelt, 1980). At $t = 0$, the oil-water interfaces occupy positions in the unit cells that compose the entrance to the network, Figure 5.1.

The two-phase flow problem is solved using the electric analog and the motion rules described in Chapter 3, and the solution is obtained in a similar stepwise manner. However, invasion simulations and solitary oil ganglion simulations differ in major aspects, especially in the boundary conditions and the formation and stranding of ganglia.

Two different types of invasion processes were analysed in the present work: free imbibition and dynamic invasion with constant pressure drop. The viscosity ratio was changed from favorable, $\kappa = 0.2$, to neutral, $\kappa = 1$, to unfavorable, $\kappa = 50$. In the dynamic invasion case the capillary number was changed from very low, $Ca = 10^{-8}$ (approaching quasistatic imbibition) to large, $Ca = 5 \times 10^{-3}$.

5.2.1 Boundary Conditions

In the simulations of the fate of a solitary oil ganglion, the boundary conditions were chosen so that the presence of the moving ganglion did not affect conditions at the network boundaries. This was achieved by using a network which was large compared to the ganglion size

The case of invasion simulations is radically different, since both the oleic and the aqueous phases may span the entire width and/or length of the network. Differ-

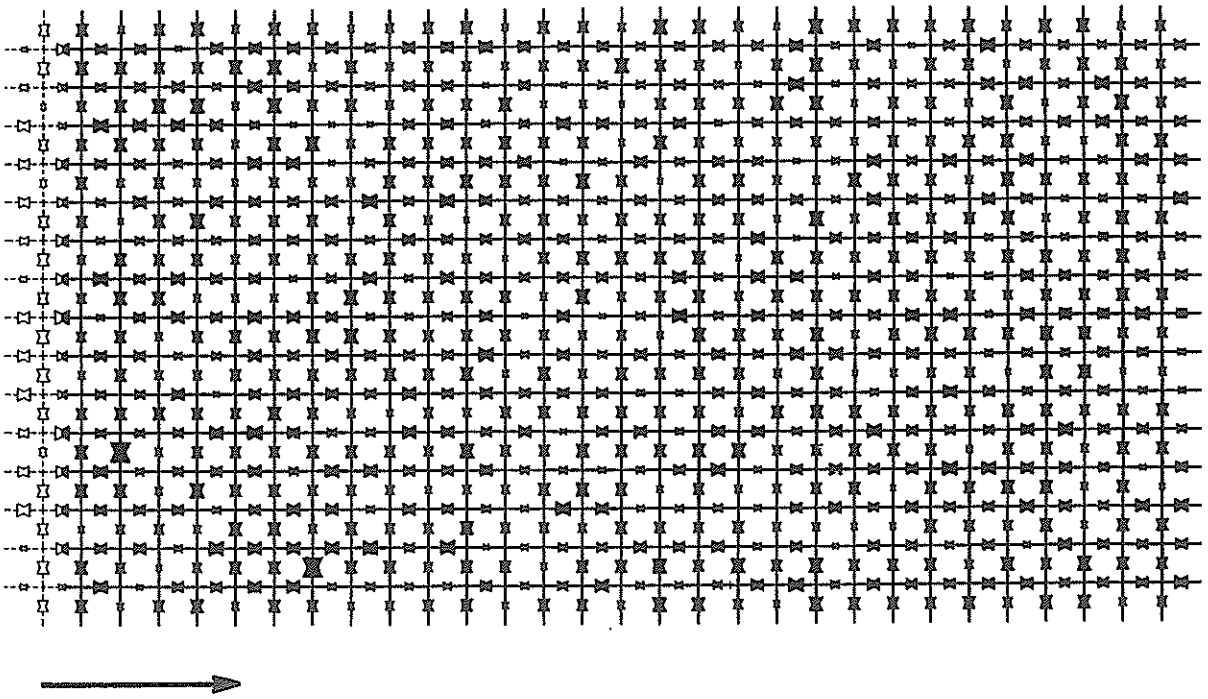


Figure 5.1

Depiction of a two-dimensional square network saturated with oil, showing the position of the oil-water interfaces at $t = 0$.

ent sets of boundary conditions have to be imposed at the unit cells at the entrance, at the exit and on both sides of the network.

The flow configuration is determined by choosing the direction of the macroscopic pressure gradient and by specifying the lateral boundary conditions.

The macroscopic pressure gradient direction is taken to be parallel to the y-axis (the longer axis of the network), that is the angle between the macroscopic pressure gradient direction and the x-axis is set at $\phi' = 90°$. The pressure drop along the network is then determined by

$$\Delta P = P_1 - P_0 = (-\nabla P)\, \ell\, N_y \,. \tag{5.1}$$

It is assumed that the entrance unit cells (left in Figure 5.1) are connected to a source of pressure P_1, and the exit unit cells (right in Figure 5.1) are connected to a sink of pressure P_0. For simplicity P_0 is set at $P_0 = 0$.

Three different types of boundary conditions can be imposed at the network sides: periodicity in the lateral direction, permeable lateral walls (i.e., water can flow in through the sides) and impermeable lateral walls (i.e., neither oil nor water can flow through the sides). Although the simulation code (see Appendix A) is prepared to deal with any of these three situations in the remainder of this work periodicity is assumed. Periodic boundary conditions are commonly used in this type of simulations, since the relatively small network used is considered to be just a representative part of a much larger porous medium. Figure 5.1 shows an example of a network with periodic boundary conditions.

5.2.1 Formation and Stranding of Ganglia

One distinct feature of invasion processes is the disconnection of the oleic phase

by the invading aqueous phase. The formation of these islands of oil, called ganglia, and their subsequent stranding due to capillary effects are responsible for the residual oil saturation at the end of the invasion process. It is then important to analyze carefully the conditions for the formation and stranding of oil ganglia.

Consider an invasion simulation in an initially oil-filled network. Under the applied pressure gradient, the water advances in the porous medium through a series of hygrons. A ganglion is formed whenever the water completely surrounds and isolates a fraction of the oil in the porous medium. Assume that at a certain instant, a portion of oil has been almost completely encircled by water, save for an oil thread connecting it to the main body of oil, and that a hygron is about to occur at the interface formed by this oil thread. The thread rupture criterion described in Section 3.7.2 is applied, and, as it turns out, the criterion leads to the rupture of the oil thread and an oil ganglion is formed. This ganglion may continue to move forward and eventually break into smaller daughter ganglia, or it may become immediately stranded.

As was discussed seen in Chapters 3 and 4, according to the present simulation algorithm, all interfaces advance or recede at the most one compartment at each time step. If a ganglion becomes stranded, its interfaces move with small steps, back and forth (so that the net effect is that the oil ganglion does not advance or recede), due to the finite time step considered.

This is an unwelcome artifact of the simulation algorithm. It is important to decide "a priori" if a ganglion is in fact stranded or not, for three major reasons:

- If the interfaces of a stranded ganglion are allowed to move back and forth, this motion creates an artificial flow field in the vicinity of the ganglion which,

in turn, may induce motion of nearby interfaces. This effect is particularly noticeable in free imbibition simulations.

- The simulation is stopped not just when the oleic phase has been disconnected but rather when all ganglia become stranded. This allows for further oil recovery after disconnection by possible motion of the ganglia.
- Upon deciding that a certain ganglion is stranded, it becomes unnecessary to follow the motion of its interfaces any further, and the computation time is reduced in this way

On the other hand, if a ganglion keeps on moving after its formation, it is important to allow it to move on, for it may eventually break into smaller ganglia, get stranded in another position or move all the way to the exit and leave the network, i.e. be produced (this last event seldom occurs).

As was seen in Chapter 4, the estimation of ganglion stranding and mobilization using the ganglion mobilization criterion developed by Ng, Payatakes and Flumerfelt (1980) is in good agreement with results obtained by the present simulation method. Due to its simplicity, this criterion is used in invasion simulations, in order to determine whether a newly formed ganglion becomes stranded or continues to move.

For each ganglion formed, a pair of gate unit cells with indexes $i = I$ and $k = K$ for which the appendix mobility factor,

$$\beta_{ki} = \frac{\Delta L_{ki} \cos(\theta_{ki})}{J_{dr,i}(\theta_r^o) - J_{lb,k}(\theta_a^o)} , \tag{5.2}$$

becomes a maximum, is identified. Here, ΔL_{ki} is the distance between throats with indices k and i, θ_{ki} is the angle between the line connecting the throats k and i and the macroscopic flow direction, $J_{dr,i}$ is the drainage curvature of the gate unit cell

with index i, and $J_{lb,k}$ is the lower bound of the imbibition curvature. The values of $J_{dr,i}$ and $J_{lb,k}$ are given by

$$J_{dr,i} = \frac{4}{d_i} \cos(\theta_r^o) \ , \tag{5.3}$$

$$J_{lb,k} = \frac{4}{a_k} \cos(\theta_a^o) \ . \tag{5.4}$$

The critical pressure drop for mobilization, ΔP_{cr} for this pair of gate unit cells, is given by

$$\Delta P_{cr} = \sigma_{ow} \left(J_{dr,I} - J_{lb,K} \right) \ . \tag{5.5}$$

Comparing this value with the pressure drop in the aqueous phase in the vicinity of the ganglion, ΔP_{KI}, if

$$\Delta P_{KI} < \Delta P_{cr} \ , \tag{5.6}$$

the ganglion is stranded. For computational purposes a zero pressure drop is imposed across the oil-water interfaces of the ganglion and the conductances of the unit cells occupied by the ganglion are set equal to zero. In effect, this creates a barrier for the water to penetrate and imposes a null flow in these unit cells. If on the other hand

$$\Delta P_{KI} \geq \Delta P_{cr} \ , \tag{5.7}$$

the ganglion is allowed to move and at each occurrence of a hygron or a xeron, it is checked again if it goes on moving, gets stranded, or breaks into smaller ganglia.

5.3 Free Imbibition Simulations

Free imbibition occurs spontaneously when the aqueous phase is allowed to

invade the initially oil saturated porous medium, driven only by the capillary forces that exist at the oil-water interfaces.

Consider then, the initially oil filled network represented in Figure 5.1. The same initial configuration is taken in all subsequent simulations. For sake of compactness, the initial stage will not be repeated in the schematic representations of the simulations that follow.

In order to simulate free imbibition conditions, a very small macroscopic pressure gradient is applied across the network so that, in effect, the process is driven only by capillary forces. The magnitude of the macroscopic pressure gradient is chosen so that the capillary number in the same network virtually depleted of oil is $Ca = 10^{-8}$.

The results of simulated imbibitions in a 15×30 network, representing a 100×200 sandpack, for $\kappa = 50$, 1 and 0.2, are shown in Figures 5.2, 5.3 and 5.4, respectively. The random network used is the same in all three simulations and equal to the one depicted in Figure 5.1 in order to make the results strictly comparable.

As was pointed out before, the capillary suction inducing the displacement remains virtually constant throughout the whole process, while the viscous resistance to the flow changes as more and more water invades the porous medium. This results in a strong dependence of the capillary number on both the flood axial direction and on the extent of the imbibition. In Figure 5.5, this effect is demonstrated by plotting Ca at various network cross-sections versus the dimensionless axial distance z/ℓ at various times during the displacement process.

The major conclusions drawn from these simulations can be summarized as

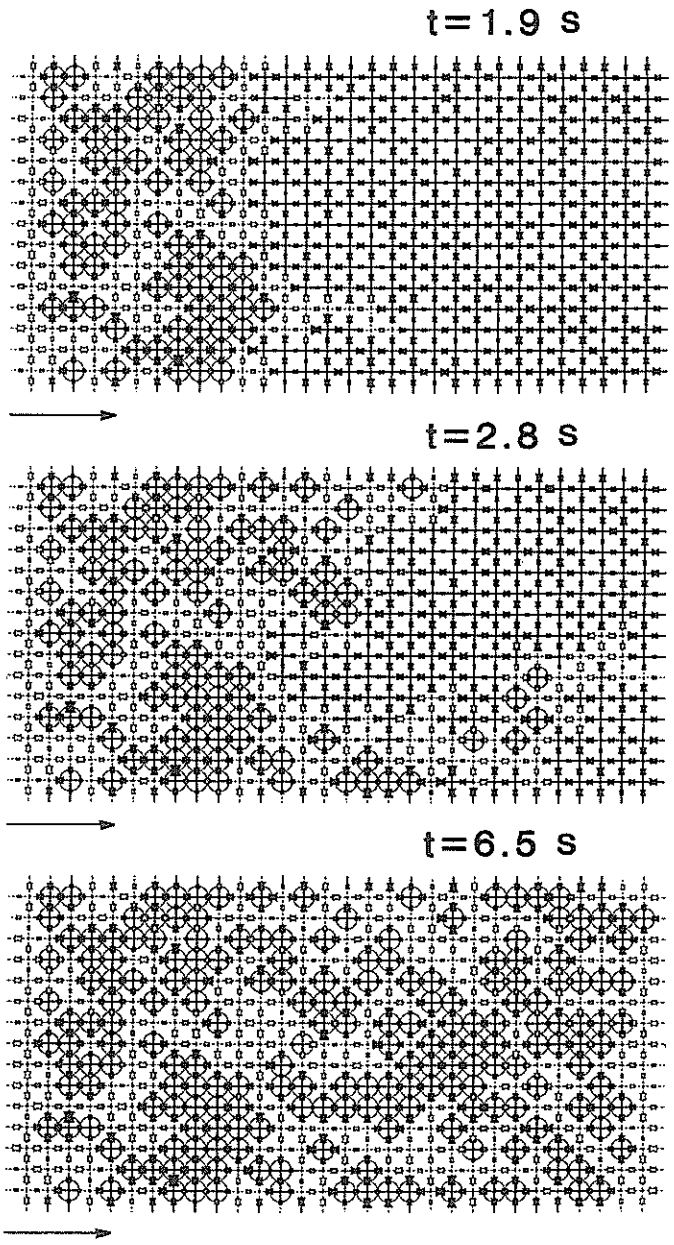


Figure 5.2

Stages of free imbibition simulations in a 15×30 network (100×200 sandpack) for $\kappa = 50$.

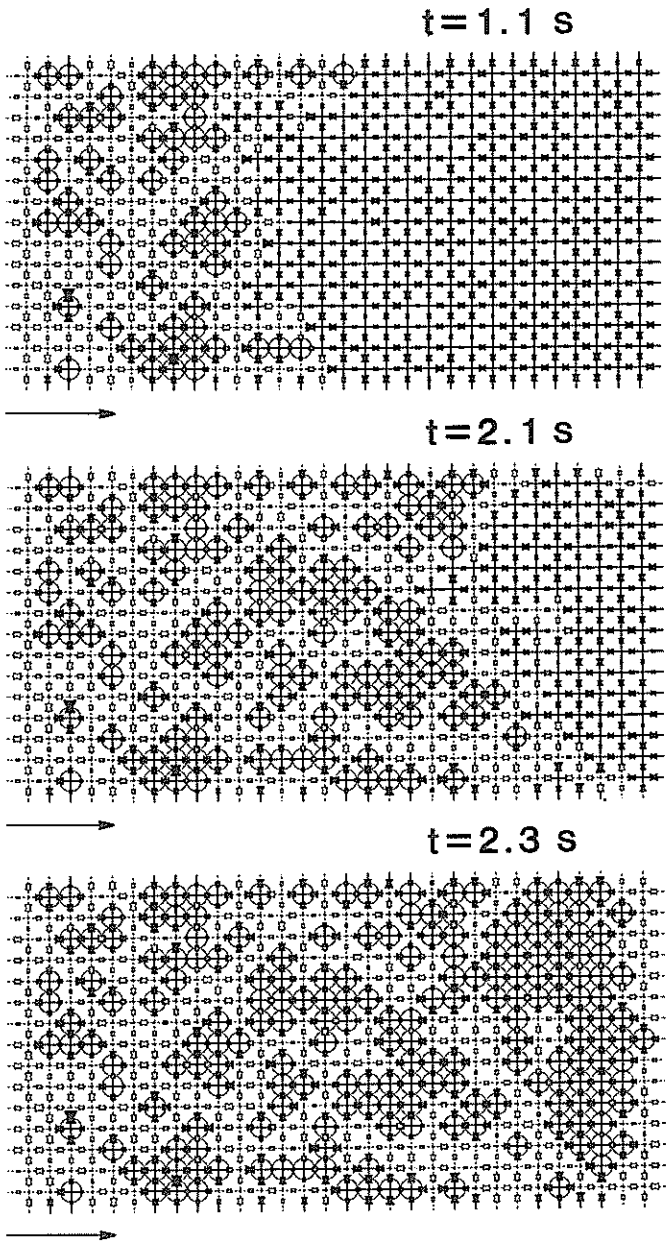


Figure 5.3

Stages of free imbibition simulations in a 15×30 network (100×200 sandpack) for $\kappa = 1$.

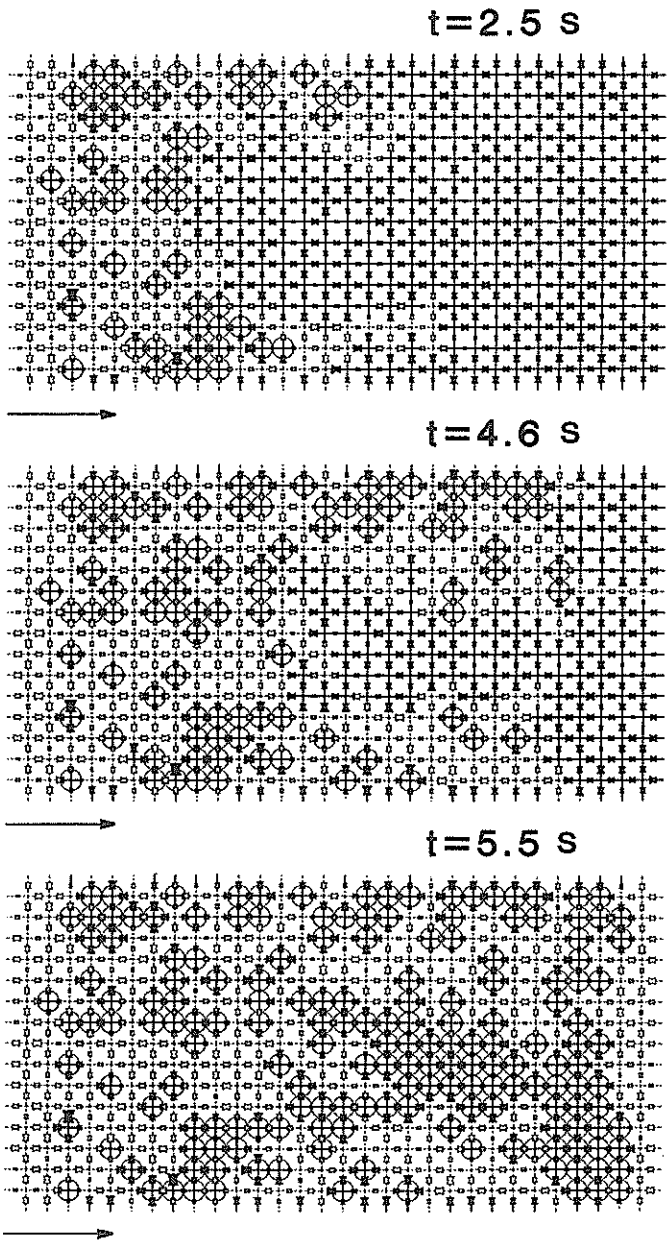


Figure 5.4

Stages of free imbibition simulations in a 15×30 network (100×200 sandpack) for $\kappa = 0.2$.

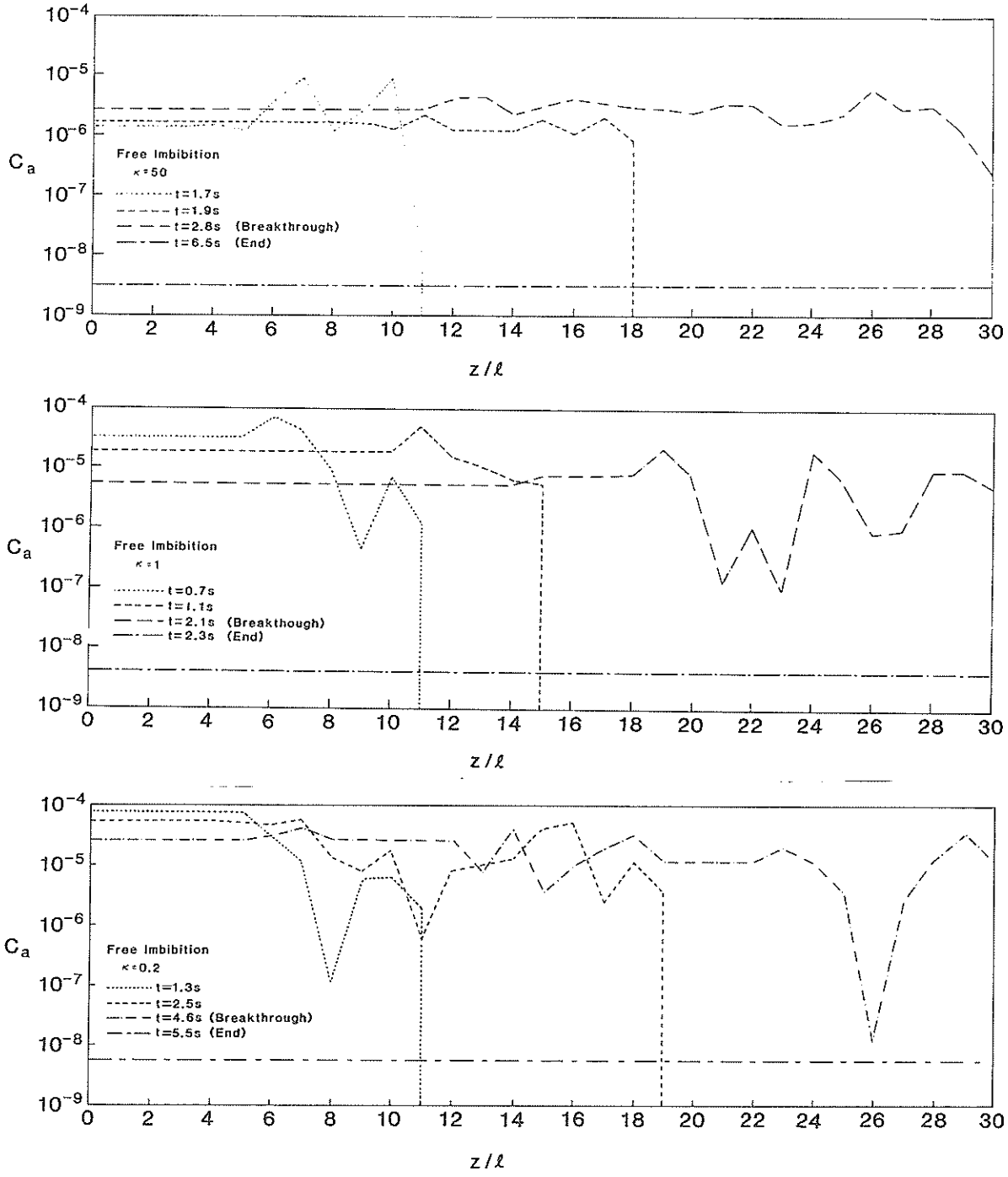


Figure 5.5

Plot of the capillary number, Ca, at various cross-sections of the network *versus* the dimensionless axial distance, z/ℓ, during a simulated free imbibition for a) $\kappa = 50$ b) $\kappa = 1$ c) $\kappa = 0.2$.

follows:

- The capillary suction induces a displacement that passes through high values of Ca.
- The lower the value of the viscosity ratio, the higher the maximum value of Ca attained.
- At the end of the displacement process, when all the oil has been disconnected and stranded, the capillary number becomes small and uniform throughout the porous medium. In fact, the limiting value of Ca is less than the initially designated value of 10^{-8} since the residual value of the oil saturation, S_{or}, is some positive value rather than nil. Hence, the relative permeability to water, k_{wr}, is smaller than unity.
- For $\kappa > 1$, the average value of Ca throughout the network increases as the water advances through the network, while for $\kappa \leq 1$, it decreases with time. This effect is supported by the experimental observation of Legait and Jacquin (1982), that during spontaneous imbibition of water in sandstone samples containing oil with viscosity $\mu_o = 225\ cP$ ($\kappa = 225$), the rate of oil displacement increased strongly with time. They also observed an increase, but much smaller, for $\kappa = 1$. Similar observations were reported by Jacquin and Legait (1983).
- The range of the final distribution of ganglion sizes is fairly wide, spanning from very large (*ca* 40 CEVS's) to rather small (1 CEVS or less). For $\kappa \leq 1$, small ganglia are formed during the initial stages of the displacement,and as the capillary number drops towards the end of the process, the ganglia become larger and larger. For $\kappa > 1$, the spatial distribution of ganglia is more uniform and fewer small ganglia are formed due to the lower Ca values attained.

The results of three different runs of simulated free imbibition for each value of the viscosity ratio, using different random networks are summarized in Figures 5.6 through 5.9. The size distributions of the resulting ganglia at the end of the displacement process are plotted in Figures 5.6 through 5.8. Each distribution is given in two ways: first, as frequency of ganglia, $f(s)$, versus the number of CEVS's occupied by the ganglion, s; second, as frequency of ganglia, $f(v^*)$, versus the reduced ganglion volume, v^*. Figure 5.9 shows the acceptance fraction, $a_d(d)$, obtained by averaging results obtained with the three runs. The acceptance fraction is defined as the number of unit cells with throat diameter d, that become occupied by the aqueous phase, divided by the total number of unit cells of that size in the network.

5.4 Imbibition and Dynamic Invasion Simulations

As in the case of free imbibition, at the beginning of the invasion process, the oleic phase is completely connected, and the two fluids are in contact with each other at a set of interfaces residing at the entrance of the porous medium (see Figure 5.1).

Contrary to the free imbibition case, where the process is controlled by capillary suction and the capillary number fluctuates on a relatively wide range, the aim now is to simulate displacements with a nearly constant capillary number. To this end, two different approaches can be used: either a high back-pressure is applied across the network or a long network is used. Both methods are equivalent, providing that in the first case a constant back-pressure be applied. Of the two approaches, the second one seems to be the more realistic. Long networks offer a much higher viscous

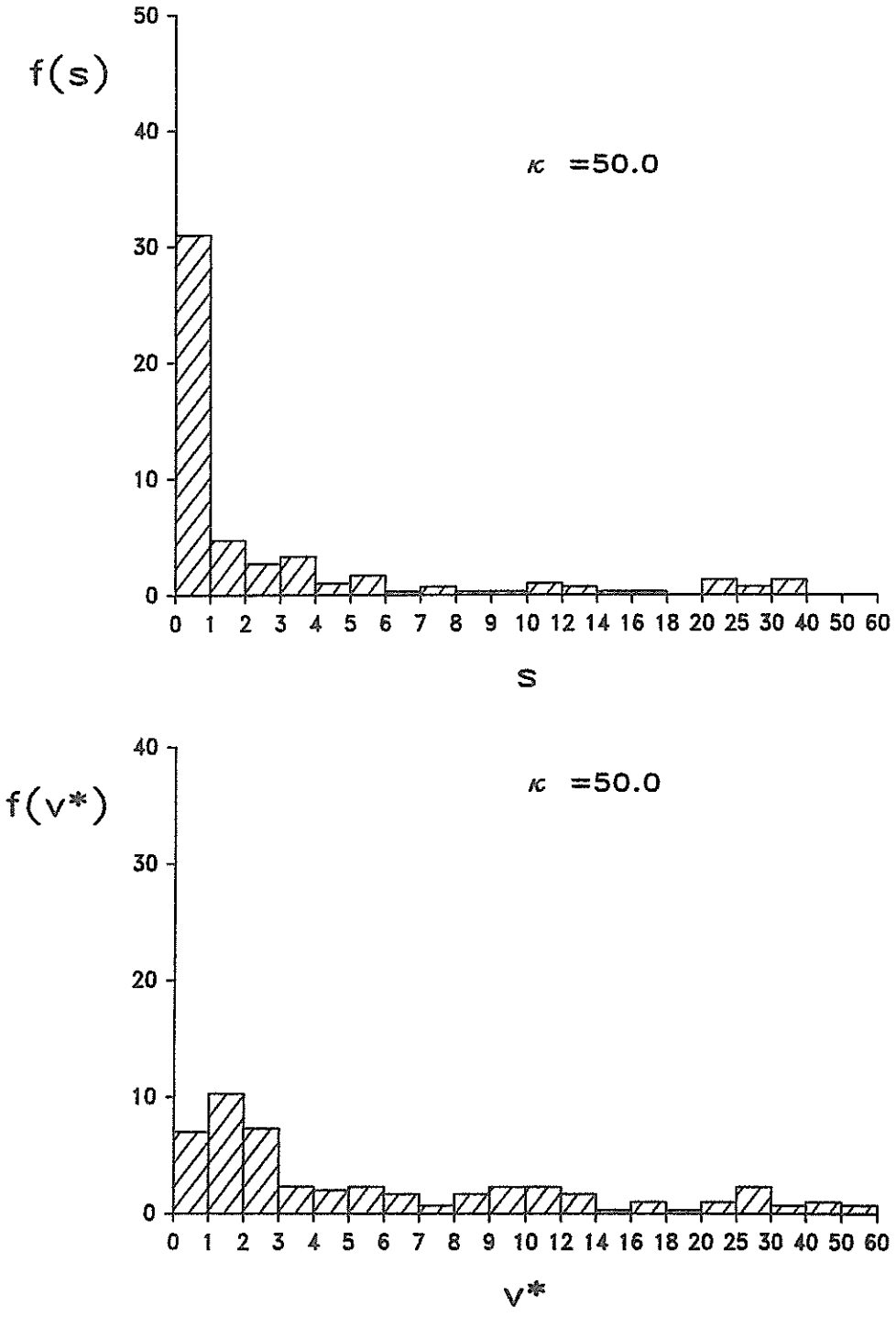


Figure 5.6

Plot of the final ganglion size frequency distribution functions for free imbibition simulations in a 15 × 30 network (100 × 200 sandpack) for $\kappa = 50$. a) frequency of ganglia, $f(s)$, *versus* the number of CEVS's occupied by the ganglion, s. b) frequency of ganglia, $f(v^*)$, *versus* the reduced ganglion volume, v^*.

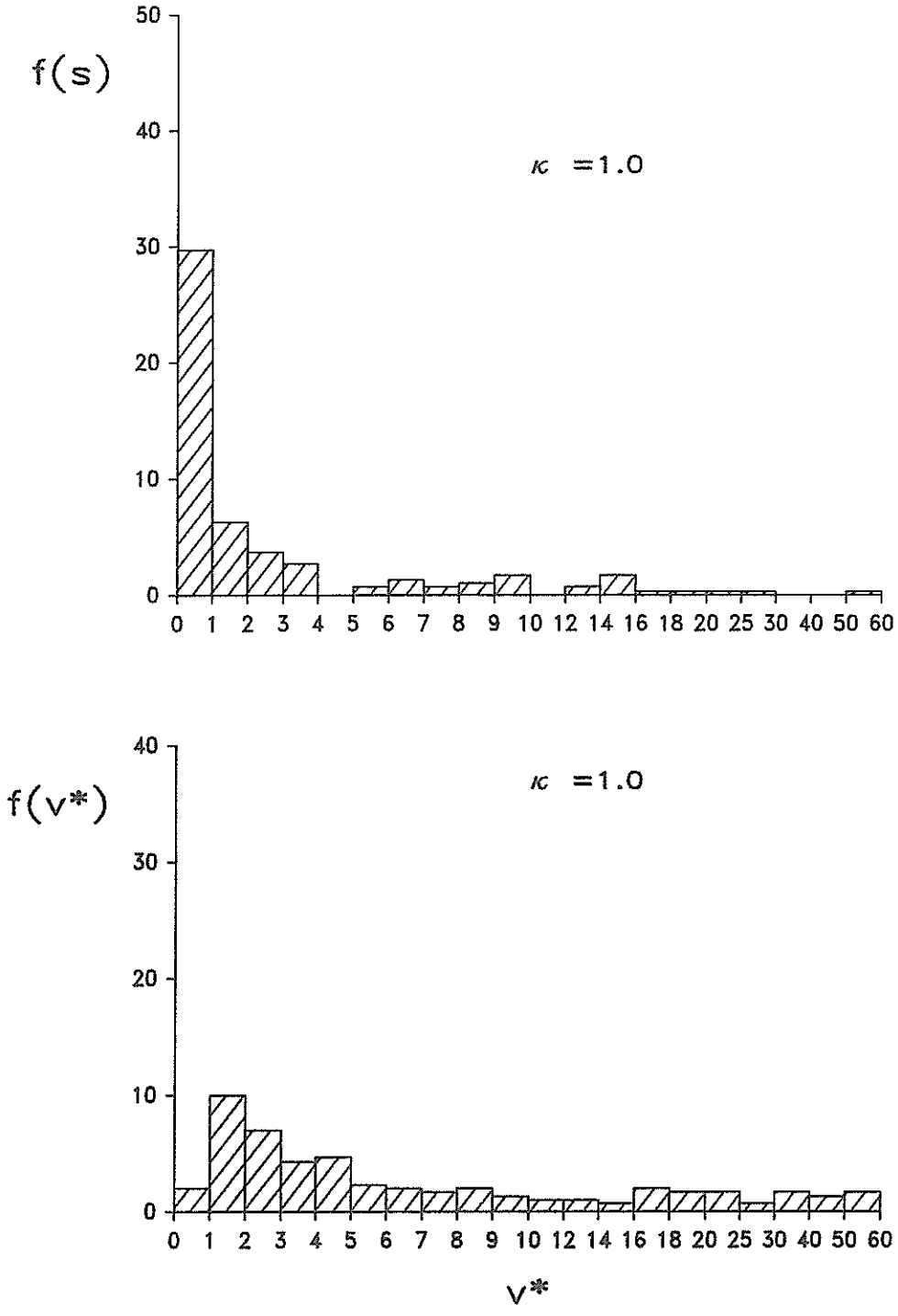


Figure 5.7

Plot of the final ganglion size frequency distribution functions for free imbibition simulations in a 15 × 30 network (100 × 200 sandpack) for $\kappa = 1$. a) frequency of ganglia, $f(s)$, *versus* the number of CEVS's occupied by the ganglion, s. b) frequency of ganglia, $f(v^*)$, *versus* the reduced ganglion volume, v^*.

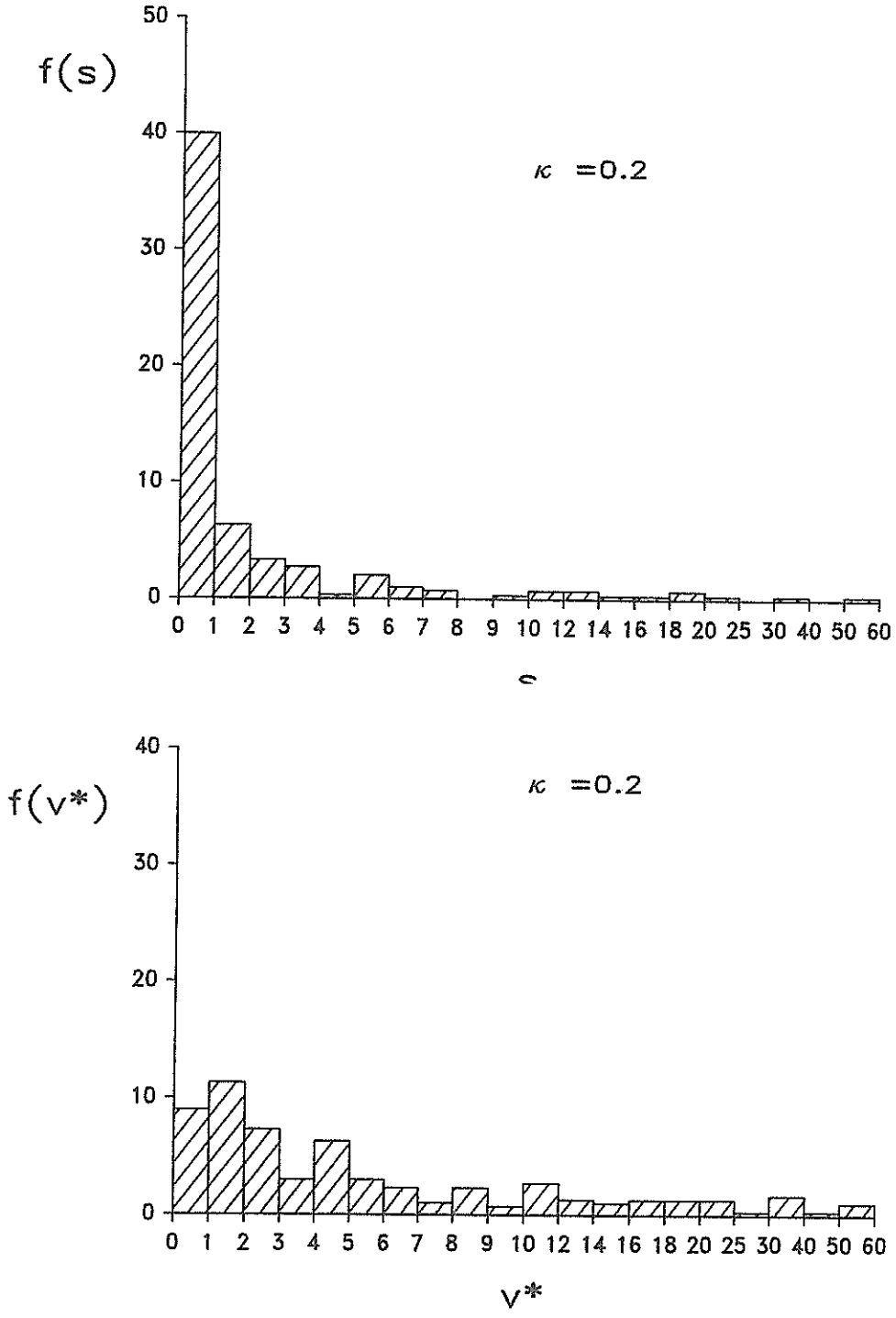


Figure 5.8

Plot of the final ganglion size frequency distribution functions for free imbibition simulations in a 15 × 30 network (100 × 200 sandpack) for $\kappa = 0.2$. a) frequency of ganglia, $f(s)$, *versus* the number of CEVS's occupied by the ganglion, s. b) frequency of ganglia, $f(v^*)$, *versus* the reduced ganglion volume, v^*.

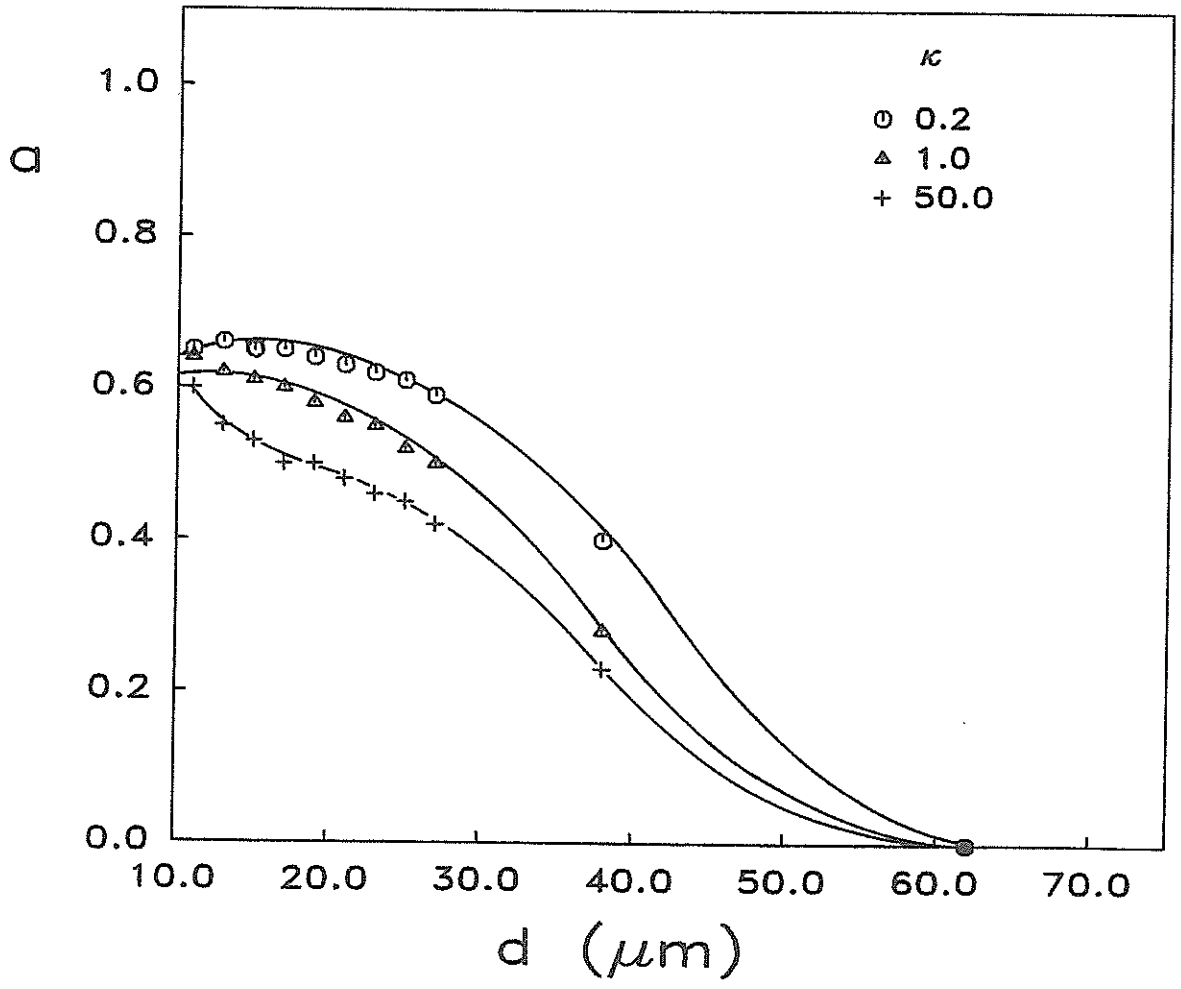


Figure 5.9

Plot of the acceptance fraction, $a_d(d)$, *versus* the unit cell throat diameter, d, for free imbibition simulations on a 15×30 network (100×200 sandpack) for various values of κ.

resistance to the flow, and the capillary number can be controlled by regulating the applied macroscopic pressure gradient.

Computational time and memory limitations require that a relatively short network be used. If this "short" network is intended to represent a small segment of a "long" network, then the exit unit cells, connected to the sink with nil pressure (see Section 5.2), are replaced by a "tail" of uniform unit cells of small hydraulic conductance. The value of the conductance of these unit cells is adjusted so that their equivalent hydraulic resistance is equal to that of the prototype. Details of the calculation of the size and conductance of these "tail" unit cells are given in Appendix D.

It is clear that this technique can only be used while the aqueous phase is still at some distance from the end of the network. In order to account for this fact, the simulations of imbibition and dynamic displacement in a 15×30 network, were actually performed in a 15×40 network with modified "tail" unit cells. Each simulation was stopped when all the oleic phase behind the thirtieth layer of unit cells becomes disconnected and stranded, so that in effect the displacement study is performed in a 15×30 segment of a much larger network. In the following figures, only this part is shown.

Typical results obtained with this simulation method are given in Figures 5.10 through 5.18. As in the case of the free imbibition simulations, the network used was random, but the same in all cases, in order to isolate the effects of the capillary number and of the viscosity ratio.

The following general qualitative observations are drawn from the inspection of these figures:

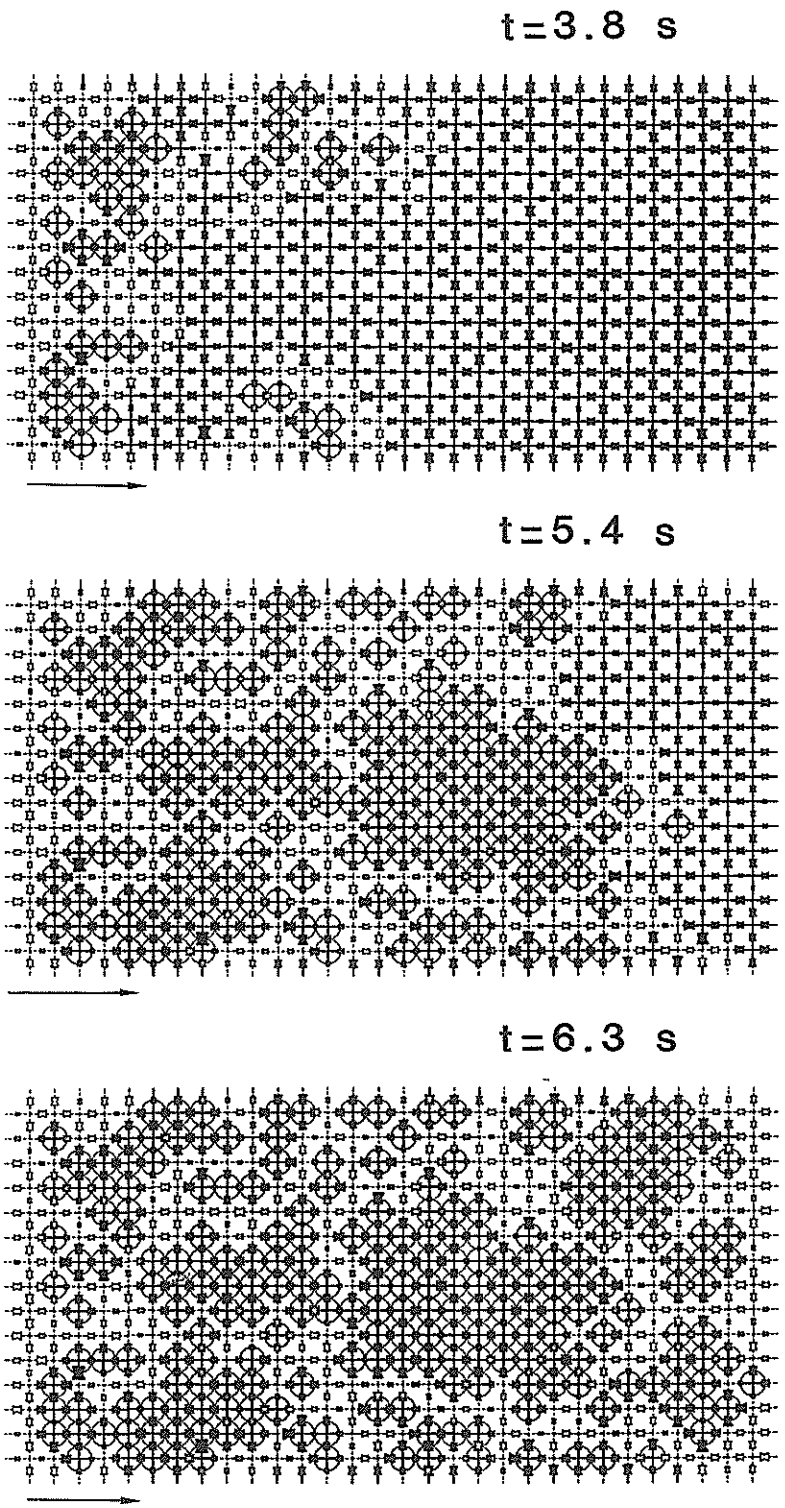


Figure 5.10

Stages of imbibition simulation in a 15 × 30 network (100 × 200 sandpack) for $Ca = 10^{-8}$ and $\kappa = 50$.

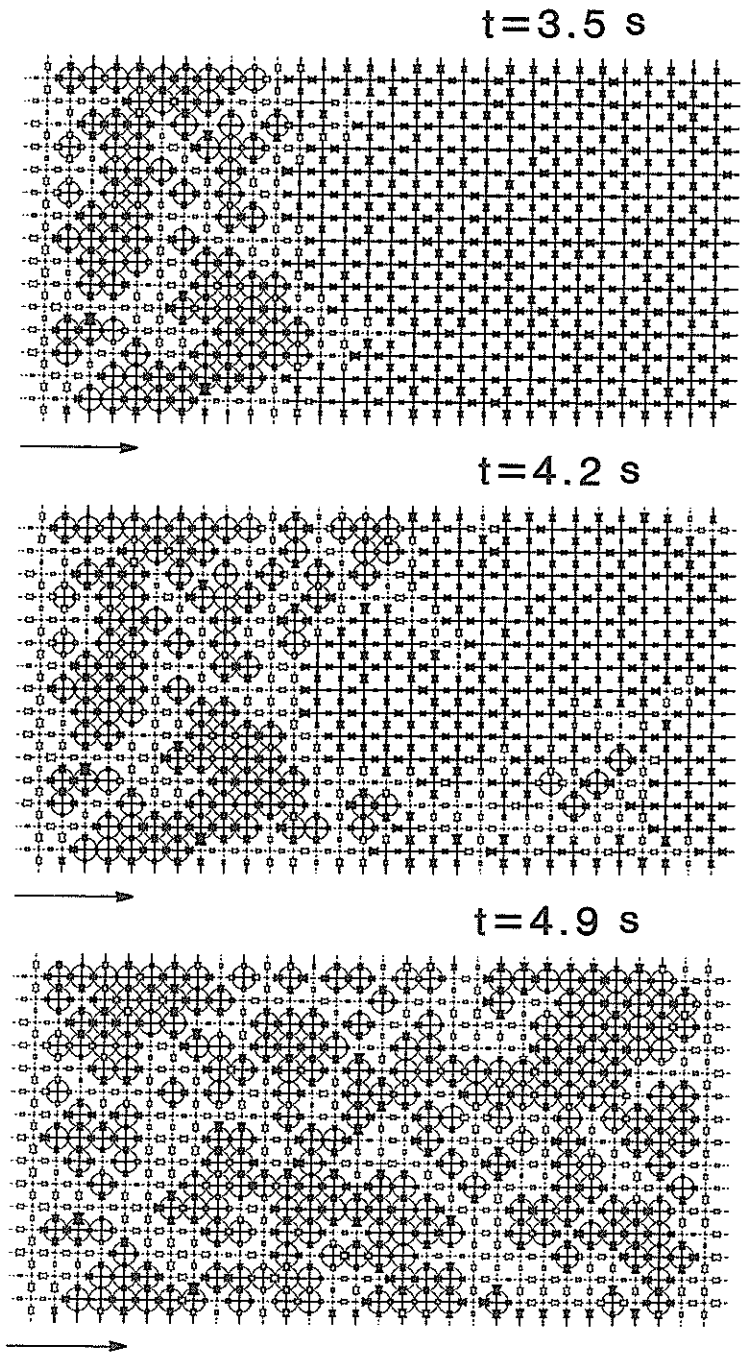


Figure 5.11

Stages of imbibition simulation in a 15×30 network (100×200 sandpack) for $Ca = 10^{-5}$ and $\kappa = 50$.

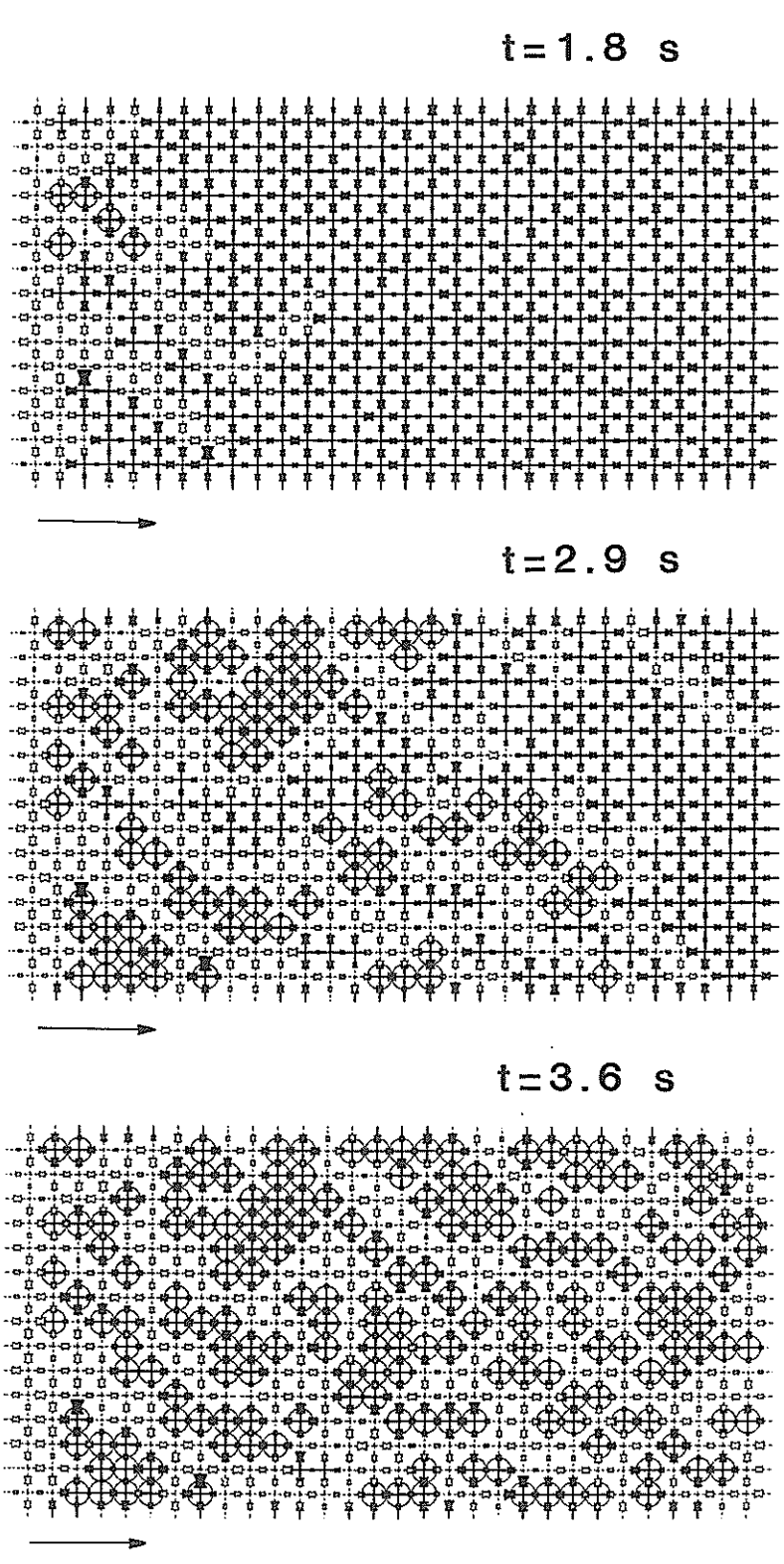


Figure 5.12

Stages of imbibition simulation in a 15 × 30 network (100 × 200 sandpack) for $Ca = 10^{-3}$ and $\kappa = 50$.

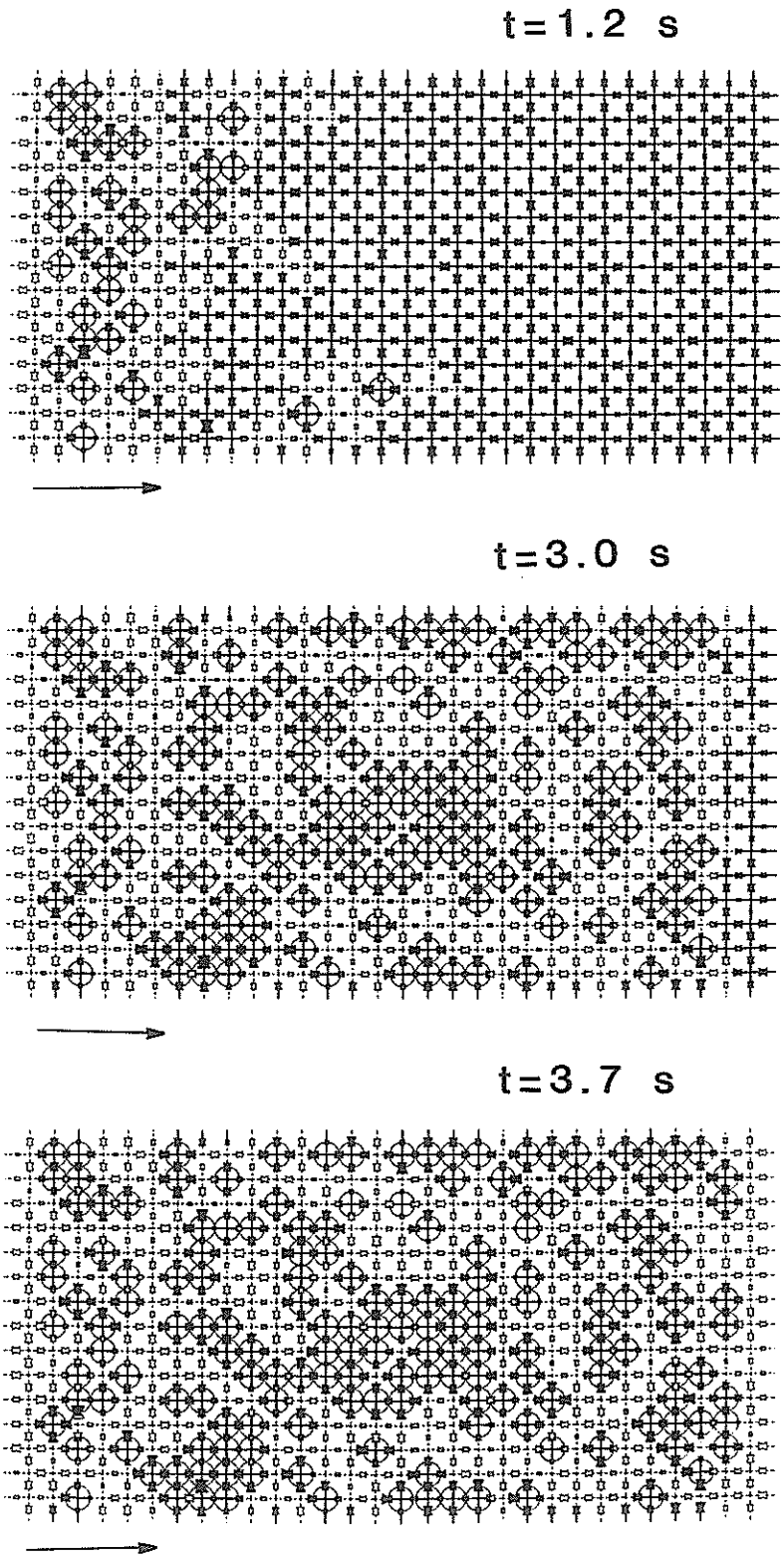


Figure 5.13

Stages of imbibition simulation in a 15 × 30 network (100 × 200 sandpack) for $Ca = 10^{-8}$ and $\kappa = 1$.

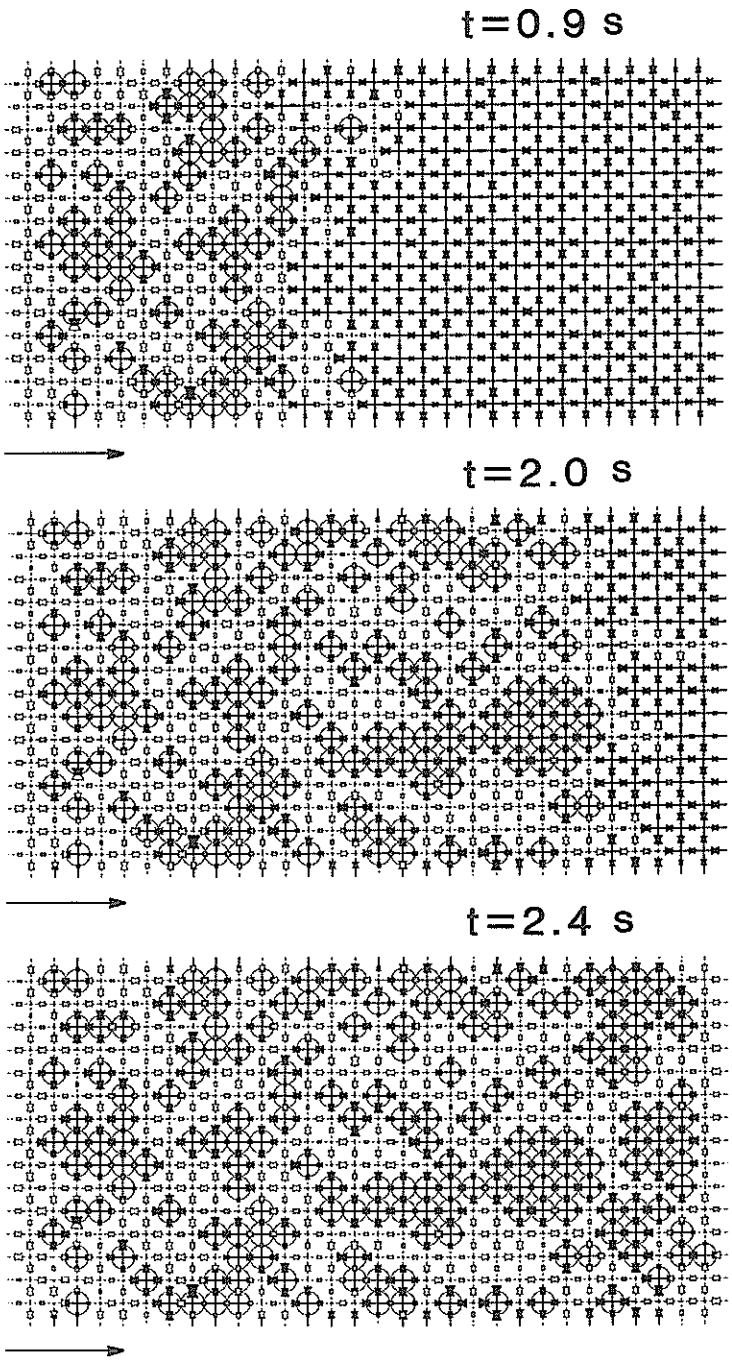


Figure 5.14

Stages of imbibition simulation in a 15 × 30 network (100 × 200 sandpack) for $Ca = 10^{-5}$ and $\kappa = 1$.

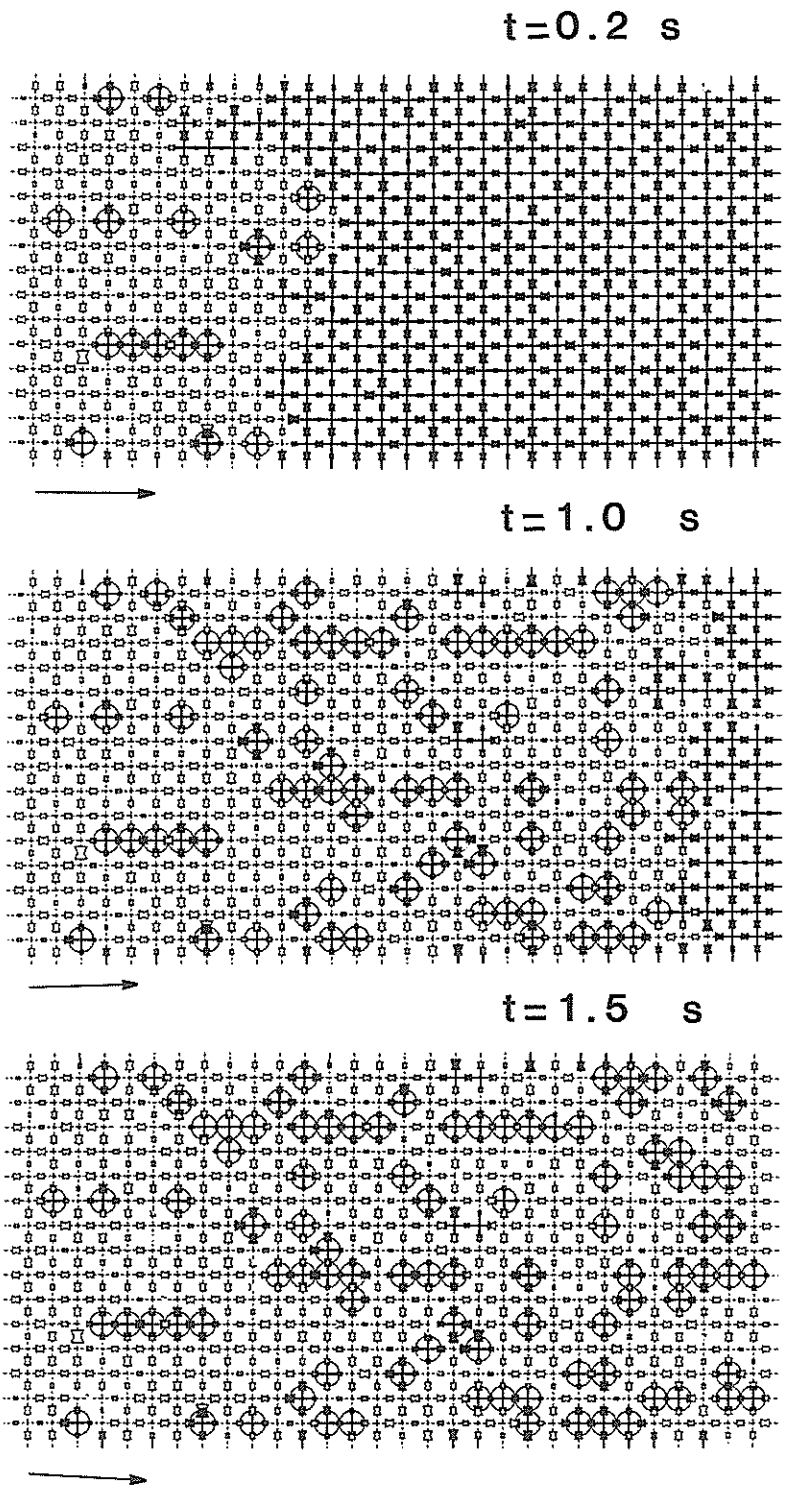


Figure 5.15

Stages of imbibition simulation in a 15 × 30 network (100 × 200 sandpack) for $Ca = 10^{-3}$ and $\kappa = 1$.

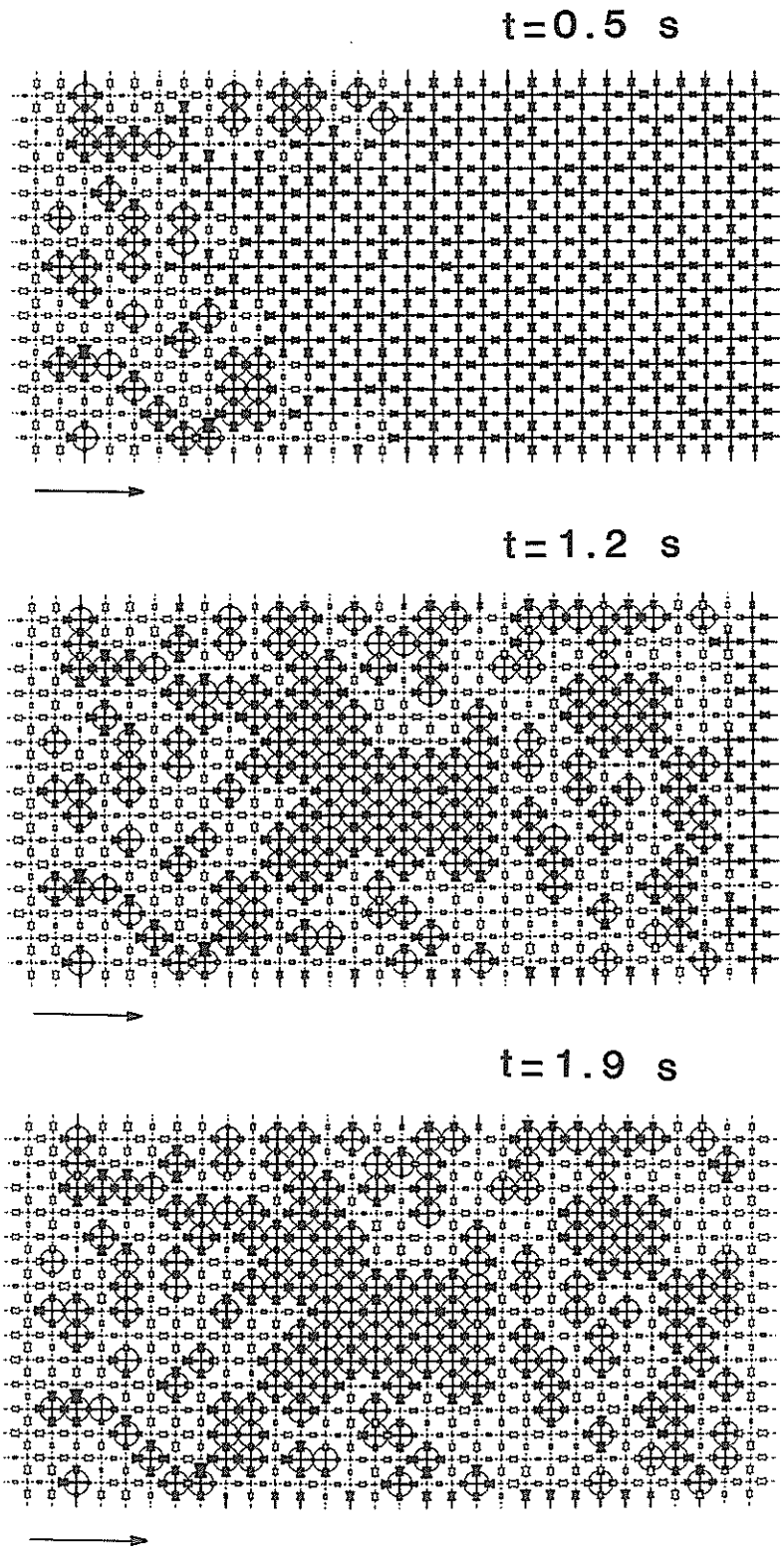


Figure 5.16

Stages of imbibition simulation in a 15×30 network (100×200 sandpack) for $Ca = 10^{-8}$ and $\kappa = 0.2$.

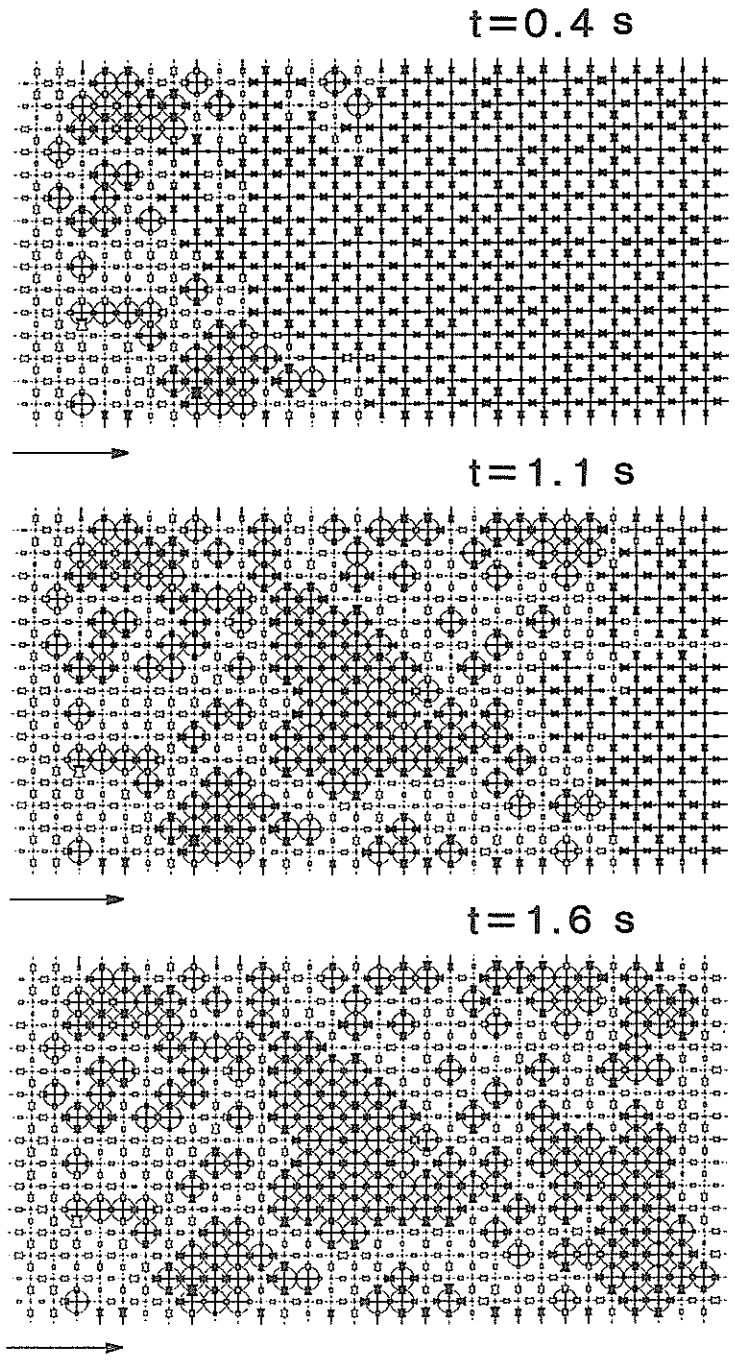


Figure 5.17

Stages of imbibition simulation in a 15 × 30 network (100 × 200 sandpack) for $Ca = 10^{-5}$ and $\kappa = 0.2$.

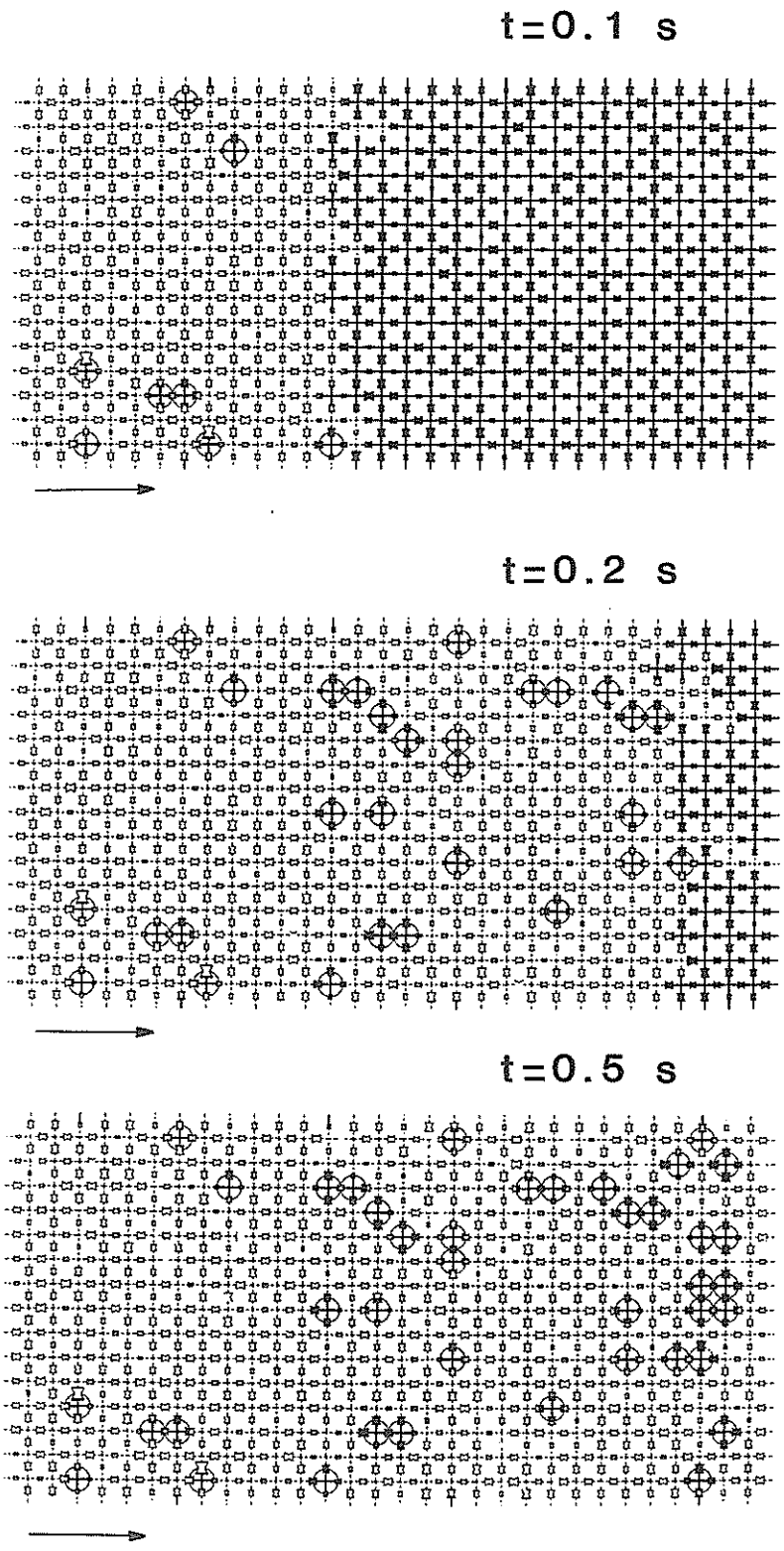


Figure 5.18

Stages of imbibition simulation in a 15×30 network (100×200 sandpack) for $Ca = 10^{-3}$ and $\kappa = 0.2$.

- For unfavorable viscosity ratio ($\kappa > 1$) and low Ca values, a high degree of microfingering is observed.
- The extent of microfingering decreases with decreasing κ and increasing Ca.
- Very high microdisplacement efficiencies are predicted in cases with favorable viscosity ratio ($\kappa < 1$) and high Ca.
- Many ganglia of various shapes and sizes are created. As the capillary number increases, fewer and fewer large ganglia are formed.
- The length of the transition zone decreases as Ca increases and/or κ decreases.

A general observation is that for moderate and high capillary numbers (say $Ca \geq 10^{-4}$), the flow regime switches from imbibition to dynamic invasion. This observation will be reinforced with the following global analysis.

Figures 5.19 through 5.27 show the final ganglion size distributions each averaged over three different realizations for different random networks. The following is observed:

- For large values of κ and Ca, the frequency of large ganglia increases due to more severe microfingering during displacement. This result is in agreement with experimental observations of Egbogah and Dawe (1981).
- The distribution $f(s)$ shows a primary maximum at $s = 1$. This means that 1-CEVS ganglia are the most numerous and contain a large portion of the residual oil. This is an important fact, since as it was seen in Chapter 4 small ganglia are difficult to remobilize, even under tertiary recovery conditions.
- The $f(v^*)$ distribution presents a primary maximum at some position well to the right of $v^* = 1$. This is due to the fact that 1-CEVS ganglia may have volumes which are larger or smaller than the average CEVS volume, v_{CEVS},

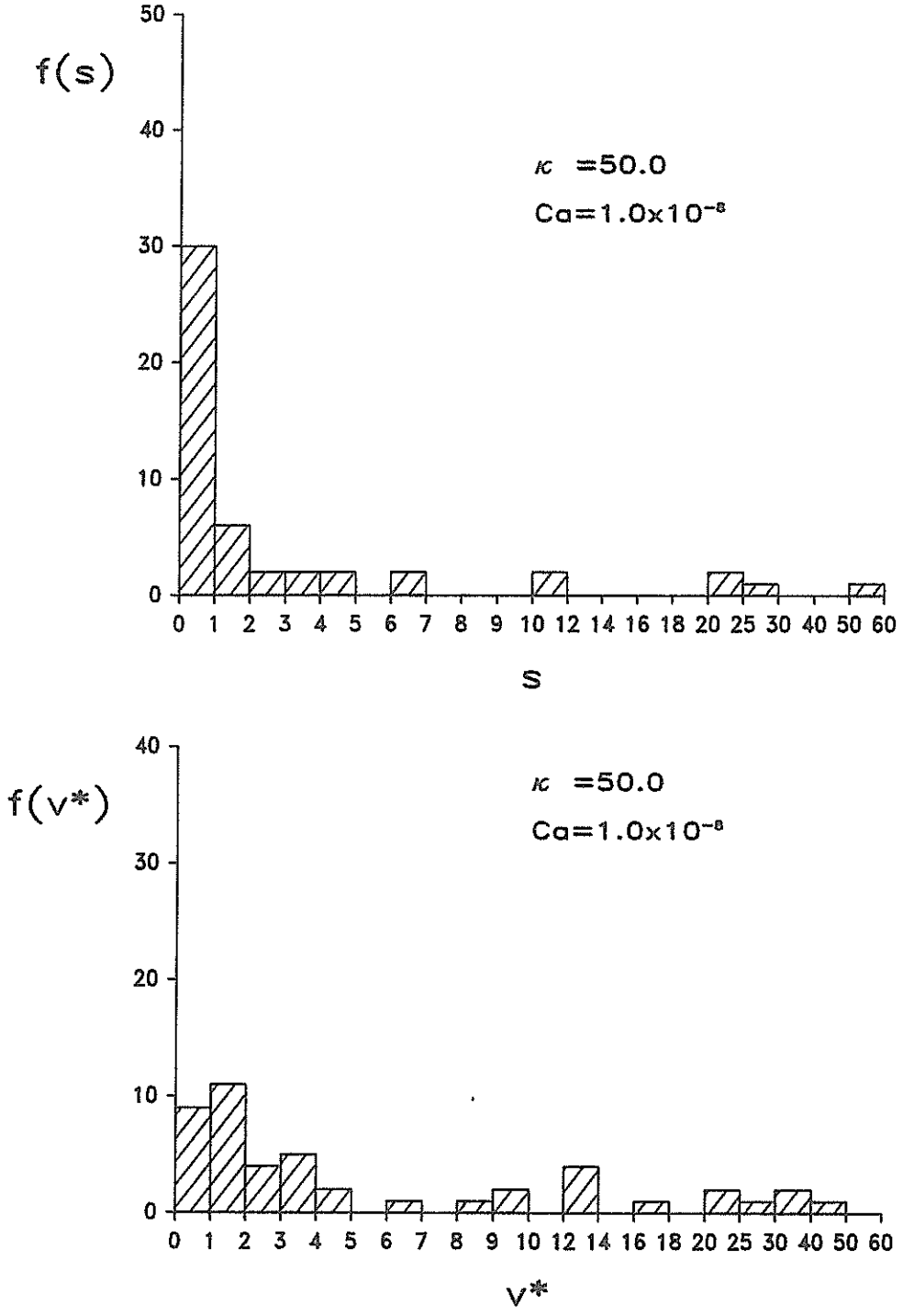


Figure 5.19

Plot of the final ganglion size frequency distribution functions for imbibition simulations in a 15×30 network (100×200 sandpack) for $Ca = 10^{-8}$ and $\kappa = 50$. a) frequency of ganglia, $f(s)$, *versus* the number of CEVS's occupied by the ganglion, s. b) frequency of ganglia, $f(v^*)$, *versus* the reduced ganglion volume, v^*.

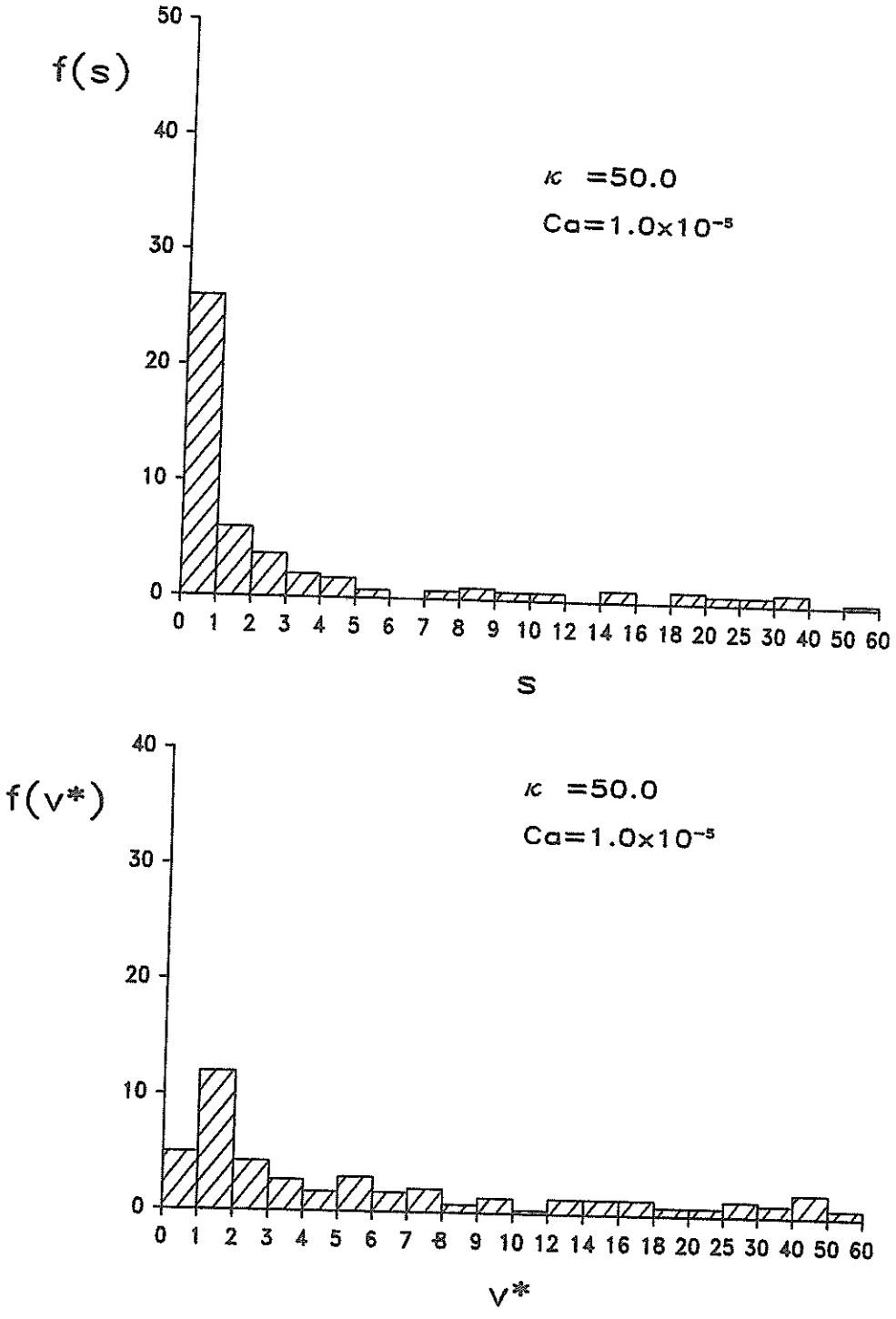


Figure 5.20

Plot of the final ganglion size frequency distribution functions for imbibition simulations in a 15×30 network (100×200 sandpack) for $Ca = 10^{-5}$ and $\kappa = 50$. a) frequency of ganglia, $f(s)$, *versus* the number of CEVS's occupied by the ganglion, s. b) frequency of ganglia, $f(v^*)$, *versus* the reduced ganglion volume, v^*.

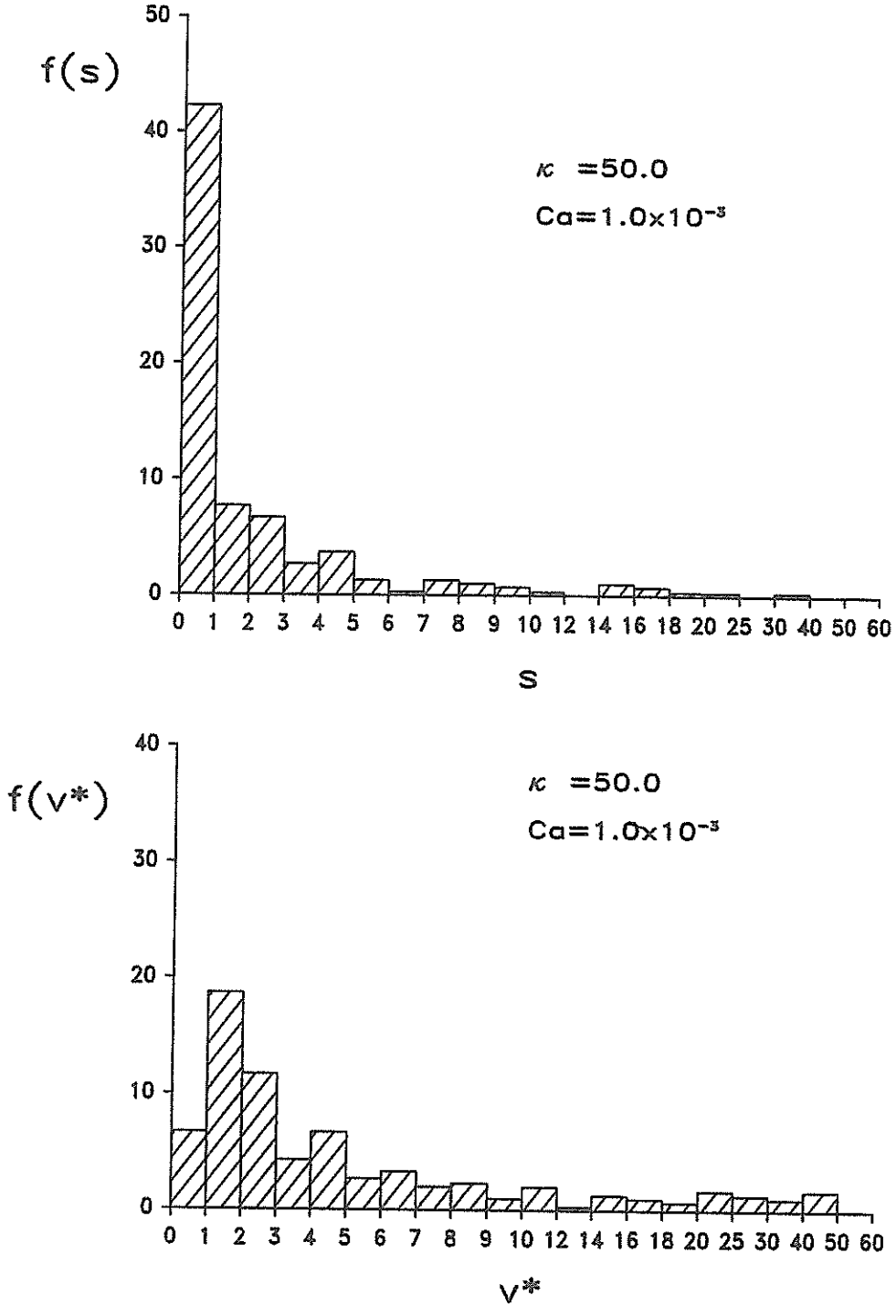


Figure 5.21

Plot of the final ganglion size frequency distribution functions for imbibition simulations in a 15×30 network (100×200 sandpack) for $Ca = 10^{-3}$ and $\kappa = 50$. a) frequency of ganglia, $f(s)$, *versus* the number of CEVS's occupied by the ganglion, s. b) frequency of ganglia, $f(v^*)$, *versus* the reduced ganglion volume, v^*.

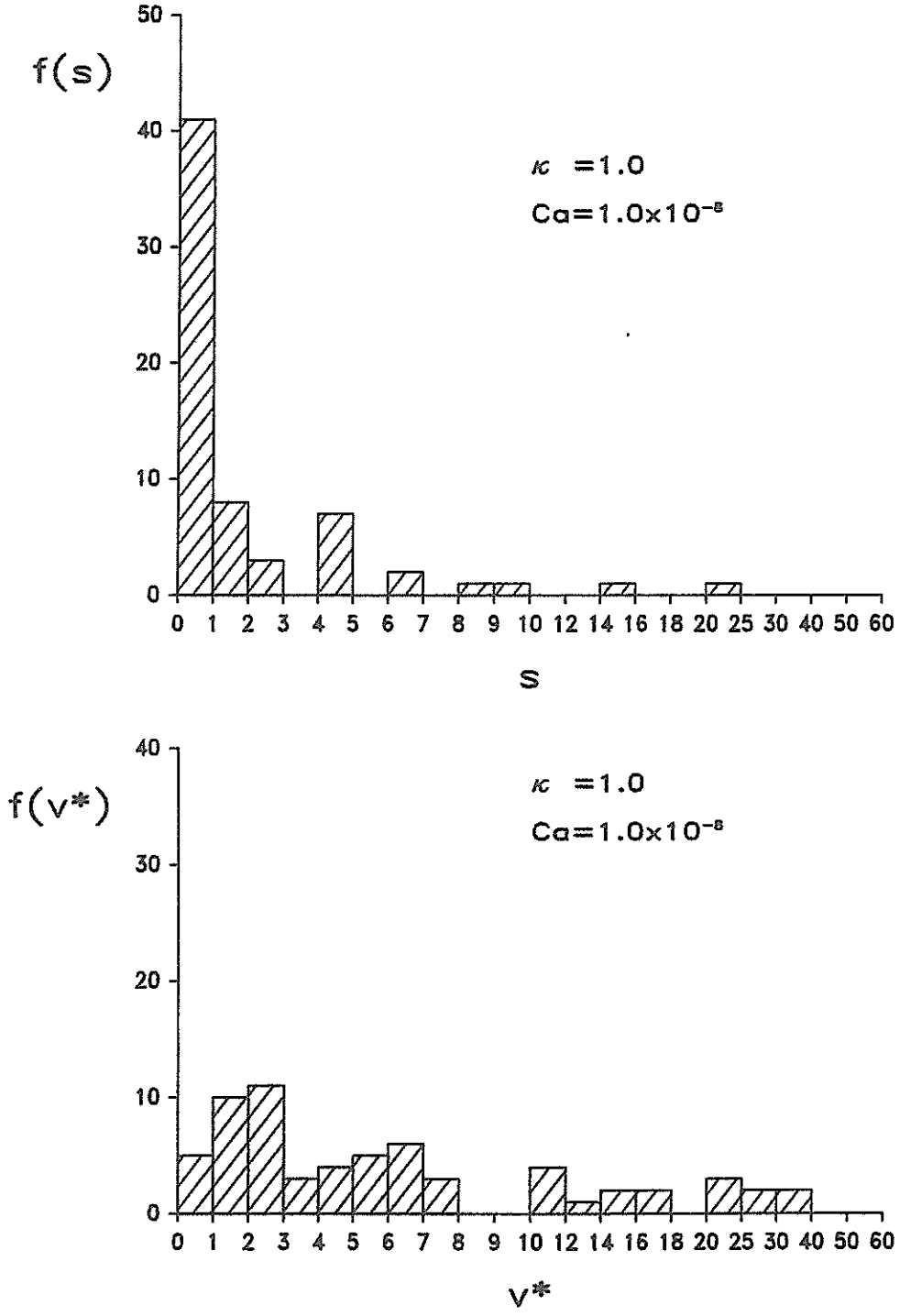


Figure 5.22

Plot of the final ganglion size frequency distribution functions for imbibition simulations in a 15×30 network (100×200 sandpack) for $Ca = 10^{-8}$ and $\kappa = 1$. a) frequency of ganglia, $f(s)$, *versus* the number of CEVS's occupied by the ganglion, s. b) frequency of ganglia, $f(v^*)$, *versus* the reduced ganglion volume, v^*.

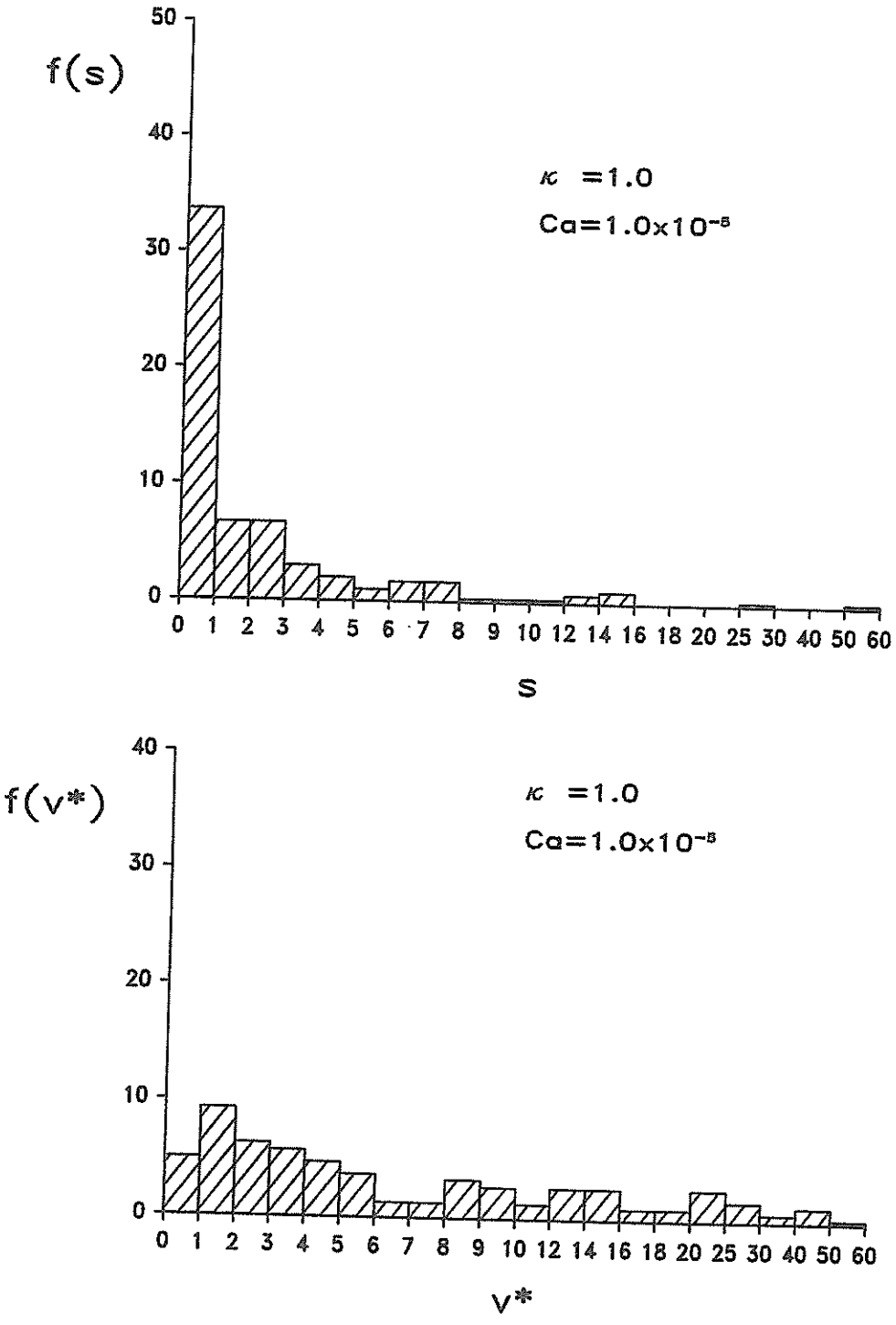
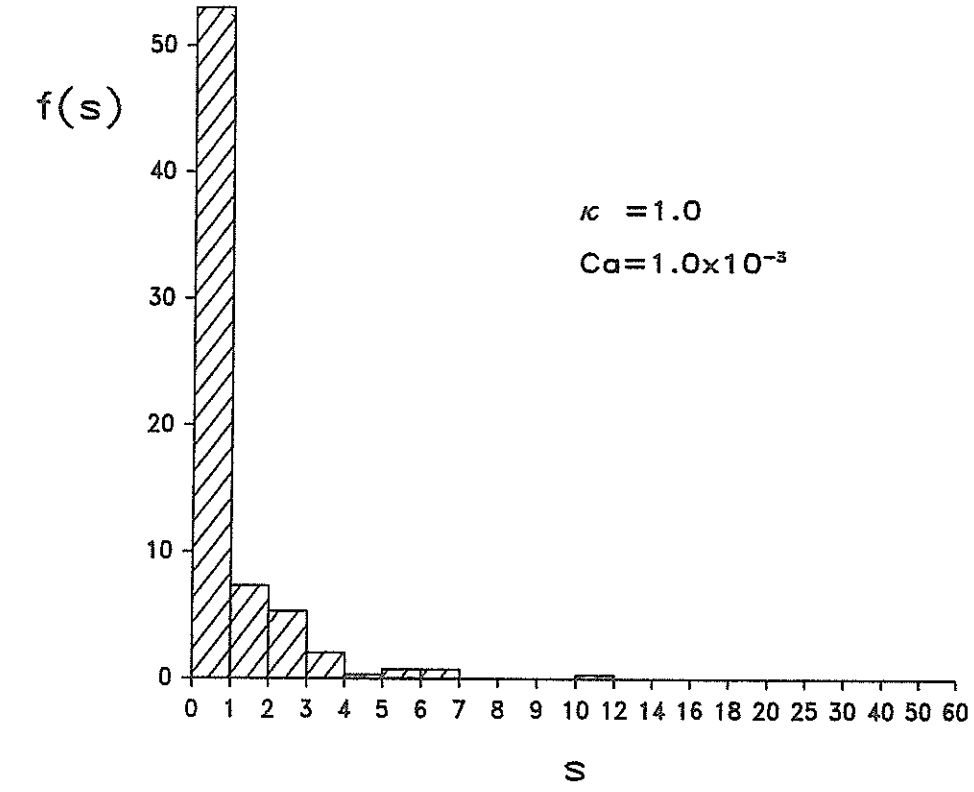


Figure 5.23

Plot of the final ganglion size frequency distribution functions for imbibition simulations in a 15×30 network (100×200 sandpack) for $Ca = 10^{-5}$ and $\kappa = 1$. a) frequency of ganglia, $f(s)$, *versus* the number of CEVS's occupied by the ganglion, s. b) frequency of ganglia, $f(v^*)$, *versus* the reduced ganglion volume, v^*.



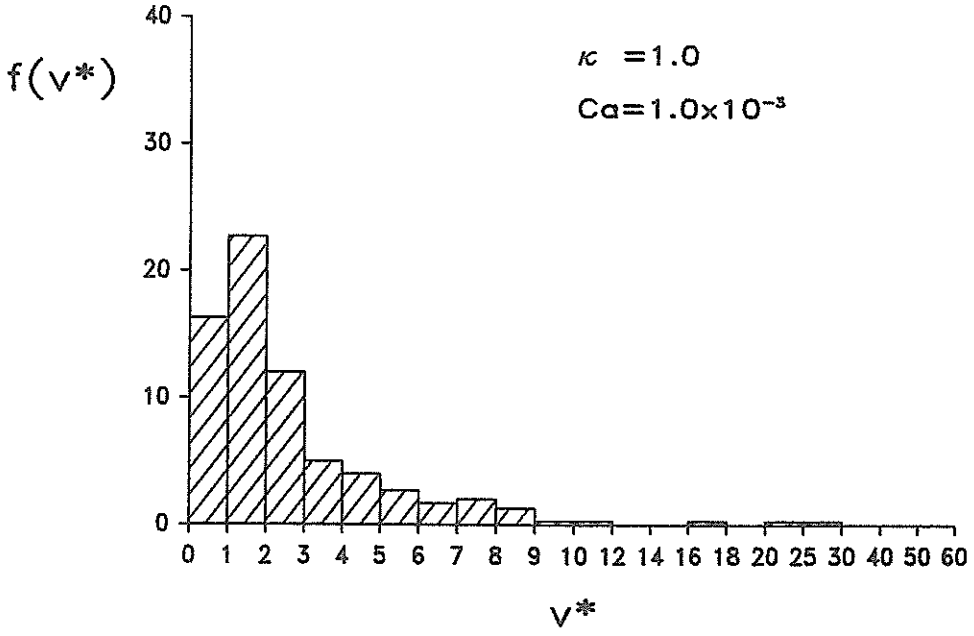


Figure 5.24

Plot of the final ganglion size frequency distribution functions for imbibition simulations in a 15×30 network (100×200 sandpack) for $Ca = 10^{-3}$ and $\kappa = 1$. a) frequency of ganglia, $f(s)$, *versus* the number of CEVS's occupied by the ganglion, s. b) frequency of ganglia, $f(v^*)$, *versus* the reduced ganglion volume, v^*.

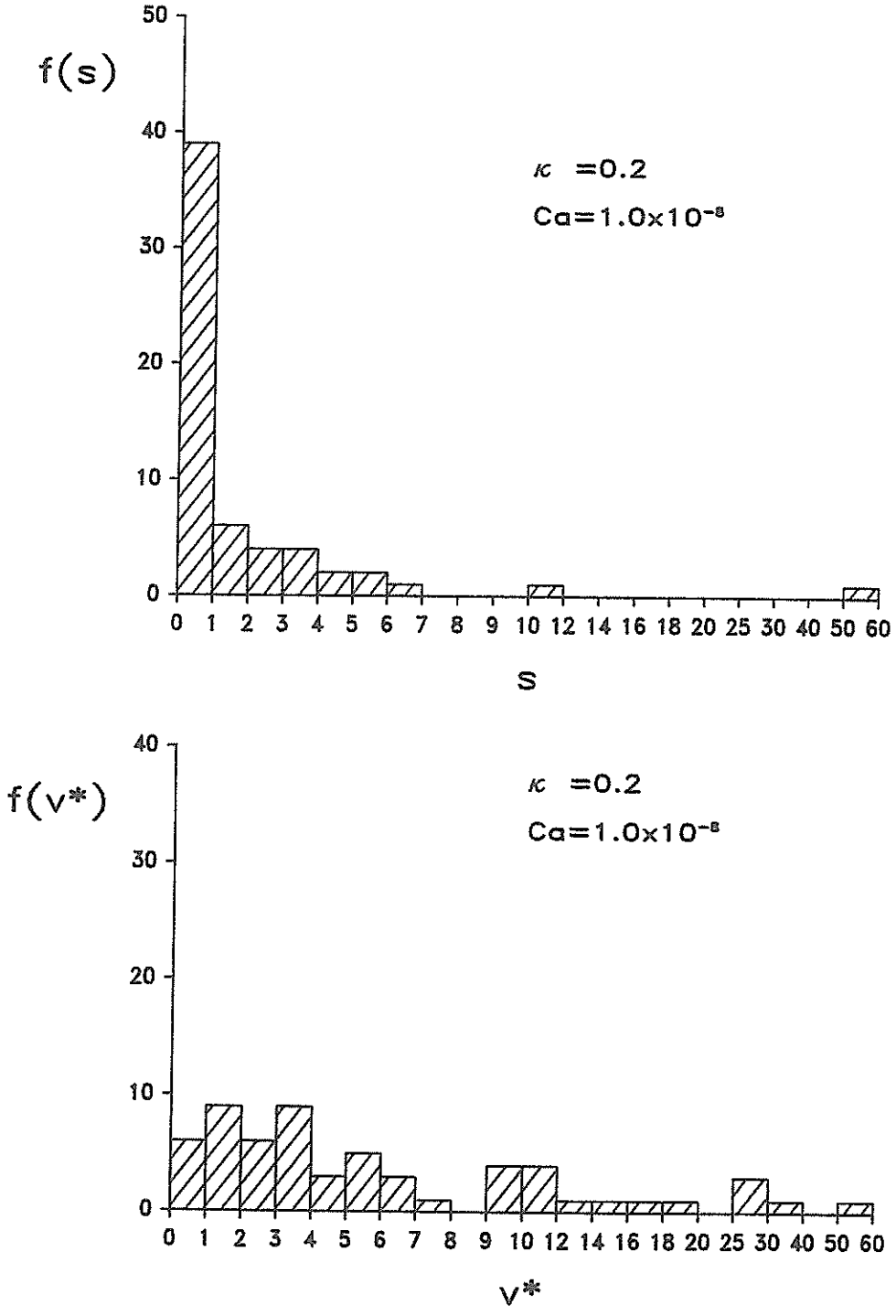


Figure 5.25

Plot of the final ganglion size frequency distribution functions for imbibition simulations in a 15×30 network (100×200 sandpack) for $Ca = 10^{-8}$ and $\kappa = 0.2$. a) frequency of ganglia, $f(s)$, *versus* the number of CEVS's occupied by the ganglion, s. b) frequency of ganglia, $f(v^*)$, *versus* the reduced ganglion volume, v^*.

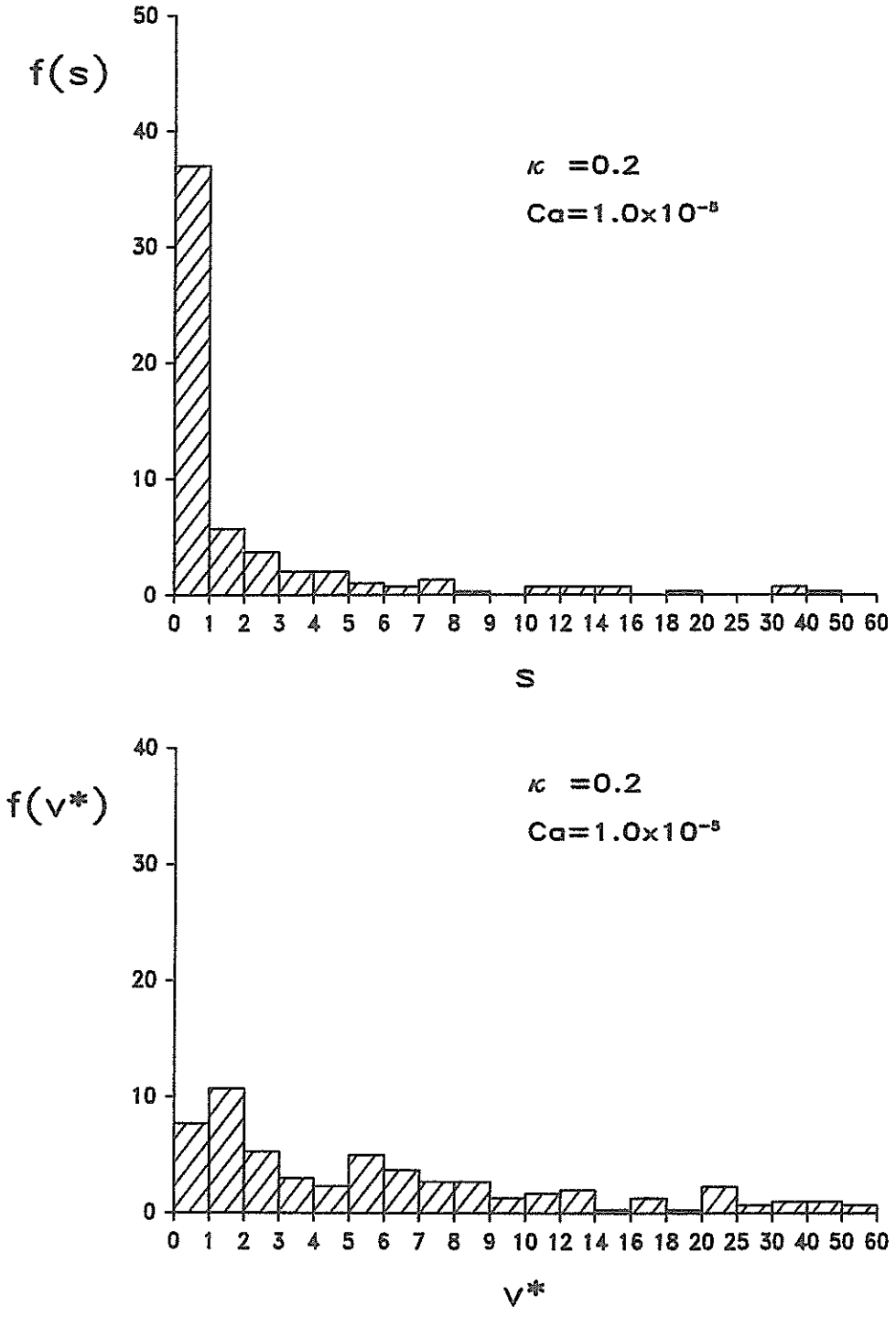


Figure 5.26

Plot of the final ganglion size frequency distribution functions for imbibition simulations in a 15×30 network (100×200 sandpack) for $Ca = 10^{-5}$ and $\kappa = 0.2$. a) frequency of ganglia, $f(s)$, *versus* the number of CEVS's occupied by the ganglion, s. b) frequency of ganglia, $f(v^*)$, *versus* the reduced ganglion volume, v^*.

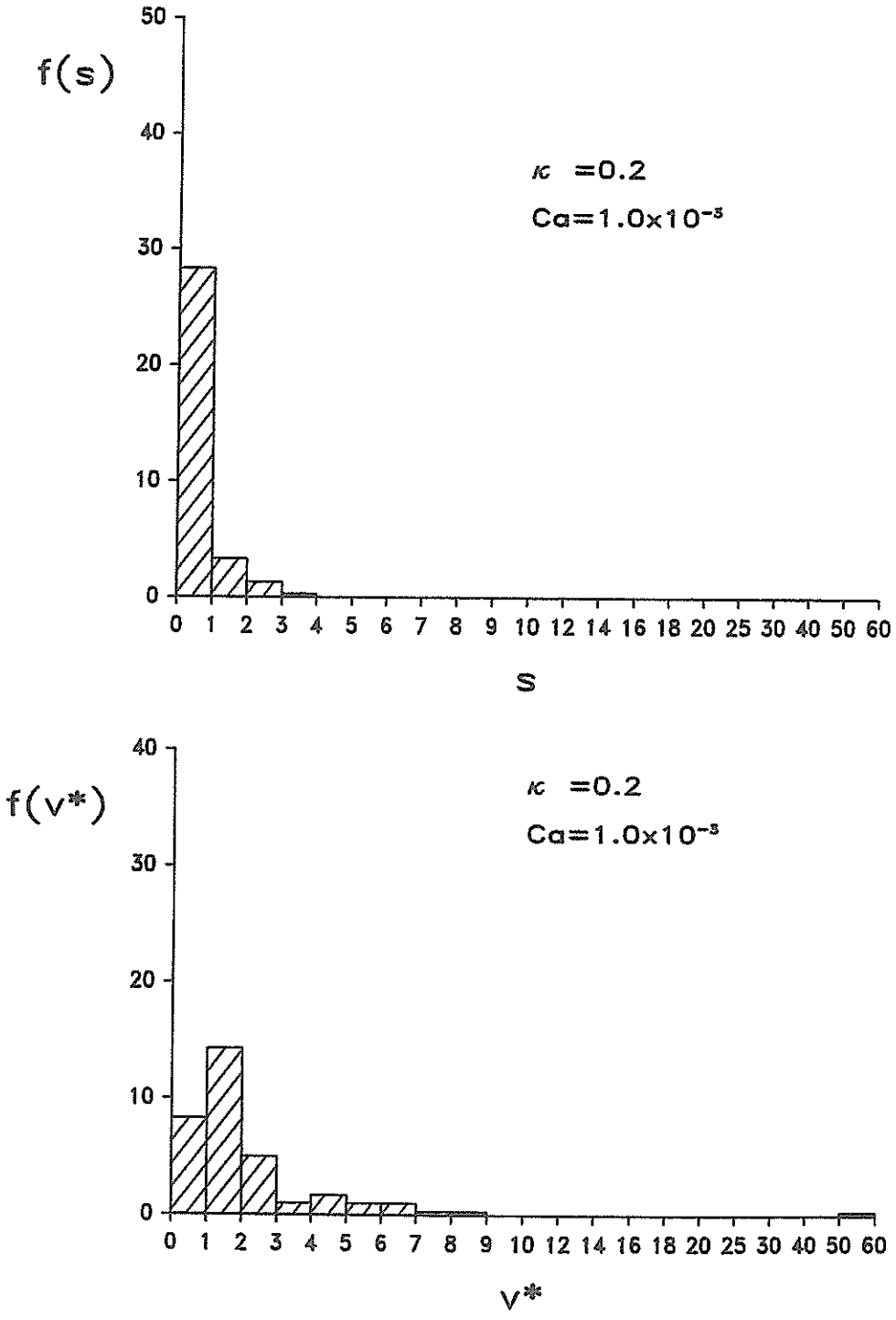


Figure 5.27

Plot of the final ganglion size frequency distribution functions for imbibition simulations in a 15×30 network (100×200 sandpack) for $Ca = 10^{-3}$ and $\kappa = 0.2$. a) frequency of ganglia, $f(s)$, *versus* the number of CEVS's occupied by the ganglion, s. b) frequency of ganglia, $f(v^*)$, *versus* the reduced ganglion volume, v^*.

and the oil accumulates preferentially in CEVS's with large volume. The form of this distribution is similar to experimental distributions reported by Chatzis, Morrow and Lim (1983). However, although these experimental results were also obtained in planar media, a direct comparison with the theoretical results is not appropriate since the former results are given in terms of the equivalent diameter of the projected area of the ganglion and not in terms of v^*.

Plots of the acceptance fraction, $a_d(d)$ for fixed values of Ca and κ, obtained by averaging results from three different runs with different networks are given in Figures 5.28 through 5.30. The analysis of these plots lead to the following observations:

- Small unit cells are invaded by the aqueous phase more frequently than large unit cells, specially for low capillary numbers.
- As Ca increases, the invading aqueous phase tends to favor larger unit cells, but there is not clearcut sorting, since unit cells of all sizes get invaded.
- For moderate to high Ca values and small κ values the acceptance fraction tends to unity for all unit cell sizes. This means that most pores get invaded, irrespective of their sizes, resulting in a very small residual oil saturation.

Figure 5.31 shows the average water saturation, $S_w - S_{wi}$, in the porous medium as a function of time with Ca and κ as parameters, and Figure 5.32 shows the residual oil saturation, S_{or}, as a function of the capillary number for various values of κ. Both results were obtained by averaging over the same three different runs of the previous figures. The following is observed:

- For $\kappa \leq 1$, the residual oil saturation remains virtually constant up to $Ca \approx 10^{-5}$, and then it starts to decrease drastically.

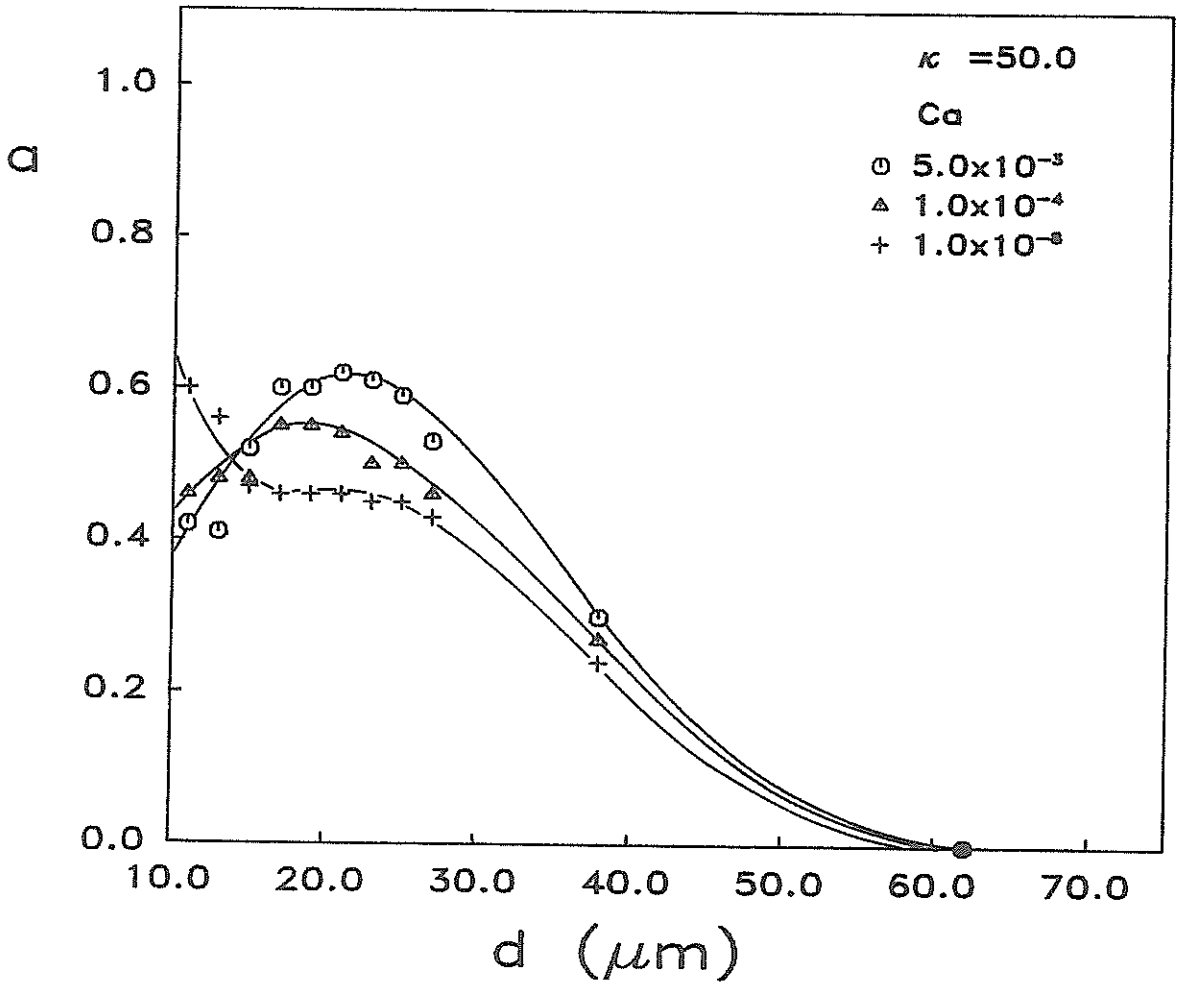


Figure 5.28

Plot of the acceptance fraction, $a_d(d)$, *versus* the unit cell throat diameter, d, for free imbibition simulations on a 15×30 network (100×200 sandpack) for $\kappa = 50$ and various Ca values.

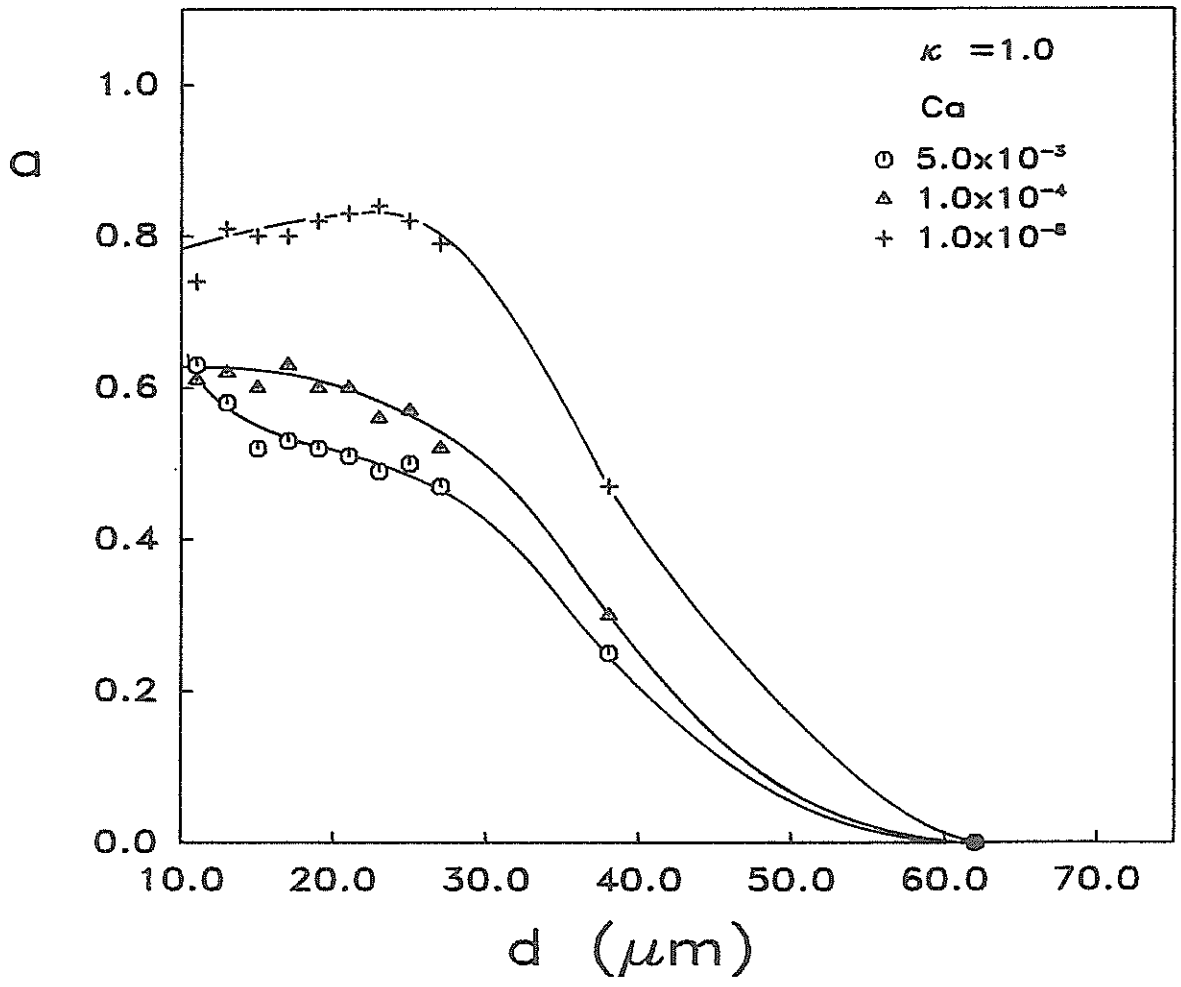


Figure 5.29

Plot of the acceptance fraction, $a_d(d)$, *versus* the unit cell throat diameter, d, for free imbibition simulations on a 15×30 network (100×200 sandpack) for $\kappa = 1$ and various Ca values.

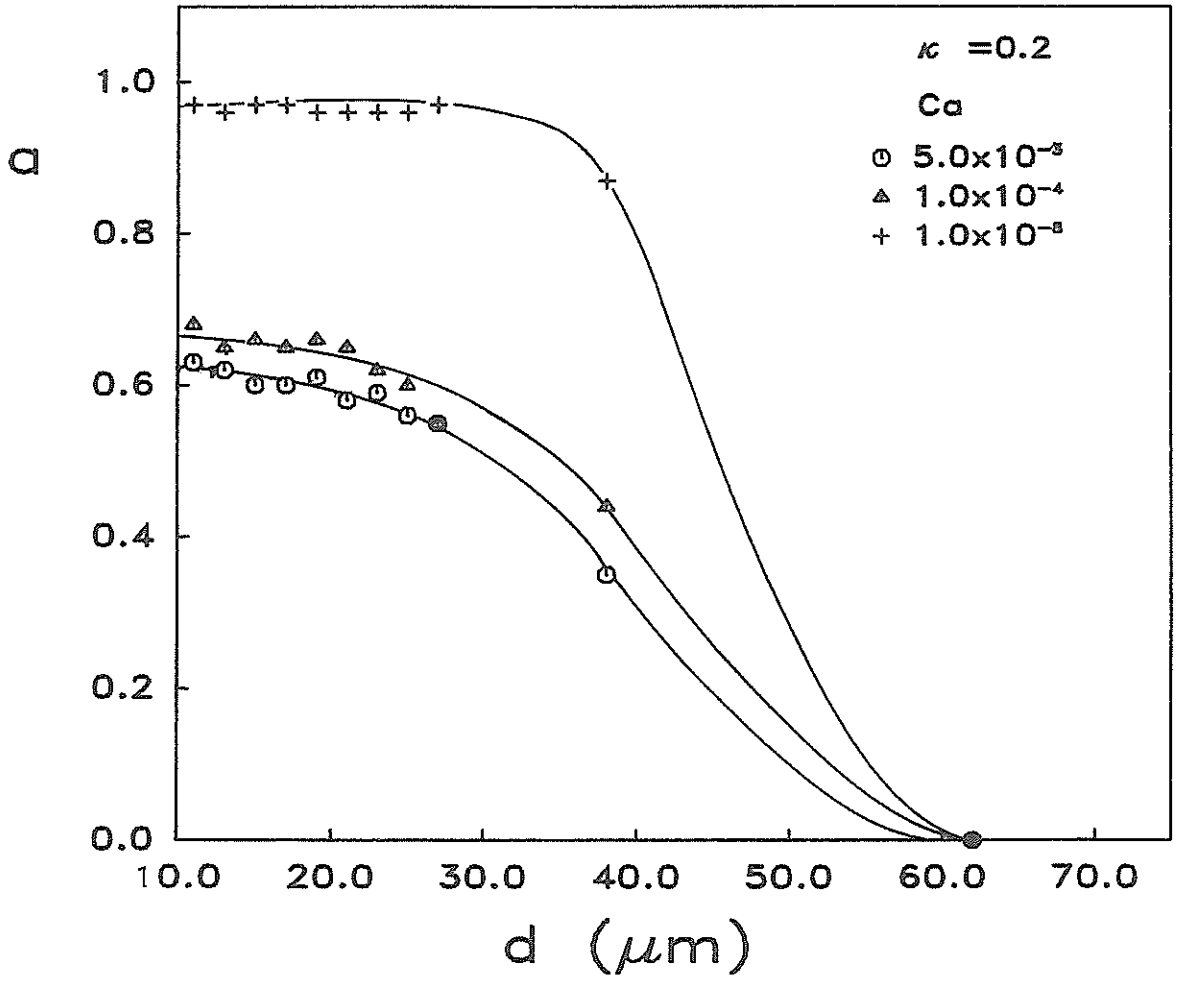


Figure 5.30 .

Plot of the acceptance fraction, $a_d(d)$, *versus* the unit cell throat diameter, d, for free imbibition simulations on a 15×30 network (100×200 sandpack) for $\kappa = 0.2$ and various Ca values.

- For $\kappa > 1$. S_{or} increases with increasing Ca up to $Ca \approx 10^{-5}$, at which point it starts decreasing rapidly.
- Both the time to achieve breakthrough and the completion time decrease with increasing Ca and/or decreasing κ

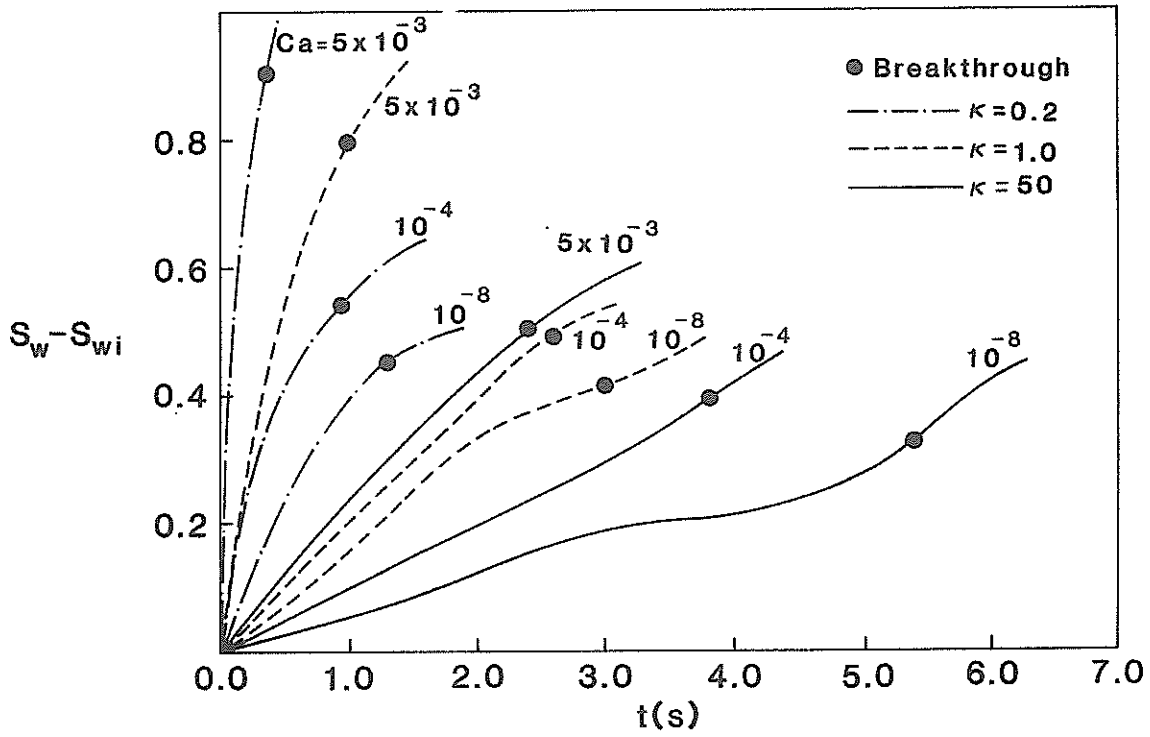


Figure 5.31

Plot of the average water saturation, $S_w - S_{wi}$, versus time, t, for imbibition simulations on a 15×30 network (100×200 sandpack), for various values of Ca and κ.

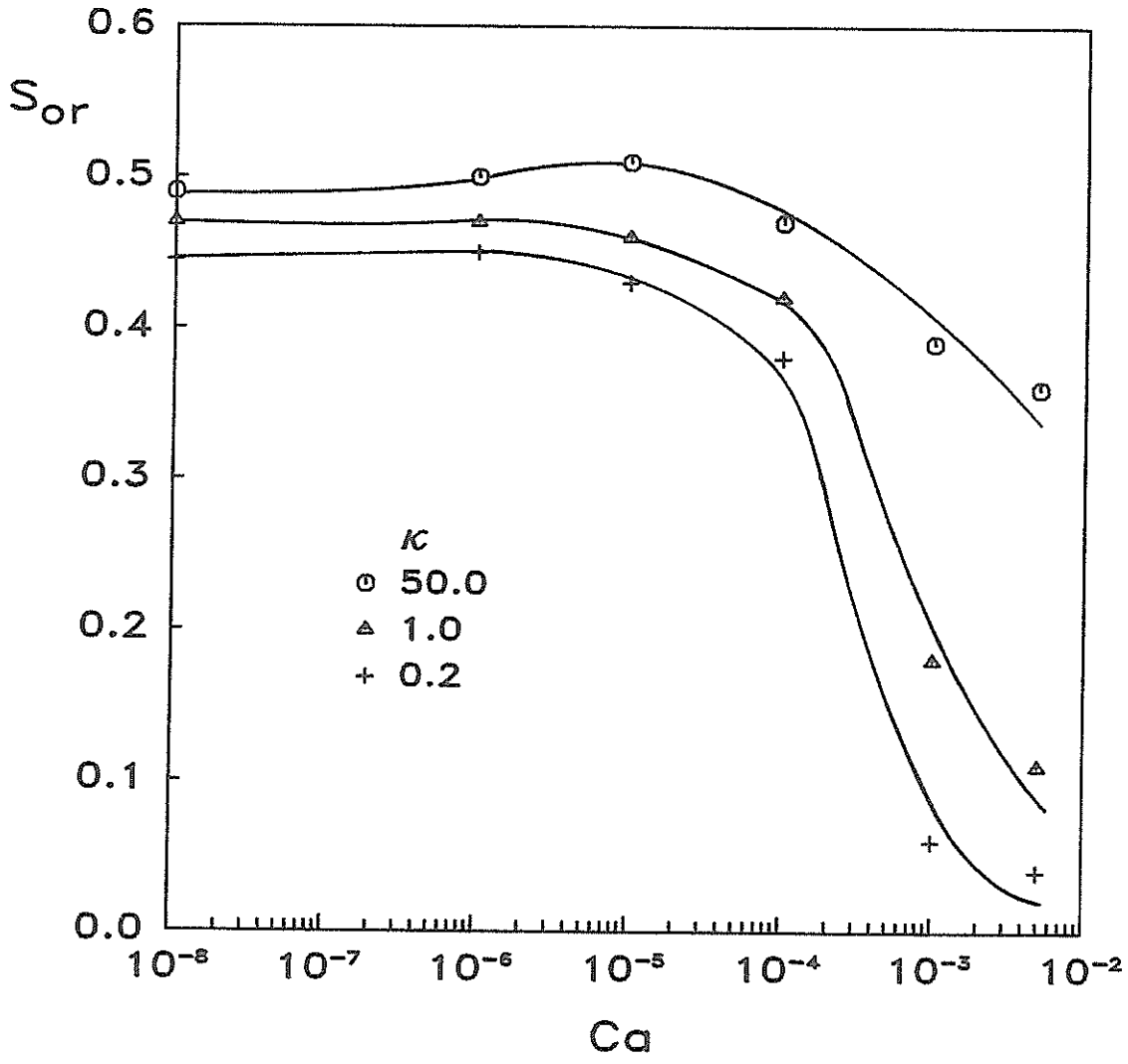


Figure 5.32

Plot of the residual oil saturation, S_{or} , versus the capillary number , Ca, for imbibition simulations on a 15 × 30 network (100 × 200 sandpack), for various values of κ.

Chapter 6

Summary and Suggestions for Future Work

6.1 Summary and Conclusions

Immiscible microdisplacement in porous media was modeled in the present work by using a network of pores of converging-diverging geometry, together with standard network analysis to calculate the pressure field and a set of rules for fluid displacement. This model was used to simulate the motion of solitary oil ganglia and the invasion by water of an initially oil-filled network (imbibition processes).

Previous attempts to simulate microdisplacement include the use of: percolation processes (Chandler *et al* , 1982; Wilkinson and Willemsen, 1983; Wilkinson, 1984); networks of the sphere-and-capillary type in conjunction with network analysis (Koplik, 1982; Koplik and Lasseter, 1982); and a stochastic simulation model based on the same porous media model used in the present work together with a mobilization criterion (Payatakes, Ng and Flumerfelt, 1980; Ng and Payatakes,

1980). Comparing these methods with the simulation method developed in the present study, the following conclusions can be drawn:

- Percolation models can be used to study some aspects of quasistatic imbibition, especially the percolation threshold (breakthrough), the residual oil saturation, and the ganglion size distribution. They can not be used, in their present form, to deal with displacement in which viscosity effects are present, or in the case where the non-wetting phase is completely disconnected (tertiary recovery). They do not have a sense of rate and do not consider the viscosity ratio. Hence they do not apply to imbibitions that have Ca values significantly larger than ca 10^{-7}. The main advantage of percolation processes is that, when they apply, the results are obtained with small computational effort. Furthermore, if percolation theory is accepted, results obtained with percolation processes are universal.

- Networks of the sphere-and-capillary type present an advantage over the model used in this work, of being more realistic when applied to consolidated porous media. On the other hand, due to the existence of wall discontinuities at the cross-sections where the cylindrical throats are connected to the spherical chambers, many menisci become constrained. This complication generates high computational times, and for this reason, the results reported so far, pertain only to cases where both fluids have the same viscosity.

- The method developed by Payatakes, Ng and Flumerfelt (1980) and Ng and Payatakes (1980) pertains exclusively to the motion of oil ganglia; it can not deal with viscosity differences between the two fluid phases; and time, as an explicit variable, is not present. Furthermore, motion of two or more interfaces

simultaneously, which is an important feature of dynamic displacement, is not allowed. This method has the advantage of producing results with relatively small computational effort, and it has been proven to produce good results for cases where the motion of ganglia occurs at the onset of mobilization.

- The simulation method developed in the present study can be used over a wide range of the physical and operational parameters, such as the capillary number and the viscosity ratio. Since the unit cell walls are defined as continuous functions, menisci are free to move at all times. Time is present as an explicit variable and rates of displacement can be evaluated. As it stands at the present time, the main disadvantages of this simulation method are: first, the porous medium model pertains to unconsolidated porous media which is not a realistic situation when it comes to simulation of oil recovery processes; and second, high computational requirements in time and memory prevent the study of a wider range of the parameters, and, especially in the case of imbibition processes, the use of large networks.

Suggestions on how to further use and improve this model and simulation method are given in the next section.

The main conclusions that can be drawn from the study done on the fate of solitary oil ganglia are the following:

- The physical and operational parameters that affect the fate of solitary oil ganglia are: the capillary number, Ca; the viscosity ratio, κ; the contact angles, namely the equilibrium contact angle, θ_e, and the advancing and receding contact angles, θ_a and θ_r, respectively; the ganglion size, expressed by the reduced ganglion volume, v^*; and the local topology of the porous medium.

- Two different types of displacement are observed, depending on the the value of the capillary number. If the capillary number is close to the critical value for mobilization, Ca_{cr}, the ganglion undergoes quasistatic displacement. It tends to become elongated and aligned with the direction of the flow. While it moves it breaks often, and the smaller daughter ganglia eventually get stranded. Restranding can occur even without break-up. If the value of Ca_{cr} is significantly exceeded, the ganglion undergoes dynamic displacement; that is, it may advance with two or more menisci simultaneously. The tendency for elongation is much smaller than in the case of quasistatic displacement, and the rate of break-up per unit length of travel is much higher, due to the presence of dynamic break-up associated with quasistatic break-up.

- The ganglion velocity can be expressed in terms of the reduced ganglion averaged velocity. u^* is smaller than unity if the the viscosity ratio is unfavorable ($\kappa \geq 1$), and larger than unity if the viscosity ratio is favorable ($\kappa < 1$) and the ganglion is large. The average velocity of a ganglion increases with increasing Ca. For ganglia larger than ca 5 pores, u^* increases with increasing ganglion size, and for very large ganglia it may reach an asymptotic value. The behaviour of smaller ganglia is more complex, and depends on the capillary number. If value of Ca is close to Ca_{cr}, u^* increases monotonically with v^*. For values of Ca that are substantially higher than Ca_{cr}, the velocity of 2 and 3-pore ganglia may be slightly larger than the velocity of larger ganglia. This effect is observed only for $\kappa \geq 1$. Studies at different values of the equilibrium and the dynamic contact angles show that u^* is largely dependent on the the values of θ_e. The critical value for mobilization decreases as θ_e increases, while

the reduced ganglion velocity for large values of Ca decreases as θ_e increases. The dependence of u^* on the values of the dynamic contact angles was found to be substantially weaker.

- Fissioning and stranding were studied in terms of the break-up and stranding coefficients and of the break-up mode probability. In general, it was found that the stranding coefficient decreases with an increase in the capillary number, while the break-up coefficient increased as Ca increased. The viscosity ratio played a lesser role on the break-up coefficient. Large ganglia seemed to be destined to break into smaller and smaller ganglia, which in turn became stranded very easily.

Analysis of imbibition and dynamic invasion simulations leads to the following conclusions:

- The physical and operational parameters that affect imbibitions processes are: the capillary number, Ca; the viscosity ratio, κ; the contact angles; the local oil saturation, S_o; the length of the porous medium and the boundary conditions; and the local topology of the porous medium.
- For favorable viscosity ratio ($\kappa < 1$), the residual oil saturation, S_{or}, decreases as Ca increases. For unfavorable viscosity ratio ($\kappa \geq 1$), S_{or} increases with Ca up to $Ca = ca\ 10^{-4}$. For higher values of Ca, the residual oil saturation decreases rapidly as Ca increases.
- A flood with favorable viscosity ratio ($\kappa < 1$) and moderate Ca values (say, $ca\ 10^{-4}$) applied right from the beginning (that is, *not after* a low Ca value flood) gives excellent microdisplacement efficiency.
- Floods with finite Ca values produce ganglion populations in which 1-pore

ganglia are the most common. The frequency of large ganglia decreases rapidly with size. Few ganglia are larger than 15-20 pores.

- As $Ca \rightarrow 0$ (quasistatic imbibition), in addition to the multitude of small ganglia, there appear a few very large ganglia, the largest of which have dimensions comparable to those of the sample. For $\kappa > 1$, microfingering becomes more intense as Ca and κ increase, and this results in the formation of some large ganglia. At the same time, the residual saturation also increases with increasing Ca for small values of Ca and decreases rapidly for $Ca > ca$ 10—4. This effect may be due to the mobilization of some large ganglia. For $\kappa < 1$, as Ca increases microfingering is reduced, fewer and smaller ganglia are formed, and the residual saturation decreases.
- The average size of the pores that become invaded by the wetting phase tends to increase with increasing Ca and κ. However, there is no clearcut sorting, as pore doublet models imply. For moderate and large Ca values, pores of all sizes get invaded (though not with equal frequency). For moderate Ca values and favorable viscosity ratio, most pores become invaded, irrespective of their size.

6.2 Suggestions for Future Work

The following suggestions emerge from the present review:

- The porous medium model used in this work can be improved by generalizing its formulation so that it applies not only to packings of grains, but also to consolidated porous media. In order to avoid the problems of sphere-and-

capillary network models, the functions representing the unit cell walls should be kept continuous. The formulation of this model will probably require the development of a method for the proper interpretation of porosimetry data combined with stereological studies of pore casts.

- Further improvement of the simulator should involve: the generalization to three dimensional networks, or at least the inclusion of two layers, in order to incorporate the non-planarity of real porous media; and the generalization to completely random networks, especially in what concerns the coordination number.
- In order to reduced the computational time, the solution of the algebraic system of equations resulting from the application of network analysis should be done in a more efficient way, namely by the use of iterative solvers. This is particularly important for three-dimensional and two-layer networks.
- The motion of small ganglia (1 to 3 pores in size) must be studied by solving the equations of motion with the appropriate boundary conditions in realistic geometries. A Washburn-type analysis of this problem is not entirely sufficient.
- The effect of other ganglia on the ganglion velocity and on the stranding and break-up coefficients must be determined.
- Snap-off should be included as one of the phenomena leading to breakup.
- The present model and simulator can be used to determine the probability of coalescence given a collision. This seems to be a very important parameter in the study of large populations of oil ganglia.
- The present model may be used to study steady state displacement over a wide range of the saturation values. The objective of this study would be to

investigate the dependence of the relative permeabilities, k_{ro} and k_{rw}, on the system parameters.

- Finally, the link between microdisplacement and macrodisplacement is not yet established. In the long run, this seems to be the overall objective of the study of immiscible microdisplacement in porous media.

Appendix A

FORTRAN 77 Listings of Computer Codes

A.1 Listing of Program GANDYN Used to Simulate the Motion of a Solitary Oil Ganglion

```
      PROGRAM GANDYN
C
C     PROGRAM *GANDYN* SIMULATES THE MOTION OF A SOLITARY OIL GANGLION
C     IN A CUBIC NETWORK, USING NETWORK ANALYSIS.
C
C     VARIABLES WITH  *  ARE INPUT VARIABLES.
C
C     AC      - VECTOR OF DIMENSIONS  NCTE  CONTAINING THE DIMENSIONLESS
C               UNIT CELL CROSS-SECTIONAL AREA FOR EACH COMPARTMENT.
C  *  AL      - LENGTH OF PERIODICITY OF THE POROUS MEDIUM.
C     AREA    - UNIT BLOCK CROSS-SECTIONAL AREA.
C  *  CAN     - CAPILARY NUMBER.
C  *  C1-C3   - UNIT CELL MODEL CONSTANTS.
C     D       - THROAT DIAMETER OF CURRENT UNIT CELL
C  *  DUC     - VECTOR OF DIMENSION  NSIZE  CONTAINING THE THROAT
C               DIAMETER FOR EACH UNIT CELL SIZE.
C  *  FCSD    - VECTOR OF DIMENSION  NSIZE+1  CONTAINING THE
C               DISTRIBUTION FUNCTION FOR THE THROAT DIAMETERS.
C     G       - ARRAY OF DIMENSIONS  4*NPT  CONTAINING THE CONDUCTANCES
C               OF EACH BRANCH.
C     GO      - CONDUCTANCE OF AN OIL FILLED DIMENSIONLESS UNIT CELL.
C     GOW     - VECTOR OF DIMENSION  NCTE  CONTAINING THE DIMENSIONLESS
C               GATE UNIT CELL CONDUCTANCE FOR EACH COMPARTMENT.
C     GRADP   - APPLIED PRESSURE GRADIENT.
C     GW      - CONDUCTANCE OF A WATER FILLED DIMENSIONLESS UNIT CELL.
C     HJ      - VECTOR OF DIMENSION  NCTE  CONTAINING THE DIMENSIONLESS
C               GATE UNIT CELL CURVATURE OF THE INTERFACE, FOR THE
C               EQUILIBRIUM CONTACT ANGLE, FOR EACH COMPARTMENT AND EACH
C               LOCAL VELOCITY.
C     HJA     - VECTOR OF DIMENSIONS  NCTE*NUI  CONTAINING THE
C               DIMENIONSLESS GATE UNIT CELL CURVATURE OF THE INTERFACE
C               FOR ADVANCING CONTACT ANGLES, FOR EACH COMPARTMENT
C               AND EACH LOCAL VELOCITY.
C     HJR     - VECTOR OF DIMENSIONS  NCTE*NUI  CONTAINING THE
C               DIMENSIONLESS GATE UNIT CELL CURVATURE OF THE INTERFACE
C               FOR RECEDING CONTACT ANGLES, FOR EACH COMPARTMENT
C               AND EACH LOCAL VELOCITY.
C     IBREAK - OUTPUT VARIABLE FROM SUBROUTINE BREAK, SUCH THAT :
C               =0  - NO FISSION OCCURRED IN THIS STEP
C               >0  - FISSION OCCURRED AND ONE OF THE DAUGHTER
C                     GANGLIA HAS IBREAK CEVS'S.
C  *  IC      - VECTOR OF DIMENSION  NBT  CONTAINING THE THROAT
C               SIZE FOR EACH BRANCH. TO BE PROVIDED BY USER IF NCSD=0.
C  *  ICL     - INDICATOR OF THE ROUGHNESS OF THE POROUS MEDIA (USED
C               TO CALCULATE CONTACT ANGLES) :
C               =0  - TAS=TRS=TE  INVARIANT WITH VELOCITY
C               =1  - NON ROUGHNED SURFACE  TAS=TRS=TE
C               =2  - SLIGHTLY ROUGHNED SURFACE
C               =3  - ROUGHNED SURFACE.
C     IND     - ARRAY OF DIMENSIONS  4*NPT  ASSIGNED SUCH THAT :
C               =0  - UC FILLED WITH WATER
C               =1  - GATE UNIT CELL
C               =2  - UC FILLED WITH OIL
C               =3  - RECEDING  EXTENDED  GUC.
C               =5  - ADVANCING  EXTENDED  GUC
C               =6  - GUC WITH TWO INTERFACES.
C  *  IP      - VECTOR OF DIMENSION  NPO  CONTAINING THE NUMBER OF EACH
C               CEVS OCCUPIED BY THE OIL BLOB. IF NBLOB=0  THE INITIAL
C               VALUES MUST BE PROVIDED BY USER IN VECTOR IPA.
C  *  IPWR    - INDICATES IF PRESSURE FIELD IS TO BE PRINTED (IPWR>0)
C               OR NOT (IPWR=0).
C     IUC     - ARRAY OF DIMENSIONS  4*NPT  CONTAINING THE SIZES OF
C               EACH BRANCH. FOR NODE "I" WE HAVE:
C                                                 I+NX -1
C                                                   J=2
C                                  I-1    J=1          I       J=3     I+1
C                                                   J=4
C                                                 I -NX+1
C     IVG     - COMPARTMENT NUMBER WHERE THE INTERFACE IS LOCATED.
C  *  IWRITE  - STEP INTERVAL AT WHICH OUTPUT SHOULD BE PRINTED.
C  *  KSIZE   - IF NCSD<0 REPRESENTS THE UNIT CELL SIZE TO BE USED.
C  *  NBLOB   - INDICATOR FOR THE INITIAL BLOB SHAPE:
C               <0  - CALCULATED TO FORM A LINEAR TRACK
C               =0  - PROVIDED BY USER
C               >0  - CALCULATED RANDOMLY
C     NBT     - TOTAL NUMBER OF BRANCHES IN THE UNIT BLOCK.
C  *  NCSD    - INDICATOR FOR THE THROAT SIZE OF EACH BRANCH:
```

```
C                  <0  - PROVIDED BY USER (EQUAL SIZES).
C                  =0  - PROVIDED BY USER (RANDOM SIZES).
C                  >1  - CALCULATED RANDOMLY.
C  *    NCT     - TOTAL NUMBER OF COMPARTMENTS IN WHICH
C                  EACH UNIT CELL IS DIVIDED.
C       NCTE    - THE SAME AS NCT FOR THE EXTENDED UNIT CELL.
C       NFLAG   - INDICATOR FOR ERROR OR BREAK-UP:
C                  = 12 DIF>E -4 OR TINC=0 OR QT>E-8.
C                  = 15 BREAK -UP OCCURED.
C       NGP     - VECTOR OF DIMENSION  NPO  CONTAINING THE NUMBER OF
C                  GUC'S FILLED WITH OIL FOR EACH CEVS.
C       NPB     - VECTOR OF DIMENSION  NPO  CONTAINING THE POSITION OF
C                  BOTH DAUGHTER GANGLIA ON OUTPUT FROM SUBROUTINE BREAK.
C  *    NPO     - TOTAL NUMBER OF CEVS'S OCCUPIED WITH OIL.
C       NPT     - TOTAL NUMBER OF NODES IN THE UNIT BLOCK.
C       NR      - NUMBER OF RANDOM NUMBERS TO BE GENERATED.
C  *    NSIZE   - NUMBER  OF UNIT CELL SIZES.
C  *    NSTEP   - MAXIMUM NUMBER OF STEPS FOR EACH SIMULATION.
C  *    NUI     - NUMBER OF INTERVALS FOR THE LOCAL VELOCITY IN THE UNIT
C                  CELLS  ( USED TO CALCULATE THE CONTACT ANGLES ).
C  *    NX      - NUMBER OF BRANCHES IN THE X-DIRECTION.
C  *    NY      - NUMBER OF BRANCHES IN THE Y-DIRECTION.
C       PD      - ARRAY OF DIMENSIONS  4*NPT  CONTAINING THE PRESSURE
C                  DROP ACROSS THE INTERFACE FOR EACH BRANCH.
C  *    PERM    - PERMEABILITY  (APROXIMATED VALUE ON INPUT. THE PROGRAM
C                  CALCULATES THE ACTUAL VALUE OF THE PERMEABILITY).
C  *    PHI     - ANGLE BETWEEN THE PRESSURE GRADIENT DIRECTION AND THE
C                  HORIZONTAL AXIS OF THE NETWORK (EXPRESSED IN PI RAD).
C  *    POR     - POROUS MEDIUM POROSITY.
C       Q       - ARRAY OF DIMENSIONS  4*NPT  CONTAINING THE
C                  FLOW RATES FOR EACH BRANCH.
C       SJI     - VECTOR OF DIMENSION  NPT  CONTAINING THE CURRENT SOURCE
C                  SOURCES FOR THE BOUNDARY PORES.
C  *    SLP     - SLOPE FOR THE CURVE CONTACT ANGLES VERSUS VELOCITY.
C  *    ST      - INTERFACIAL TENSION BETWEEN OIL AND WATER.
C       TAS     - ADVANCING CONTACT ANGLE WHEN U=0.
C  *    TE      - EQUILIBRIUM CONTACT ANGLE.
C       TRS     - RECEDING CONTACT ANGLE WHEN U=0.
C       U       - LOCAL VELOCITY AT THE INTERFACE IN A GUC.
C  *    UMAX    - MAXIMUM LOCAL VELOCITY IN A GUC ( USED TO CALCULATE
C                  THE CONTACT ANGLES ).
C       VEUC    - VOLUME OF AN EXTENDED DIMENSIONLESS UNIT CELL.
C       VG      - ARRAY OF DIMENSIONS  4*NPT  CONTAINING THE VOLUME OF
C                  OIL FOR EACH UNIT CELL.
C  *    VISR    - VISCOSITY RATIO (OIL/WATER).
C  *    VISW    - VISCOSITY OF WATER.
C       VO      - TOTAL VOLUME OF OIL.
C       VOG     - VOLUME OF OIL IN GUC'S.
C       VOO     - VOLUME OF OIL IN NON-GUC'S.
C       VUC     - VOLUME OF A DIMENSIONLESS UNIT CELL.
C       X       - VECTOR OF DIMENSION  NPT  CONTAINIG THE NODE PRESSURES.
C       XCG     - X-COORDINATE OF CENTER OF GRAVITY OF GANGLION.
C       YCG     - Y-COORDINATE OF CENTER OF GRAVITY OF GANGLION.
C       XVG     - VECTOR OF DIMENSION  NCTE  CONTAINING THE PARTIAL
C                  VOLUME FOR EACH COMPARTEMENT.
C       Y       - ARRAY OF DIMENSION  NPT*NX  USED BY SUBROUTINE NET.
C       ZI      - VECTOR OF DIMENSION  NCTE  CONTAINING THE POSITION OF
C                  THE INTERFACE FOR EACH COMPARTMENT.
C
C     SUBROUTINES CALLED :
C
C     SUBROUTINE BREAK (N1,NPO,IND,IP,IBREAK,NPB)
C      - CHECKS IF FISSION OCCURRED.
C
C     SUBROUTINE CGCC (N1,NXM1,NPO,IP,IUC,IND,VUC,VG,XCG,YCG,XVG,DUC,ZI)
C      - CALCULATES THE COORDINATES OF CENTER OF GRAVITY OF GANGLION.
C
C     SUBROUTINE COMP (VEUC,VUC,AC,ZI,XVG)
C      - DIVIDES THE UC'S IN COMPARTMENTS AND CALCULATES THE VOLUME AND
C        POSITION OF INTERFACE FOR EACH COMPARTMENT.
C
C     SUBROUTINE COND (ZI,GW,GO,GOW)
C      - CALCULATES THE DIMENSIONLESS UNIT CELL CONDUCTANCE
C        FOR EACH COMPARTMENT
C
C     SUBROUTINE CSD (ICSD,NBT,FCSD,IC,IUC)
C      - ASSIGNS THROAT SIZES TO EACH UNIT CELL.
C
C     SUBROUTINE CURV (N1,ZI,HJ,HJA,HJR)
C      - CALCULATES THE DIMENSIONLESS UNIT CELL INTERFACE CURVATURE
```

```
C        FOR EACH COMPARTMENT AND FOR EQUILIBRIUM, ADVANCING AND
C        RECEDING CONTACT ANGLES.
C
C     SUBROUTINE GGUBS (NR)
C      - PSEUDO-RANDOM NUMBER GENERATOR.
C
C     SUBROUTINE LEQ1PB (A,N,NC,IA,B,IB,M,IDGT,D1,D2,IER)
C      - SOLVES THE ALGEBRIC SYSTEM OF EQUATIONS (CALLED BY NET).
C
C     SUBROUTINE LUDAPB (A,N,NC,IA,A,IA,D1,D2,IER)
C      - CALLED INTERNALLY BY LEQ1PB.
C
C     SUBROUTINE LUELPB (UL,B.N,NC,IA,X)
C      - CALLED INTERNALLY BY LEQ1PB.
C
C     SUBROUTINE MATCH (I,J,IN,JN)
C      - MATCHES CONNECTING UC'S.
C
C     SUBROUTINE NET (NPT,NX,G,X,Y)
C      - ORGANIZES THE NODE MATRIX IN BAND SYMMETRIC FORM.
C
C     SUBROUTINE SELECT (IVG,D,X,XVG)
C      - CHOSES COMPARTMENT NUMBER WHERE INTERFACE IS LOCATED.
C
C     SUBROUTINE SHAPE (ICASE,NPO,IPA,NPB)
C      - GENERATES A RANDOM SHAPE FOR THE GANGLION.
C
C     SUBROUTINE SLCTU (U,IU)
C      - SELECTS THE RANGE FOR THE LOCAL VELOCITY.
C
C     SUBROUTINE UERTST (IER,NAME)
C      - CALLED INTERNALLY BY LEQ1PB.
C
C     SUBROUTINE UGETIO (1,NIN,IOUNIT)
C      - CALLED INTERNALLY BY UERTST.
C
C
      IMPLICIT DOUBLE PRECISION (A-H,O-Z)
      INTEGER DNC,DNX,DNY,DNPT,DNBT,DNYA,DND,DFC,DNCT,DNU
      PARAMETER (DNC=4)
      PARAMETER (DNX=21,DNY=41)
      PARAMETER (DNPT=(DNX-1)*(DNY-1))
      PARAMETER (DNBT=(DNX+DNX-1)*(DNY-1)+(DNX-1))
      PARAMETER (DNYA=DNPT*DNX)
      PARAMETER (DND=13,DFC=DND+1)
      PARAMETER (DPAR=10)
      PARAMETER (DNG=300,DNGP=50)
      PARAMETER (DNCT=31,DNU=20)
      DIMENSION VG(DNC,DNPT),Q(DNC,DNPT),PD(DNC,DNPT)
      DIMENSION G(DNC,DNPT),IND(DNC,DNPT),IUC(DNC,DNPT)
      DIMENSION IP(DNPT),SJI(DNPT),X(DNPT)
      DIMENSION IC(DNBT),IUA(DNBT),IVGA(DNBT)
      DIMENSION DUC(DND),FCSD(DFC)
      DIMENSION GOW(DNCT),AC(DNCT),XVG(DNCT),ZI(DNCT),HJ(DNCT)
      DIMENSION HJA(DNCT,DNU),HJR(DNCT,DNU),JVOID(DNC)
      DIMENSION Y(DNYA)
      DIMENSION NGP(DNPT),NPB(DNPT)
      CHARACTER TITLE*20
      CHARACTER*5 SIDE(2)
      COMMON /CTAN/ SLP,TE,TAS,TRS,ICL
      COMMON /NTW/  NX,NY
      COMMON /VIS/  VISW,VISR
      COMMON /UCC/  C1,C2,C3,PI
      COMMON /EXT/  NCT,NCTE,NSIZE
      COMMON /UN/   UMAX,NUI
      COMMON /ALC/  AL
      COMMON /SEED/ DSEED,R(DNBT)
      DATA SIDE /'LEFT','RIGHT'/
C
C     READ INPUT VARIABLES
C
      READ (08,*) TITLE
      READ (08,*) C1,C2,C3,AL,POR,PERM
      READ (08,*) NSIZE
      READ (08,*) (DUC(I),I=1,NSIZE)
      READ (08,*) (FCSD(I),I=1,NSIZE+1)
      READ (08,*) ST,VISW,VISR,CAN,NPO
      READ (08,*) NX,NY,NCT,PHI,SEED
      READ (08,*) NCSD,NBLOB,KSIZE,NSTEP,IWRITE,IPWR
```

```
      READ (08,*) NUI,ICL,TE,UMAX,SLP
C
      DSEED=SEED
      KSTEPS=0
      TAS=0.
      TRS=0.
      DO 10 I=1,DNYA
      Y(I)=0.
   10 CONTINUE
      NXM1=NX-1
      NXM2=NX-2
      NXM12=NXM1/2-1
      NYM1=NY-1
      NPT=NXM1*NYM1
      NP2=NPT-NXM1
      NP3=NPT-NXM2
      NP4=NP3-NXM1
      NP5=NPT-1
      NBT=(NX*2-1)*NYM1+NXM1
      WRITE (6,1200) TITLE,AL,POR,PHI,UMAX,NUI,
     &               NCT,NX,NY,NPT,NBT
      NCTE=NCT*(1.+1./C3)/2.
      NCPE=NCTE+1
      NXVG=NCT*.15
      IF (NXVG.EQ.1) NXVG=2
      PI=ATAN(1.)*4
      PI4=PI/4.
      PH=PI*PHI
      DY=SIN(PH)
      IF (PHI.EQ.0.0) DY=0.
      DX=COS(PH)
      IF (PHI.EQ.0.5) DX=0.
      D2=NY*DY
      D1=NX*DX
      D0=NY*DY+NX*DX
      AREA=(NXM1*DY+NYM1*DX)*AL*AL
C
C     ASSIGN THROAT SIZES TO EACH BRANCH
C
      IF (NCSD.EQ.0) READ (08,*) (IC(I),I=1,NBT)
      IF (NCSD.LT.0) THEN
       NCSD=0
       DO 100 I=1,NBT
  100  IC(I)= KSIZE
      END IF
      CALL CSD (NCSD,NBT,FCSD,IC,IUC)
      WRITE (6,9000)
      DO 115 I=1,NPT,NXM1
      I2=NPT+1-I
      I1=I2-NXM1+1
      WRITE (6,2500) (IUC(2,J),J=I1,I2)
      WRITE (6,2600) (IUC(1,J),J=I1,I2),IUC(3,I2)
  115 CONTINUE
      WRITE (6,2500) (IUC(4,J),J=1,NXM1)
C
C     CALCULATE VOLUME AND POSITION OF INTERFACE FOR
C     EACH COMPARTMENT
C
      CALL COMP (VEUC,VUC,AC,ZI,XVG)
      VEUCE=XVG(NCPE)
C
C     CALCULATE DIMENSIONLESS UNIT CELL CURVATURE FOR EACH COMPARTMENT
C
      CALL CURV (31,ZI,HJ,HJA,HJR)
      WRITE (6,2700) ICL,SLP,TE,TAS,TRS
C
      ST2=ST*2.
      VWOST=VISW/ST
      WRITE (6,1300) VISW,VISR,ST
C
C     CALCULATE DIMENSIONLESS UNIT CELL CONDUCTANCE FOR EACH COMPARTMENT
C
      CALL COND (ZI,GW,GO,GOW)
C
      ICAN=0
      IF (ST.NE.0.) THEN
       GRADP=ST*CAN/PERM
      ELSE
```

```
       GRADP=.1*CAN/PERM
       ICAN=1
      END IF
  120 P=GRADP*AL
C
C     DETERMINE  CURRENT SOURCES ON THE BOUNDARY NODES
C
      DO 125 I=1,NPT
      SJI(I)=0.
      DO 125 J=1,4
      D=DUC(IUC(J,I))
      G(J,I)=GW*D*D*D
  125 CONTINUE
      DO 130 I=1,NXM1
      I1=NP2+I
      SJI(I)=SJI(I)+P*G(4,I)*(D0-FLOAT(I)*DX)
      SJI(I1)=SJI(I1)+P*G(2,I1)*(D1-FLOAT(I)*DX)
  130 CONTINUE
      DO 140 J=1,NYM1
      J1=1+(J-1)*NXM1
      J2=J1+NX-2
      SJI(J1)=SJI(J1)+P*G(1,J1)*(D0-FLOAT(J)*DY)
      SJI(J2)=SJI(J2)+P*G(3,J2)*(D2-FLOAT(J)*DY)
  140 CONTINUE
C
C     CALCULATE  TOTAL FLOW RATE AND SUPERFICIAL VELOCITY
C
      DO 145 I=1,NPT
      X(I)=SJI(I)
  145 CONTINUE
      CALL NET (NPT,NX,G,X,Y)
      QTT=0.
      DO 160 I=NXM2,NP5,NXM1
      QTT=QTT+(X(I)-X(I+1))*G(3,I)
  160 CONTINUE
      DO 170 I=NP4,NP2
      QTT=QTT+(X(I)-X(I+NXM1))*G(2,I)
  170 CONTINUE
      VF=QTT/AREA
C
C     CALCULATE PERMEABILITY
C
      IF (ICAN.EQ.0) THEN
       CANO=VISW*VF/ST
       PERM=ST*CANO/GRADP
       GRADP=ST*CAN/PERM
       ICAN=ICAN+1
       GO TO 120
      END IF
C
C     OUTPUT PRESSURE FIELD
C
      IF (IPWR.NE.0) THEN
       DO 182 I=1,2
       WRITE (6,1040) SIDE(I)
       II=(I-1)*(NXM12+1)
       DO 180 IY=NYM1,1,-1
       I1=(IY-1)*NXM1+1+II
       I2=I1+NXM12
       WRITE (6,1020) (ZERO,J=I1,I2)
       WRITE (6,1030) ((ZERO,X(J)),J=I1,I2),ZERO
  180  CONTINUE
       WRITE (6,1020) (ZERO,J=I1,I2)
  182  CONTINUE
      END IF
C
      IF (NBLOB.LT.0) THEN
       IP(1)=4*NXM1+NX/2
       DO 185 I=2,NPO
       IP(I)=IP(I-1)+NXM1
  185  CONTINUE
      ELSE
       IF (NBLOB.GT.0) THEN
        CALL SHAPE (-1,NPO,IPA,NPB)
       ELSE
        READ (08,*) (IP(I),I=1,NPO)
       END IF
      END IF
      WRITE (6,6500) (IP(I),I=1,NPO)
      IWR=0
```

```
      K5TEP=0
      IBREAK=0
      NFLAG=0
C
C     ASSIGN  0  TO  ALL UNIT CELLS
C
      DO 200 I=1,NPT
      X(I)=0.
      DO 200 J=1,4
      VG(J,I)=0.
      PD (J,I)=0.
      IND(J,I)=0
  200 CONTINUE
      IF (NPO.NE.0) THEN
C
C     ASSIGN  1  TO GUC
C
       DO 210 I=1,NPO
       DO 210 J=1,4
       IND(J,IP(I))=1
  210  CONTINUE
C
C     ASSIGN  2    TO UC FILLED WITH OIL
C
       DO 220 I=1,NPO
       NP=IP(I)
       DO 220 J=1,4
       CALL MATCH (NP,J,IN,JN)
       IND(J,NP)=IND(J,NP)+IND(JN,IN)
       IF (IND(J,NP).EQ.3) IND(J,NP)=2
  220  CONTINUE
C
C     ASSIGN VOLUME OF OIL TO GUC'S
C
       NGUC=0
       DO 240 I=1,NPO
       NP=IP(I)
       DO 230 J=1,4
       IF (IND(J,NP).NE.2) THEN
        NGUC=NGUC+1
        D=DUC(IUC(J,NP))
        VG(J,NP)=.5*VUC*D*D*D
        CALL SELECT (IVG,D,VG(J,NP),XVG)
        IVGA(NGUC)=IVG
        IUA(NGUC)=0
        G(J,NP)=GOW(IVG)*D*D*D
        PD(J,NP)=HJ(IVG)*ST2/D
        CALL MATCH (NP,J,IN,JN)
        G(JN,IN)=G(J,NP)
        PD(JN,IN)=-PD(J,NP)
       END IF
  230  CONTINUE
  240  CONTINUE
       TT=0.
C
C     RETURN POINT IF XERON OR HYGRON OCCURED
C
  900  CONTINUE
       NPOS=NPO
C
C     CHECK IF BREAK-UP OCCURED
C
         CALL BREAK (4,NPO,IND,IP,IBREAK,NPB)
         IF (IBREAK.NE.0) THEN
          WRITE (6,8000)
          GO TO 800
         END IF
C
C     INITIALIZE PD AND G
C
       IF (K5TEP.NE.0) THEN
        DO 300 I=1,NPT
        DO 300 J=1,4
        D=DUC(IUC(J,I))
        PD(J,I)=0.
        G(J,I)=GW*D*D*D
  300   CONTINUE
       END IF
C
```

```
C     RETURN POINT IF NO XERON OR HYGRON OCCURED
C
  910  CONTINUE
       IWR=0
       IF (KSTEP.EQ.NSTEP) GO TO 800
      END IF
      KSTEP=KSTEP+1
      IF (KSTEP.EQ.NSTEP) IWRIT=IWRITE
C
C     INITIALIZE X
C
      DO 930 I=1,NPT
      X(I)=SJI(I)
  930 CONTINUE
      IWRIT=IWRIT+1
      IF (IWRIT.GE.IWRITE) THEN
       IWR=1
       IWRIT=0
      END IF
      IF (NPO.NE.0) THEN
C
C     CALCULATE THE TOTAL VOLUME OF OIL AND  CHECK IF (VO.EQ.VOI)
C     AND
C     ASSIGN CONDUCTANCE VALUES FOR EACH UNIT CELL FILLED WITH OIL
C
       VOG=0.
       VOO=0.
       DO 360 I=1,NPO
       NGP(I)=0
       NP=IP(I)
       DO 360 J=1,4
       IF (IND(J,NP).NE.2) THEN
        NGP(I)=NGP(I)+1
        IF (VG(J,NP).GT.0.) VOG=VOG+VG(J,NP)
       ELSE
        D=DUC(IUC(J,NP))
        D3=D*D*D
        VOO=VOO+.5*VUC*D3
        G(J,NP)=GO*D3
       END IF
  360  CONTINUE
       VO=VOO+VOG
       IF (KSTEP.EQ.1) VOI=VO
       DIF=VO-VOI
       IF (ABS(DIF).GE.1.E-8) THEN
        NFLAG=12
        WRITE (6,3500) KSTEP,TINC,TT
        WRITE (6,4500)
        DO 380 I=1,NPO
        IF (NGP(I).NE.0) THEN
         NP=IP(I)
         DO 370 J=1,4
         IF (IND(J,NP).NE.2) THEN
          D=DUC(IUC(J,NP))
          D3=D*D*D
          VGX=VG(J,NP)/(VUC*D3)
          VGY=VG(J,NP)/(VEUC*D3)
          WRITE (6,5000) J,NP,Q(J,NP),VG(J,NP),
     &          VGX,VGY,IND(J,NP),IUC(J,NP),IVGA(N),IUA(N)
         END IF
  370    CONTINUE
      END IF
  380   CONTINUE
      GO TO 800
       END IF
       VI=VF/POR
       IF (KSTEP.EQ.1) THEN
        WRITE (6,2900) CAN,NPO,VOG,VOO,VO
        WRITE (6,3000) GRADP,PERM,VF,VI
       ELSE
C
C     ASSIGN CONDUCTANCE AND PRESSURE DROP ACROSS THE INTERFACE
C     VALUES FOR EACH GATE UNIT CELL
C
        NGUC=0
        DO 460 I=1,NPO
        IF (NGP(I).NE.0) THEN
         N=0
```

```
          NP=IP(I)
          DO 450 J=1,4
          IF (IND(J,NP).NE.2) THEN
           NGUC=NGUC+1
           D=DUC(IUC(J,NP))
           DU2=D*D
           D3=D*D*D
           N=N+1
           VGX=VG(J,NP)
           IF (VGX.GT.0.) THEN
            IF (IND(J,NP).EQ.6) THEN
             CALL MATCH (NP,J,IN,JN)
             VGY=VG(JN,IN)
             VGZ=VGX+VGY
             IF (VGZ.GT.0.9999*VUC*D3) THEN
              IND(J,NP)=2
              VG(J,NP)=0.
              IND(JN,IN)=2
              VG(JN,IN)=0.
              PD (J,NP)=0.
              G(J,NP)=GO*D3
             ELSE
              CALL SELECT (IVG,D,VGX,XVG)
              CALL SELECT (IVY,D,VGY,XVG)
              CALL SELECT (IVZ,D,VGZ,XVG)
              G(J,NP)=GOW(IVZ)*D3
              U=Q(J,NP)/(AC(IVG)*DU2)
              CALL SLCTU (ABS(U),IU)
              IVGA(NGUC)=IVG
              IUA(NGUC)=IU
              IF (U.GE.0.) PD(J,NP)=(HJA(IVG,IU)-HJR(IVY,IU))*ST2/D
              IF (U.LT.0.) PD(J,NP)=(HJR(IVG,IU)-HJA(IVY,IU))*ST2/D
             END IF
            ELSE
             CALL SELECT (IVG,D,VGX,XVG)
             G(J,NP)=GOW(IVG)*D3
             U=Q(J,NP)/(AC(IVG)*DU2)
             CALL SLCTU (ABS(U),IU)
             IVGA(NGUC)=IVG
             IUA(NGUC)=IU
             IF (U.GE.0.) PD(J,NP)=HJA(IVG,IU)*ST2/D
             IF (U.LT.0.) PD(J,NP)=HJR(IVG,IU)*ST2/D
            END IF
           ELSE
            IVGA(NGUC)=1
            G(J,NP)=0.
            PD (J,NP)=0.
           END IF
           CALL MATCH (NP,J,IN,JN)
           G(JN,IN)=G(J,NP)
           PD(JN,IN)=-PD(J,NP)
           IF (N.EQ.NGP(I)) GO TO 460
          END IF
  450     CONTINUE
         END IF
  460    CONTINUE
        END IF
       END IF
C
C      OUTPUT
C
       IF (IWR.NE.0) THEN
         WRITE (6,8500) KSTEP,TINC,TT
         WRITE (6,4500)
         N=0
         DO 495 I=1,NPO
         IF (NGP(I).NE.0) THEN
          NP=IP(I)
          DO 490 J=1,4
          IF (IND(J,NP).NE.2) THEN
           D=DUC(IUC(J,NP))
           D3=D*D*D
           N=N+1
           VGX=VG(J,NP)/(VUC*D3)
           VGY=VG(J,NP)/(VEUC*D3)
           WRITE (6,5000) J,NP,Q(J,NP),VG(J,NP),
     &                    VGX,VGY,IND(J,NP),IUC(J,NP),IVGA(N),IUA(N)
          END IF
  490     CONTINUE
         END IF
```

```
  495   CONTINUE
        WRITE (6,9500)
        CALL SHAPE (IBREAK,NPO,IP,NPB)
        CALL CGCC (4,NXM1,NPO,IP,IUC,IND,VUC,VG,XCG,YCG,XVG,DUC,ZI)
        XCG=XCG/VO
        YCG=YCG/VO
        WRITE (6,3050) XCG,YCG
      END IF
C
C     UPDATE  X  FOR EACH NODE
C
      DO 500 I=1,NPT
      DO 500 J=1,4
      X(I)=X(I)+PD(J,I)*G(J,I)
  500 CONTINUE
C
C     SOLVE FOR THE PRESSURES IN EACH PORE BY NODE ANALYSIS
C
      CALL NET (NPT,NX,G,X,Y)
C
C     OUTPUT PRESSURE FIELD
C
      IF ((IWR.NE.0.AND.IPWR.NE.0).OR.NPO.EQ.0) THEN
       DO 520 I=1,2
       WRITE (6,1040) SIDE(I)
       II=(I-1)*(NXM12+1)
       DO 510 IY=NYM1,1,-1
       I1=(IY-1)*NXM1+1+II
       I2=I1+NXM12
       WRITE (6,1020) (PD(2,J),J=I1,I2)
       WRITE (6,1030) ((PD(1,J),X(J)),J=I1,I2),PD(3,I2)
  510  CONTINUE
       WRITE (6,1020) (PD(4,J),J=I1,I2)
  520  CONTINUE
      END IF
C
C     CALCULATE THE FLOW RATES IN THE GUC'S AND THE NEXT
C     TIME INCREMENT
C
      TINC=1000.
      QT=0.
      DO 550 I=1,NPO
      IF (NGP(I).NE.0) THEN
       N=0
       NP=IP(I)
       DO 540 J=1,4
       IF (IND(J,NP).NE.2) THEN
        D=DUC(IUC(J,NP))
        D3=D*D*D
        N=N+1
        CALL MATCH (NP,J,IN,JN)
        Q0=G(J,NP)*(X(NP)-X(IN)-PD(J,NP))
        QT=QT+Q0
        Q(J,NP)=Q0
        IF (Q0.NE.0.) THEN
         IF ((J.EQ.2.OR.J.EQ.3).AND.IND(J,NP).EQ.3.AND.Q0.GT.0.)
     &            IND(J,NP)=5
         IF ((J.EQ.1.OR.J.EQ.4).AND.IND(J,NP).EQ.5.AND.Q0.LT.0.)
     &            IND(J,NP)=3
         VGX=VG(J,NP)
         CALL SELECT (IVG,D,VGX,XVG)
         T=ABS((XVG(IVG+1)-XVG(IVG))*D3/Q0)
         IF (VGX.GT.0.) THEN
          IF (IVG.EQ.1.AND.Q0.LT.0.) T=ABS(VGX/Q0)
          IF (IND(J,NP).EQ.1.AND.IVG.EQ.NCT.AND.Q0.GT.0.)
     &                                T=ABS((VUC*D3-VGX)/Q0)
          IF (IND(J,NP).EQ.5.AND.IVG.EQ.NCTE.AND.Q0.GT.0.)
     &                                 T=ABS((VEUCE*D3-VGX)/Q0)
         END IF
         IF (TINC.GT.T) TINC=T
        END IF
        IF (N.EQ.NGP(I)) GO TO 550
       END IF
  540  CONTINUE
      END IF
  550 CONTINUE
      IF (TINC.EQ.0.OR.QT.GE.1E-7) THEN
       NFLAG=12
       GO TO 800
```

```
      END IF
  560 TT=TT+TINC
C
C     UPDATE VG
C
      DO 580 I=1,NPO
      IF (NGP(I).NE.0) THEN
       NP=IP(I)
       DO 570 J=1,4
       IF (IND(J,NP).NE.2) THEN
        VG(J,NP)=VG(J,NP)+TINC*Q(J,NP)
        IF (VG(J,NP).LT.1E-13) VG(J,NP)=0.
       END IF
  570  CONTINUE
      END IF
  580 CONTINUE
C
C     CHECK FOR XERON,HYGRON,ETC.
C
      IWARN=0
      DO 750 I=1,NPO
      IF (NGP(I).NE.0) THEN
       N=0
       NVOID=0
       NP=IP(I)
       DO 640 J=1,4
       IF (IND(J,NP).NE.2) THEN
        D=DUC(IUC(J,NP))
        D3=D*D*D
        N=N+1
C
C     CHECK IF XERON OCCURED
C
        IF (IND(J,NP).NE.3) THEN
         IF (IND(J,NP).EQ.5.OR.IND(J,NP).EQ.7) THEN
          CALL MATCH (NP,J,IN,JN)
          VAD=0.
          DO 590 J0=1,4
          IF (J0.NE.JN) THEN
           D=DUC(IUC(J0,IN))
           VAD=VAD+XVG(NXVG)*D*D*D
          END IF
  590     CONTINUE
          VS=VG(J,NP)-VUC*D3
          IF (VS.GE.VAD) THEN
           VG(JN,IN)=0.
           IND(JN,IN)=2
           WRITE (6,6400) J,NP
           IWARN=IWARN+1
           NPOS=NPOS+1
           IP(NPOS)=IN
           VG(J,NP)=0.
           IND(J,NP)=2
           VSS=0.
           DO 600 J0=1,4
           IF (J0.NE.JN) THEN
            D=DUC(IUC(J0,IN))
            VSS=VSS+VUC*D*D*D
           END IF
  600      CONTINUE
           DO 610 J0=1,4
           IF (J0.NE.JN) THEN
            D=DUC(IUC(J0,IN))
            VG(J0,IN)=VS*VUC*D*D*D/VSS
            IND(J0,IN)=1
            CALL MATCH (IN,J0,INN,JNN)
            Q(J0,IN)=(X(IN)-X(INN)-PD(J0,IN))*G(J0,IN)
            IF (IND(JNN,INN).EQ.1) THEN
             IND(J0,IN)=6
             IND(JNN,INN)=6
            END IF
           END IF
  610      CONTINUE
           GO TO 750
          ELSE
           IF (VG(J,NP).GE.0.9999*VEUCE*D3) IND(J,NP)=7
          END IF
         ELSE
```

```
          IF (VG(J,NP).LT.0.9999*VUC*D3) THEN
           IF (VG(J,NP).LE.0.) THEN
            NVOID=NVOID+1
            JVOID(NVOID)=J
            WRITE (6,6000) J,NP,NVOID
           END IF
          ELSE
           IND(J,NP)=5
          END IF
         END IF
        ELSE
         IF (VG(J,NP).LT.0.9999*VUC*D3) IND(J,NP)=1
        END IF
        IF (N.EQ.NGP(I)) GO TO 650
       END IF
  640  CONTINUE
C
C      CHECK IF HYGRON OCCURED
C
  650  IF (NVOID.NE.0) THEN
        VAD=0.
        VADD=0.
        VMVE=0.
        V55=0.
        JDN5=JVOID(NVOID)+2
        IF (JDN5.GT.4) JDN5=JDN5-4
        IF (IND(JDN5,NP).NE.2) THEN
         DO 670 J=1,4
         IF (IND(J,NP).EQ.2) JDN5=J
  670    CONTINUE
        END IF
        CALL MATCH (NP,JDN5,IN,JN)
        D=DUC(IUC(JN,IN))
        VMVE=(VEUCE-VUC)*D*D*D*.9
        NVOID=0
        DO 680 J=1,4
        IF (J.NE.JDN5) THEN
         IF (IND(J,NP).NE.2) THEN
          NVOID=NVOID+1
          JVOID(NVOID)=J
          VAD=VAD+VG(J,NP)
         ELSE
          D=DUC(IUC(J,NP))
          V5=VUC*D*D*D
          V55=V55+V5
          VADD=VADD+V5*0.5
         END IF
        END IF
  680   CONTINUE
        IF (VADD.GE.VMVE) VADD=VMVE*0.9999
        VAD=VAD+VADD
        IF (VAD.LE.VMVE) THEN
         IP(I)=1000
         IWARN=IWARN+1
         DO 710 J=1,4
         DO 690 JV=1,NVOID
         IF (J.EQ.JVOID(JV)) THEN
          IF (IND(J,NP).EQ.6) THEN
           CALL MATCH (NP,J,IN,JN)
           IND(JN,IN)=1
          END IF
          GO TO 700
         END IF
  690    CONTINUE
         CALL MATCH (NP,J,IN,JN)
         D=DUC(IUC(JN,IN))
         V5=VUC*D*D*D
         IF (J.EQ.JDN5) THEN
          VG(JN,IN)=V5+VAD
          IND(JN,IN)=3
         ELSE
          VG(JN,IN)=V5-V5*VADD/V55
          IND(JN,IN)=1
         END IF
         CALL MATCH (IN,JN,INN,JNN)
         Q(JN,IN)=(X(IN)-X(INN)-PD(JN,IN))*G(JN,IN)
  700    VG(J,NP)=0.
         IND(J,NP)=0
  710    CONTINUE
         WRITE (6,6200) NP
```

```
        ELSE
         V5=0.
         NV=0
         NF=0
         DO 730 J=1,4
         IF (IND(J,NP).NE.2) THEN
          VGX=VG(J,NP)
          IF (VGX.GT.0.) THEN
           D=DUC(IUC(J,NP))
           D3=D*D*D
           CALL SELECT (IVG,D,VGX,XVG)
           IF (IVG.EQ.1) THEN
            V1=XVG(IVG)*D3*0.5
           ELSE
            V1=(XVG(IVG)-XVG(IVG-1))*D3
           END IF
           IF (VGX.LT.V1) GO TO 730
           VG(J,NP)=VGX-V1
           V5=V5+V1
           NF=NF+1
          ELSE
           NV=NV+1
           JVOID(NV)=J
          END IF
         END IF
  730    CONTINUE
         V5=V5/FLOAT(NV)
         VAD=0.
         DO 740 J=1,4
         IF (IND(J,NP).NE.2.AND.VG(J,NP).EQ.0.) THEN
          IF (IND(J,NP).EQ.6) THEN
           D=DUC(IUC(J,NP))
           D3=D*D*D
           CALL MATCH (NP,J,IN,JN)
           IF ((VG(JN,IN)+V5).GT.0.9999*VUC*D3) THEN
            VG(J,NP)=VUC*D3-VG(JN,IN)
            VAD=V5-VG(J,NP)
            GO TO 740
           END IF
          END IF
          VG(J,NP)=V5
         END IF
  740    CONTINUE
         IF (VAD.GT.0.) THEN
          VAD=VAD/FLOAT(NF)
          DO 746 J=1,4
          IF (IND(J,NP).NE.2) THEN
           DO 745 JV=1,NV
           IF (J.EQ.JVOID(JV)) GO TO 746
  745      CONTINUE
           VG(J,NP)=VG(J,NP)+VAD
          END IF
  746     CONTINUE
        END IF
       END IF
       END IF
      END IF
  750 CONTINUE
C
C     IF NO XERON OR HYGRON OCCURED RETURN TO 910
C
      IF (IWARN.EQ.0) GO TO 910
C
C     RENUMBER IP(I)
C
      IO=0
      DO 770 I=1,NPOS
      K=NPOS+1-I
      IF(IP(K).EQ.1000) THEN
       IO=IO+1
       DO 760 J=K,NPOS
       IP(J)=IP(J+1)
  760  CONTINUE
      END IF
  770 CONTINUE
      NPO=NPOS-IO
      DO 780 I=NPO+1,NPOS
      IP(I)=0
  780 CONTINUE
```

```
      DO 790 I=1,NPO
      K1=NPO+1-I
      DO 790 K=I+1,NPO
      K2=NPO+1-K
      IF (IP(K1).LE.IP(K2)) THEN
       IT=IP(K2)
       IP(K2)=IP(K1)
       IP(K1)=IT
      END IF
  790 CONTINUE
      WRITE (6,6500) (IP(I),I=1,NPO)
C
C     XERON OR HYGRON OCCURED. RETURN TO 900
C
      GO TO 900
  800 CONTINUE
      IF (NFLAG.EQ.15) THEN
       NBREAK=IBREAK
       NB=1
       DO 820 K=1,2
       VOO=0.
       DO 810 I=NB,NBREAK
       NP=NPB(I)
       DO 810 J=1,4
       D=DUC(IUC(J,NP))
       IF (IND(J,NP).EQ.2) VOO=VOO+.5*VUC*D*D*D
       IF (IND(J,NP).NE.2) VOO=VOO+VG(J,NP)
  810  CONTINUE
       WRITE (6,9100) K,VOO/VO
       WRITE (6,6500) (NPB(N),N=NB,NBREAK)
       NBREAK=NPO
       NB=IBREAK+1
  820  CONTINUE
      END IF
      WRITE (6,9500)
      CALL SHAPE (IBREAK,NPO,IP,NPB)
      CALL CGCC (4,NXM1,NPO,IP,IUC,IND,VUC,VG,XCG,YCG,XVG,DUC,ZI)
      XCG=XCG/VO
      YCG=YCG/VO
      WRITE (6,3050) XCG,YCG
      DO 830 I=1,NPO
      IP(I)=0
      NPB(I)=0
  830 CONTINUE
      KSTEPS=KSTEPS+KSTEP
      WRITE (6,2000) KSTEP,KSTEPS
      IF (NFLAG.EQ.12) WRITE (6,7500) KSTEP,DIF,TINC,QT
      STOP
 1020 FORMAT (6(10X,E10.3))
 1030 FORMAT (13E10.3)
 1040 FORMAT (1H1//'       PRESSURE FIELD  ',A6,'SIDE'//)
 1200 FORMAT (///A20,2X,'L    =',F6.3,
     &     4X,'POR=',F8.4,3X,'PHI=',F5.2
     &     //' UMAX =',F7.2,8X,'NUI =',I3,7X,'NCT=',I4
     &     //' NX   =',I3,12X,'NY  =',I3,7X,'NPT=',I4,7X,'NBT=',I4)
 1300 FORMAT (//' VISW =',F6.2,8X,'VISR=',F6.2,8X,' ST   =',F7.2)
 2000 FORMAT (//2I6)
 2500 FORMAT (2X,30(1X,I1))
 2600 FORMAT (2X,31(I1,1X))
 2700 FORMAT (//' ICL  =',I3,12X,'SLP =',F5.2,5X,
     &         'TE =',F6.1,5X,'TAS=',F5.1,3X,'TRS=',F5.1)
 2900 FORMAT (//' CA.NO =',E10.2,3X,'NPO  =',I3//
     &   ' VOG  =',E12.5,2X,'VOO  =',E12.5,2X,'VO  ='E12.5)
 3000 FORMAT (/' GRADP=',E12.5,2X,'PERM =',E10.3,2X,'VF =',E12.4,
     &         2X,'VI =',E12.4)
 3050 FORMAT (/' CENTER OF GRAVITY:    X=',F5.2,4X,'Y=',F5.2)
 3500 FORMAT (///' KSTEP=',I4,4X
     &         'TINC=',E15.7,3X,'TTOTAL=',E15.7)
 4000 FORMAT (/' IU=',20I3)
 4500 FORMAT (/3X,'J  NP',10X,'Q',11X,'VG'9X,'VG/VUC',3X,'VG/VEUC',
     &         3X,'IND',3X'IUC',3X,'IVG',3X,'IU'/)
 5000 FORMAT (2I4,4X,2E12.4,2X,2F9.4,2(3X,I3),4X,I3,2X,I3)
 6000 FORMAT (/2I4,2X,'NVOID=',I3)
 6200 FORMAT (/I5,4X,'HYGRON')
 6400 FORMAT (/2I5,4X,'XERON')
 6500 FORMAT (/' IP',18I4)
 7500 FORMAT (//2X,' KSTEP=',I3,3X,'DIF=',E12.3,3X,'TINC=',E12.3,
     &         3X,'QT=',E12.3)
 8000 FORMAT (//' BREAK-UP OCCURED')
 8200 FORMAT (20I3)
 8300 FORMAT (3I6,2E15.7,2I3)
 8400 FORMAT (20I4)
 8500 FORMAT (4E20.12)
 9100 FORMAT (/' DAUGHTER GANGLION',I3,3X,'VOLUME RATIO=',F8.3)
 9000 FORMAT (1H1)
 9500 FORMAT (/)
      END
```

A.2 Listing of Program IMBSIM Used for Imbibition and Dynamic Invasion Simulations

```
      PROGRAM IMBSIM
C
C
C
C     PROGRAM *IMBSIM* SIMULATES THE INVASION BY WATER OF AN INITIALLY
C     OIL-FILLED NETWORK, USING NETWORK ANALYSIS.
C
C      VARIABLES WITH  *  ARE INPUT VARIABLES.
C
C      AC      - VECTOR OF DIMENSIONS  NCTE  CONTAINING THE DIMENSIONLESS
C                UNIT CELL CROSS-SECTIONAL AREA FOR EACH COMPARTMENT.
C  *   AL      - LENGTH OF PERIODICITY OF THE POROUS MEDIUM.
C      AREA    - UNIT BLOCK CROSS-SECTIONAL AREA.
C  *   CAN     - CAPILARY NUMBER.
C  *   C1-C3   - UNIT CELL MODEL CONSTANTS.
C      D       - THROAT DIAMETER OF CURRENT UNIT CELL
C  *   DUC     - VECTOR OF DIMENSION  NSIZE  CONTAINING THE THROAT
C                DIAMETER FOR EACH UNIT CELL SIZE.
C  *   FCSD    - VECTOR OF DIMENSION  NSIZE+1  CONTAINING THE
C                DISTRIBUTION FUNCTION FOR THE THROAT DIAMETERS.
C      G       - ARRAY OF DIMENSIONS  4*NPT  CONTAINING THE CONDUCTANCES
C                OF EACH BRANCH.
C      GO      - CONDUCTANCE OF AN OIL FILLED DIMENSIONLESS UNIT CELL.
C      GOW     - VECTOR OF DIMENSION  NCTE  CONTAINING THE DIMENSIONLESS
C                GATE UNIT CELL CONDUCTANCE FOR EACH COMPARTMENT.
C      GRADP   - APPLIED PRESSURE GRADIENT.
C      GW      - CONDUCTANCE OF A WATER FILLED DIMENSIONLESS UNIT CELL.
C      HJ      - VECTOR OF DIMENSION  NCTE  CONTAINING THE DIMENSIONLESS
C                GATE UNIT CELL CURVATURE OF THE INTERFACE, FOR THE
C                EQUILIBRIUM CONTACT ANGLE, FOR EACH COMPARTMENT AND EACH
C                LOCAL VELOCITY.
C      HJA     - VECTOR OF DIMENSIONS  NCTE*NUI  CONTAINING THE
C                DIMENIONSLESS GATE UNIT CELL CURVATURE OF THE INTERFACE
C                FOR ADVANCING CONTACT ANGLES, FOR EACH COMPARTMENT
C                AND EACH LOCAL VELOCITY.
C      HJR     - VECTOR OF DIMENSIONS  NCTE*NUI  CONTAINING THE
C                DIMENSIONLESS GATE UNIT CELL CURVATURE OF THE INTERFACE
C                FOR RECEDING CONTACT ANGLES, FOR EACH COMPARTMENT
C                AND EACH LOCAL VELOCITY.
C  *   IBC     - INDICATES THE TYPE OF BOUNDARY CONDITIONS TO BE
C                USED ON THE LATERAL WALLS:
C                =1  - PERMEABLE TO WATER.
C                =2  - IMPERMEABLE WALL.
C                =3  - PERIODIC.
C  *   IC      - VECTOR OF DIMENSION  NBT  CONTAINING THE THROAT
C                SIZE FOR EACH BRANCH. TO BE PROVIDED BY USER IF NCSD=0.
C  *   ICL     - INDICATOR OF THE ROUGHNESS OF THE POROUS MEDIA (USED
C                TO CALCULATE CONTACT ANGLES) :
C                =0  - TAS=TRS=TE  INVARIANT WITH VELOCITY
C                =1  - NON ROUGHNED SURFACE  TAS=TRS=TE
C                =2  - SLIGHTLY ROUGHNED SURFACE
C                =3  - ROUGHNED SURFACE.
C  *   IGWR    - INDICATES WHETHER CONDUCTANCE FIELD IS TO BE PRINTED
C                (>0) OR NOT (=0).
C  *   ILONG   - INDICATES WHETHER SHORT NETWORK IS TO BE USED (=0)
C                OR LONG NETWORK (>0).
C      IND     - ARRAY OF DIMENSIONS  4*NPT  ASSIGNED SUCH THAT :
C                =0  - UC FILLED WITH WATER
C                =1  - GATE UNIT CELL
C                =2  - UC FILLED WITH OIL
C                =3  - RECEDING  EXTENDED  GUC.
C                =5  - ADVANCING  EXTENDED  GUC
C                =6  - GUC WITH TWO INTERFACES.
C  *   IP      - VECTOR OF DIMENSION  NPO  CONTAINING THE NUMBER OF EACH
C                CEVS OCCUPIED BY THE OIL BLOB. IF NBLOB=0  THE INITIAL
C                VALUES MUST BE PROVIDED BY USER IN VECTOR IPA.
C  *   IPWR    - INDICATES WHETHER PRESSURE FIELD IS TO BE PRINTED (>0)
C                OR NOT (=0).
C  *   IQWR    - INDICATES WHETHER FLOW-RATE FIELD IS TO BE PRINTED (>0)
C                OR NOT (=0).
C  *  ISTART   - INDICATES WHETHER THE SIMULATION IS TO BE RESTARTED (>0)
C                OR NOT (=0).
```

```
C       IUC    - ARRAY OF DIMENSIONS  4*NPT  CONTAINING THE SIZES OF
C                EACH BRANCH. FOR NODE "I" WE HAVE:
C                                                 I+NX -1
C                                                   J=2
C                                    I-1    J=1      I       J=3     I+1
C                                                   J=4
C                                                 I -NX+1
C       IVG    - COMPARTMENT NUMBER WHERE THE INTERFACE IS LOCATED.
C  *    I09    - STEP INTERVAL AT WHICH FILE 009 IS TO BE UPDATED.
C                FILE 009 IS USED TO RESTART THE SIMULATION IF NECESSARY.
C  *    KSIZE  - IF NCSD<0 REPRESENTS THE UNIT CELL SIZE TO BE USED.
C  *    KWRITE - STEP INTERVAL AT WHICH OUTPUT SHOULD BE PRINTED
C                INTO FILE 010.
C       NBT    - TOTAL NUMBER OF BRANCHES IN THE UNIT BLOCK.
C  *    NCSD   - INDICATOR FOR THE THROAT SIZE OF EACH BRANCH:
C                <0  - PROVIDED BY USER (EQUAL SIZES).
C                =0  - PROVIDED BY USER (RANDOM SIZES).
C                >1  - CALCULATED RANDOMLY.
C  *    NCT    - TOTAL NUMBER OF COMPARTMENTS IN WHICH
C                EACH UNIT CELL IS DIVIDED.
C       NCTE   - THE SAME AS NCT FOR THE EXTENDED UNIT CELL.
C       NFLAG  - INDICATOR FOR ERROR:
C                = 12 TINC=0.
C       NGP    - ARRAY OF DIMENSION  NG*NGPT  CONTAINING THE CEVS NUMBER
C                BELONGING TO EACH STRANDED GANGLION.
C       NGPT   - VECTOR OF DIMENSION  NG  CONTAINING THE TOTAL NUMBER OF
C                CEVS'S IN EACH STRANDED GANGLION.
C       NPT    - TOTAL NUMBER OF NODES IN THE UNIT BLOCK.
C       NR     - NUMBER OF RANDOM NUMBERS TO BE GENERATED.
C  *    NSIZE  - NUMBER  OF UNIT CELL SIZES.
C  *    NSTEP  - MAXIMUM NUMBER OF STEPS FOR EACH SIMULATION.
C  *    NUI    - NUMBER OF INTERVALS FOR THE LOCAL VELOCITY IN THE UNIT
C                CELLS  ( USED TO CALCULATE THE CONTACT ANGLES ).
C  *    NX     - NUMBER OF BRANCHES IN THE X-DIRECTION.
C  *    NY     - NUMBER OF BRANCHES IN THE Y-DIRECTION.
C       PD     - ARRAY OF DIMENSIONS  4*NPT  CONTAINING THE PRESSURE
C                DROP ACROSS THE INTERFACE FOR EACH BRANCH.
C  *    PERM   - PERMEABILITY  (APROXIMATED VALUE ON INPUT. THE PROGRAM
C                CALCULATES THE ACTUAL VALUE OF THE PERMEABILITY).
C  *    PHI    - ANGLE BETWEEN THE PRESSURE GRADIENT DIRECTION AND THE
C                HORIZONTAL AXIS OF THE NETWORK (EXPRESSED IN PI RAD).
C  *    POR    - POROUS MEDIUM POROSITY.
C       Q      - ARRAY OF DIMENSIONS  4*NPT  CONTAINING THE
C                FLOW RATES FOR EACH BRANCH.
C       SJI    - VECTOR OF DIMENSION  NPT  CONTAINING THE CURRENT SOURCE
C                SOURCES FOR THE BOUNDARY PORES.
C  *    SLP    - SLOPE FOR THE CURVE CONTACT ANGLES VERSUS VELOCITY.
C  *    ST     - INTERFACIAL TENSION BETWEEN OIL AND WATER.
C       TAS    - ADVANCING CONTACT ANGLE WHEN U=0.
C  *    TE     - EQUILIBRIUM CONTACT ANGLE.
C       TRS    - RECEDING CONTACT ANGLE WHEN U=0.
C       U      - LOCAL VELOCITY AT THE INTERFACE IN A GUC.
C  *    UMAX   - MAXIMUM LOCAL VELOCITY IN A GUC ( USED TO CALCULATE
C                THE CONTACT ANGLES ).
C       VEUC   - VOLUME OF AN EXTENDED DIMENSIONLESS UNIT CELL.
C       VG     - ARRAY OF DIMENSIONS  4*NPT  CONTAINING THE VOLUME OF
C                OIL FOR EACH UNIT CELL.
C  *    VISR   - VISCOSITY RATIO (OIL/WATER).
C  *    VISW   - VISCOSITY OF WATER.
C       VUC    - VOLUME OF A DIMENSIONLESS UNIT CELL.
C       X      - VECTOR OF DIMENSION  NPT  CONTAINIG THE NODE PRESSURES.
C       XVG    - VECTOR OF DIMENSION  NCTE  CONTAINING THE PARTIAL
C                VOLUME FOR EACH COMPARTEMENT.
C       Y      - ARRAY OF DIMENSION  NPT*NX  USED BY SUBROUTINE NET.
C       ZI     - VECTOR OF DIMENSION  NCTE  CONTAINING THE POSITION OF
C                THE INTERFACE FOR EACH COMPARTMENT.
C
C     SUBROUTINES CALLED :
C
C     SUBROUTINE COMP (VEUC,VUC,AC,ZI,XVG)
C      - DIVIDES THE UC'S IN COMPARTMENTS AND CALCULATES THE VOLUME AND
C        POSITION OF INTERFACE FOR EACH COMPARTMENT.
C
C     SUBROUTINE COND (ZI,GW,GO,GOW)
C      - CALCULATES THE DIMENSIONLESS UNIT CELL CONDUCTANCE
C        FOR EACH COMPARTMENT
C
C     SUBROUTINE CSD (ICSD,NBT,FCSD,IC,IUC)
C      - ASSIGNS THROAT SIZES TO EACH UNIT CELL.
C
C     SUBROUTINE CURV (N1,ZI,HJ,HJA,HJR)
C      - CALCULATES THE DIMENSIONLESS UNIT CELL INTERFACE CURVATURE
C        FOR EACH COMPARTMENT AND FOR EQUILIBRIUM, ADVANCING AND
C        RECEDING CONTACT ANGLES.
C
```

```
C      SUBROUTINE GANG (DNG,NPO,NG,IP,NGPT,IND,NGP)
C       - GANG  IDENTIFIES GANGLIA FORMED DURING IMBIBITION.
C
C      SUBROUTINE GGUBS (NR)
C       - PSEUDO-RANDOM NUMBER GENERATOR.
C
C      SUBROUTINE LEQ1PB (A,N,NC,IA,B,IB,M,IDGT,D1,D2,IER)
C       - SOLVES THE ALGEBRIC SYSTEM OF EQUATIONS (CALLED BY NET).
C
C      SUBROUTINE LUDAPB (A,N,NC,IA,A,IA,D1,D2,IER)
C       - CALLED INTERNALLY BY LEQ1PB.
C
C      SUBROUTINE LUELPB (UL,B.N,NC,IA,X)
C       - CALLED INTERNALLY BY LEQ1PB.
C
C      SUBROUTINE MATCH (I,J,IN,JN)
C       - MATCHES CONNECTING UC'S.
C
C      SUBROUTINE NETIMB (NPT,NX,G,X,Y)
C       - ORGANIZES THE NODE MATRIX IN BAND SYMMETRIC FORM.
C
C      SUBROUTINE SELECT (IVG,D,X,XVG)
C       - CHOSES COMPARTMENT NUMBER WHERE INTERFACE IS LOCATED.
C
C      SUBROUTINE SLCTU (U,IU)
C       - SELECTS THE RANGE FOR THE LOCAL VELOCITY.
C
C      SUBROUTINE UERTST (IER,NAME)
C       - CALLED INTERNALLY BY LEQ1PB.
C
C      SUBROUTINE UGETIO (1,NIN,IOUNIT)
C       - CALLED INTERNALLY BY UERTST.
C
C
C
      IMPLICIT DOUBLE PRECISION (A-H,O-Z)
      INTEGER DNC,DNX,DNY,DNPT,DNBT,DNYA,DND,DFC,DPAR,DNG,DNGP,DNCT,DNU
      PARAMETER (DNC=4)
      PARAMETER (DNX=21,DNY=41)
      PARAMETER (DNPT=(DNX-1)*(DNY-1))
      PARAMETER (DNBT=(DNX+DNX-1)*(DNY-1)+(DNX-1))
      PARAMETER (DNYA=DNPT*DNX)
      PARAMETER (DND=13,DFC=DND+1)
      PARAMETER (DPAR=10)
      PARAMETER (DNG=100,DNGP=100)
      PARAMETER (DNCT=31,DNU=20)
      DIMENSION VG(DNC,DNPT),Q(DNC,DNPT),PD(DNC,DNPT)
      DIMENSION G(DNC,DNPT),IND(DNC,DNPT),IUC(DNC,DNPT)
      DIMENSION IP(DNPT),SJI(DNPT),X(DNPT),CA(DNY),QQ(DNY)
      DIMENSION IC(DNBT),IUA(DNBT),IVGA(DNBT)
      DIMENSION DUC(DND),FCSD(DFC)
      DIMENSION GOW(DNCT),AC(DNCT),XVG(DNCT),ZI(DNCT),HJ(DNCT)
      DIMENSION HJA(DNCT,DNU),HJR(DNCT,DNU),JVOID(DNC)
      DIMENSION Y(DNYA)
      DIMENSION NGPT(DNG),NGP(DNG,DNGP),NGPTO(DNG),NGPO(DNG,DNGP)
      CHARACTER TITLE*20
      CHARACTER*5 SIDE(2)
      COMMON /CTAN/ SLP,TE,TAS,TRS,ICL
      COMMON /NTW/  NX,NY
      COMMON /VIS/  VISW,VISR
      COMMON /UCC/  C1,C2,C3,PI
      COMMON /EXT/  NCT,NCTE,NSIZE
      COMMON /UN/   UMAX,NUI
      COMMON /ALC/  AL
      COMMON /SEED/ DSEED,R(DNBT)
      COMMON /ONE/  IPO(DNBT)
      COMMON /TWO/  IGT(DNBT)
      DATA SIDE /'LEFT','RIGHT'/
C
C     READ INPUT VARIABLES
C
      READ (08,*) TITLE
      READ (08,*) C1,C2,C3,AL,POR,PERM
      READ (08,*) NSIZE
      READ (08,*) (DUC(I),I=1,NSIZE)
      READ (08,*) (FCSD(I),I=1,NSIZE+1)
      READ (08,*) ST,VISW,VISR,CAN
      READ (08,*) NX,NY,NCT,PHI,SEED
      READ (08,*) NCSD,KSIZE,NSTEP,KWRITE,ISTART,I09
```

```
      READ (08,*) IPWR,IQWR,IGWR
      READ (08,*) NUI,ICL,TE,UMAX,SLP
      READ (08,*) IBC,ILONG
C
      DSEED=SEED
      KSTEPS=0
      ZERO=0.0D0
      TAS=0.0D0
      TRS=0.0D0
      RL=0.0D0
      DO 10 I=1,DNYA
      Y(I)=0.0D0
   10 CONTINUE
      DO 20 I=1,DNG
      NGPTO(I)=0
      NGPT(I)=0
      DO 20 J=1,DNGP
      NGPO(I,J)=0
      NGP(I,J)=0
   20 CONTINUE
      NXM1=NX-1
      NXM2=NX-2
      NXM12=NXM1/2-1
      NYM1=NY-1
      NPT=NXM1*NYM1
      NPF=NXM1*(NY-ILONG)
      NP2=NPT-NXM1
      NP3=NPT-NXM2
      NP4=NP3-NXM1
      NBT=(NX*2-1)*NYM1+NXM1
      NCTE=NCT*(1.+1./C3)/2.
      NCPE=NCTE+1
      NC2=NCT/2
      NXVG=NCT*.15D0
      IF (NXVG.EQ.1) NXVG=2
      PI=DATAN(1.D0)*4.D0
      PI2=PI*0.5D0
      PH=PI*PHI
      DY=DSIN(PH)
      IF (PHI.EQ.0.0D0) DY=0.0D0
      DX=DCOS(PH)
      IF (PHI.EQ.0.5D0) DX=0.0D0
      D2=NY*DY
      D1=NX*DX
      D0=NY*DY+NX*DX
      AREA=(NXM1*DY+NYM1*DX)*AL*AL
      COSTE=DCOS(TE)
      NINE=9
      NTEN=10
      WRITE (06,5000) ISTART
      WRITE (10) ISTART
      WRITE (10) TITLE,AL,POR,PHI,UMAX,NUI,NCT,NCTE,
     &           NX,NY,NPT,NBT,C1,C2,C3
      WRITE (10) NSTEP,NSIZE,KVR,KCAN,IBC,ILONG,NCSD,KSIZE,PHI,SEED
C
C     ASSIGN THROAT SIZES TO EACH BRANCH
C
      IF (NCSD.EQ.0) READ (08,8200) (IC(I),I=1,NBT)
      IF (NCSD.LT.0) THEN
       NCSD=0
       DO 80 I=1,NBT
   80  IC(I)= KSIZE
      END IF
      CALL CSD (NCSD,NBT,FCSD,IC,IUC)
      IF (IBC.GT.1) THEN
       DO 100 I=1,NP3,NXM1
       IF (IBC.EQ.2) IUC(1,I)=13
       IUC(3,I+NXM2)=IUC(1,I)
  100  CONTINUE
      END IF
      WRITE (10) ((IUC(J,K),J=1,4),K=1,NPT)
C
C     CALCULATE VOLUME AND POSITION OF INTERFACE FOR
C     EACH COMPARTMENT
C
      CALL COMP (VEUC,VUC,AC,ZI,XVG)
      VEUCE=XVG(NCPE)
      WRITE (10) VUC,VEUC,VEUCE,(DUC(I),I=1,NSIZE)
```

```
C
C     CALCULATE CURVATURE FOR EACH COMPARTMENT
C
      CALL CURV (DNCT,ZI,HJ,HJA,HJR)
      WRITE (10) ICL,SLP,TE,TAS,TRS
C
      VISO=VISR*VISW
      ST=STA(KVR)
      ST2=ST*2.D0
      VWOST=VISW/ST
C
C     CALCULATE CONDUCTANCE FOR EACH COMPARTMENT
C
      CALL COND (ZI,GW,GO,GOW)
C
      ICAN=0
      IF (ST.NE.0.0D0) THEN
       GRADP=ST*CAN/PERM
      ELSE
       GRADP=.1D0*CAN/PERM
       ICAN=1
      END IF
  110 CONTINUE
      P=GRADP*AL
      IF (ICAN.EQ.1.AND.ILONG.GT.0) THEN
       RL=4.D0*PERM*COSTE/(VISR*CAN*DUC(5))
       DUC(13)=(AL*AL*PERM/(VISO*RL*GO))**0.333333D0
       P=P*RL/(AL*NY)
       DO 115 I=NP3,NPT
       DO 115 J=1,3
       IUC(J,I)=13
  115  CONTINUE
      END IF
      P1=P*NY
      P0=0.0D0
C
C     DETERMINE  CURRENT SOURCES ON THE BOUNDARY NODES
C
      DO 120 I=1,NPT
      SJI(I)=0.0D0
      DO 120 J=1,4
      D=DUC(IUC(J,I))
      G(J,I)=GW*D*D*D
  120 CONTINUE
      DO 125 I=1,NXM1
      I1=NP2+I
      SJI(I)=SJI(I)+P*G(4,I)*(D0-DFLOAT(I)*DX)
      SJI(I1)=SJI(I1)+P*G(2,I1)*(D1-DFLOAT(I)*DX)
  125 CONTINUE
      IF (IBC.EQ.1) THEN
       DO 130 J=1,NYM1
       J1=1+(J-1)*NXM1
       J2=J1+NX-2
       SJI(J1)=SJI(J1)+P*G(1,J1)*(D0-DFLOAT(J)*DY)
       SJI(J2)=SJI(J2)+P*G(3,J2)*(D2-DFLOAT(J)*DY)
  130  CONTINUE
      END IF
C
C     CALCULATE  TOTAL FLOW RATE AND SUPERFICIAL VELOCITY
C
      DO 135 I=1,NPT
      X(I)=SJI(I)
  135 CONTINUE
      CALL NETIMB (IER,IBC,NPT,NX,G,X,Y)
      IF (IER.NE.0) THEN
       KSTEP=0
       WRITE (06,9200) KSTEP,IER
       GO TO 800
      END IF
      QTT=0.0D0
      DO 140 I=NP4,NP2
      QTT=QTT+(X(I)-X(I+NXM1))*G(2,I)
  140 CONTINUE
      VF=QTT/AREA
C
C     CALCULATE PERMEABILITY
C
      IF (ICAN.EQ.0) THEN
       CANO=VWOST*VF
       PERM=ST*CANO/GRADP
```

```
       GRADP=ST*CAN/PERM
       ICAN=ICAN+1
       GO TO 110
      END IF
      KSTEP=0
      IBREAK=0
      IDISC=0
      ILAST=0
      NFLAG=0
      K09=I09
C
C     CALCULATE FLOW RATES
C
       DO 155 I=1,NPT
       DO 150 J=1,4
       IF (IBC.EQ.2.OR.IND(J,I).EQ.8) THEN
        Q(J,I)=0.0D0
       ELSE
        IF (I.LE.NXM1.AND.J.EQ.4) THEN
         Q(J,I)=G(J,I)*(X(I)-P1)
        ELSE
         IF (I.GE.NP3.AND.J.EQ.2) THEN
          Q(J,I)=G(J,I)*(X(I)-P0)
         ELSE
          CALL MATCH (I,J,IN,JN)
          Q(J,I)=G(J,I)*(X(I)-X(IN))
         END IF
        END IF
       END IF
  150  CONTINUE
  155  CONTINUE
C
C     OUTPUT CONDUCTANCE, FLOW RATE AND PRESSURE FIELDS
C
      IF (IGWR.NE.0) THEN
       WRITE (06,9000)
       DO 165 I=1,2
       WRITE (06,1041) KSTEP,SIDE(I)
       II=(I-1)*(NXM12+1)
       DO 160 IY=NYM1,1,-1
       I1=(IY-1)*NXM1+1+II
       I2=I1+NXM12
       WRITE (06,1020) (G(2,J),J=I1,I2)
       WRITE (06,1035) (G(1,J),J=I1,I2),G(3,I2)
  160  CONTINUE
       WRITE (06,1020) (G(4,J),J=I1,I2)
  165  CONTINUE
      END IF
      IF (IQWR.NE.0) THEN
       WRITE (06,9000)
       DO 166 I=1,NY
       QQ(I)=0.0D0
  166  CONTINUE
       DO 175 I=1,2
       WRITE (06,1042) KSTEP,SIDE(I)
       II=(I-1)*(NXM12+1)
       DO 170 IY=NYM1,1,-1
       I1=(IY-1)*NXM1+1+II
       I2=I1+NXM12
       DO 167 J=I1,I2
       QQ(IY+1)=QQ(IY+1)+Q(2,J)
  167  CONTINUE
       WRITE (06,1020) (Q(2,J),J=I1,I2),QQ(IY+1)
       WRITE (06,1035) (Q(1,J),J=I1,I2),G(3,I2)
  170  CONTINUE
       DO 171 J=I1,I2
       QQ(IY)=QQ(IY)+Q(2,J)
  171  CONTINUE
       WRITE (06,1020) (Q(4,J),J=I1,I2),QQ(1)
  175  CONTINUE
      END IF
      IF (IPWR.NE.0) THEN
       WRITE (06,9000)
       DO 185 I=1,2
       WRITE (06,1040) KSTEP,SIDE(I)
       II=(I-1)*(NXM12+1)
       DO 180 IY=NYM1,1,-1
       I1=(IY-1)*NXM1+1+II
       I2=I1+NXM12
```

```
       WRITE (06,1020) (ZERO,J=I1,I2)
       WRITE (06,1030) ((ZERO,X(J)),J=I1,I2),ZERO
  180  CONTINUE
       WRITE (06,1020) (ZERO,J=I1,I2)
  185  CONTINUE
      END IF
      WRITE (10) VISW,VISR,ST,CAN,GRADP,PERM,VF,RL,DUC(13)
      IF (ISTART.EQ.0) THEN
       NGO=0
       NG=0
C
C     TO START A SIMULATION
C
C     ASSIGN  2  TO  ALL UNIT CELLS
C
       DO 190 I=1,NPT
       X(I)=0.0D0
       DO 190 J=1,4
       VG(J,I)=0.0D0
       PD (J,I)=0.0D0
       IND(J,I)=2
       D=DUC(IUC(J,I))
       G(J,I)=GO*D*D*D
  190  CONTINUE
C
C     ASSIGN  0    TO UC FILLED WITH WATER
C
       DO 195 I=1,NXM1
       DO 195 J=1,4
       IND(J,I)=0
       D=DUC(IUC(J,I))
       G(J,I)=GW*D*D*D
  195  CONTINUE
C
C     ASSIGN  1  TO GUC
C
       NPO=0
       DO 200 I=NX,NX+NXM2
       NPO=NPO+1
       IP(NPO)=I
       IND(4,I)=1
  200  CONTINUE
       TT=0.0D0
       TINC=0.0D0
C
C     ASSIGN VOLUME OF OIL TO GUC'S
C
       NGUC=0
       DO 210 I=1,NPO
       NP=IP(I)
       DO 210 J=1,4
       IF (IND(J,NP).NE.2) THEN
        NGUC=NGUC+1
        D=DUC(IUC(J,NP))
        IUA(NGUC)=0
        VG(J,NP)=.5D0*VUC*D*D*D
        CALL SELECT (IVG,D,VG(J,NP),XVG)
        IVGA(NGUC)=IVG
        G(J,NP)=GOW(IVG)*D*D*D
        PD(J,NP)=HJ(IVG)*ST2/D
        CALL MATCH (NP,J,IN,JN)
        G(JN,IN)=G(J,NP)
        PD(JN,IN)=-PD(J,NP)
       END IF
  210  CONTINUE
      ELSE
C
C     TO RESTART A SIMULATION
C
       READ (09,8100) ICASE,ISTART
       READ (09,8300) KSTEP,NPO,NGUC,TINC,TT,IBREAK,IDISC
       READ (09,8400) (IP(I),I=1,NPO)
       READ (09,8400) (IVGA(I),I=1,NGUC)
       READ (09,8400) (IUA(I),I=1,NGUC)
       READ (09,8200) ((IND(J,I),J=1,4),I=1,NPT)
       READ (09,8500) (CA(I),I=1,NYM1)
       READ (09,8500) ((G(J,I),J=1,4),I=1,NPT)
       READ (09,8500) ((VG(J,I),J=1,4),I=1,NPT)
```

```
       READ (09,8200) NGO
       IF (NGO.GT.0) THEN
        READ (09,8200) (NGPTO(I),I=1,NGO)
        READ (09,8200) ((NGPO(I,I1),I1=1,NGPTO(I)),I=1,NGO)
       END IF
       K09=K5TEP+K09
      END IF
       WRITE (10) NPO,(IP(I),I=1,NPO)
      KWRIT=KWRITE
C
C     RETURN POINT IF XERON OR HYGRON OCCURED
C
  900 CONTINUE
      NPO5=NPO
      KWRIT=KWRIT+1
C
C     INITIALIZE PD AND G
C
      IF (K5TEP.NE.0) THEN
       DO 240 I=1,NPT
       DO 240 J=1,4
       D=DUC(IUC(J,I))
       PD(J,I)=0.0D0
       IF (IND(J,I).NE.2) THEN
        G(J,I)=GW*D*D*D
       ELSE
        G(J,I)=GO*D*D*D
       END IF
  240  CONTINUE
      END IF
C
C     RETURN POINT IF NO XERON OR HYGRON OCCURED
C
  910 CONTINUE
C
      IF (IBREAK.GT.0.AND.IDI5C.EQ.0) THEN
       DO 245 I=1,NPO
       NP=IP(I)
       DO 245 J=1,4
       IF (IND(J,NP).NE.2.AND.
     &      IND(J,NP).NE.10.AND.IND(J,NP).NE.17) GO TO 250
  245  CONTINUE
       N5TEP=K5TEP+5
       IDI5C=1
       WRITE (06,6650) K5TEP
       KWRIT=KWRITE
      END IF
C
C     CHECK IF GANGLIA HAVE BEEN CREATED
C
  250 CALL GANG (DNG,NPO,NG,IP,NGPT,IND,NGP)
      IF (NG.NE.NGO) THEN
       IF (NG.GT.NGO) THEN
        DO 270 I=1,NG
        DO 255 I1=1,NGO
        DO 255 I2=1,NGPT(I)
        DO 255 I3=1,NGPTO(I1)
        IF (NGP(I,I2).EQ.NGPO(I1,I3)) GO TO 270
  255   CONTINUE
        IF (NGPT(I).GT.1) THEN
         BKI=0.0D0
         NPK=NGP(I,1)
         NPI=NPK
         JK=1
         JI=1
         DLJ=0.0D0
         DO 259 I1=1,NGPT(I)-1
         NP1=NGP(I,I1)
         R1=NP1/NXM1
         NR1=INT(R1)
         IF (DFLOAT(NR1).EQ.R1) NR1=NR1-1
         DO 258 J=1,4
         IF (IND(J,NP1).NE.2) THEN
          HJ1=1.D0/(C1*DUC(IUC(J,NP1)))
          DO 257 I2=I1+1,NGPT(I)
          NP2=NGP(I,I2)
          R2=DFLOAT(NP2)/DFLOAT(NXM1)
          NR2=INT(R2)
          IF (DFLOAT(NR2).EQ.R2) NR2=NR2-1
          NLY=NR2-NR1
```

```
          NLX=IABS(NP1-(NP2-NLY*NXM1))
          IF (NLY.NE.0.AND.NLX.NE.0) THEN
           CKI=DCOS(PI2-DATAN(DFLOAT(NLY)/DFLOAT(NLX)))
          ELSE
           IF (NLY.EQ.0) CKI=0.0D0
           IF (NLX.EQ.0) CKI=1.D0
          END IF
          NLY=NLY+1
          NLX=NLX+1
          DLKI=AL*DSQRT(DFLOAT(NLY*NLY+NLX*NLX))*CKI
          DO 256 J0=1,4
          IF (IND(J0,NP2).NE.2) THEN
           HJ2=1.D0/DUC(IUC(J0,NP2))
           DJ=DABS(HJ1-HJ2)*4.D0*COSTE
           BKIN=DLKI/DJ
           IF (BKIN.GT.BKI) THEN
            BKI=BKIN
            NPK=NP1
            NPI=NP2
            JK=J
            JI=J0
            DLJ=DJ
           END IF
          END IF
 256      CONTINUE
 257      CONTINUE
         END IF
258      CONTINUE
259      CONTINUE
         CALL MATCH (NPK,JK,IN,JN)
         CALL MATCH (NPI,JI,INN,JNN)
         DLP=DABS(X(IN)-X(INN))
         IF (DLP.GT.DLJ) GO TO 270
        END IF
        NGO=NGO+1
        NGPTO(NGO)=NGPT(I)
        VS=0.0D0
        VSS=0.0D0
        DO 260 I1=1,NGPT(I)
        NP=NGP(I,I1)
        NGPO(NGO,I1)=NP
        DO 260 J=1,4
        IF (IND(J,NP).NE.2) THEN
         IF (IND(J,NP).EQ.6.OR.IND(J,NP).EQ.16) THEN
          CALL MATCH (NP,J,IN,JN)
          IF (IND(JN,IN).EQ.16) THEN
           IND(JN,IN)=17
           IND(J,NP)=17
          ELSE
           IND(J,NP)=16
          END IF
         ELSE
          IND(J,NP)=10
          VS=VS+VG(J,NP)
          D=DUC(IUC(J,NP))
          VSS=VSS+VUC*D*D*D
         END IF
        END IF
260     CONTINUE
        DO 265 I1=1,NGPT(I)
        NP=NGP(I,I1)
        DO 265 J=1,4
        IF (IND(J,NP).EQ.10) THEN
         D=DUC(IUC(J,NP))
         VG(J,NP)=VS*VUC*D*D*D/VSS
        END IF
265     CONTINUE
        IF (NGO.EQ.NG) GO TO 305
270     CONTINUE
       ELSE
        ING=0
        DO 285 I=1,NGO
        DO 275 I1=1,NG
        DO 275 I2=1,NGPTO(I)
        DO 275 I3=1,NGPT(I1)
        IF (NGPO(I,I2).EQ.NGP(I1,I3)) GO TO 285
275     CONTINUE
        ING=ING+1
        DO 280 I2=1,NGPTO(I)
```

```
          NP=NGPO(I,I2)
          DO 280 J=1,4
          IF (IND(J,NP).EQ.16) IND(J,NP)=6
          IF (IND(J,NP).EQ.17) THEN
           IND(J,NP)=6
           CALL MATCH (NP,J,IN,JN)
           IND(JN,IN)=16
          END IF
          IF (IND(J,NP).EQ.10) THEN
           D=DUC(IUC(J,NP))
           IF (VG(J,NP).GT.VUC*D*D*D) THEN
            IF (J.EQ.2.OR.J.EQ.3) IND(J,NP)=5
            IF (J.EQ.1.OR.J.EQ.4) IND(J,NP)=3
           ELSE
            IND(J,NP)=1
           END IF
          END IF
  280     CONTINUE
          NGPTO(I)=0
          IF ((NGO-ING).EQ.NG) GO TO 290
  285     CONTINUE
  290     I1=0
          DO 300 I=1,NGO
          IF (NGPTO(I).NE.0) THEN
           I1=I1+1
           NGPTO(I1)=NGPTO(I)
           DO 295 I2=1,NGPTO(I)
           NGPO(I1,I2)=NGPO(I,I2)
  295      CONTINUE
          END IF
  300     CONTINUE
          NGO=I1
         END IF
  305    IF (NGO.EQ.NG) KWRIT=KWRITE
        END IF
C
        KWR=0
        IF (KSTEP.GE.NSTEP) GO TO 800
        KSTEP=KSTEP+1
        IF (KSTEP.EQ.NSTEP) THEN
         KWRIT=KWRITE
         ILAST=1
        END IF
C
        IF ((KWRIT.GE.KWRITE.AND.KWRITE.GT.0).OR.KWRITE.EQ.0) THEN
         KWRIT=0
         KWR=1
        END IF
C
        IF (KSTEP.NE.1) THEN
C
C       ASSIGN CONDUCTANCE AND PRESSURE DROP ACROSS INTERFACE
C       FOR EACH GATE UNIT CELL
C
         NGUC=0
         DO 325 I=1,NPO
         NP=IP(I)
         DO 320 J=1,4
         IF (IND(J,NP).NE.2) THEN
          NGUC=NGUC+1
          D=DUC(IUC(J,NP))
          DU2=D*D
          D3=D*D*D
          VGX=VG(J,NP)
          IF (VGX.GT.0.0D0.AND.D.NE.0.0D0) THEN
           IF (IND(J,NP).EQ.10.OR.IND(J,NP).EQ.17) THEN
            IF (IDISC.EQ.0) THEN
             CALL MATCH (NP,J,IN,JN)
             PD(J,NP)=X(NP)-X(IN)
            ELSE
             PD(J,NP)=0.0D0
            END IF
           ELSE
            IF (IND(J,NP).EQ.6.OR.IND(J,NP).EQ.16) THEN
             CALL MATCH (NP,J,IN,JN)
             VGY=VG(JN,IN)
             VGZ=VGX+VGY
             IF (VGZ.GT.0.9999D0*VUC*D3) THEN
```

```
            VGX=XVG(NC2)*D3
            VGY=XVG(NC2-2)*D3
            VG(J,NP)=VGX
            VG(JN,IN)=VGY
            VGZ=VGX+VGY
           END IF
           CALL SELECT (IVG,D,VGX,XVG)
           CALL SELECT (IVY,D,VGY,XVG)
           CALL SELECT (IVZ,D,VGZ,XVG)
           G(J,NP)=GOW(IVZ)*D3
           IF (AC(IVG).NE.0.0D0) U=Q(J,NP)/(AC(IVG)*DU2)
           CALL SLCTU (DAB5(U),IU)
           IVGA(NGUC)=IVG
           IUA(NGUC)=IU
           IF (U.GE.0.0D0) PD(J,NP)=(HJA(IVG,IU)-HJR(IVY,IU))*ST2/D
           IF (U.LT.0.0D0) PD(J,NP)=(HJR(IVG,IU)-HJA(IVY,IU))*ST2/D
          ELSE
           CALL SELECT (IVG,D,VGX,XVG)
           G(J,NP)=GOW(IVG)*D3
           IF (AC(IVG).NE.0.0D0) U=Q(J,NP)/(AC(IVG)*DU2)
           CALL SLCTU (DAB5(U),IU)
           IVGA(NGUC)=IVG
           IUA(NGUC)=IU
           IF (U.GE.0.0D0) PD(J,NP)=HJA(IVG,IU)*ST2/D
           IF (U.LT.0.0D0) PD(J,NP)=HJR(IVG,IU)*ST2/D
          END IF
         END IF
        ELSE
         IVGA(NGUC)=1
         G(J,NP)=0.0D0
         PD (J,NP)=0.0D0
        END IF
        IF (IND(J,NP).NE.8.OR.IBC.EQ.3) THEN
         CALL MATCH (NP,J,IN,JN)
         G(JN,IN)=G(J,NP)
         PD(JN,IN)=-PD(J,NP)
        END IF
       END IF
  320  CONTINUE
  325  CONTINUE
      END IF
      IF (NGO.GT.0) THEN
       DO 345 I=1,NGO
       DO 330 I1=1,NGPTO(I)
       NP=NGPO(I,I1)
       DO 330 J=1,4
       IF (IND(J,NP).EQ.16) GO TO 335
       G(J,NP)=1.D-20
       CALL MATCH (NP,J,IN,JN)
       G(JN,IN)=1.D-20
  330  CONTINUE
       GO TO 345
  335  DO 340 I1=1,NGPTO(I)
       NP=NGPO(I,I1)
       DO 340 J=1,4
       D=DUC(IUC(J,NP))
       IF (IND(J,NP).EQ.2) THEN
        G(J,NP)=GO*D*D*D
       ELSE
        VGX=VG(J,NP)
        IF (IND(J,NP).EQ.6.OR.IND(J,NP).EQ.16) THEN
         CALL MATCH (NP,J,IN,JN)
         VGX=VGX+VG(JN,IN)
        END IF
        CALL SELECT (IVG,D,VGX,XVG)
        G(J,NP)=GOW(IVG)*D*D*D
       END IF
       CALL MATCH (NP,J,IN,JN)
       G(JN,IN)=G(J,NP)
  340  CONTINUE
  345  CONTINUE
      END IF
C
C     OUTPUT
C
      IF (KWR.NE.0) THEN
       IR=0
       DO 352 I1=1,NPT,NXM1
       IR=IR+1
       QT=0.0D0
```

```
        QTT=0.0D0
        IWF=0
        DO 350 I=I1,I1+NXM2
        Q0=Q(2,I)
        QTT=QTT+Q0
        CALL MATCH (I,2,IN,JN)
        IF (IND(2,I).EQ.0.AND.IND(JN,IN).EQ.0) THEN
         QT=QT+Q0
         IWF=IWF+1
        END IF
  350   CONTINUE
        QQ(IR)=QT
        IF (IWF.NE.0) THEN
         CA(IR)=VWOST*DABS(QT)/AREA
        ELSE
         CA(IR)=0.0D0
        END IF
  352   CONTINUE
        WRITE (6,9999) NTEN,KSTEP
        WRITE (10) KSTEP,NPO,NGUC,TINC,TT,IBREAK,IDISC,ILAST
        WRITE (10) (IP(I),I=1,NPO)
        WRITE (10) (IVGA(I),I=1,NGUC)
        WRITE (10) (IUA(I),I=1,NGUC)
        WRITE (10) ((IND(J,I),J=1,4),I=1,NPT)
        WRITE (10) QTT,(QQ(I),I=1,NYM1)
        WRITE (10) (CA(I),I=1,NYM1)
        WRITE (10) ((VG(J,IP(I)),J=1,4),I=1,NPO)
        WRITE (10) ((Q(J,IP(I)),J=1,4),I=1,NPO)
        WRITE (10) NGO
        IF (NGO.NE.0) THEN
         WRITE (10) (NGPTO(I),I=1,NGO)
         WRITE (10) ((NGPO(I,I1),I1=1,NGPTO(I)),I=1,NGO)
        END IF
       END IF
       IF (KSTEP.EQ.K09.OR.ILAST.GT.0) THEN
        K09=K09+I09
        WRITE (6,9999) NINE,KSTEP
        REWIND (09)
        WRITE (09,8100) ICASE,ISTART
        WRITE (09,8900) KSTEP,NPO,NGUC,TINC,TT,IBREAK,IDISC
        WRITE (09,8400) (IP(I),I=1,NPO)
        WRITE (09,8400) (IVGA(I),I=1,NGUC)
        WRITE (09,8400) (IUA(I),I=1,NGUC)
        WRITE (09,8200) ((IND(J,I),J=1,4),I=1,NPT)
        WRITE (09,8500) (CA(I),I=1,NYM1)
        WRITE (09,8500) ((Q(J,I),J=1,4),I=1,NPT)
        WRITE (09,8500) ((VG(J,I),J=1,4),I=1,NPT)
        WRITE (09,8200) NGO
        IF (NGO.NE.0) THEN
         WRITE (09,8200) (NGPTO(I),I=1,NGO)
         WRITE (09,8200) ((NGPO(I,I1),I1=1,NGPTO(I)),I=1,NGO)
        END IF
       END IF
C
C      UPDATE  X  FOR EACH NODE
C
       DO 360 I=1,NPT
       X(I)=SJI(I)
  360  CONTINUE
       DO 365 I=1,NPT
       DO 365 J=1,4
       X(I)=X(I)+PD(J,I)*G(J,I)
  365  CONTINUE
C
C      SOLVE FOR THE PRESSURES IN EACH PORE BY NODE ANALYSIS
C
       CALL NETIMB (IER,IBC,NPT,NX,G,X,Y)
       IF (IER.NE.0) THEN
        WRITE (6,9200) KSTEP,IER
        GO TO 800
       END IF
C
C      OUTPUT CONDUCTANCE, FLOW RATE AND PRESSURE FIELDS
C
       IF ((KWR.NE.0.AND.IGWR.NE.0)) THEN
        WRITE (06,9000)
        DO 375 I=1,2
        WRITE (06,1041) KSTEP,SIDE(I)
        II=(I-1)*(NXM12+1)
```

```
      DO 370 IY=NYM1,1,-1
      I1=(IY-1)*NXM1+1+II
      I2=I1+NXM12
      WRITE (06,1020) (G(2,J),J=I1,I2)
      WRITE (06,1035) (G(1,J),J=I1,I2),G(3,I2)
  370 CONTINUE
      WRITE (06,1020) (G(4,J),J=I1,I2)
  375 CONTINUE
     END IF
     IF ((KWR.NE.0.AND.IQWR.NE.0)) THEN
      WRITE (06,9000)
      DO 386 I=1,NY
      QQ(I)=0.0D0
  386 CONTINUE
      DO 395 I=1,2
      WRITE (06,1042) KSTEP,SIDE(I)
      II=(I-1)*(NXM12+1)
      DO 390 IY=NYM1,1,-1
      I1=(IY-1)*NXM1+1+II
      I2=I1+NXM12
      DO 387 J=I1,I2
      QQ(IY+1)=QQ(IY+1)+Q(2,J)
  387 CONTINUE
      WRITE (06,1020) (Q(2,J),J=I1,I2),QQ(IY+1)
      WRITE (06,1035) (Q(1,J),J=I1,I2),G(3,I2)
  390 CONTINUE
      DO 391 J=I1,I2
      QQ(1)=QQ(1)+Q(4,J)
  391 CONTINUE
      WRITE (06,1020) (Q(4,J),J=I1,I2),QQ(1)
  395 CONTINUE
     END IF
     IF ((KWR.NE.0.AND.IPWR.NE.0)) THEN
      WRITE (06,9000)
      DO 405 I=1,2
      WRITE (06,1040) KSTEP,SIDE(I)
      II=(I-1)*(NXM12+1)
      DO 400 IY=NYM1,1,-1
      I1=(IY-1)*NXM1+1+II
      I2=I1+NXM12
      WRITE (06,1020) (PD(2,J),J=I1,I2)
      WRITE (06,1030) ((PD(1,J),X(J)),J=I1,I2),PD(3,I2)
  400 CONTINUE
      WRITE (06,1020) (PD(4,J),J=I1,I2)
  405 CONTINUE
     END IF
C
C    CALCULATE FLOW RATES
C
     DO 410 I=1,NPT
     DO 410 J=1,4
     IF (IBC.EQ.2.AND.IND(J,I).EQ.8) THEN
      Q(J,I)=0.0D0
     ELSE
      IF (I.LE.NXM1.AND.J.EQ.4) THEN
       Q(J,I)=G(J,I)*(X(I)-P1)
      ELSE
       IF (I.GE.NP3.AND.J.EQ.2) THEN
        Q(J,I)=G(J,I)*(X(I)-P0)
       ELSE
        CALL MATCH (I,J,IN,JN)
        Q(J,I)=G(J,I)*(X(I)-X(IN)-PD(J,I))
       END IF
      END IF
     END IF
  410 CONTINUE
C
C    CALCULATE TIME INCREMENT
C
     TINC=1000.0D0
     DO 415 I=1,NPO
     NP=IP(I)
     DO 415 J=1,4
     IF (IND(J,NP).NE.2) THEN
      D=DUC(IUC(J,NP))
      D3=D*D*D
      Q0=Q(J,NP)
      IF (Q0.NE.0.0D0.AND.IND(J,NP).NE.10.AND.
```

```
     &       IND(J,NP).NE.16.AND.IND(J,NP).NE.17) THEN
          IF ((J.EQ.2.OR.J.EQ.3).AND.IND(J,NP).EQ.3.AND.Q0.GT.0.0D0)
     &          IND(J,NP)=5
          IF ((J.EQ.1.OR.J.EQ.4).AND.IND(J,NP).EQ.5.AND.Q0.LT.0.0D0)
     &          IND(J,NP)=3
          VGX=VG(J,NP)
          CALL SELECT (IVG,D,VGX,XVG)
          T=DABS((XVG(IVG+1)-XVG(IVG))*D3/Q0)
          IF (VGX.GT.0.0D0) THEN
           IF (IVG.EQ.1.AND.Q0.LT.0.0D0) T=DABS(VGX/Q0)
           IF (IND(J,NP).EQ.1.AND.IVG.EQ.NCT.AND.Q0.GT.0.0D0)
     &                                T=DABS((VUC*D3-VGX)/Q0)
           IF (IND(J,NP).EQ.5.AND.IVG.EQ.NCTE.AND.Q0.GT.0.0D0)
     &                                 T=DABS((VEUCE*D3-VGX)/Q0)
          END IF
          IF (TINC.GT.T.AND.T.NE.0.0D0) TINC=T
         END IF
        END IF
  415 CONTINUE
        IF (TINC.EQ.0) THEN
         NFLAG=12
         GO TO 800
        END IF
        TT=TT+TINC
C
C       UPDATE VG
C
        DO 425 I=1,NPO
        NP=IP(I)
        DO 420 J=1,4
        IF (IND(J,NP).NE.2) THEN
         IF (IND(J,NP).NE.10.AND.IND(J,NP).NE.16.AND.IND(J,NP).NE.17)
     &                    VG(J,NP)=VG(J,NP)+TINC*Q(J,NP)
         IF (VG(J,NP).LT.1D-13) VG(J,NP)=0.0D0
        END IF
  420 CONTINUE
  425 CONTINUE
C
C       CHECK FOR XERON,HYGRON,ETC.
C
        IWARN=0
        DO 700 I=1,NPO
        NVOID=0
        NP=IP(I)
        DO 530 J=1,4
        IF (IND(J,NP).NE.2.AND.IND(J,NP).NE.10.AND.IND(J,NP).NE.16.AND.
     &      IND(J,NP).NE.17) THEN
         D=DUC(IUC(J,NP))
         D3=D*D*D
C
C       CHECK IF XERON OCCURED
C
         IF (IND(J,NP).NE.3) THEN
          IF (IND(J,NP).EQ.5.OR.IND(J,NP).EQ.7) THEN
           IF (VG(J,NP).LT.0.9999D0*VUC*D3) THEN
            IND(J,NP)=1
           ELSE
            CALL MATCH (NP,J,IN,JN)
            IF (IN.GT.NPT.OR.IN.LT.NX) THEN
             VG(J,NP)=.5D0*VUC*D3
            ELSE
             VAD=0.0D0
             DO 500 J0=1,4
             IF (J0.NE.JN) THEN
              D=DUC(IUC(J0,IN))
              VAD=VAD+XVG(NXVG)*D*D*D
             END IF
  500        CONTINUE
             VS=VG(J,NP)-VUC*D3
             IF (VS.GE.VAD) THEN
              VG(JN,IN)=0.0D0
              IND(JN,IN)=2
              IF (IPWR.NE.0) WRITE (6,6400) J,NP
              IWARN=IWARN+1
              NPOS=NPOS+1
              IP(NPOS)=IN
              VG(J,NP)=0.0D0
              IND(J,NP)=2
              VSS=0.0D0
              DO 510 J0=1,4
```

```
            IF (J0.NE.JN) THEN
             D=DUC(IUC(J0,IN))
             V55=V55+VUC*D*D*D
            END IF
  510       CONTINUE
            DO 520 J0=1,4
            IF (J0.NE.JN) THEN
             D=DUC(IUC(J0,IN))
             VG(J0,IN)=V5*VUC*D*D*D/V55
             IND(J0,IN)=1
             IF (IBC.LT.3) THEN
              NPROW=(IN/NXM1)*NXM1
              IF ((J0.EQ.1.AND.IN.EQ.NPROW+1).OR.
     &            (J0.EQ.3.AND.IN.EQ.NPROW)) THEN
               IND(J0,IN)=8
               IF (IBC.EQ.2) THEN
                Q(J,NP)=0.0D0
                GO TO 520
               END IF
              END IF
             END IF
             CALL MATCH (IN,J0,INN,JNN)
             Q(J0,IN)=(X(IN)-X(INN)-PD(J0,IN))*G(J0,IN)
             IF (IND(JNN,INN).EQ.2.OR.IND(JNN,INN).EQ.0) THEN
              IND(JNN,INN)=IND(JNN,INN)
             ELSE
              IND(J0,IN)=6
              IF (IND(JNN,INN).NE.1.AND.IND(JNN,INN).NE.10) THEN
               D=DUC(IUC(JNN,INN))
               VG(JNN,INN)=0.5D0*VUC*D*D*D
              END IF
              IF (IND(JNN,INN).EQ.10) THEN
               IND(JNN,INN)=16
              ELSE
               IND(JNN,INN)=6
              END IF
             END IF
            END IF
  520       CONTINUE
            GO TO 700
           ELSE
            IF (VG(J,NP).GE.0.9999D0*VEUCE*D3) IND(J,NP)=7
           END IF
          END IF
         END IF
        ELSE
         IF (VG(J,NP).LT.0.9999D0*VUC*D3) THEN
          IF (VG(J,NP).LE.0.0D0) THEN
           NVOID=NVOID+1
           JVOID(NVOID)=J
           IF (IPWR.NE.0) WRITE (6,6000) J,NP,NVOID
          END IF
         ELSE
          IF (IND(J,NP).NE.8.OR.IBC.EQ.3) IND(J,NP)=5
         END IF
        END IF
       ELSE
        IF (VG(J,NP).LT.0.9999D0*VUC*D3) IND(J,NP)=1
       END IF
      END IF
  530 CONTINUE
C
C     CHECK IF HYGRON OCCURED
C
       IF (NVOID.NE.0) THEN
        J=4
        VAD=0.0D0
        VADD=0.0D0
        VMVE=0.0D0
        V55=0.0D0
        IF (IBC.LT.3) THEN
         NPROW=(NP/NXM1)*NXM1
         IF (NP.EQ.NPROW+1.OR.NP.EQ.NPROW) THEN
          IF (NP.EQ.NPROW+1) J=1
          IF (NP.EQ.NPROW) J=3
          D=DUC(IUC(J,NP))
          IF (IND(J,NP).NE.8.OR.VG(J,NP).GT.0.9999D0*VUC*D*D*D.OR.
     &        IBC.EQ.2) THEN
           IND(J,NP)=8
```

```
          VG(J,NP)=VUC*D*D*D
         END IF
        END IF
       END IF
       JDN5=JVOID(NVOID)+2
       IF (JDN5.GT.4) JDN5=JDN5-4
       IF (IND(JDN5,NP).NE.2) THEN
        DO 550 J=1,4
        IF (IND(J,NP).EQ.2) JDN5=J
550    CONTINUE
       END IF
       CALL MATCH (NP,JDN5,IN,JN)
       D=DUC(IUC(JN,IN))
       VMVE=(VEUCE-VUC)*D*D*D*.9D0
       NVOID=0
       DO 560 J=1,4
       IF (J.NE.JDN5) THEN
        IF (IND(J,NP).NE.2) THEN
         NVOID=NVOID+1
         JVOID(NVOID)=J
         VAD=VAD+VG(J,NP)
        ELSE
         D=DUC(IUC(J,NP))
         V5=VUC*D*D*D
         V55=V55+V5
         VADD=VADD+V5*0.5D0
        END IF
       END IF
560    CONTINUE
       IF (VADD.GE.VMVE) VADD=VMVE*0.9999D0
       VAD=VAD+VADD
       IF (VAD.LE.VMVE) THEN
        IP(I)=1000
        IWARN=IWARN+1
        DO 640 J=1,4
        DO 570 JV=1,NVOID
        IF (J.EQ.JVOID(JV)) THEN
         IF (IND(J,NP).EQ.6.OR.IND(J,NP).EQ.16) THEN
          CALL MATCH (NP,J,IN,JN)
          IF (IND(JN,IN).EQ.16) THEN
           IND(JN,IN)=10
          ELSE
           IND(JN,IN)=1
          END IF
         END IF
         GO TO 630
        END IF
570     CONTINUE
        CALL MATCH (NP,J,IN,JN)
        IF (IN.LE.NPT) THEN
         IF (IBC.LT.3) THEN
          INROW=(IN/NXM1)*NXM1
          IF ((NP.EQ.NPROW.AND.IN.EQ.INROW+1).OR.
     &        (NP.EQ.NPROW+1.AND.IN.EQ.INROW)) GO TO 630
         END IF
         D=DUC(IUC(JN,IN))
         V5=VUC*D*D*D
         IF (J.EQ.JDN5) THEN
          V555=0.0D0
          IDN5=0
          DO 580 J0=1,4
          IF (IND(J0,IN).EQ.2) THEN
           IDN5=IDN5+1
           GO TO 590
          ELSE
           D=DUC(IUC(J0,IN))
           V555=V555+VUC*D*D*D
          END IF
580       CONTINUE
590       IF (IDN5.NE.0) THEN
           VG(JN,IN)=V5+VAD
           IND(JN,IN)=3
          ELSE
           DO 600 J0=1,4
           D=DUC(IUC(J0,IN))
           VG(J0,IN)=VAD*VUC*D*D*D/V555
           IND(J0,IN)=1
600        CONTINUE
```

```
        END IF
       ELSE
        VG(JN,IN)=VS-VS*VADD/VSS
        IND(JN,IN)=1
       END IF
       DO 610 K=1,NPOS
       IF (IP(K).EQ.IN) GO TO 620
610    CONTINUE
       NPOS=NPOS+1
       IP(NPOS)=IN
620    CALL MATCH (IN,JN,INN,JNN)
       Q(JN,IN)=(X(IN)-X(INN)-PD(JN,IN))*G(JN,IN)
       IF (ILONG.GT.0.AND.IBREAK.EQ.0.AND.IN.GT.NPF) THEN
       WRITE (6,6600) KSTEP
       IBREAK=1
       IWRIT=IWRITE
       KWRIT=KWRITE
       IDISC=1
       NSTEP=KSTEP+5
      END IF
     ELSE
      IF (IBREAK.EQ.0) THEN
       WRITE (6,6600) KSTEP
       IBREAK=1
       IWRIT=IWRITE
       KWRIT=KWRITE
      END IF
     END IF
630  IND(J,NP)=0
640  CONTINUE
     IF (IPWR.NE.0) WRITE (6,6200) NP
    ELSE
     VS=0.0D0
     NV=0
     NF=0
     DO 650 J=1,4
     IF (IND(J,NP).NE.2) THEN
      VGX=VG(J,NP)
      IF (VGX.GT.0.0D0) THEN
       D=DUC(IUC(J,NP))
       D3=D*D*D
       CALL SELECT (IVG,D,VGX,XVG)
       IF (IVG.EQ.1) THEN
        V1=XVG(IVG)*D3*0.5D0
       ELSE
        V1=(XVG(IVG)-XVG(IVG-1))*D3
       END IF
       IF (VGX.LT.V1) GO TO 650
       VG(J,NP)=VGX-V1
       VS=VS+V1
       NF=NF+1
      ELSE
       IF (IBC.EQ.2.AND.IND(J,NP).EQ.8) GO TO 650
       NV=NV+1
       JVOID(NV)=J
      END IF
     END IF
650  CONTINUE
     VS=VS/DFLOAT(NV)
     VAD=0.0D0
     DO 660 J=1,4
     IF (IBC.EQ.2.AND.IND(J,NP).EQ.8) GO TO 660
     IF (IND(J,NP).NE.2.AND.VG(J,NP).EQ.0.0D0) THEN
      IF (IND(J,NP).EQ.6) THEN
       D=DUC(IUC(J,NP))
       D3=D*D*D
       CALL MATCH (NP,J,IN,JN)
       IF ((VG(JN,IN)+VS).GT.0.9999D0*VUC*D3) THEN
        VG(J,NP)=VUC*D3-VG(JN,IN)
        VAD=VS-VG(J,NP)
        GO TO 660
       END IF
      END IF
      VG(J,NP)=VS
     END IF
660  CONTINUE
     IF (VAD.GT.0.0D0) THEN
      VAD=VAD/DFLOAT(NF)
      DO 680 J=1,4
      IF (IND(J,NP).NE.2) THEN
```

```
            DO 670 JV=1,NV
            IF (J.EQ.JVOID(JV)) GO TO 680
  670       CONTINUE
            VG(J,NP)=VG(J,NP)+VAD
           END IF
  680      CONTINUE
         END IF
        END IF
       END IF
  700 CONTINUE
C
C      IF NO XERON OR HYGRON OCCURED RETURN TO 910
C
       IF (IWARN.EQ.0) GO TO 910
C
C      RENUMBER IP(I)
C
       DO 720 I=1,NPOS-1
       IN=IP(I)
       DO 710 K=I+1,NPOS
       IF (IP(K).EQ.IN) THEN
        IP(I)=1000
        GO TO 720
       END IF
  710  CONTINUE
  720  CONTINUE
       IO=0
       DO 740 I=1,NPOS
       K=NPOS+1-I
       IF(IP(K).EQ.1000) THEN
        IO=IO+1
        DO 730 J=K,NPOS
        IP(J)=IP(J+1)
  730   CONTINUE
       END IF
  740  CONTINUE
       NPO=NPOS-IO
       DO 750 I=NPO+1,NPOS
       IP(I)=0
  750  CONTINUE
       DO 760 I=1,NPO
       K1=NPO+1-I
       DO 760 K=I+1,NPO
       K2=NPO+1-K
       IF (IP(K1).LE.IP(K2)) THEN
        IT=IP(K2)
        IP(K2)=IP(K1)
        IP(K1)=IT
       END IF
  760  CONTINUE
C       WRITE (6,6500) (IP(I),I=1,NPO)
C
C      XERON OR HYGRON OCCURED. RETURN TO 900
C
       GO TO 900
  800  CONTINUE
       WRITE (10) NSTEP+1,NPO,NGUC,TINC,TT,IBREAK,IDISC,ILAST
       KSTEPS=KSTEPS+KSTEP
       WRITE (6,2000) KSTEP,KSTEPS
       IF (NFLAG.EQ.12) WRITE (6,7500) KSTEP,TINC
       NFLAG=0
       STOP
 1020 FORMAT (6(10X,E10.3))
 1030 FORMAT (13E10.3)
 1035 FORMAT (6(E10.3,10X),E10.3)
 1040 FORMAT (//'  KSTEP=',I5/'       PRESSURE FIELD  ',A6,'SIDE'//)
 1041 FORMAT (//'  KSTEP=',I5/'   CONDUCTANCE FIELD  ',A6,'SIDE'//)
 1042 FORMAT (//'  KSTEP=',I5/'     FLOW RATE FIELD  ',A6,'SIDE'//)
 2000 FORMAT (//2I6)
 5000 FORMAT (//'ISTART=',I2//)
 6000 FORMAT (2I4,2X,'NVOID=',I3)
 6200 FORMAT (I5,4X,'HYGRON')
 6400 FORMAT (2I5,4X,'XERON')
 6500 FORMAT (/' IP',25I3)
 6600 FORMAT (//' KSTEP=',I5,'    BREAKTHROUGH'//)
 6650 FORMAT (//' KSTEP=',I5,'    OIL DISCONNECTED'//)
 7500 FORMAT (//2X,' KSTEP=',I5,3X,'TINC=',E12.3)
 8100 FORMAT (2I6)
 8200 FORMAT (20I3)
 8300 FORMAT (3I6,2E15.7,3I3)
 8400 FORMAT (20I4)
 8500 FORMAT (4E20.12)
 9000 FORMAT (1H1)
 9200 FORMAT (//' KSTEP=',I5,' IER=',I5//)
 9999 FORMAT ('     WRITING TO FILE',I4,'  AT STEP',I6)
      END
```

A.3 Listing of Subroutines Called by Programs GANDYN and/or IMBSIM

```
      SUBROUTINE BREAK (N1,NPO,IND,IP,IBREAK,NPB)
C
C     BREAK  CHECKS IF FISSION OCCURRED
C
      IMPLICIT DOUBLE PRECISION (A-H,O-Z)
      DIMENSION IND(N1,1),IP(1),NPB(1),NPBT(100)
      COMMON /NTW/ NX,NY
      NP=IP(1)
      IBREAK=1
      NPB(IBREAK)=NP
      J1=1
      J2=J1+3
   10 DO 20 J=J1,J2
      J0=J
      IF (J.GT.4) J0=J-4
      IF (IND(J0,NP).EQ.2) GO TO 90
   20 CONTINUE
      IF (IBREAK.NE.NPO) THEN
       IC=1
       DO 60 I=1,NPO
       NP=IP(I)
       DO 30 J=1,IBREAK
       IF (NP.EQ.NPB(J)) GO TO 60
   30  CONTINUE
       DO 40 J=1,4
       IF (IND(J,NP).EQ.2) THEN
        CALL MATCH (NP,J,IN,JN)
        DO 45 J0=1,IBREAK
        IF (IN.EQ.NPB(J0)) GO TO 50
   45   CONTINUE
       END IF
   40  CONTINUE
       NPBT(IC)=NP
       IC=IC+1
       GO TO 60
   50  IBREAK=IBREAK+1
       NPB(IBREAK)=NP
   60  CONTINUE
       IF (IBREAK.NE.NPO) THEN
        DO 70 I=1,IC
        NPB(IBREAK+I)=NPBT(I)
   70   CONTINUE
       ELSE
        GO TO 75
       END IF
      ELSE
   75  IBREAK=0
       DO 80 I=1,NPO
       NPB(I)=0
   80  CONTINUE
      END IF
      RETURN
   90 CALL MATCH (NP,J0,IN,JN)
      NP=IN
      IF (IN.EQ.IP(1)) THEN
       J1=JN+1
       J2=J1+1
      ELSE
       DO 100 I=1,IBREAK
       IF (NP.EQ.NPB(I)) GO TO 110
  100  CONTINUE
       IBREAK=IBREAK+1
       NPB(IBREAK)=NP
  110  J1=JN+1
       IF (JN.EQ.4) J1=1
       J2=J1+3
      END IF
      GO TO 10
      END
```

```
      SUBROUTINE CGCC (N1,NXM1,NPO,IP,IUC,IND,VUC,VG,XCG,YCG,
     &                 XVG,DUC,ZI)
C
C     CGCC CALCULATES THE COORDINATES OF THE GANGLION CENTER OF GRAVITY
C
      IMPLICIT DOUBLE PRECISION (A-H,O-Z)
      DIMENSION IUC(N1,1),IND(N1,1),VG(N1,1),IP(1)
      DIMENSION XVG(1),DUC(1),ZI(1)
      COMMON /UCC/ C1,C2,C3,PI
      COMMON /ALC/ AL
      C22=C2*0.25D0
      C2C3=C2*C3*0.25D0
      XCG=0.D0
      YCG=0.D0
      DO 50 I=1,NPO
      NP=IP(I)
      IX=NP
      IY=1
   10 IF (IX.GT.NXM1) THEN
       IX=IX-NXM1
       IY=IY+1
       GO TO 10
      END IF
      X=IX*AL
      Y=IY*AL
      DO 40 J=1,4
      D=DUC(IUC(J,NP))
      IF (IND(J,NP).NE.2) THEN
       VGX=VG(J,NP)
       CALL SELECT (IVG,D,VGX,XVG)
       Z=C22*D*(ZI(IVG)+C3)
       VI=VGX
      ELSE
       Z=C2C3*D
       VI=VUC*D*D*D*0.5D0
      END IF
      IF (J.EQ.1.OR.J.EQ.4) THEN
       ISIGN=-1
      ELSE
       ISIGN=1
      END IF
      IF (J.EQ.1.OR.J.EQ.3) THEN
       XCG=XCG+VI*(X+ISIGN*Z)
       YCG=YCG+VI*Y
      ELSE
       XCG=XCG+VI*X
       YCG=YCG+VI*(Y+ISIGN*Z)
      END IF
   40 CONTINUE
   50 CONTINUE
      XCG=XCG/AL
      YCG=YCG/AL
      RETURN
      END
```

```
      SUBROUTINE COMP (VEUC,VUC,AC,ZI,XVG)
C
C     COMP  DIVIDES THE UC'S IN COMPARTMENTS AND CALCULATES THE VOLUME
C           AND THE POSITION OF THE INTERFACE FOR EACH COMPARTMENT.
C
      IMPLICIT DOUBLE PRECISION (A-H,O-Z)
      DIMENSION ZI(1),XVG(1),AC(1)
      COMMON /UCC/ C1,C2,C3,PI
      COMMON /EXT/ NCT,NCTE,NSIZE
      F0(X)=A1*X-A2*DSIN(PI*X)+A4*DSIN(A5*X)
      A0(X)=(C1P1-C1M1*DCOS(PI*X))**2
      C1P1=C1+1.D0
      C1M1=C1-1.D0
      A1=(C1P1*C1P1+0.5D0*C1M1*C1M1)*PI
      A2=2.D0*(C1*C1-1.D0)
      A4=C1M1*C1M1*0.25D0
      A5=2.D0*PI
      NCP=NCT+1
      NC2=NCT/2
      NC1=NC2+1
      NCP1=NCP+1
      DZ=C3/FLOAT(NC2)
      C232=C2/32.D0
      PI16=PI/16.D0
      F1=F0(1.D0)
      F3=F0(C3)
      VEUC=C232*(F1+F3)
      VUC=C232*F3*2.D0
      ZCL=0.D0
      FL=0.D0
      XVG(NC1)=F3*C232
      DO 10 I=1,NC2
      I1=I+NC2
      I2=NCP-I1
      IA=NC1+I
      IB=NCP1-IA
      ZC=ZCL+DZ
      ZCI=ZCL+DZ*0.5D0
      ZI(I1)=ZCI
      ZI(I2)=-ZCI
      A=A0(ZCI)*PI16
      AC(I1)=A
      AC(I2)=A
      F=F0(ZC)
      VC=(F-FL)*C232
      XVG(IA)=XVG(IA-1)+VC
      XVG(IB)=XVG(IB+1)-VC
      ZCL=ZC
      FL=F
   10 CONTINUE
      XVG(1)=0.
      DO 20 I=NCP1,NCTE+1
      I1=I-1
      ZC=ZCL+DZ
      ZCI=ZCL+DZ/2.
      ZI(I1)=ZCI
      AC(I1)=A0(ZCI)*PI16
      F=F0(ZC)
      VC=(F-FL)*C232
      XVG(I)=XVG(I-1)+VC
      ZCL=ZC
      FL=F
   20 CONTINUE
      RETURN
      END
```

```
      SUBROUTINE COND (ZI,GW,GO,GOW)
C
C     COND  CALCULATES THE DIMENSIONLESS UNIT CELL CONDUCTANCE
C           FOR EACH COMPARTMENT
C
      IMPLICIT DOUBLE PRECISION (A-H,O-Z)
      DIMENSION ZI(1),GOW(1)
      COMMON /VIS/ VISW,VISR
      COMMON /UCC/ C1,C2,C3,PI
      COMMON /EXT/ NCT,NCTE,NSIZE
      PSI(X,A,B)=ABS(A*B*(B*(A1*B+A2)+A3))+A4*ATAN(A5*TAN(X/2.))
      NCP=NCT+1
      NC2=NCT/2
      B0=(C1-1.D0)/(C1+1.D0)
      B1=B0*B0
      B2=1.D0-B1
      A1=B0/(B2*3.D0)
      A2=5.D0*B0/(6.D0*B2*B2)
      A3=B0*(11.D0+4.D0*B1)/(6.D0*B2*B2*B2)
      A4=(2.D0+3.D0*B1)/(B2**3.5D0)
      A5=SQRT(B2)/(1.D0-B0)
      AI=(1024.D0*C2/(PI**2)/(C1+1.D0)**4)*VISW
      X=C3*PI
      A=DSIN(X)
      B=1.D0/(1.D0-B0*DCOS(X))
      PSP=PSI(X,A,B)
      GWI=AI*PSP
      GOI=GWI*VISR
      GW=0.5D0/GWI
      GO=0.5D0/GOI
      DO 10 J=1,NC2
      J1=J+NC2
      J2=NCP-J
      X=ZI(J1)*PI
      A=DSIN(X)
      B=1.D0/(1.D0-B0*DCOS(X))
      PSZ=PSI(X,A,B)
      GOW(J1)=1.D0/(AI*(VISR*PSZ+(PSP-PSZ))+GOI)
      X=ZI(J2)*PI
      A=DSIN(X)
      B=1.D0/(1.D0-B0*DCOS(X))
      PSZ=PSI(X,A,B)
      GOW(J)=1.D0/(AI*(PSZ+VISR*(PSP-PSZ))+GWI)
   10 CONTINUE
      DO 20 J=NCT+1,NCTE
      X=ZI(J)*PI
      A=DSIN(X)
      B=1.D0/(1.D0-B0*DCOS(X))
      PSZ=PSI(X,A,B)
      GOW(J)=1.D0/(AI*VISR*PSZ+GOI)
   20 CONTINUE
      RETURN
      END


      SUBROUTINE CSD (ICSD,NBT,FC,IC,IUC)
C
C     CSD  ASSIGNS THROAT SIZES TO EACH UNIT CELL.
C
      IMPLICIT DOUBLE PRECISION (A-H,O-Z)
      DIMENSION IC(NBT),IUC(4,1),FC(1)
      COMMON /NTW/ NX,NY
      COMMON /SEED/ DSEED,R(1)
      IF (ICSD.GT.0) THEN
       CALL GGUBS (NBT)
       DO 30 I=1,NBT
       RI=R(I)
       IF (RI.LT.1.D0) THEN
        J=1
   10   IF (RI.LT.FC(J).OR.RI.GE.FC(J+1)) THEN
         J=J+1
         GO TO 10
        END IF
       ELSE
        J=12
       END IF
       IC(I)=J
   30  CONTINUE
      END IF
      NX2=NX*2-1
      NXM1=NX-1
      NYM1=NY-1
      DO 50 IY=1,NYM1
      DO 50 IX=1,NXM1
      IP=(IY-1)*NXM1+IX
      IB=(IY-1)*NX2+IX
      IUC(1,IP)=IC(IB+NXM1)
      IUC(2,IP)=IC(IB+NX2)
      IUC(3,IP)=IC(IB+NXM1+1)
      IUC(4,IP)=IC(IB)
   50 CONTINUE
      RETURN
      END
```

```
      SUBROUTINE CURV (N1,ZI,HJ,HJA,HJR)
C
C     CURV  CALCULATES THE DIMENSIONLESS UNIT CELL INTERFACE CURVATURE
C           FOR EACH COMPARTMENT AND FOR EQUILIBRIUM, ADVANCING AND
C           RECEDING CONTACT ANGLES.
C
      IMPLICIT DOUBLE PRECISION (A-H,O-Z)
      DIMENSION ZI(1),HJ(1),HJA(N1,1),HJR(N1,1)
      COMMON /UCC/ C1,C2,C3,PI
      COMMON /CTAN/ SLP,TE,TAS,TRS,ICL
      COMMON /EXT/ NCT,NCTE,NSIZE
      COMMON /UN/ UMAX,NUI
      FA(U)=TAS+1.D0/(AKA/U+DTAM)
      FR(U)=TRS+1.D0/(AKR/U+DTRM)
      C1P1=C1+1.D0
      C1M1=C1-1.D0
      A1=C1M1*PI*0.5D0/C2
      PID=PI/180.D0
      TA=0.D0
      TR=0.D0
      TEP=TE*PID
C
C     CONTACT ANGLE CALCULATIONS
C
      IF (ICL.NE.0) THEN
       IF (ICL.EQ.1) THEN
        TAS=TE
        TRS=TE
       ELSE
        IF (ICL.EQ.2) THEN
         TAS=1.14D0*TE
         TRS=0.D0
         IF (TE.GT.22.D0) TRS=1.14D0*(TE-22.D0)
        ELSE
         TAS=0.D0
         TRS=0.D0
         IF (TE.GT.21.6D0) THEN
          TAS=2.D0*(TE-21.6D0)
          TRS=.525635548D0*TE-1.5D0
         END IF
        END IF
       END IF
      ELSE
       TA=TEP
       TR=TEP
      END IF
      IF (SLP.NE.0.D0) THEN
       AK=UMAX*(1.D0/SLP-1.D0)
       DTAM=1.D0/(60.D0-TAS)
       AKA=DTAM*AK
       IF (TRS.NE.0.D0) THEN
        DTRM=-1.D0/TRS
        AKR=DTRM*AK
       END IF
      ELSE
       TA=TAS*PID
       TR=TAS*PID
      END IF
      DU=UMAX/NUI
      DO 70 J=1,NCTE
      Z=ZI(J)*PI
      TALF=A1*DSIN(Z)
      TRW=(DSQRT(1.D0+TALF*TALF))*(C1P1-C1M1*DCOS(Z))*0.25D0
      HJ(J)=(DCOS(TEP)+DSIN(TEP)*TALF)/TRW
      U=DU*0.5D0
      DO 70 I=1,NUI
      IF (ICL.NE.0.AND.SLP.NE.0.D0) THEN
       TA=FA(U)*PID
       IF (TRS.NE.0.D0) TR=FR(U)*PID
      END IF
      HJA(J,I)=(DCOS(TA)+DSIN(TA)*TALF)/TRW
      HJR(J,I)=(DCOS(TR)+DSIN(TR)*TALF)/TRW
      U=U+DU
   70 CONTINUE
      RETURN
      END
```

```
      SUBROUTINE CURVR (N1,ZI,HJ,HJA,HJR)
C
C     CURVR  CALCULATES THE DIMENSIONLESS UNIT CELL INTERFACE CURVATURE
C           FOR EACH COMPARTMENT AND FOR EQUILIBRIUM, ADVANCING AND
C           RECEDING CONTACT ANGLESAS REPORTED BY HINKLEY (1983).
C
      IMPLICIT DOUBLE PRECISION (A-H,O-Z)
      DIMENSION ZI(1),HJ(1),HJA(N1,1),HJR(N1,1)
      DIMENSION TA(21),TR(21)
      COMMON /UCC/ C1,C2,C3,PI
      COMMON /CTAN/ SLP,TE,TAS,TRS,ICL
      COMMON /EXT/ NCT,NCTE,NSIZE
      COMMON /UN/ UMAX,NUI
      DATA TA /26.9D0,27.5D0,28.45D0,29.4D0,30.25D0,
     &         31.D0,31.7D0,32.3D0,32.85D0,33.45D0,
     &         33.95D0,34.45D0,34.85D0,35.3D0,35.75D0,36.2D0,
     &         36.65D0,37.D0,37.35D0,37.7D0,38.D0/
      DATA TR /25.1D0,24.45D0,23.45D0,22.6D0,22.05D0,
     &         21.75D0,21.6D0,21.45D0,21.35D0,21.25D0,
     &         21.2D0,21.15D0,21.1D0,21.08D0,
     &         21.05D0,21.02D0,21.D0,21.D0,21.D0,21.D0,21.D0/
      TAS=TA(1)
      TRS=TR(1)
      C1P1=C1+1.D0
      C1M1=C1-1.D0
      A1=C1M1*PI*0.5D0/C2
      PID=PI/180.D0
      TEP=TE*PID
      DO 70 J=1,NCTE
      Z=ZI(J)*PI
      TALF=A1*DSIN(Z)
      TRW=(SQRT(1.D0+TALF**2))*(C1P1-C1M1*DCOS(Z))*0.25D0
      HJ(J)=(DCOS(TEP)+DSIN(TEP)*TALF)/TRW
      DO 70 I=1,NUI
      TAP=TA(I+1)*PID
      TRP=TR(I+1)*PID
      HJA(J,I)=(DCOS(TAP)+DSIN(TAP)*TALF)/TRW
      HJR(J,I)=(DCOS(TRP)+DSIN(TRP)*TALF)/TRW
   70 CONTINUE
      RETURN
      END
```

```
      SUBROUTINE GANG (N,NPO,NG,IP,NGPT,IND,NGP)
C
C     GANG  IDENTIFIES GANGLIA FORMED DURING IMBIBITION
C
      DIMENSION IP(1),NGPT(1),IND(4,1),NGP(N,1)
      COMMON /NTW/ NX,NY
      COMMON /ONE/ IPO(1)
      COMMON /TWO/ IGT(1)
      NXM1=NX-1
      NPT=NXM1*(NY-1)
      NP1=NPT-(NX-2)
      DO 20 I=1,NPO
      IPO(I)=IP(I)
   20 CONTINUE
      IPC=0
      DO 100 IL=NP1,NPT
      IF (IND(2,IL).EQ.2) THEN
       IC=IL
   40  DO 60 I=1,NPO
       IF (IC.EQ.IP(I)) THEN
        IPO(I)=-1
        IPC=IPC+1
        GO TO 80
       END IF
   60  CONTINUE
   80  IF (IND(4,IC).EQ.2) THEN
        IC=IC-NXM1
        GO TO 40
       END IF
      END IF
  100 CONTINUE
      NG=0
  160 DO 180 I=1,NPO
      IF (IPO(I).GT.0) GO TO 200
  180 CONTINUE
      RETURN
  200 NP=IP(I)
      NPO=NP
      J00=0
      IPO(I)=-2
      IGP=1
      IGT(1)=NP
      J1=1
      J2=4
  250 DO 300 J=J1,J2
      J0=J
      IF (J0.GT.4) J0=J-4
      IF (IND(J0,NP).EQ.2) THEN
       IF (NP.EQ.NPO) THEN
        IF (J00.EQ.0) THEN
         J00=J0
        ELSE
         IF (J0.EQ.J00) GO TO 305
        END IF
       END IF
       GO TO 400
      END IF
  300 CONTINUE
  305 NG=NG+1
      DO 310 I=1,IGP
      NGP(NG,I)=IGT(I)
  310 CONTINUE
      IF (IGP.GE.9) THEN
       I=0
  320  I=I+1
       NP=NGP(NG,I)
       DO 360 J=1,4
       IF (IND(J,NP).EQ.2) THEN
        CALL MATCH (NP,J,IN,JN)
        DO 340 IG=1,IGP
        IF (IN.EQ.NGP(NG,IG)) GO TO 360
  340   CONTINUE
        IGP=IGP+1
        NGP(NG,IGP)=IN
       END IF
  360  CONTINUE
       IF (I.LE.IGP) GO TO 320
```

```
      END IF
      NGPT(NG)=IGP
      GO TO 160
  400 CALL MATCH (NP,J0,IN,JN)
      NP=IN
      IF (NP.EQ.NP0) THEN
       IF (JN.EQ.4) GO TO 800
       J1=JN+1
       J2=J1+1
      ELSE
       DO 450 I=1,NP0
       IF (NP.EQ.IP(I).AND.IP0(I).EQ.-1) GO TO 800
  450  CONTINUE
       DO 500 I=1,IGP
       IF (NP.EQ.IGT(I)) GO TO 700
  500  CONTINUE
       IGP=IGP+1
       IGT(IGP)=NP
       DO 600 I=1,NP0
       IF (NP.EQ.IP(I)) IP0(I)=0
  600  CONTINUE
  700  J1=JN+1
       IF (JN.EQ.4) J1=1
       J2=J1+3
      END IF
      GO TO 250
  800 DO 850 I=1,IGP
      IPC=IPC+1
      DO 850 IL=1,NP0
      IF (IP(IL).EQ.IGT(I)) IP0(IL)=-1
  850 CONTINUE
      GO TO 160
      END
```

```
      SUBROUTINE GGUB5 (NR)
C
C     GGUB5  IS A PSEUDO-RANDOM NUMBER GENERATOR.
C            (CALLED BY CSD AND SHAPE)
C
      IMPLICIT DOUBLE PRECISION (A-H,O-Z)
      COMMON /SEED/ DSEED,R(1)
      D2P31M=2147483647.D0
      D2P31 =2147483655.D0
      DO 10  I=1,NR
      DSEED=DMOD(16807.D0*DSEED,D2P31M)
      R(I)=DSEED/D2P31
   10 CONTINUE
      RETURN
      END
```

```
      SUBROUTINE LEQ1PB (A,N,NC,IA,B,IB,M,IDGT,D1,D2,IER)
C
C     LEQ1PB  SOLVES THE ALGEBRIC SYSTEM OF EQUATIONS
C             (CALLED BY NET).
C
      IMPLICIT DOUBLE PRECISION (A-H,O-Z)
      DIMENSION A(IA,1),B(IB,1)
      IER=0
      CALL LUDAPB (A,N,NC,IA,A,IA,D1,D2,IER)
      IF (IER.NE.0) GO TO 9000
      DO 5 I=1,M
      CALL LUELPB (A,B(1,I),N,NC,IA,B(1,I))
    5 CONTINUE
      GO TO 9005
 9000 CONTINUE
      CALL UERTST (IER,'LEQ1PB')
 9005 RETURN
      END
```

```
      SUBROUTINE LUDAPB (A,N,NC,IA,UL,IU,D1,D2,IER)
C
C     LUDAPB  IS USED TO DECOMPOSE A POSITIVE, DEFINITE,
C             BAND SYMMETRIC MATRIX (CALLED BY LEQ1PB)
C
      IMPLICIT DOUBLE PRECISION (A-H,O-Z)
      DIMENSION A(IA,1),UL(IU,1)
      DATA ZERO/0.0D0/FOUR/4.0D0/SIXTN/16.0D0/
     &     SIXTH/.0625D0/ONE/1.0D0/
      IER=0
      RN=ONE/(N*SIXTN)
      D1=ONE
      D2=ZERO
      NCP1=NC+1
      IF (NC.EQ.0) GO TO 15
      DO 10 I=1,NC
      DO 5  J=I,NC
      K=NCP1-J
      UL(I,K)=ZERO
    5 CONTINUE
   10 CONTINUE
   15 DO 60 I=1,N
      IMNCP1=I-NCP1
      I1=MAX0(1,1-IMNCP1)
      DO 60 J=I1,NCP1
      L=IMNCP1+J
      I2=NCP1-J
      SUM=A(I,J)
      JM1=J-1
      IF (JM1) 30,30,20
   20 DO 25 K=1,JM1
      M=I2+K
      SUM=SUM-UL(I,K)*UL(L,M)
   25 CONTINUE
   30 IF (J.NE.NCP1) GO TO 55
      TEMP=A(I,J)+SUM*RN
      IF (TEMP.LE.A(I,J)) GO TO 65
      UL(I,J)=ONE/SQRT(SUM)
      D1=D1*SUM
   35 IF (ABS(D1)-ONE) 45,45,40
   40 D1=D1*SIXTH
      D2=D2+FOUR
      GO TO 35
   45 IF (ABS(D1)-SIXTH) 50,50,60
   50 D1=D1*SIXTN
      D2=D2-FOUR
      GO TO 45
   55 UL(I,J)=SUM*UL(L,NCP1)
   60 CONTINUE
      GO TO 9005
   65 IER=129
 9000 CONTINUE
      CALL UERTST (IER,'LUDAPB')
 9005 RETURN
      END
```

```
      SUBROUTINE LUELPB (UL,B,N,NC,IA,X)
C
C     LUELPB  IS USED FOR THE ELIMINATION PART OF THE SOLUTION OF AX=B,
C             WHERE A IS A POSITIVE DEFINITE BAND SYMMETRIC MATRIX
C             (CALLED BY LEQ1PB)
C
      IMPLICIT DOUBLE PRECISION (A-H,O-Z)
      DIMENSION UL(IA,1),B(1),X(1)
      DATA ZERO/0.0D0/
      NC1=NC+1
      IW=0
      L=0
      DO 15 I=1,N
      SUM=B(I)
      IF (NC.LE.0) GO TO 10
      IF (IW.EQ.0) GO TO 9
      L=L+1
      IF (L.GT.NC) L=NC
      K=NC1-L
      KL=I-L
      DO 5 J=K,NC
      SUM=SUM-X(KL)*UL(I,J)
      KL=KL+1
    5 CONTINUE
      GO TO 10
    9 IF (SUM.NE.ZERO) IW=1
   10 X(I)=SUM*UL(I,NC1)
   15 CONTINUE
   20 X(N)=X(N)*UL(N,NC1)
      IF (N.LE.1) GO TO 40
      N1=N+1
      DO 35 I=2,N
      K=N1-I
      SUM=X(K)
      IF (NC.LE.0) GO TO 30
      KL=K+1
      K1=MIN0(N,K+NC)
      L=1
      DO 25 J=KL,K1
      SUM=SUM-X(J)*UL(J,NC1-L)
      L=L+1
   25 CONTINUE
   30 X(K)=SUM*UL(K,NC1)
   35 CONTINUE
   40 RETURN
      END
```

```
      SUBROUTINE MATCH (I,J,IN,JN)
C
C     MATCH   MATCHES CONNECTING UC'S, TAKING INTO ACCOUNT THAT:
C
C                X(1,I)=X(3,I-1)
C                X(2,I)=X(4,I+NXM1)
C                X(3,I)=X(1,I+1)
C                X(4,I)=X(2,I-NXM1)
C
      COMMON /NTW/ NX,NY
      NXM1=NX-1
      NXM2=NX-2
      K=1
      IS=1
      JS=1
      IF(J.EQ.2.OR.J.EQ.4) K=NXM1
      IF (J.EQ.1.OR.J.EQ.4) IS=-1
      IF (J.EQ.3.OR.J.EQ.4) JS=-1
      IN=I+IS*K
      JN=J+JS*2
      IROW=(I/NXM1)*NXM1
      IF (I.EQ.IROW+1.AND.J.EQ.1) IN=I+NXM2
      IF (I.EQ.IROW.AND.J.EQ.3) IN=I-NXM2
      RETURN
      END
```

```
      SUBROUTINE NET (N,NX,G,X,Y)
C
C     NET   ORGANIZES THE NODE MATRIX IN BAND SYMMETRIC FORM.
C
      IMPLICIT DOUBLE PRECISION (A-H,O-Z)
      DIMENSION Y(N,NX),X(N),G(4,N)
      NXM1=NX-1
      DO 20 I=1,N
      DO 20 J=1,4
   20 Y(I,NX)=Y(I,NX)+G(J,I)
      J=1
      DO 40 I=1,N
      IF (I.GE.NX) Y(I,1)=-G(4,I)
      IF (I.NE.J) THEN
       Y(I,NXM1)=-G(1,I)
      ELSE
      J=J+NXM1
      END IF
   40 CONTINUE
      CALL LEQ1PB (Y,N,NXM1,N,X,N,1,0,D1,D2,IER)
      DO 10 I=1,N
      DO 10 J=1,NX
   10 Y(I,J)=0.D0
      RETURN
      END



      SUBROUTINE NETIMB (IER,IBC,N,NX,G,X,Y)
C
C     NETIMB ORGANIZES THE NODE MATRIX
C     IN A BAND SYMMETRIC FORM TO BE SOLVED BY LEQ1PB
C     USED BY IMBIBITION VERSION
C
      IMPLICIT DOUBLE PRECISION (A-H,O-Z)
      DIMENSION Y(N,NX),X(N),G(4,N)
      NXM1=NX-1
      DO 20 I=1,N
      DO 20 J=1,4
   20 Y(I,NX)=Y(I,NX)+G(J,I)
      J=1
      K=NXM1
      DO 40 I=1,N
      IF (I.GE.NX) Y(I,1)=-G(4,I)
      IF (I.NE.J) THEN
       Y(I,NXM1)=-G(1,I)
       IF (IBC.EQ.3.AND.I.EQ.K) THEN
        Y(I,2)=-G(3,I)
        K=K+NXM1
       END IF
      ELSE
      J=J+NXM1
      END IF
   40 CONTINUE
      CALL LEQ1PB (Y,N,NXM1,N,X,N,1,0,D1,D2,IER)
      DO 10 I=1,N
      DO 10 J=1,NX
   10 Y(I,J)=0.D0
      RETURN
      END



      SUBROUTINE SELECT (IVG,D,X,XVG)
C
C     SELECT  CHOSES COMPARTMENT NUMBER WHERE INTERFACE IS LOCATED.
C
      IMPLICIT DOUBLE PRECISION (A-H,O-Z)
      DIMENSION XVG(1)
      COMMON /EXT/ NCT,NCTE,NSIZE
      D3=D*D*D
      IF (X.LE.XVG(1)*D3) THEN
       IVG=1
       RETURN
      END IF
      DO 10 J=1,NCTE
      IF (X.GT.XVG(J)*D3.AND.X.LE.XVG(J+1)*D3) GO TO 20
   10 CONTINUE
      IVG=NCTE
      RETURN
   20 IVG=J
      RETURN
      END
```

```
      SUBROUTINE SHAPE (ICASE,NPO,IPA,NPB)
C
C     SHAPE GENERATES A RANDOM SHAPE FOR THE GANGLION
C     SHAPE   GENERATES A RANDOM SHAPE FOR THE GANGLION
C
      IMPLICIT DOUBLE PRECISION (A-H,O-Z)
      DIMENSION IPA(1),NPB(1),IPOP(100)
      CHARACTER*30 PRI,PR(50)
      CHARACTER CHAR,STAR,PLUS,BLNK
      COMMON /SEED/ DSEED,R(2000)
      COMMON /NTW/ NX,NY
      IF (NPO.EQ.1) RETURN
      NXM1=NX-1
      IF (ICASE.LT.0) THEN
       IF (ICASE.EQ.-1) ICASE=0
       CALL GGUBS (1000)
       NXI=NX
       NXIM1=NXM1
       NX=2*NXIM1+1
       NXM1=NX-1
       IPA(1)=NPO*(NX-1)+NX/2
       IRG=1
       NSAMP=1
       IP=1
   10  NPOP=0
       DO 40 I=1,IP
       NP=IPA(I)
       DO 30 J=1,4
       CALL MATCH (NP,J,IN,JN)
       DO 20 K=1,IP
       IF (IN.EQ.IPA(K)) GO TO 30
   20  CONTINUE
       NPOP=NPOP+1
       IPOP(NPOP)=IN
   30  CONTINUE
   40  CONTINUE
       RI=R(IRG)
       IRG=IRG+1
       IF (RI.LT.1.D0) THEN
        DR=1./NPOP
        RN=0.
        I=0
   45   I=I+1
        RN=RN+DR*I
        IF (RI.GT.RN) GO TO 45
       ELSE
        I=NPOP
       END IF
       IP=IP+1
       IPA(IP)=IPOP(I)
       DO 50 I=1,IP-1
       K1=IP-I+1
       DO 50 K=I+1,IP
       K2=IP+1-K
       IF (IPA(K1).GT.IPA(K2)) GO TO 50
       IT=IPA(K2)
       IPA(K2)=IPA(K1)
       IPA(K1)=IT
   50  CONTINUE
       IF (IP.LT.NPO) GO TO 10
       ICOL=1000
       DO 70 I=1,NPO
       ICO=IPA(I)
   60  ICO=ICO-NXM1
       IF (ICO.GT.NXM1) GO TO 60
       IF (ICO.LT.ICOL) ICOL=ICO
   70  CONTINUE
       IDIF=ICOL-3
       DO 80 I=1,NPO
       IPA(I)=IPA(I)-IDIF
   80  CONTINUE
       IROW=IPA(1)/NXM1
       IDIF=(IROW-2)*NXM1
       DO 90 I=1,NPO
       IPA(I)=IPA(I)-IDIF
   90  CONTINUE
       DO 100 J=1,NPO
```

```
      JROW=IPA(J)/NXM1
      IPA(J)=IPA(J)-JROW*NXIM1
  100 CONTINUE
      NX=NXI
      NXM1=NXIM1
     END IF
     IF (ICASE.GE.0) THEN
      STAR='*'
      PLUS='+'
      BLNK=' '
      IROW=IPA(1)/NXM1
      ICOL=1000
      DO 120 I=1,NPO
      ICO=IPA(I)
  110 ICO=ICO-NXM1
      IF (ICO.GT.NXM1) GO TO 110
      IF (ICO.LT.ICOL) ICOL=ICO
  120 CONTINUE
      PRI=BLNK
      KROW=IROW
      KCOL=ICOL
      NROW=1
      J=1
  130 IF (J.LE.NPO) THEN
       JROW=IPA(J)/NXM1
       IF (JROW.EQ.KROW) THEN
        JCOL=IPA(J)
  140   JCOL=JCOL-NXM1
        IF (JCOL.GT.NXM1) GO TO 140
  160   IF (JCOL.EQ.KCOL) THEN
         IF (ICASE.GT.0) THEN
          DO 170 I=1,ICASE
          IF (IPA(J).EQ.NPB(I)) THEN
           CHAR=STAR
           GO TO 180
          END IF
  170     CONTINUE
         END IF
         CHAR=PLUS
  180    PRI=PRI(:KCOL-ICOL+1)//CHAR
         KCOL=KCOL+1
         J=J+1
         GO TO 130
        ELSE
         PRI=PRI(:KCOL-ICOL+1)//BLNK
         KCOL=KCOL+1
         GO TO 160
        END IF
       ELSE
        PR(NROW)=PRI
        NROW=NROW+1
        PRI=BLNK
        KROW=KROW+1
        KCOL=ICOL
        GO TO 130
       END IF
      END IF
      PR(NROW)=PRI
     END IF
     DO 200 J=NROW,1,-1
     WRITE (6,1000) PR(J)
  200 CONTINUE
 1000 FORMAT (5X,A30)
     RETURN
     END


     SUBROUTINE SLCTU (U,IU)
C
C    SLCTU  SELECTS THE RANGE FOR THE LOCAL VELOCITY.
C
     IMPLICIT DOUBLE PRECISION (A-H,O-Z)
     COMMON /UN/ UMAX,NUI
     DU=UMAX/NUI
     DO 10 I=1,NUI
     UL=DU*FLOAT(I)
     IF (U.LT.UL) GO TO 20
   10 CONTINUE
     IU=NUI
     RETURN
   20 IU=I
     RETURN
     END
```

```
      SUBROUTINE UERTST (IER,NAME)
C
C     UERTST  IS USED TO PRINT A MESSAGE REFLECTING AN ERROR CONDITION
C             (CALLED BY LEQ1PB AND LUDAPB)
C
      IMPLICIT DOUBLE PRECISION (A-H,O-Z)
      CHARACTER*6 NAME
      CHARACTER*6 NAMSET,NAMEQ
      CHARACTER IEQ
      DATA NAMSET/'UERSET'/
      DATA NAMEQ /'      '/
      DATA LEVEL/4/IEQDF/0/IEQ/'='/
      IF (IER.GT.999) GO TO 25
      IF (IER.LT.-32) GO TO 55
      IF (IER.LE.128) GO TO 5
      IF (LEVEL.LT.1) GO TO 30
      CALL UGETIO (1,NIN,IOUNIT)
      IF (IEQDF.EQ.1) WRITE (IOUNIT,35) IER,NAMEQ,IEQ,NAME
      IF (IEQDF.EQ.0) WRITE (IOUNIT,35) IER,NAME
      GO TO 30
    5 IF (IER.LE.64) GO TO 10
      IF (LEVEL.LT.2) GO TO 30
      CALL UGETIO (1,NIN,IOUNIT)
      IF (IEQDF.EQ.1) WRITE (IOUNIT,40) IER,NAMEQ,IEQ,NAME
      IF (IEQDF.EQ.0) WRITE (IOUNIT,40) IER,NAME
      GO TO 30
   10 IF (IER.LE.32) GO TO 15
      IF (LEVEL.LT.3) GO TO 30
      CALL UGETIO (1,NIN,IOUNIT)
      IF (IEQDF.EQ.1) WRITE (IOUNIT,45) IER,NAMEQ,IEQ,NAME
      IF (IEQDF.EQ.0) WRITE (IOUNIT,45) IER,NAME
      GO TO 30
   15 CONTINUE
      IF (NAME.NE.NAMSET) GO TO 25
      LEVOLD=LEVEL
      LEVEL=IER
      IER=LEVOLD
      IF (LEVEL.LT.0) LEVEL=4
      IF (LEVEL.GT.4) LEVEL=4
      GO TO 30
   25 CONTINUE
      IF (LEVEL.LT.4) GO TO 30
      CALL UGETIO (1,NIN,IOUNIT)
      IF (IEQDF.EQ.1) WRITE (IOUNIT,50) IER,NAMEQ,IEQ,NAME
      IF (IEQDF.EQ.0) WRITE (IOUNIT,50) IER,NAME
   30 IEQDF=0
      RETURN
   35 FORMAT (19H *** TERMINAL ERROR,10X,7H(IER = ,I3,
     &        20H) FROM IMSL ROUTINE ,A6,A1,A6)
   40 FORMAT (36H *** WARNING WITH FIX ERROR  (IER = ,I3,
     &        20H) FROM IMSL ROUTINE ,A6,A1,A6)
   45 FORMAT (18H *** WARNING ERROR,11X,7H(IER = ,I3,
     &        20H) FROM IMSL ROUTINE ,A6,A1,A6)
   50 FORMAT (20H *** UNDEFINED ERROR,9X,7H(IER = ,I5,
     &        20H) FROM IMSL ROUTINE ,A6,A1,A6)
   55 IEQDF=1
      NAMEQ=NAME
   65 RETURN
      END


      SUBROUTINE UGETIO (IOPT,NIN,NOUT)
C
C     UGETIO   IS CALLED INTERNALLY BY USERTST
C
      IMPLICIT DOUBLE PRECISION (A-H,O-Z)
      DATA NIND/5/NOUTD/6/
      IF (IOPT.EQ.3) GO TO 10
      IF (IOPT.EQ.2) GO TO 5
      IF (IOPT.NE.1) GO TO 9005
      NIN=NIND
      NOUT=NOUTD
      GO TO 9005
    5 NIND=NIN
      GO TO 9005
   10 NOUTD=NOUT
 9005 RETURN
      END
```

Appendix B

Description of Dimensionless Unit Cell

As is clear from the formulation of the unit cell model, the volume and single phase conductance of the unit cell, and the volume of oil. the conductance and the pressure drop across the interface for a gate unit cell depend on the unit cell size. In order to avoid calculating all these quantities for all possible sizes of the unit cells, the following dimensionless variables are used in the simulation code. Define the dimensionless axial coordinate in the unit cell as

$$z^{*} = \frac{z}{h/2} \,, \tag{B.1}$$

so that,$(z = h'/2, z^{*} = 1)$ and $(z = h'/2, z^{*} = c_3)$ (see Figure 3.6).

The volume of oil in unit cell is given by

$$v(z_i) = f(z_i^{*})\, d^3 \,, \tag{B.2}$$

where

$$f(z^{*}) = \frac{c_2}{16}\left\{\left[(c_1+1)^2 + \frac{(c_1-1)^2}{2}\right]\pi z^{*} - 2\left(c_1^2-1\right)\sin(\pi z^{*}) + \frac{(c_1-1)^2}{4}\sin(2\pi z^{*})\right\} \,, \tag{B.3}$$

and d is the unit cell throat diameter. Similarly,

$$v_{UC} = f(c_3)\, d^3 \tag{B.4}$$

$$v_{EUC} = f(1)\, d^3 \ , \tag{B.5}$$

where v_{UC} is the unit cell volume, and v_{EUC} is the volume of the extended unit cell.

The conductance of a gate unit cell is given by

$$G(z_i) = G^*(z_i^*)\, d^3 \ , \tag{B.6}$$

where z_i is the axial position of the interface,

$$G^*(z_i^*) = \left\{ \frac{2^{10}\mu_w c_2}{\pi^2 (c_1+1)^4} \left[\Psi\left(-c_3, z_i^*\right) + \kappa \Psi\left(z_i^*, c_3\right) \right] \right\}^{-1} \ , \tag{B.7}$$

and $\Psi(z_1^*, z_2^*)$ is given by Equation 3.26, noting that now

$$x = \frac{2\pi z}{c_2 d} = \pi\, c_3 \tag{B.8}$$

Finally, the pressure drop across an interface is given by

$$\Delta P_i(z_i) = \frac{1}{d}\, \Delta P_i^*(z_i^*) \ , \tag{B.9}$$

where

$$\Delta P_i^*(z_i^*) = 2\, \sigma_{ow}\, \frac{\cos(\beta)}{r_w^*(z_i^*)} \ , \tag{B.10}$$

$$r_w^*(z^*) = \frac{1}{4}\left[(c_1+1) - (c_1-1)\cos\left(\pi z^*\right) \right] \ , \tag{B.11}$$

$$\cos(\beta) = \frac{\cos(\theta) + \sin(\theta)\tan(\alpha)}{\left(1+\tan^2(\alpha)\right)^{1/2}} \ , \tag{B.12}$$

$$\tan(\alpha) = \frac{d\left(r_w(z)\right)}{dz} = \frac{\pi}{2c_2}(c_1-1)\sin\left(2\pi z^*\right) \ , \tag{B.13}$$

Appendix C

Determination of the Porous Medium Model Constants for the Monolayer Square Beadpack Network

Consider the unit cell of Figure 3.1. The wall profile is given by

$$r_w(z) = \frac{1}{4}\left[(a+d) - (a-d)\cos\left(\frac{2\pi z}{h}\right)\right] , \qquad (C.1)$$

where d is the throat diameter, $a = c_1 d$ and $h = c_2 d$. The unit cell corresponds to the segment $(-h'/2 < z \leq h'/2)$, where $h' = c_2 c_3 d$.

The unit cell volume is obtained by integration of Equation C.1

$$v_{UC} = f(c_1, c_2, c_3)\, d^3 , \qquad (C.2)$$

where

$$f(c_1, c_2, c_3) = \frac{c_2}{16}\left\{\left[(c_1+1)^2 + \frac{(c_1-1)^2}{2}\right]\pi c_3 - 2\left(c_1^2 - 1\right)\sin(\pi c_3) + \frac{(c_1-1)^2}{4}\sin(2\pi c_3)\right\} , \qquad (C.3)$$

The values of d, c_1, c_2 and c_3 corresponding to the Monolayer Square Beadpack Apparatus used by Hinkley (1983) are calculated below.

Due to the density difference between the oleic and the aqueous phases, the oil ganglion is contained in the space between the upper half section of the glass beads and the overlying plate. For this reason, only this space is considered in the remainder of this calculation. Furthermore, experimental data shows that the ganglion does not occupy the total pore volume, v_{pore}. The void volume fraction that is not occupied by oil is defined as

$$S \equiv \frac{v_{pore} - v_{CEVS}}{v_{pore}} , \qquad (C.3)$$

where v_{CEVS} is the volume of the CEVS, i.e. the actual volume of oil in the pore. By geometrical considerations, it follows that

$$v_{CEVS} = \frac{1}{2}\left(1 - \frac{\pi}{6}\right)(1 - S) d_g^3 , \qquad (C.4)$$

where d_g is the diameter of the glass bead. By definition of CEVS

$$v_{UC} = \frac{1}{2} v_{CEVS} = \frac{1}{4}\left(1 - \frac{\pi}{6}\right)(1 - S)\, d_g^3 . \qquad (C.5)$$

The cross-sectional area at the pore throat is given by

$$A_d = \left(\frac{1}{2} - \frac{\pi}{8}\right)(1 - S)\, d_g^2 = \frac{\pi}{4} d^2 , \qquad (C.6)$$

and the cross-sectional area at the pore chamber is given by

$$A_D = \frac{1}{2}(1 - S)\, d_g^2 = \frac{\pi}{4} a^2 . \qquad (C.7)$$

Rearranging Equations C.6 and C.7, it follows that

$$d = \sqrt{\left(\frac{2}{\pi} - \frac{1}{2}\right)(1 - S)}\, d_g , \qquad (C.8)$$

and

$$a = \sqrt{\frac{2}{\pi}(1 - S)}\, d_g \ . \qquad (C.9)$$

Equating $a = c_1 d$, it follows

$$c_1 = \sqrt{\frac{4}{4 - \pi}} \ . \qquad (C.10)$$

Finally, c_2 and c_3 are correlated by imposing the same volume for the prototype and the unit cell model

$$v_{UC} = f(c_1, c_2, c_3)\, d^3 = \frac{1}{4}\left(1 - \frac{\pi}{6}\right)(1 - S)\, d_g^3 \ . \qquad (C.11)$$

To close the problem c_2 was calculated for several values of c_3 , and the pair of values giving the best values of k, the absolute permeability, and of R_{min} and R_{max}, the minimum and maximum radii of curvature, was chosen.

Appendix D

Determination of the Hydraulic Conductance Equivalent to a Long Network

Consider a network of unit cells with unit block size equal to $N_x \times N_y$. The pressure drop across the length of the network (ℓN_y) is given by ΔP. In the remainder of this Appendix this network will be referred as the "short" network.

Replace the last column of unit cells in the far right with a set of resistors, $\{R_1, R_2 \ldots R_{N_x-1}\}$, whose equivalent resistance, $\mathcal{R}$, corresponds to a network of length L. The short network is assumed to be much shorter than the "long" network ($L \gg \ell N_y$). L is calculated so that the imposed pressure drop, ΔP_L, across the entire network results in a nearly constant value of the capillary number

$$Ca = \frac{v_f \mu_w}{\sigma_{ow}} \ . \tag{D.1}$$

For a network initially filled with oil, Darcy's law gives

$$v_f = \frac{k}{\mu_o} \nabla P = \frac{k}{\mu_o} \frac{\Delta P_L}{L} \ . \tag{D.2}$$

Combining Equations D.1 and D.2

$$L = \frac{k}{\kappa Ca \sigma_{ow}} \Delta P_L \ . \tag{D.3}$$

In order to keep a constant capillary number, the imposed pressure drop has to be of the same order of magnitude of the pressure drop resulting from the capillary forces, $\Delta P_L = O(\Delta P_c)$. The capillary pressure drop may be estimated as

$$\Delta P_c = \frac{4\sigma_{ow}\cos(\theta)}{\langle d \rangle} \ , \tag{D.4}$$

where $\langle d \rangle$ is the average throat diameter. Replacing in Equation D.3

$$L = \frac{4k\cos(\theta)}{\kappa Ca\,\langle d \rangle} \ . \tag{D.5}$$

The equivalent resistance is given by

$$\mathcal{R} = \frac{R_L}{N_x - 1} = \frac{1}{(N_x - 1)G_L} \ , \tag{D.6}$$

where the resistors $\{R_1 . R_2 \ldots R_{N_x - 1}\}$ are assumed to have all the same resistance value, R_L , or conversely, the same conductance, G_L . Rearranging

$$\mathcal{G} = \frac{1}{\mathcal{R}} = (N_x - 1)G_L \ , \tag{D.7}$$

where $\mathcal{G}$ is the equivalent conductance.

The total flow rate, Q, can be expressed in terms of ΔP_L as

$$Q = \mathcal{G}\Delta P_L \ . \tag{D.8}$$

Combining equations D.2, D.7 and D.8,

$$G_L = \frac{A\,k}{(N_x - 1)\mu_o L} \ , \tag{D.9}$$

where A, the network cross-sectional area can be expressed as

$$A = \ell^2(N_x - 1) \ . \tag{D.10}$$

Replacing above

$$G_L = \frac{\ell^2 k}{\mu_o L} \ . \qquad (D.11)$$

For computational reasons, it is convenient to express this result in terms of an equivalent unit cell diameter. Equation B.6 cam be expressed as

$$G_L = G^* d_L^3 \ , \qquad (D.12)$$

where G^* is the hydraulic conductance of the dimensionless unit cell. Rearranging and combining with Equation D.11

$$d_L = \left(\frac{\ell^2 k}{\mu_o L G^*} \right)^{\frac{1}{3}} \ . \qquad (D.13)$$

Notation

Roman letters

a	maximum diameter of the extended unit cell, Figure 3.1
a'	maximum diameter of the unit cell, Figure 3.1
$a_d(d)$	acceptance fraction
a_{jk}	element of matrix $\underline{\underline{A}}$
a_K	maximum diameter of the gate unit cell with index K
$\underline{a}_1, \underline{a}_2, \underline{a}_3, \underline{a}_4$	parameter vectors, Equations 2.14 and 2.15
A	network cross-sectonal area
$\underline{\underline{A}}$	reduced incidence matrix
A_d	cross-sectional area at the pore throat
A_D	cross-sectional area at the pore chamber
b	constant defined by Equation 3.27
c_1, c_2, c_3	modified P-T-T unit cell model constants defined by Equations 3.2 and 3.3
C_{ij}	probability of coalescence given a collision
Ca	capillary number
Ca_{cr}	critical capillary number for ganglion mobilization
d	throat diameter
d_g	grain diameter
d_I	throat diameter of the gate unit cell with index I
d_L	diameter of each unit cell forming the "tail" corresponding to the "long" network, Equation D.13
D	chamber diameter

D_b	chamber diameter corresponding to P_b
D_{bc}	chamber diameter corresponding to P_{bc}
D_{xy}	variable used to calculate the pressure drop along the network, Equation 3.18
$f(s)$	ganglion size frequency distribution function, expressed in terms of s
$f(v^*)$	ganglion size frequency distribution function, expressed in terms of v^*
f_0	extrapolated value of $f(s)$ at $s = 1$
$F_d(d)$	throat size probability distribution function
g_{ik}	element of matrix $\underline{\underline{G}}$
G	hydraulic conductance of unit cell
$\mathcal{G}$	conductance equivalent to the "long" network, Equation D.7
G^*	dimensionless hydraulic conductance of unit cell
$\underline{\underline{G}}$	branch conductance matrix
G_{eff}	effective conductance for a gate unit cell
G_L	conductance of each unit cell forming the "tail" corresponding to the "long" network, Equation D.7
Gm	ganglion mobilization number, Equation 2.10
h	length of extended unit cell, Figure 3.1
h'	length of unit cell, Figure 3.1
J	gaussian curvature of the oil-water interface
J_{dr}	maximum stable curvature or drainage curvature
$J_{dr,I}$	drainage curvature in the gate unit cell with index I
$J_{imb,K}$	imbibition curvature in the gate unit cell with index K
J_{imb}	minimum stable curvature or imbibition curvature
J_{neck}	curvature of oil-water interface formed by an oil thread
k	absolute permeability
$\underline{\underline{k}}$	permeability tensor
k_{ij}	element of permeability tensor $\underline{\underline{k}}$
k_{rw}	relative permeability to water
K_{ij}	collision-coalescence kernel functions
ℓ	length of periodicity of the porous medium, Figure 3.2
L	length of liquid column, Equation 2.1; also length of "long" network, Figure D.1
L_g	projected length of ganglion
m	fraction of fluid remaining in the tube, Equation 2.3a
$n(z,t;v)\Delta v$	number of moving v-ganglia per unit porous medium volume
N_b	total number of branches in the unit block
N_c	number of compartments in which a unit cell is divided

N_I, N_N	number of unt cells along the y-axis up to positions I and N in the network, respectively, Figure 3.5
N_J, N_M	number of unt cells along the x-axis up to positions J and M in the network, respectively, Figure 3.5
N_p	total number of nodes in the unit block
N_x	number of unit cells along the x-axis in the unit block
N_y	number of unit cells along the y-axis in the unit block
N_z	number of unit cells along the z-axis in the unit block
$\underline{p}$	node voltage vector
p_k	element of vector $\underline{p}$
P	pressure
P_b	applied back pressure to attain quasistatic imbibition invasion percolation
P_{bc}	percolation threshold
$P_I, P_J,$ P_M, P_N	pressure at locations I, J, M and N, respectively, Figure 3.5
P_o	pressure in oleic phase
P_w	pressure in aqueous phase
P_0, P_1	pressure at plane 0 and plane 1, respectively, Figure 3.5
$\underline{q}$	branch current vector
q_j	element of vector $\underline{q}$
$\underline{q}_s$	node current source vector
q_{s_k}	element of $\underline{q}_s$
q_{uc}	flow rate through unit cell
r	tube radius
$r_w(z)$	unit cell radius at axial position z, Figure 3.1
r_w^*	dimensionless unit cell radius
$\mathcal{R}$	resistance equivalent to the "long" network, Equation D.6
R_{ij}	collision kernel functions for interception
R_L	resistance of each unit cell forming the "tail" corresponding to the "long" network, Equation D.6
R_{max}, R_{min}	maximum and minimum radii of curvature in the monolayer square beadpack, respectively. Equations 4.1 and 4.2
R_1, R_2	principal radii of curvature
Re	Reynolds number
s	number of CEVS's (chambers) occupied by ganglion
S	volume fraction not occupied by oil in Hinkley's (1983) experimental apparatus, Equation C.1
S_{or}	residual oil saturation
S_w	water saturation

S_{wi}	initial water saturation
t	time
u^*	reduced time-averaged ganglion velocity
u_i	local velocity of the interface
u_z	ganglion velocity
$\overline{u}_z$	time-averaged ganglion velocity
v	volume of oil ganglion
v^*	reduced ganglion volume
$\underline{v}$	velocity vector
$\underline{v}_b$	branch voltage vector
v_{b_j}	element of vector $\underline{v}_b$
v_{CEVS}	average volume of CEVS
v_{EUC}	volume of extended unit cell
v_f	superficial velocity of flood
v_i	interstitial velocity of aqueous phase
v_{pore}	average volume of pore
$\underline{v} - s$	branch voltage source vector
v_{s_j}	element of vector $\underline{v}_s$
v_{UC}	volume of unit cell
v_0	mean velocity at the throat cross section in a unit cell
w	volume of a w-ganglion
$W(u,v)\Delta v$	probability that a moving w-ganglion will break into two daughter ganglia, one of which is a v-ganglion
x	variable defined by Equation 3.28
y_{kk}	self admitance of node k; element of matrix $\underline{\underline{Y}}$
y_{lk}	mutual admitance between nodes l and k; element of matrix $\underline{\underline{Y}}$
$\underline{\underline{Y}}$	node conductance matrix
z	cartesian coordinate in the direction of the flood; also, axial coordinate in the unit cell, Figure 3.1
z^*	dimensionless axial coordinate in the unit cell, Equation B.1
z_i	axial coordinate of the position of the interface in the unit cell
z'	axial coordinate in the unit cell taken from the end of the unit cell, Figure 3.6

Greek letters

$\beta(z,t;v)\Delta v$	number of v-ganglia that fissioned a position z per unit porous medium volume
β_{KI}	maximum value of the appendix mobility factor, Equation 2.9

γ	exponent, Equation 2.5
δ	thickness of traveling slug of v-ganglia
$\underline{\underline{\delta}}$	Kronecker delta tensor
δ_{ij}	element of $\underline{\underline{\delta}}$
ΔL_{KI}	distance between throats of gate unit cells with indexes K and I
ΔP	pressure drop
ΔP^*	dimensionless pressure drop along an extended unit cell
ΔP_c	capillary pressure drop across an oil-water interface
ΔP_{cr}	critical pressure drop for ganglion mobilization, Equation 5.5
ΔP_{eff}	effective pressure drop across an oil-water interface
ΔP_i	pressure drop across an oil-water interface
ΔP_i^*	dimensionless pressure drop across an oil-water interface
ΔP_L	pressure drop across "long" network, Equation d.2
ΔP_{uc}	pressure drop along a unit cell
ΔP_1^*	value of ΔP^* at $Re = 1$
ϵ	porosity of the porous medium
ζ	reduced average radius of influence of ganglion presence on the pressure field
θ	apparent contact angle as measured from the wetting phase
θ_a, θ_r	advancing and receding dynamic contact angles
θ_a^o, θ_r^o	advancing and receding dynamic contact angles in the limit as u_i tends to zero
θ_e	equilibrium contact angle
θ_{KI}	angle between the line connecting the throats of gate unit cells K and I and the macroscopic flow direction
θ_1, θ_2	contact angles at the sphere surface and at the overlying plate, respectively, in monolayer square beadpack
κ	oil-water viscosity ratio
λ	stranding coefficient, Equation 4.3
μ	viscosity
μ_o	viscosity of oleic phase
μ_w	viscosity of aqueous phase
ν	kinematic viscosity
ξ	dimensionless film thickness, Equation 2.3b
ρ	density
$\sigma(z,t;v)\Delta v$	number of stranded v-ganglia per unit porous medium volume
σ_{os}	interfacial tension at the oil-solid interface
σ_{ow}	interfacial tension at the oil-water interface
σ_{ws}	interfacial tension at the water-solid interface

τ	transformed time, Equation 4.2
ϕ	breakup coefficient, Equation 4.4
ϕ'	angle between the direction of the macroscopic pressure gradient and the horizontal axis
χ	number of v-ganglia moving at position z divided by the initial number of v-ganglia, Equation 4.7
ψ	number of v-ganglia stranded in the interval $(z - \Delta z/2, z + \Delta z/2)$ divided by the initial number of v-ganglia, Equation 4.8
Ψ	function defined by Equation 2.28
ω	number of v-ganglia fissioned in the interval $(z - \Delta z/2, z + \Delta z/2)$ divided by the initial number of v-ganglia, Equation 4.9

Literature References

- Arriola, A., Willhite, G.P. and Green, D.W., "Trapping of Oil Drops in a Noncircular Pore Throat and Mobilization upon Contact with a Surfactant", *Soc. Pet. Eng. J.*, 23, 99–114 (1983)
- Barber, A.D. and Hartland, S., "The Effects of Surface Viscosity on the Axisymmetric Drainage of Planar Liquid Films", *The Can. J. Chem. Eng.*, 54, 279–284 (1976)
- Bartell, F.E. and Shepperd, J.W., "Surface Roughness as Related to Hysteresis of Contact Angles. I", *J. Phys. Chem.*, 57, 211–215 (1953)
- Bartell, F.E. and Shepperd, J.W. , "Surface Roughness as Related to Hysteresis of Contact Angles. II", *J. Phys. Chem.*, 57, 455–458 (1953)
- Batycky, J.P., "Dependence of Residual Oil Mobilization on Wetting and Roughness", in *Surface Phenomena in Enhanced Oil Recovery*, D.O. Shah (ed.), Plenum Press, New York, 1981
- Batycky, J.P. and Singhal, A.K., "Mobilization of Entrapped Ganglia", Research Report RR-35, Petroleum Recovery Institute, Calgary, Canada, 1977
- Bear, J., *Dynamics of Fluids in Porous Media*, American Elsevier, New york, 1972
- Bikerman, J.J., *Surface Chemistry*, Academic Press, New York, 1958
- Blake, T.D., *The Contact Angle and Two-Phase Flow*, Ph.D. Thesis, Univ. of Bristol, Great Britain, 1968
- Blake, T.D., Everett, D.H. and Haynes, J.M., "Some Basic Considerations Concerning the Kinetics of Wetting Processes in Capillary Systems", *Soc. Chem. Ind., London*, Monograph No. 25, 164–173 (1967)
- Blake, T.D. and Haynes, J.M., "Kinetics of Liquid/Liquid Displacement", *J. Colloid Interface Sci.*, 30, 421–423 (1969)
- Blumberg, R.L., Shlifer, G. and Stanley H.E., "Monte Carlo Tests of Universality in a Correlated-Site Percolation", *J. Phys. A*, 13, L147–L152 (1980)

Interface Sci., 47(2), 337–349 (1974)
- Dullien, F.A.L. and Dhawan, G.K., "Effects of Pore Structure and Capillary and Flow Phenomena in Sandstones", *J. Can. Pet. Tech.*, 14(3), 48–55 (1975)
- Dullien, F.A.L. and Dhawan, G.K., "Bivariate Pore-Size Distribution of Some Sandstones", *J. Colloid Interface Sci.*, 52(1), 129–135 (1975)
- Dussan V., E.B., "On the Spreading of Liquids on Solids Surfaces: Static and Dynamic Contact Lines", *Ann. Rev. Fluid Mech.*, 11, 371–400 (1979)
- Dussan V., E.B., "The Moving Contact Line: The Slip Boundary Condition", *J. Fluid Mech.*, 77, 665–684 (1976)
- Dussan V., E.B. and Davis, S.H., "On the Motion of a Fluid-Fluid Interface Along a Solid Interface", *J. Fluid Mech.*, 65, 71–95 (1974)
- Egbogah, E.O. and Dawe, A., "A Model of Oil Ganglion Movement in Porous Media", SPE 10115, 56th Annual Fall Tech. Conf. and Exhib. of SPE, San Antonio, Texas, Oct. 5–7, 1981
- Ehrlich, R. and Crane, F.E., "A Model for Two-Phase Flow in Consolidated Materials", *Soc. Pet. Eng. J. Trans.*, 246, 221–231 (1969)
- Elliot, G.E.P. and Riddiford, A.C., "Dynamic Contact Angles I. The Effect of Impressed Motion", *J. Colloid Interface Sci.*, 23, 389–398 (1967)
- Essam, J.W., "Percolation Theory", *Rep. Prog. Phys.*, 43, 833–912 (1980)
- Fairbrother, F. and Stubbs, A.E., "Studies in Electro-Endosmosis VI. 'Bubble-Tube' Method of Measurement", *J. Chem. Soc.*, 1, 527–529 (1935)
- Fatt, I., "The Network Model of Porous Media I. Capillary Pressure Characteristics", *Trans. AIME*, 207, 44–159 (1956a)
- Fatt, I., "The Network Model of Porous Media II. Dynamic Properties of a Single Size Tube Network", *Trans. AIME*, 207, 160–163 (1956b)
- Fatt, I., "The Network Model of Porous Media III. Dynamic Properties of Networks with Tube Radius Distribution", *Trans. AIME*, 207, 164–181 (1956c)
- Fedkiw, P. and Newman J., "Mass Transfer at High Péclet Numbers for Creeping Flow in a Packed Bed Reactor", *AIChE J.*, 23, 255–263 (1977)
- Fisher, L.R. and Lark, P.D., "An Experimental Study of the Washburn Equation for Liquid Flow in Very Fine Capillaries", *J. Colloid Interface Sci.*, 69, 486–492 (1979)
- Flumerfelt, R.W., Catalano, A.B. and Tong, C.H., in *Surface Phenomena in Enhanced Oil Recovery*, D.O.Shah (ed.), Plenum Press, New York, 1981
- Flumerfelt, R.W., Oppenheim, J.P. and Son, J.R., "Magnitude and Role of Dynamic Interfacial Effects in Low Tension Flooding", *AIChE J.*, 212, 113–126 (1982)
- Fontugne, D.J., *Permeability Measurements in Anisotropic Media*, M.S. Thesis, Syracuse University, Syracuse, New York, 1969
- Frisch, H.L. and Hammersley, J.M., "Percolation Processes and Related Topics", *J. Soc. Ind. Appl. Math.*, 11, 894–918 (1963)

- Broadbent, S.R. and Hammersley, J.M., "Percolation Processes I. Crystals and Mazes", *Proc. Cambridge Phil. Soc.*, 53, 629–645 (1957)
- Bretherton, F.P., "The Motion of Long Bubbles in Tubes", *J. Fluid Mech.*, 10, 166–186 (1961)
- Buckley, S.E. and Leverett, M.C., "Mechanisms of Fluid Displacement in Sands", *Trans. AIME*, 146, 107–116 (1942)
- Chandler, R., Koplik, J., Lerman, K. and Willemsen, J.F., "Capillary Displacement and Percolation in Porous Media", *J. Fluid Mech.*, 119, 249–267 (1982)
- Chatzis, I. and Dullien, F.A.L., "Mercury Porosimetry Curves of Sandstones. Mechanisms of Mercury Penetration and Withdrawal", *Powder Tech.*, 29, 117–125 (1981)
- Chatzis, I. and Dullien, F.A.L., "Dynamic Immiscible Displacement in Pore Doublets. Theory versus Expertiment", *J. Colloid Interface Sci.*, 91, 199–222 (1983)
- Chatzis, I., Morrow, N.R. and Lim, H.T., "Magnitude and Detailed Structure of Residual Oil Saturation", *Soc. Pet. Eng. J.*, 23, 311–326 (1983)
- Chen, J.D. and Slattery, J.C., "Effects of London-van der Walls Forces in the Thinning of a Dimpled Liquid Film as a Small Drop or Bubble Approaches a Horizontal Solid Plane", *AIChE J.*, 28, 955–963 (1982)
- Choquette, P.W. and Pray, L.C., "Geological Nomenclature and Classification of Porosity in Sedimentary Carbonates", in *Carbonate Rocks II : Porosity and Classification of Reservoir Rocks*, AAPG Repr. Ser., 5, 154–197 (1972)
- Chow, J.C.F. and Soda, K., "Laminar Flow in Tubes with Constriction", *Phys. Fluids*, 15, 1700–1706 (1972)
- Claridge, E.L., "Discussion of the Use of Capillary Tube Networks in Reservoir Performance Studies",*Soc. Pet. Eng. J.*, 12, 352–361 (1972)
- Cox, B.G., "On Driving a Viscous Fluid Out of a Tube", *J. Fluid Mech.*, 14, 81–96 (1963)
- Craig, F.F.,Jr., *The Reservoir Engineering Aspects of Waterflooding*, SPE of AIME Monograph, Dallas, Texas, 1971
- Davis, J.A. and Jones, S.C., "Displacement Mechanisms of Micellar Solutions", *J. Pet. Tech.*, 20, 1415–1428 (1968)
- de Gennes, P.G. and Guyon, E., "Lois Générales pour l'Injection d'un Fluid dans un Millieux Alièatoire", *J. de Mécanique*, 7, 403–432 (1978)
- Deiber, J.A. and Schowalter, W.R., "Flow Through Tubes with Sinusoidal Axial Variations in Diameter", *AIChE J.*, 25, 638–644 (1979)
- Desoer, C.A. and Huh, E.S., *Basic Circuit Theory*, McGraw-Hill, 1969
- Dettre, R.H. and Johnson, R.E., Jr., "Contact Angle Hysteresis II. Contact Angle Measurements on Rough Surfaces", in *Contact Angle, Wettability and Adhesion : Advances in Chemistry Series*, American Chemical Society, 43, 136–144 (1964)
- Dullien, F.A.L. and Dhawan, G.K., "Characterization of Pore Structure by a Combination of Quantitative Photomicrography and Mercury Porosimetry", *J. Colloid*

- Giordano, R.M. and Slattery, J.C., "Stability of Static Interfaces in a Sinusoidal Capillary", *J. Colloid Interface Sci.*, 92, 13–24 (1983)
- Goldsmith, H.L. and Mason, S.G., "The Flow of Suspensions Through Tubes II. Single Layer Bubbles", *J. Colloid Interface Sci.*, 18, 237–261 (1963)
- Goren, S.L., "The Instability of an Annular Thread of Fluid", *J. Fluid Mech.*, 12, 309–312 (1962)
- Greenkorn, R.A., Johnson, C.R. and Shallenberger, L.K., "Directional Permeability of Heterogeneuos Anisotropic Porous Media", *Soc. Pet. Eng. J.*, 4, 124–132 (1964)
- Haines, W.B., "Studies in the Physical Properties of Soil V. The Hysteresis Effect in Capillary Properties and the Modes of Moisture Distribution Associated Therewith", *J. Agric. Sci.*, 20, 97–116 (1930)
- Hall, A.C., Collins, S.H. and Melrose, J.C., "Stability of Aqueous Wetting Films in Athabasca Tar Sands", 23, 249–258 (1983)
- Hammond, P.S., "Non-linear Adjustment of a Thin Annular Film of Viscous Fluid Surrounding a Thread of Another Within a Circular Cylindrical Pipe", *J. Fluid Mech.*, in press (1983)
- Hammond, P.S., "Non-Linear Adjustment of an Annular Film of Viscous Fluid Within an Axisymmetric Constricted Pipe", *J. Fluid Mech.*, to be submitted (1984)
- Handy, L.L., Datta, P., "Fluid Distributions During Immiscible Displacements in Porous Media". *Soc. Pet. Eng. J.*, 6, 261–266 (1966)
- Haring, R.E. and Greenkorn, R.A., "Statistical Model of a Porous Medium with Non-uniform Pores", *AIChE J.*, 16, 477–483 (1970)
- Hartland, S., "The Coalescence of a Liquid Drop at a Liquid-Liquid Interface. Part II. Film Thickness", *Trans. Inst. Chem. Engrs. (London)*, 45, T102–T108 (1967)
- Healy, R.N. and Reed, R.L., "Physicochemical Aspects of Microemulsion Flooding", *Soc. Pet. Eng. J.*, 14, 491–501 (1976)
- Healy, R.N., Reed, R.L. and Stenmark, D.G., "Multiphase Microemulsion Systems", *Soc. Pet. Eng. J.*, 16, 147–160 (1976)
- Heller, J.P., "The Drying Through the Top Surface of a Vertical Porous Column", *Soil. Sci. Soc. Am. Proc.*, 32, 778–786 (1968)
- Hinkley, R.E., *Oil Ganglion Motion*, M.S. Thesis, Univ. of Houston, Houston, Texas, 1982
- Hocking, L.M., "A Moving Fluid Interface on a Rough Surface", *J. Fluid Mech.*, 76, 801–817 (1976)
- Hocking, L.M., "A Moving Fluid Interface. Part 2. The Removal of the Force Singularity by a Slip Flow", *J. Fluid Mech.*, 79, 209–229 (1977)
- Hoffman, R.L., "A Study of the Advancing Interface I. Interface Shape in Liquid-Gas Systems", *J. Colloid Interface Sci.*, 50, 228–241 (1975)
- Hubbert, M.K., "Systematic Packing of Spheres - with Particular Relation to Porosity and Permeability", *J. Geology*, 43, 785–944 (1940)

- Huh, C. and Mason, S.G., "The Steady Movement of a Liquid Meniscus in a Capillary Tube", *J. Fluid Mech.*, 81, 401–419 (1977a)
- Huh, C. and Mason, S.G., "Effects of Surface Roughness on Wetting (Theoretical)", *J. Colloid Interface Sci.*, 60, 11–38 (1977b)
- Huh, C. and Scriven, L.E., "Hydrodynamic Model of Steady Movement of a Solid-Liquid-Fluid Contact Line", *J. Colloid Interface Sci.*, 35, 85–101 (1971)
- Jacquin, C. and Legait, B., "Influence of Capillarity and Viscosity During Spontaneous Imbibition in Porous Media and in Capillaries", to appear, 1983
- Jamin, J., "Mémoire sur l'Équilibre et le Movement des Liquides dans les Corps Poreux", *C.R.H. Acad. Sci. Paris*, 50, 172,176 (1860)
- Jeffreys, V. and Davies, G.A., "Coalescence of Liquid Droplets and Liquid Dispersions", in *Recent Advances in Liquid-Liquid Extratcion*, C. Hanson (ed.), Pergamon Press, 1971
- Johnson, R.E., Jr. and Dettre, R.E., "Contact Angle Hysteresis I. Study of an Idealized Rough Surface", in *Contact Angle, Wettability and Adhesion : Advances in Chemistry Series*, American Chemical Society, 46, 112–135 (1964)
- Johnson, W.E. and Breston, J.N., "Directional Permeability Measurements on Oil Sandstones from Various States", *Prod. Monthly*, 15(4), 10–19 (1951)
- Johnson, W.E. and Hughes, R.V., "Directional Permeability Measurements on Oil Sandstones and their Significance", *Prod. Monthly*, 13(1), 17–25 (1948)
- Josselin de Jong, G., "Longitudinal and Transverse Diffusion in Granular Deposits", *Trans. Am. Geophys. Union*, 39, 67–74 (1958)
- Kafka, F.Y. and Dussan V., E.B., "On the Interpretation of Dynamic Contact Angles in Capillaries", *J. Fluid Mech.*, 95, 539–565 (1979)
- Kloubek, J., "Volume and Contact Angle Hysteresis in Mercury Porosimetry of ASC-Whetlerite", *J. Colloid Interface Sci.*, 95, 135–141 (1983)
- Koplik, J., "Creeping Flow in Two-dimensional Networks", *J. Fluid Mech.*, 119, 219–247 (1982)
- Koplik, J. and Lasseter, T.J., "Two-Phase Flow in Random Network Models of Porous Media", SPE 11014, 57th Annual Fall Tech. Conf. and Exhib. of SPE, New Orleans, Louisiana, Sept. 26–29, 1982
- Laidlaw, W.G. and N.C. Wardlaw, "A Theoretical and Experimental Investigation of Trapping in Pore Doublets", *Can. J. Chem. Eng.*, 61, 719–727 (1983)
- Laplace, P.S., "Theory of Capillary Attraction", supplements to the 10^{th} book of *Celestial Mechanics* (1806, 1807), translated and annotated by N. Bowditch (1839). Reprinted by Chelsea, New York, 1966
- Larson, R.G., Davis, H.T. and Scriven, L.E., "Displacement of Residual Nonwetting Fluid from Porous Media", *Chem. Eng. Sci.*, 36, 75–85 (1981)
- Larson, R.G., Scriven, L.E. and Davis, H.T., "Percolation Theory of Residual Phases in Porous Media", *Nature*, 268, 409–413 (1977)

- Larson, R.G., Scriven, L.E. and Davis, H.T., "Percolation Theory of Two Phase Flow in Porous Media", *Chem. Eng. Sci.*, 36, 57–73 (1981)
- Lefevre du Pray, E.J., "Factors Affecting Liquid-Liquid Relative Permeabilities of a Consolidated Porous Medium", *Soc. Pet. Eng. J.*, 13, 39–47 (1973)
- Legait, B., "Influence des Forces d'Inertie et de Viscosité sur la Différence de Pression Nécessaire au Passage d'une Goute, Immiscible avec le Fluid en Place, à Travers un Col", *C.R. Acad. Sci. Paris*, 292, Sér. II, 1111–1114 (1981a)
- Legait, B., "Rupture, en Écoulement Capillaire Diphasique, de la Phase Non Mouillante lors du Passage par un Rétrécissement", Inst. Français du Pét., Réf. 29142, 1981b
- Legait, B., "Laminar Flow of Two-Phases Through a Capillary Tube with Variable Square Cross Section", *J. Colloid Interface Sci.*, 96, 28–38 (1983)
- Legait, B. and Jacquin, C., "Conditions Nécessaires au Passage d'un Col par une Goutte en déplacement dans un Capillaire de Section Carrée, en Régime de Stokes", *C.R. Acad. Sci. Paris*, 294, Sér. II, 487–492 (1982)
- Legait, B., Sourieau, P. and Combarnous, M., "Inertia, Viscosity, and Capillary Forces During Two-Phase Flow in a Constricted Capillary Tube", *J. Colloid Interface Sci.*, 91, 400–411 (1983)
- Lenormand, R. and Bories, S., "Description d'un Mécanisme de Connexion de Liaison Destiné a l'Étude du Drainage avec Piégeage en Millieux Poreux", *C.R. Acad. Sci. Paris*, 291, Sér. B, 279–283 (1980)
- Lenormand, R., Zarcone, C. and Sarr, A., "Mechanism of the Displacement of One Fluid by Another in a Network of Capillary Ducts", *J. Fluid Mech.*, in press (1983)
- Leverett, M.C., "Flow in Oil-Water Mixtures Through Unconsolidated Sands", *Trans. AIME*, 132, 149–171 (1938)
- Leverett, M.C., "Capillary Behaviour in Porous Solids", *Trans. AIME*, 142, 152–169 (1941)
- Lin, C. and Cohen, N.H., "Quasistatic Methods for Microgeometry Modelling", *J. Appl. Phys.*, 53, 4152–4165 (1982)
- Lin. C. and Hamasaki, J., "Pore Geometry: A New System for Quantitative Analysis and 3–D Displays", *J. of Sedimentary Petrology*, 53(2), 670–672 (1983)
- Lin, C.Y. and Slattery, J.C., "Three-Dimensional, Randomized, Network Model for Two-Phase Flow Through Porous Media", *AIChE J.*, 28, 311–324 (1982)
- Lucas, R., "Ueber das Zeitgestz des Kapillaren Aufstiegs von Fhüssigkeiten", *Kolloid Z.*, 23, 15–22 (1918)
- Mahers, E.G., Wright, R.J. and Dawe, R.A., "Visualization of the Behaviour of EOR Reagents in Displacement in Porous Media", European Symposium on Enhanced Oil Recovery, Bournemouth, England, Sept. 21–23, 1981
- Marchessault, R.H. and Mason, S.G., "Flow of Entrapped Bubbles Through a Capillary", *Ind. Eng. Chem.*, 52(1), 79–84 (1960)

- Mason, G. and Yadav, G.D., "Capillary Hysteresis in the Pore Space of a Packing of Spheres Measured by the Movement of Blobs", *J. Colloid Interface Sci.*, 95, 120–130 (1983)
- Mast, R.F and Potter, P.E., "Sedimentary Structures, Sand Shape Fabrics and Permeability, II". *J. of Geology*, 71, 548–565 (1963)
- Mattax, C.C. and Kyte, J.R., "Ever See a Waterflood?", *Oil and Gas J.*, 59 (Oct. 16), 115–128 (1961)
- McKay, G.P. and Mason, S.G., "The Gravity Approach and Coalescence of Fluid Drops at Liquid Interfaces", *The Can. J. Chem. Eng.*, 41, 203–212 (1963)
- McKellar, M. and Wardlaw, N.C., "A Method of Making Two-dimensional Glass Micromodels of Pore Systems", *J. Can. Pet. Tech.*, 21, 39–41 (1982)
- Melrose, J.C., "Wettability as Related to Capillary Action in Porous Media", *Soc. Pet. Eng. J.*, 5, 259–271 (1965)
- Melrose, J.C., "Interfacial Phenomena as Related to Oil Recovery Mechanisms", *The Can. J. Chem. Eng.*, 48, 638–644 (1970)
- Melrose, J.C. and Brandner, C.F., "Role of Capillary Forces in Determining Microscopic Displacement Efficiency for Oil Recovery by Water Flooding", *Can. J. Pet. Tech.*, 13(4), 54–62 (1974)
- Meseguer, J., "The Breaking of Axisymmetric Slender Liquid Bridges", *J. Fluid Mech.*, 130, 123–151 (1983)
- Michael, D.H., "Meniscus Stability", *Ann. Rev. Fluid Mech.*, 13, 189–215 (1981)
- Mikami, R., Cox, R.G. and Mason, S.G., "Breakup of Extended Liquid Threads", *Int. J. Multiphase Flow*, 2, 113–138 (1975)
- Miller, E.E. and Miller, R.D., "Physical Theory for Capillary Flow Phenomena", *J. Appl. Phys.*, 27, 324–332 (1956)
- Mohanty, K.K. and Salter, S.J.,"Multiphase Flow in Porous Media: II. Pore-Level Modelling", SPE 11018 57th Annual Fall Tech. Conf. and Exhib. of SPE, New Orleans, Louisiana, Sept. 26–29, 1982
- Moore, T.F. and Slobod, R. L., "The Effect of Viscosity and Capillarity on the Displacement of Oil by Water", *Prod. Monthly*, 20(10), 20–30 (1956)
- Morrow, N.R., "The Effects of Surface Roughness on Contact Angles with Special Reference to Petroleum Recovery", *J. Can. Pet. Tech.*, 14, 42–53 (1975)
- Muskat, M., *The Flow of Homogeneous Fluids Through Porous Media*, McGraw-Hill, New-York, 1937
- Neira, M.A. and Payatakes, A.C., "Collocation Solution of Creeping Newtonian Flow Through Periodically Constricted Tubes with Piecewise Continuous Wall Profile", *AIChE J.*, 24, 43–54 (1978)
- Neira, M.A. and Payatakes, A.C., "Collocation Solution of Creeping Newtonian Flow Through Sinusoidal Tubes", *AIChE J.*, 25, 725–730 (1979)

- Nelson, R.C. and Pope, G.A., "Phase Relationships in Chemical Flooding", SPE 6773, Cos. Pet. Eng., Dallas, Texas, 1977
- Ng, K.M., *Oil Ganglia Dynamics in Flow Through Porous Media*, Ph.D. Thesis, Univ. of Houston, Houston, Texas, 1980
- Ng, K.M., Davis, H.T. and Scriven, L.E., "Visualization of Blob Mechanisms in Flow Through Porous Media", *Chem. Eng. Sci.*, 33, 1009–1017 (1978)
- Ng, K.M. and Payatakes, A.C., "Stochastic Simulation of the Motion, Break-up and Stranding of Oil Ganglia in Water-Wet Granular Porous Media During Immiscible Displacement", *AIChE J.*, 26, 419–429 (1980)
- Oh, S.G. and Slattery, J.C., "Interfacial Tension Required for Significant Displacement of Oil", *Soc. Pet. Eng. J.*, 19, 83–96 (1974)
- Olbritch, W.L. and Leal, L.G., "The Creeping Motion of Immiscible Drops Through a Circular Tube of Comparable Diameter: The Effect of Density Differences Between Liquids", *J. Fluid Mech.*, 115, 187–216 (1983)
- Olbritch, W.L. and Leal, L.G., "The Creeping Motion of Immiscible Drops Through Converging/Diverging Tubes", *J. Fluid Mech.*, in press (1983)
- Oppenheim, J.P., *Film Drainage: A Mathematical Model*, Ph.D. Thesis, Univ. of Houston, Houston, Texas, 1983
- Padday, J.F., "Theory of Surface Tension", in *Surface and Colloid Science*, E. Matijevic (ed.), 1, 39–251, Wiley, New York, 1969
- Padday, J.F., "Spreading Hysteresis of Water on Wax", 3rd International Congress of Surface Activity, Academic Press, New York, 1960
- Payatakes, A.C., "Dynamics of Oil Ganglion During Immiscible Displacement in Water-Wet Porous Media", *Ann. Rev. Fluid Mech.*, 14, 365–393 (1982)
- Payatakes, A.C. and Dias, M.M., "Immiscible Microdisplacement and Ganglion Dynamics in Porous Media", *Rev. Chem. Eng.*, in press (1984)
- Payatakes, A.C. and Neira, M.A., "Model of the Constricted Unit Cell Type for Isotropic Granular Porous Media", *AIChE J.*, 23, 922–930 (1977)
- Payatakes, A.C., Ng, K.M. and Flumerfelt, R.W., "Oil Ganglia Dynamics During Immiscible Displacement. Model Formulation", *AIChE J.*, 20, 430–443 (1980)
- Payatakes, A.C., Tien, Chi and Turian, R.M., "A New Model for Granular Porous Media-Part I. Model Formulation", *AIChE J.*, 19, 67–76 (1973)
- Payatakes, A.C., Woodham, G. and Ng, K.M., "On the Fate of Oil Ganglia During Immiscible Displacement in Water Wet Granular Porous Media", in *Surface Phenomena in Enhanced Oil Recovery*, D.O. Shah (ed.), Plenum Press, New York, 1981
- Peaceman, D.W., *Fundamentals of Numerical Reservoir Simulation*, Elsevier, Amsterdam, 1977
- Pickell, J.J., Swanson, B.F. and Hickerman, W.B., "Application of Air-Mercury and Oil-Air Capillary Pressure Data in the Study of Pore Structure and Fluid Distribution", *Soc. Pet. Eng. J.*, 6, 55–61 (1966)

- Plateau, J., "The Figures of Equilibrium of a Liquid Mass Withdrawn from the Action of Gravity", *Annual Rep. of the Board of Regents of the Smithsonian Institution*, 83, 228–285 (1864)
- Poiseuille, J.L.M., "Recherches Experimentales sur le Movement des Liquides dans les Tubes de Trés Petits Diamétres", *C.R.H. Acad. Sci. Paris*, 11, 961–967 (1840a); 11, 1041–1048 (1840b); 15, 1167–1186 (1842)
- Potter, P.E., and Mast, R.F "Sedimentary Structures, Sand Shape Fabrics and Permeability, I",*J. of Geology*, 71, 441–471 (1963)
- Prasad, S., *Flow of Newtonian Fluids Through Axisymmetric Converging-Diverging Channels*, M.S. Thesis, Univ. of Houston, Houston, Texas, 1978
- Rapin, S., *Behaviour of Non-Wetting Oil Ganglia Displaced by an Aqueous Phase*, M. S. Thesis, Univ. of Houston, Houston, Texas, 1980
- Rayleigh, Lord, "On the Capillary Phenomena of Jets", *Proc. Roy. Soc., London*, 27, 71–97 (1879)
- Rayleigh, Lord, "On the Instability of a Cylinder of Viscous Liquid under Capillary Force", *Phil. Mag.*, 34, 145–154 (1892)
- Rice, P.A., Fontugne, D.J., Latini R.G. and Barduhn, A.J., "Anisotropic Permeability in Porous Media", *Ind. Eng. Chem.*, 62(6), 23–31 (1970)
- Rillaerts, E. and Joos, P., "The Dynamic Contact Angle", *Chem. Eng. Sci.*, 35, 883–887 (1980)
- Roof, J.G., "Snap-Off of Oil Droplets in Water-Wet Pores", *Soc. Pet. Eng. J. Trans.*, 249, 85–90 (1970)
- Rose, W., "Fluid-Fluid Interfaces in Steady Motion", *Nature*, 191, 242–243 (1961)
- Rose, W. and Cleary, J., "Further Indication of Pore Doublet Theory", *Prod. Monthly*, 22(3), 20–31 (1958)
- Rose, W. and Heins, R.W., "Moving Interfaces and Contact Angle Rate Dependency", *J. Colloid Interface Sci.*, 17, 39–48 (1962)
- Rose, W. and Witherspoon, R.A., "Trapping Oil in a Pore Doublet", *Prod. Monthly*, 21(2), 32–37 (1956)
- Ruschak, K.J., "Boundary Conditions at a Liquid/Air Interface in Lubrication Flows", *J. Fluid Mech.*, 119, 107–120 (1982)
- Sheffield, R.E. and Metzner, A.B., "Flows of Nonlinear Fluids Through Porous Media", *AIChE J.*, 22, 736–744 (1976)
- Scheidegger, A.E., *The Physics of Flow Through Porous Media*, University of Toronto Press, Toronto, Canada, 1974
- Schmidt, V., McDonald, D.A and Platt, R.L., "Pore Geometry and Reservoir Aspects of Secondary Porosity in Sandstones", *Bull. Can. Pet. Geol.*, 25(2), 271–290 (1977)
- Schwartz, A.M., Rader, C.A. and Huey, E., "Resistance to Flow in Capillary Systems of Positive Contact Angle", in *Contact Angle, Wettability and Adhesion :*

Advances in Chemistry Series, American Chemical Society, 43, 250–267 (1964)

- Shante, V.K.S. and Kirkpatrick, S., "An Introduction to Percolation Theory", *Advan. Phys.*, 20, 325–357 (1971)
- Shepperd, J.W. and Bartell, F.E., "Surface Roughness as Related to Hysteresis of Contact Angles. III", *J. Phys. Chem.*, 57, 458–463 (1953)
- Singhal, A.K. and Dranchuk, P.M., "Motion of an Oil-Droplet Through a Water Filled Uneven Pore", *Rév. Inst. Français du Pét.*, 35, 993–1010 (1980)
- Singhal, A.K. and Somerton, W.H., "Quantitative Modelling of Immiscible Displacement in Porous Media", *Rév. Inst. Français du Pét.*, 32, 897–920 (1977)
- Slattery, J.C., "Interfacial Effects in the Entrapment and Displacement of Residual Oil", *AIChE J.*, 20, 1145–1154 (1974)
- Slobod, R.L., "Comments on Trapping Oil in a Porous Doublet", *Prod. Monthly*, 21(3), 17 (1957)
- Spielman, L.A. and Goren, S.L., "Progress in Induced Coalescence and a new Theoretical Framework for Coalescence in by Flow Through Porous Media", *Ind. Eng. Chem.*, 62 (Oct.), 10–24 (1970)
- Spielman, L.A. and Goren, S.L., "Theory of Coalescence in by Flow Through Porous Media", *Ind. Eng. Chem. Fund.*, 66, 66–72 (1972a)
- Spielman, L.A. and Goren, S.L., "Experiments in Coalescence in by Flow Through Porous Media", *Ind. Eng. Chem. Fund.*, 66, 73–83 (1972b)
- Spielman, L.A., Su, Y., "Coalescence of Oil-in-Water Suspensions by Flow Through Porous Media", *Ind. Eng. Chem. Fund.*, 16, 272–282 (1977)
- Stegemeier, G.L., "Mechanisms of Entrapment and Displacement of Oil in Porous Media", 81st AIChE meeting, Kansas City, Missouri, April 11–14, 1976
- Stauffer, D., "Scaling Theory of Percolation Clusters", *Phys. Repts.*, 54, 1–74 (1979)
- Sur, A., Lebowitz, J.C., Marro, J., Kalos, M.H. and Kirkpatrick, S., "Monte Carlo Studies of Percolation Phenomena for a Simple Cubic Lattice", *J. Stat. Phys.*, 15, 345–353 (1976)
- Taylor, G.I., "The Formation of Emulsions in Definable Fields of Flow", *Proc. Roy. Soc., London*, A146, 501–523 (1934)
- Taylor, G.I., "Deposition of a Viscous Fluid on the Wall of a Tube", *J. Fluid Mech.*, 10, 161–165 (1961)
- Tilton J.N. and Payatakes, A.C., "Collocation Solution of Creeping Newtonian Flow Through a Sinusoidal Tube: A Correction", *AIChE J.*, in press (1984)
- Tomotika, S., "On the Instability of a Cylindrical Thread of a Viscous Liquid Surrounded by Another", *Proc. Roy. Soc., London*, 150, 392–337 (1935)
- Tomotika, S., "Breaking up of a Drop of Viscous Liquid Immersed in Another Viscous Fluid Which is Extending at a Uniform Rate", *Proc. Roy. Soc., London*, 153, 302–318 (1936)

- van Brakel, N.C., "Pore Space Models for Transport Phenomena in Porous Media. Review and Evaluation with Special Emphasis on Capillary Liquid Transport", *Powder Technol.*, 11, 205–236 (1975)
- Wardlaw, N.C., "Pore Geometry in Dolomites and its Influence on Capillary Behaviour". Symposium on Advances in Petroleum Recovery, New York, April 4–9, 1976a
- Wardlaw, N.C., "Pore Geometry of Carbonate Rocks as Revealed by Pore Casts and Capillary Pressure", *Amer. Assoc. Pet. Geol. Bull.*, 60(2), 245–257 (1976b)
- Wardlaw, N.C., "The Effects of Pore Structure on Displacement Efficiency in Reservoir Rocks and in Glass Micromodels",SPE 8843, First Joint SPE/DOE Symposium on Enhanced Oil Recovery, Tulsa, Oklahoma, April 20–23, 1980
- Wardlaw, N. C. and Cassan, J. P., "Estimation of Recovery Efficiency by Visual Observation of Pore Systems in Reservoir Rocks", *Bull. Can. Pet. Geol.*, 26(4), 572–585 (1978)
- Wardlaw, N. C. and Cassan, J. P., "Oil Recovery Efficiency and the Rock-Pore Properties of Some Sandstone Reservoirs", *Bull. Can. Pet. Geol.*, 27(2), 117–138 (1979)
- Wardlaw, N.C. and McKellar, M., "Mercury Porosimetry and the Interpretation of Pore Geometry in Sedimentary Rocks and Artificial Models", *Powder Tech.*, 29, 127–143 (1981)
- Wardlaw, N.C. and Taylor, R.P., "Mercury Capillary Pressure Curves and the Interpretation of Pore Structure and Capillary Behaviour in Reservoir Rocks", *Bull. Can. Pet. Geol.*, 24(2), 225–262 (1976)
- Wasan, D.T., McNamara, J.J., Shah, S.M., Sampath, K. and Aderangi, N., "The Role of Coalescence Phenomena and Interfacial Rheological Properties in Enhanced Oil Recovery: An Overview", *J. of Rheology*, 23, 181–207 (1979)
- Wasan, D.T., Sampath, K., McNamara, J.J., Perl, J., Aderangi, N., Shah, S.M., Chan, M., Neverkar, P., Pasquarelli, C., Srivatsa, S. and Venkataraman, K., "The Mechanisms of Oil Bank Formation, Coalescence in Porous Media and Emulsion Stability", Proc. 4th DOE Annual Symposium on Enhanced Oil Recovery and Improved Drilling Methods", Tulsa, Oklahoma, Aug. 28–31, 1978
- Wasan, D.T., Shah, S.M., Aderangi, N., Chan, M.S. and McNamara, J.J., "Observation on the Coalescence Behaviour of Oil Droplets and Emulsions Stability in Enhanced Oil Recovery", *Soc. Pet. Eng. J.*, 18, 409–417 (1978)
- Washburn, E.W., "The Dynamics of Capillary Flow", *Phys. Rev.*, 17, 273–283 (1921)
- Weiland, R.H. and Davis, S.H., "Moving Contact Lines and Rivulet Instabilities. Part 2. Long Waves on Flat Rivulets", *J. Fluid Mech.*, 102, 135–141 (1983)
- Welygan, D.G. and Burns, C.M., "Dynamic Contact Angles of Viscous Liquids", *J. Adhesion*, 11, 41–55 (1980)

- Wenzel, R.N., "Resistance of Solid Surfaces to Wetting by Water", *Ind. Eng. Chem.*, 28, 988–994 (1936)
- West, G.D., "On the Resistance to the Motion of a Thread of Mercury in a Glass Tube", *Proc. Roy. Soc., London*, A86, 20–25 (1911/12)
- Wilkinson, D. "A Percolation Model of Immiscible Displacement in the Presence of Buoyancy Forces", *Phys. Rev. A*, in press (1984)
- Wilkinson, D. and Willensen, J., "Invasion Percolation: A New Form of Percolation Theory", *J. Phys. A*, 16, 3365–3376 (1983)
- Wooding, R.A. and Morel-Seytoux, H.J., "Multiphase Fluid Flow Through Porous Media", *Ann. Rev. Fluid Mech.*, 8, 233–274 (1976)
- Young, T., "An Essay on the Cohesion of Fluids", *Philos. Trans. Roy. Soc., London*, 95, 65–87 (1805)